UCLA
UCLA Electronic Theses and Dissertations

Title
Mean-Field Games: Computation, Modeling, and Applications

Permalink
https://escholarship.org/uc/item/46x3c5xb

Author
Liu, Siting

Publication Date
2022

Peer reviewed|Thesis/dissertation

UNIVERSITY OF CALIFORNIA

Los Angeles

Mean-Field Games: Computation, Modeling, and Applications

A dissertation submitted in partial satisfaction

of the requirements for the degree

Doctor of Philosophy in Mathematics

by

Siting Liu

2022

ABSTRACT OF THE DISSERTATION

Mean-Field Games: Computation, Modeling, and Applications

by

Siting Liu

Doctor of Philosophy in Mathematics

University of California, Los Angeles, 2022

Professor Stanley J. Osher, Chair

Mean-field game(MFG) systems are revolutionary models to describe complex multi-agent dynamic systems, such as competition between asset managers in finance and traffic congestion in population dynamics. They combine mean-field approximation techniques to describe the population with optimal control approaches to characterize a representative player.

This thesis investigates both computation and modeling aspects of the mean-field games. We propose a computational method for nonlocal MFGs. Our approach relies on kernel-based representations of mean-field interactions and feature-space expansions, which yields a dimension reduction. Based on the monotone inclusion formulation, we further generalize the splitting method for nonlocal MFGs to solve a class of non-potential MFGs. In terms of modelings, we integrate the spatial epidemic models with mean-field control (MFC) models to control the propagation of pandemics. We also apply MFCs to study the optimal vaccine distribution strategy. Numerical experiments demonstrate that the proposed model effectively separates infected patients in a spatial domain and transports vaccines efficiently. Finally, we study an inverse MFG problem. We propose a model recovery algorithm to reconstruct the ground metrics and interactions in the running costs with some noisy observations.

The dissertation of Siting Liu is approved.

Guido Fra Montufar Cuartas

Deanna M. Hunter

Wilfrid Dossou Gangbo

Stanley J. Osher, Committee Chair

University of California, Los Angeles

2022

To my parents and Qi

for their unconditional love and support.

TABLE OF CONTENTS

LIST OF FIGURES

LIST OF TABLES

ACKNOWLEDGMENTS

First, I would like to express my deepest gratitude to my advisor, Professor Stanley Osher. His immense knowledge, invaluable guidance on research directions, and expertise in methodology have been extraordinary to me and made me an independent researcher. His constant encouragement, patience, passion, and humor have always been a great support throughout my Ph.D. years.

I would like first to thank the members of my dissertation committee members, Prof. Guido Montúfar, Prof. Deanna Needell and Prof. Wilfrid Gangbo for their insightful comments and kind suggestions.

I thank all my collaborators for their hard work and advice: Wuchen Li, Levon Nurbekyan, Yat Tin Chow, Samy Wu Fung, Wonjun Lee, Karthik Elamvazhuthi, Matthew Jacobs, and Yuhan Kang. I always enjoy insightful discussions, which not bring in new ideas but also help me build up skills in various aspects: proposing questions, presentations, writings, etc.

I want to give special thanks to my friends and colleagues at UCLA: Fei Feng, Yuejiao Sun, Xuchen Han, Kaiyan Peng, Xia Li, Alex Lin, Minh Pham, Michael Puthawala, Bohyun Kim, Victoria Kala. Especially thank you to my boyfriend Qi Wu for all his love and support. My journey through graduate school would not have been as much of pleasure without them.

Most of all, I would like to thank my parents for their unconditional love and support and always being there for me from the other side of the planet.

2016	B.S. (Mathematics), Shanghai Jiao Tong University.
2017	M.A. (Mathematics), University of Wisconsin-Madison.
2019	Candidate in Philosophy in Mathematics, UCLA.
2021	Dissertation Year Fellowship, UCLA.

PUBLICATIONS

Liu, Siting, Matthew Jacobs, Wuchen Li, Levon Nurbekyan, and Stanley J. Osher. Computational Methods for First-Order Nonlocal Mean Field Games with Applications. *SIAM Journal on Numerical Analysis 59, no. 5 (2021): 2639-2668.*

Liu, Siting, and Levon Nurbekyan. Splitting methods for a class of non-potential mean field games. *Journal of Dynamics & Games 8, no. 4 (2021): 467.*

Lee, Wonjun, Siting Liu, Hamidou Tembine, Wuchen Li, and Stanley Osher. Controlling propagation of epidemics via mean-field control. *SIAM Journal on Applied Mathematics 81, no. 1 (2021): 190-207.*

Lee, Wonjun, Siting Liu, Wuchen Li, and Stanley Osher. Mean field control problems for vaccine distribution.*arXiv:2104.11887 (2021). Submitted to Research in the Mathematical Sciences*

Chow, Yat Tin, Samy Wu Fung, Siting Liu, Levon Nurbekyan, and Stanley Osher. A numerical algorithm for inverse problem from partial boundary measurement arising from mean field game problem. *arXiv:2204.04851 (2022). Submitted to Inverse Problems.*

CHAPTER 1

Introduction

We first consider a continuous differential game, where each rational player takes actions to minimize their own cost. When the number of players is small, the state of the system is determined by the state of every player. A single player, by itself, may significantly change the system's evolution. In such a scenario, the study of Nash equilibrium requires tracking every player and their actions. Therefore, the problem becomes intractable if we want to use agent-based models when the number of players is large. Nevertheless, tracking the state of the individual player usually does not provide practice insights into the model. Mean-field games were firstly introduced independently by J-M. Lasry and P-L. Lions, and by M. Huang, R.P. Malhamé, and P. E. Caines as a new approach to optimization problems involving a large number of interacting players. Mean-field games study strategic decision-making in large populations of identical rational players, where the individual agent interacts in a non-cooperative manner through a certain quantity in the mean-field. At the Nash equilibrium, a consensual state is reached, in which no players have further incentive to change their strategy unilaterally. Indeed, when the number of players is significant, an individual player's contribution to the system state is relatively small. Mean-field games connect the microscopic (individual player) with the macroscopic (overall system state). Such MFG systems can be described using the system of PDEs, which consist Hamilton–Jacobi equations and a Fokker–Planck equations.

1.1 Review of the literature

Mean-field game was initiated by Lasry and Lions [LL06a, LL06b, LL07], and by Huang Malhamé and Caines [HMC06, HCM07]. Since then, the research on mean-field games have been thriving, in theory, computations, and applications.

The classical mean-field games are described using a system of a Hamilton–Jacobi equation and a Fokker–Planck equation, which is derived by Lions and Lasry in their original paper. The existence of solutions for the MFG systems are carefully studied. For the first order and second order Hamilton–Jacobi equation with smooth dependence on the measure, the existence is proved via fixed point argument [Car13a]. As for the MFG systems with local couplings, various models are discussed [Gue09, CLL12, GPS12, Car15, BF16]. The uniqueness of classical solution of MFGs are proved via Lions-Lasry monotonicity method. Potential mean-field game models, which admits variational formulations that allows the use of calculus of variations and duality techniques, are also studied in[LL07, ACC12, Car13b, BCS17]. Such variational problems are also connected to the Benamou-Brenier formulation for the optimal transport problem [BB00]. The linear-quadratic mean-field game that consists a linear adjoint equation is considered in [HCM07, Bar12, NH12, BSY16]. In the probabilistic view, MFG system can be analyzed as a backward stochastic differential equations with a mean-field McKean-Vlasov type, see [BDL09, AD11]. Forward-backward stochastic differential equations are also used to study NFGs [CD13a, CD13b, CL15]. A more general formulation of mean-field games, referred as master equation, is thoroughly investigated [CD14, BFY15, CDL19]. Related research directions include well-posedness of second order master equations with non-smooth data [MZ19], long time behavior of master equation [CP19], large deviations principle [DLR20], and Hamilton-Jacobi equations in probability space of potential games [GNT08, GS15, GM20]. For a detailed introduction and review of MFG theory we refer to[LL07, GLL11, Car13a, GS14].

MFG system has a special forward-backward in time structure. Moreover, the two

equations are coupled with nonlinear terms, making the system difficult to analyze. Therefore, numerical methods are crucial for understanding the qualitative and quantitative behaviors of the MFG systems. Pioneering works of numerical methods for the MFGs are investigated using a finite difference scheme [ACC12]. Proximal point algorithm[BKS18] and Newton's method[AC10, ACC12, ACC13] are applied to solve the finite difference system. The discrete approximations of the MFG model rely on monotone approximations of the Hamiltonian. The existence and uniqueness of the discretized problems are proved[AC10]. Semi-Lagrangian approaches are studied in [CS12, CS14, CS15, CS18]. For MFG and MFC problems with a variational structure, optimization methods are applied, including Augmented Lagrangian [FG00, BC15b], Alternating Direction Method of Multipliers (ADMM) [EB92, BB00, AL16, And17], and Primal–dual Hybrid Gradient (PDHG) [CP11, CP16, BKS18, BKK19]. Monotone deformation flow is studied in [GS21], while basis method for non-local interactions are handled in [NS18, LN21, LJL21, ALF22, MYZ22]. An approach that solves the Hamilton-Jacobi equation in density space via the Hopf formula is discussed in [CLO19]. Numerical methods for stationary MFG equations are studied in [AFG17]. MFG systems are solved using game theory approaches, such as fictitious play[CH17, Had17, HS19, BLP21]. Deep learning approaches are also explored in the context of MFGs [ROL20, LFL21, CCS21], optimal transport [FJN20, OWL21], and optimal control [ONL21b, ONL21a]. Reinforcement leaning methods are also developed to compute MFG and MFC problems in a model-free fashion [YYT18, GHX20, AFL21, AFL22]. For surveys of numerical methods of MEGs, see [AL20, Lau21, HL22].

Mean-field games offer powerful descriptions ranging from social-economical to biodiversity ecology, and have brought significant impact in the understanding of finance[LLL16, CL18, CJ19, FC17, LRS19, CJ20], economics[GLL11, ABL14, GNP15, AHL17, CL18], biology[NCM11, SS21], epidemics[CPP20, EHT20, LLT21, ACD22], opinion dynamics[BTB16, GLB22], and data science[WHL19, GHX19, CLT19, FJN20]. In [WHL19], they analyze deep learning by recasting it as an optimal control problem. In population dynamics, MFGs were used to

study crowd motions[LW11, BDM14, DTT17, AD18, AL19] and traffics[CLM15, ZYL19]. MFG models have various applications in engineering, including robotic controls[KC12, SPB19, EB19, GLK22], demand management in power grids [MLT13, BB14, KSM19] and others [BFY13, BLY21]. For example, in [KLZ21], they use MFG models to generate trajectories for mobile vehicle networks.

1.2 Outline of the thesis

In this thesis, we study three different aspects of the mean-field games: computations, modelings, and applications.

In Chapter 2,3, we present two projects on computational approaches for mean-field games. This part is based on the papers [LJL21] and [LN21].

We first introduce a novel framework to model and solve first-order mean-field game systems with nonlocal interactions extending the results in [NS18]. Our approach relies on kernel-based representations of mean-field interactions and feature-space expansions in the spirit of kernel methods in machine learning. We demonstrate the flexibility of our approach by modeling various interaction scenarios between agents. Additionally, our method yields a computationally efficient saddle-point reformulation of the original problem that is amenable to state-of-the-art convex optimization methods such as the primal–dual hybrid gradient method (PDHG). We also discuss the potential applications of our methods to multi-agent trajectory planning problems.

Next, we extend the methods from [NS18, LJL21] to a class of non-potential mean-field game (MFG) systems with mixed couplings. Up to now, splitting methods have been applied to potential MFG systems that can be cast as convex-concave saddle-point problems. Here, we show that a class of non-potential MFG can be cast as primal-dual pairs of monotone inclusions and solved via extensions of convex optimization algorithms such as PDHG algorithm. A critical feature of our approach is in considering dual variables of nonlocal couplings in Fourier

or feature spaces.

The main contribution of this part is the numerical method for nonlocal MFGs and a type of non-potential MFGs.

In Chapter 4,5, we address some modeling of MFGs to the epidemic model. This chapter is based on the papers [LLT21] and [LLL21b].

We incorporate the mean-field control framework with SIR and SIRV model, and introduce a mean-field control model for controlling the propagation of epidemics on a spatial domain. The coronavirus disease 2019 (COVID-19) pandemic is changing and impacting lives on a global scale. As the propagation of COVID-19 has a significant spatial characteristic, it is crucial to have a spatial-type SIR model to study the spread of infectious diseases and the movement of individuals. Beyond this, mean-field games (controls) provide a perspective to study and understand the underlying population dynamics. The control variable – the spatial velocity – is first introduced for the classical disease models, such as the SIR model. We provide fast numerical algorithms based on proximal primal-dual methods for this proposed model. Numerical experiments demonstrate that the proposed model illustrates how to separate infected patients in a spatial domain effectively.

Later, with the invention of the COVID-19 vaccine, shipping and distributing is crucial in controlling the pandemic. We extend this work by using the concept of mean-field control to study the optimal transportation strategy for vaccine distribution. Numerical examples demonstrate that the proposed model provides practical strategies for vaccine distribution in a spatial domain.

The main contribution is to generalize the mean-field control problems to the epidemic models. Numerical algorithms are derived to solve the proposed models, with experiments demonstrating that our models can effectively control the propagation of the pandemic.

In Chapter 6, we propose a new mean-field game inverse problem. This part is based on the paper [CFL22].

We aim to recover the mean-field game model parameters that govern the underlying interactions among the population based on a limited set of noisy partial observations of the population dynamics under the limited aperture. Due to its severe ill-posedness, obtaining a good quality reconstruction is very difficult. Nonetheless, it is vital to recover the model parameters stably and efficiently to uncover the underlying causes for population dynamics for practical needs. Based on insights from [NS18, LJL21, LN21] we postulate a feature expansion representation for the interaction kernel K and formulate the forward problem as a convex-concave saddle point problem. Furthermore, we design a three-operator splitting scheme [DY17] for the resulting inverse problem with a saddle-point constraint. The algorithm reduces to a forward-backward splitting for the parameter updates, a primal-dual hybrid gradient for the forward saddle point problem update, and a proximal-point algorithm for the adjoint problem update.

The main contribution of this part is that we propose a novel MFG inverse problem with non-invasive partial boundary measurements. We propose a model recovery algorithm to recover the model coefficients numerically. Intriguingly, our algorithm applies to inverse problems whose forward problem has a saddle point structure beyond MFG.

CHAPTER 2

Computational Methods for Nonlocal Mean-field games

In this chapter, we propose a novel computational framework to solve nonlinear PDE arising in mean-field games (MFG) theory. These PDEs characterize equilibria in large systems of interacting agents that solve optimal control problems. When interactions are nonlocal, the PDEs contain integral terms that are computationally expensive to handle with existing algorithms. Our approach solves this problem by approximating these interactions with suitable bases in the spirit of Fourier or feature-space expansions in machine learning. We demonstrate the flexibility of our approach in terms of choices of bases and compatibility with existing computational methods for MFGs with local interactions and optimal control problems. The work builds on a theoretical analysis performed in[GS21].

This chapter has the following organization. Firstly, we introduce the nonlocal mean-field games and discuss motivations on efficient computational method for this certain type of MFGs in Section2.1. In Section 2.2, we provide a detailed description of our method. In Section 2.3, we devise a PDHG algorithm to solve (2.1.1) based on our method and discuss the computational efficiency of our approach. In Section 2.4, we show how to model and approximate interactions using kernel methods from machine learning. Next, in Section 2.5, we discuss potential applications of our methods to multi-agent trajectory planning problems. Finally, in Section 2.6 we provide several numerical experiments.

The contributions in this chapter were first presented in the joint work with Matthew Jacobs, Wuchen Li, Levon Nurbekyan, and Stanley Osher in [LJL21].

2.1 Introduction

We study computational and modeling aspects of first-order nonlocal mean-field game systems. Specifically, we are interested in the system

$$
\begin{cases}
-\phi_t + H(x, \nabla\phi) = f\left(x, \int_\Omega K(x,y)\rho(y,t)dy\right) \\
\rho_t - \nabla \cdot (\rho\nabla_p H(x, \nabla\phi)) = 0 \\
\rho(x,0) = \rho_0(x), \ \ \phi(x,1) = g\left(x, \int_\Omega S(x,y)\rho(y,1)dy\right)
\end{cases}
\tag{2.1.1}
$$

Above, $\Omega \subset \mathbb{R}^d$ is either the flat torus, $\mathbb{T}^d$, or a closure of a domain with smooth boundary, $H : \Omega \times \mathbb{R}^d \to \mathbb{R}$ is the Hamiltonian, $K, S : \Omega \times \Omega \to \mathbb{R}$ are interaction kernels, and $f, g : \Omega \times \mathbb{R} \to \mathbb{R}$ are interaction functions.

System (2.1.1) describes Nash equilibria in an infinite-dimensional differential game where a continuum of agents interact through their distribution in the state-space. In (2.1.1), $\rho(\cdot, t)$ represents the population density at time t, and ρ_0 is an initial distribution. Furthermore, $(x,t) \mapsto \phi(x,t)$ is a value function that measures the optimal value of an agent at position x and time t. Functions f, g and kernels K, S model the interaction between a single agent and the population.

In general, (2.1.1) does not admit classical solutions, and a suitable notion of a weak solution is necessary. A pair (ϕ, ρ) is a weak solution of (2.1.1) if ϕ is a viscosity solution for HJB, and ρ is a distribution solution for the continuity equation with a no-flux boundary condition. For the existence, uniqueness, and regularity theory of (2.1.1) we refer to [LL07, Car13a] for $\Omega \in \{\mathbb{T}^d, \mathbb{R}^d\}$ and [CC18, CCC19, CCC21] for bounded Ω with smooth boundary.

Our goal is to develop computational and modeling methods for (2.1.1). There are several general purpose numerical methods for MFG that can be used to approximate the solutions of (2.1.1). In [AC10, Ach13, ACC13], the authors develop and analyze finite-difference methods for second-order versions of (2.1.1). Their approach is based on a solution of the discrete problem applying Newton's method. Although the authors consider second-order systems

with a positive viscosity parameter, their numerical experiments indicate robustness with respect to the vanishing viscosity and can be used to approximate first-order systems such as (2.1.1) (see [AC10, Test 6] and Section 2.6.6 here).

For so-called *potential* MFG systems, there are several primal-dual convex optimization methods such as alternating direction method of multipliers (ADMM) [BC15a, BCS17] and primal-dual hybrid gradient (PDHG) [AKS18, AKK19] (the latter employing the discretization in [AC10]). These methods are extensions of the celebrated Brenier-Benamou method for computation of optimal transport maps [BB00] to the MFG setting. Although originally designed for local interactions, these methods can be naturally adapted to nonlocal ones: see Section 2.3.3 for further details.

Here, our goal is to develop computational and modeling methods specifically for nonlocal MFG systems. The term nonlocal refers to expressions

$$f\left(x, \int_\Omega K(x,y)\rho(y,t)dy\right), \quad g\left(x, \int_\Omega S(x,y)\rho(y,1)dy\right).$$

Indeed, the calculation of these terms at x requires the knowledge of $\rho(y,t)$ at all y. For general MFG systems, these terms are replaced by $f(x,\rho)$, $g(x,\rho)$ where one allows local interactions as well; that is, $f(x,\rho) = \tilde{f}(x,\rho(x,t))$, and $g(x,\rho) = \tilde{g}(x,\rho(x,1))$ where, $\tilde{f}, \tilde{g}: \Omega \times \mathbb{R}_+ \to \mathbb{R}$ are some functions, and $\rho(x,t)$ is the density of ρ. Note that for local interactions, the calculation of f, g terms at x requires information only at x.

Existing methods in the literature discretize interaction terms directly in the state-space. For local interactions such discretizations are economical. For the nonlocal case though, the calculation of interaction terms requires matrix multiplication on a full grid to evaluate the expressions $\int_\Omega K(x,y)\rho(y,t)dy$, $\int_\Omega S(x,y)\rho(y,1)dy$. Our approach solves this problem by encoding the interactions in a small number of *expansion coefficients*.

Furthermore, a critical feature of primal-dual methods mentioned above is that one of the proximal steps results in a decoupled system of one-dimensional convex optimization problems at the grid-points. Therefore, this step is parallelizable and yields a linear computational

cost in the number of grid-points. However, direct applications of these methods to nonlocal problems yield fully coupled systems that are not parallelizable and yield a superlinear computational cost. Our method solves this problem as well. The expansion coefficients, that encode the interactions, decouple the aforementioned systems. Furthermore, we update these coefficients by an explicit proximal step that yields a linear computational cost.

Our method is also well-suited for the Lagrangian framework. Indeed, in [NS18], where this approach was introduced, the authors solved (2.1.1) in Lagrangian coordinates. Thus, this approach paves a way to efficient computational methods for high-dimensional MFG problems.

Another appealing feature of our method is the flexibility of modeling interactions. We expand K, S in a basis that can be interpreted as features from kernel methods in ML [MRT18, Chapter 6]. This allows us to design various interactions by only manipulating the basis. In particular, we can easily model heterogeneous regimes where agents interact only within specific subdomains and other interesting scenarios. Additionally, we can handle nonlocal interactions that are given by differential operators [AC10, Tests 5, 6].

Finally, we would like to point out potential applications of our methods to multi-agent trajectory-planning. In general, even single-agent trajectory-panning problems are highly complex. With the number of agents increasing in a system, problems quickly become computationally overwhelming.

A critical difficulty comes from modeling and computing the interactions. MFG theory provides a flexible framework to solve this problem. Theoretically, MFG solutions are optimal only when the number of agents is infinite. Nevertheless, one can generate sub-optimal trajectories that have appealing properties such as no-collision. Since our method provides a way of encoding mean-field interactions in a few coefficients independent of the number of agents, it is potentially applicable to large multi-agent trajectory planning problems.

2.2 The method of coefficients

We assume that Ω is either the flat torus, $\mathbb{T}^d$, or a closure of a bounded domain with C^2 boundary. Additionally, we assume that f, g, K, S are C^2 functions. To alleviate the presentation, we first discuss the periodic case and assume that interactions are given by $f(x, \zeta) = \zeta$, and $g(x, \zeta) = g(x)$. We provide remarks on the non-periodic case and more general interactions in Remark 2.

Thus, assume that $\Omega = \mathbb{T}^d$, $\rho_0 \in \mathcal{P}(\Omega) \cap L^\infty(\Omega)$, and $H \in C^2(\Omega \times \mathbb{R}^d)$ is such that

$$\frac{1}{C} I_d \leq \nabla_{pp}^2 H(x, p) \leq C I_d, \ \forall (x, p) \in \Omega \times \mathbb{R}^d,$$

$$-C(1 + |p|^2) \leq \nabla_x H(x, p) \cdot p, \ \forall (x, p) \in \Omega \times \mathbb{R}^d,$$

for some constant $C > 0$. Assuming $f(x, \zeta) = \zeta$, and $g(x, \zeta) = g(x)$, (2.1.1) reduces to

$$\begin{cases} -\phi_t + H(x, \nabla \phi) = \int_\Omega K(x, y) \rho(y, t) dy \\ \rho_t - \nabla \cdot (\rho \nabla_p H(x, \nabla \phi)) = 0 \\ \rho(x, 0) = \rho_0(x), \ \phi(x, 1) = g(x) \end{cases} \tag{2.2.1}$$

It is proved in [LL07] (see also [Car13a, Car13b]) that (2.2.1) admits solutions $\phi \in W^{1,\infty}(\Omega \times [0, 1])$ and $\rho \in L^\infty(\Omega \times [0, 1]) \cap C([0, 1]; \mathcal{P}(\Omega))$, where ϕ is a viscosity solution of the HJB, and ρ is a weak-solution of the continuity equation. Additionally, when the mean-field interaction is monotone; that is,

$$\int_{\Omega^2} K(x, y)(\rho_2(x) - \rho_1(x))(\rho_2(y) - \rho_1(y)) dx dy \geq 0, \quad \forall \rho_1, \rho_2 \in \mathcal{P}(\Omega) \tag{2.2.2}$$

the solution is unique.

The essence of the method of coefficients is in an expansion of $K(x, y)$ in a family of functions. More precisely, assume that $\{f_i\}_{i=1}^r \subset C^2(\Omega)$ is an arbitrary family of functions. Furthermore, suppose that

$$K(x, y) = \sum_{i,j=1}^r k_{ij} f_i(x) f_j(y) \tag{2.2.3}$$

11

Remark 1. *In general, K may not have the form (2.2.3). In these cases, we approximate K with kernels of such form [NS18, Section 4].*

We denote by $\mathbf{K} = (k_{ij}) \in M_{r \times r}(\mathbb{R})$. A straightforward calculation yields that

$$\int_{\Omega} K(x, y) \rho(y, t) dt = \sum_{i=1}^{r} a_i(t) f_i(x),$$

where

$$a_i(t) = \sum_{j=1}^{r} k_{ij} \int_{\Omega} f_j(y) \rho(y, t) dy.$$

Thus, for an arbitrary probability measure ρ, the expression $\int_{\Omega} K(x, y) \rho(y, t) dy$ is a combination of $\{f_i\}_{i=1}^{r}$ with some *unknown coefficients $a_1, a_2, \cdots, a_r$*. These coefficients encode all necessary information about the interactions. Thus, (a_i) will be our new unknowns. Note that once we find (a_i) we can solve (2.2.1) by solving decoupled HJB and continuity equations.

It turns out that (a_i) are zeroes of an operator that is *monotone* if $\rho \mapsto \int_{\Omega} K(x, y) \rho(y) dy$ is monotone, and a *gradient* when K is symmetric. To state the results precisely, denote by ϕ_a the viscosity solution of the HJB

$$\begin{cases} -\phi_t + H(x, \nabla \phi) = \sum_{i=1}^{r} a_i(t) f_i(x) \\ \phi(x, 1) = g(x) \end{cases} \tag{2.2.4}$$

Furthermore, denote by ρ_a the distributional solution of the continuity equation

$$\begin{cases} \rho_t - \nabla \cdot (\rho \nabla_p H(x, \nabla \phi_a)) = 0 \\ \rho(x, 0) = \rho_0(x) \end{cases} \tag{2.2.5}$$

The following two theorems are the basis of our approach.

Theorem 2.2.1. *[NS18, Theorem 2.3] The functional $a \mapsto \int_{\Omega} \phi_a(x, 0) \rho_0(x) dx$ is concave and everywhere Fréchet differentiable. Moreover,*

$$\frac{\delta}{\delta a_i} \int_{\Omega} \phi_a(x, 0) \rho_0(x) dx = \int_{\Omega} f_i(x) \rho_a(x, \cdot) dx, \ 1 \le i \le r. \tag{2.2.6}$$

12

Theorem 2.2.2. *[NS18, Theorem 3.1]*

i. *A pair (ϕ, ρ) is a solution of (2.2.1) if and only if $(\phi, \rho) = (\phi_a, \rho_a)$ for some $a \in C([0,1]; \mathbb{R}^r)$ such that*

$$a = \mathbf{K} \frac{\delta}{\delta a} \int_\Omega \phi_a(x, 0) \rho_0(x) dx \qquad (2.2.7)$$

ii. *If $\mathbf{K}$ is strictly monotone; that is, $\xi^\top \mathbf{K} \xi > 0$ for all $\xi \in \mathbb{R}^r \backslash \{0\}$, then (2.2.7) is equivalent to finding a zero of a monotone operator $a \mapsto \mathbf{K}^{-1} a - \frac{\delta}{\delta a} \int_\Omega \phi_a(x, 0) \rho_0(x) dx$, $a \in C([0,1]; \mathbb{R}^r)$.*

iii. *Additionally, if $\mathbf{K}$ is symmetric, (2.2.7) is equivalent to the convex optimization problem*

$$\inf_{a \in C([0,1]; \mathbb{R}^r)} \frac{\langle \mathbf{K}^{-1} a, a \rangle}{2} - \int_\Omega \phi_a(x, 0) \rho_0(x) dx, \qquad (2.2.8)$$

where $\langle a, b \rangle = \sum_{i=1}^r \int_0^1 a_i(t) b_i(t) dt$ for $a, b \in C([0,1]; \mathbb{R}^r)$.

Remark 2. *Several remarks are in order.*

1. *Theorem 2.2.2 asserts that instead of finding (ϕ, ρ) in (2.2.1) we just need to find the right coefficients (a_i) and then solve the decoupled equations (2.2.4), (2.2.5).*

2. *Here, we do not concentrate on technical aspects of Theorems 2.2.1, 2.2.2, such as well-posedness of (2.2.1), (2.2.4), (2.2.5), that are discussed for the periodic case in [NS18]. For the non-periodic case in a bounded domain, (2.2.1) must be complemented with a no-flux Neumann boundary condition*

$$-\nabla_p H(x, \nabla \phi(x, t)) \cdot \nu(x) = 0, \quad x \in \partial\Omega \cap \operatorname{supp}(\rho(\cdot, t)), \quad t \in (0, 1),$$

where $\nu(x)$ is the outer unit normal to Ω at x, and $\nabla \phi$ should be understood in a suitable sense. Informally speaking, $\nabla \phi$ is the gradient of ϕ "from inside Ω." Additionally, viscosity solutions must be understood in the constrained sense. We refer to [CC18, CCC19, CCC21] for precise definitions and statements.

In this context, Theorems 2.2.1, 2.2.2 should be modified accordingly. Indeed, ϕ_a is still well-defined as a unique constrained viscosity solution of (2.2.4). However, unlike the unconstrained case, ϕ_a is not regular enough in general for (2.2.5) to be well-posed. Consequently, the functional $a \mapsto \int_\Omega \phi_a(x,0)\rho_0(x)dx$ is concave but not necessarily Fréchet differentiable.

Hence, in Theorems 2.2.1, 2.2.2 we should replace Fréchet derivatives by superdifferentials and instead of working with ρ_a work with probability measures supported on minimizing trajectories as it is done in [CC18, CCC19, CCC21]. Furthermore, solutions $\rho(\cdot, t)$ of (2.2.1) might not be absolutely continuous with respect to the Lebesgue measure. Nevertheless, we believe that suitable extensions of Theorems 2.2.1, 2.2.2 and the saddle-point formulation (2.3.2) are valid in the constrained case based on the results in [CC18, CCC19, CCC21]. We will address this intriguing point in our future work.

For now, we proceed informally and impose a no-flux boundary condition $m \cdot \nu = 0$ on $\partial\Omega$, where $m = \rho v$, and $v = -\nabla_p H(x, \nabla\phi)$ is the optimal velocity field. Note that we do not exploit the relation between m and $\nabla\phi$ explicitly but impose the no-flux boundary condition directly on m instead of $\nabla\phi$. This approach is consistent with the results obtained in [CCC21, Section 4].

3. According to [NS18, Lemma 4.1], **K** is monotone if and only if the interaction is monotone; that is, (2.2.2) holds. As mentioned above, this condition is essential for the uniqueness of solutions of (2.2.1) [LL07, CC18].

4. **K** is symmetric if and only if K is symmetric; that is, $K(x,y) = K(y,x)$ for all $x, y \in \Omega$.

5. For monotone interactions, (a_i) are solutions of a monotone variational inequality or a convex optimization problem. Therefore, one can apply powerful convex optimization techniques to find (a_i).

6. Equation (2.2.6) is critical for update rules of (a_i). Indeed, it gives the ascent direction

14

$\int_\Omega \phi_a(x,0)\rho_0(x)dx$ *with respect to* (a_i). *Moreover, this direction depends on* ρ_a, *which is available once* ϕ_a *is (approximately) computed at current* (a_i). *As we shall see below, this property yields extremely simple update rules for* (a_i).

7. *These previous points are also very appealing for potential applications of our methods to multi-agent trajectory planning problems.*

8. *Optimization problem (2.2.8) is equivalent to the infinite-dimensional optimal control problem (58)-(59) in [LL07].*

9. *There is nothing special about the choice* $f(x,\zeta) = \zeta$, $g(x,\zeta) = g(x)$ *except simplicity. Analogous results are valid for general* f, g *as well. This topic is discussed in a companion paper [LN21].*

10. *Similar theorems are valid for stochastic systems as well.*

2.3   A primal-dual hybrid gradient algorithm for symmetric kernels

Here, we assume that **K** is symmetric and formulate (2.2.8) as a convex-concave saddle point problem. Furthermore, we devise a primal-dual hybrid gradient (PDHG) algorithm of Chambolle and Pock [CP11, CP16] to solve it.

2.3.1 A saddle-point problem formulation

Introducing a Lagrange multiplier for the HJB equation in (2.2.4) we obtain

$$
\begin{aligned}
&\inf_{a \in C([0,1];\mathbb{R}^r)} \frac{\langle \mathbf{K}^{-1}a, a \rangle}{2} - \int_\Omega \phi_a(x,0)\rho_0(x)dx \\
&= \inf_{\phi,a} \left\{ \frac{\langle \mathbf{K}^{-1}a, a \rangle}{2} - \int_\Omega \phi(x,0)\rho_0(x)dx \text{ s.t. (2.2.4) holds} \right\} \\
&= \inf_{\substack{\phi(x,1)=g \\ a}} \sup_\rho \left\{ \frac{\langle \mathbf{K}^{-1}a, a \rangle}{2} - \int_\Omega \phi(x,0)\rho_0(x)dx \right. \\
&\qquad \left. + \int_\Omega \int_0^1 \rho \left(-\phi_t + H(x,\nabla\phi) - \sum_{i=1}^r a_i(t)f_i(x) \right) dtdx \right\} \\
&= \inf_{\substack{\phi(x,1)=g \\ a}} \sup_{\rho,v} \left\{ \frac{\langle \mathbf{K}^{-1}a, a \rangle}{2} - \int_\Omega \phi(x,0)\rho_0(x)dx - \int_\Omega \int_0^1 (\rho\phi_t + \rho v \cdot \nabla\phi)\, dtdx \right. \\
&\qquad \left. - \int_\Omega \int_0^1 \rho \left(L(x,v) + \sum_{i=1}^r a_i(t)f_i(x) \right) dtdx \right\},
\end{aligned}
$$

$$(2.3.1)$$

where we used the convex duality

$$
H(x,\nabla\phi) = \sup_v -v \cdot \nabla\phi - L(x,v).
$$

The saddle point problem in (2.3.1) is convex in (ϕ, a) but not concave in (ρ, v). Non-concavity comes from the terms $\rho v \cdot \phi$ and $\rho L(x,v)$. Following [BB00], we remedy this problem by replacing v with a flux variable $m = \rho v$. Thus, we obtain an equivalent saddle point problem

$$
\begin{aligned}
&\inf_{\substack{\phi(x,1)=g \\ a}} \sup_{\rho,m} \left\{ \frac{\langle \mathbf{K}^{-1}a, a \rangle}{2} - \int_\Omega \phi(x,0)\rho_0(x)dx - \int_\Omega \int_0^1 (\rho\phi_t + m \cdot \nabla\phi)\, dxdt \right. \\
&\qquad \left. - \int_\Omega \int_0^1 \rho \left(L \left(x, \frac{m}{\rho} \right) + \sum_{i=1}^r a_i(t)f_i(x) \right) dxdt \right\} \\
&= \inf_{\substack{\phi(x,1)=g \\ a}} \sup_{\rho,m} \mathcal{L}(\phi, a, \rho, m)
\end{aligned}
$$

$$(2.3.2)$$

Note that $(\phi, a) \mapsto \mathcal{L}(\phi, a, \rho, m)$ is convex, $(\rho, m) \mapsto \mathcal{L}(\phi, a, \rho, m)$ is concave, and the coupling between (ϕ, a) and (ρ, m) is bilinear. Thus, we can apply PDHG [CP11, CP16] to solve

(2.3.2). Also, note that the first-order optimality conditions for ϕ are

$$
\begin{cases}
\rho_t + \nabla \cdot m = 0 & \text{in} \quad \Omega \times (0,1) \\
m(x,t) \cdot \nu = 0 & \text{in} \quad \partial\Omega \times (0,1) \\
\rho(x,0) = \rho_0(x) & \text{in} \quad \Omega
\end{cases}
$$

Therefore, the no-flux boundary condition for m and the initial condition for ρ are incorporated in (2.3.2), and no extra considerations are necessary.

Furthermore, we must add a constraint $\rho \geq 0$ to account for ρ being a probability distribution. This adjustment is coherent with the derivation (2.3.1) because the viscosity-solution constraint (2.2.4) should be replaced by pointwise constraints $-\partial_t \phi + H(x, \nabla\phi) \leq \sum_{i=1}^{r} a_i(t) f_i(x)$, $\phi(x,1) \leq g(x)$. Additionally, the expression $L\left(x, \frac{m}{\rho}\right)$ must be understood in the following sense

$$
L\left(x, \frac{m}{\rho}\right) = \begin{cases}
L\left(x, \frac{m}{\rho}\right), & \text{when } \rho > 0 \\
0, & \text{when } m = 0, \ \rho = 0 \\
+\infty, & \text{when } m \neq 0, \ \rho = 0
\end{cases}
$$

We refer to [BCS17] for further details.

2.3.2 PDHG updates

As illustrated in [JLL19, JL20], the choices of spaces for variables are crucial when applying PDHG. Correct choices render algorithms with grid-size-independent convergence rates. For a, ρ, m we choose L^2 spaces, whereas for ϕ we choose H^1. The motivation for this choice comes from convergence analysis of PDHG. Indeed, upper bounds on the step-sizes depend on the inverse of the norm of the bilinear coupling

$$
\left| \int_\Omega \int_0^1 (\rho \phi_t + m \cdot \nabla\phi) \, dx dt \right| \leq \|(\rho, m)\|_{L^2} \cdot \|\phi\|_{H^1}
$$

This norm is finite if we choose L^2 norm for (ρ, m) and H^1 norm for ϕ. If we chose L^2 norm for ϕ, the bilinear coupling would have infinite norm. Therefore the corresponding norm

of the finite-dimensional coupling on a grid would depend on the grid-size and converge to infinity as grid gets finer. Consequently, the step-sizes that guarantee the convergence of the algorithm would shrink to 0 and yield an impractically slow algorithm. The H^1 norm, on the other hand, yields convergence guarantees and rates that are grid-independent.

For step-sizes $\tau_{\nabla\phi}, \tau_{\phi_t}, \tau_{\phi(0)}, \tau_\rho, \tau_m$, and current iterates $(a^k, \phi^k, \rho^k, m^k, \bar{a}^k, \bar{\phi}^k)$ the update rules for PDHG are

$$
\begin{cases}
(\rho^{k+1}, m^{k+1}) & = \underset{\rho,m}{\operatorname{argmax}} \left\{ \mathcal{L}(\bar{\phi}^k, \bar{a}^k, \rho, m) - \frac{1}{2\tau_\rho}\|\rho - \rho^k\|^2_{L^2_{x,t}} - \frac{1}{2\tau_m}\|m - m^k\|^2_{L^2_{x,t}} \right\} \\[2mm]
(a^{k+1}, \phi^{k+1}) & = \underset{a,\phi}{\operatorname{argmin}} \left\{ \mathcal{L}(\phi, a, \rho^{k+1}, m^{k+1}) + \frac{1}{2\tau_{\phi(0)}}\|\phi(\cdot,0) - \phi^k(\cdot,0)\|^2_{L^2_x} \right. \\[2mm]
& \qquad \left. + \frac{1}{2\tau_{\nabla\phi}}\|\nabla\phi - \nabla\phi^k\|^2_{L^2_{x,t}} + \frac{1}{2\tau_{\phi_t}}\|\phi_t - \phi^k_t\|^2_{L^2_{x,t}} + \frac{1}{2\tau_a}\|a - a^k\|^2_{L^2_t} \right\} \\[2mm]
(\bar{a}^{k+1}, \bar{\phi}^{k+1}) & = 2(a^{k+1}, \phi^{k+1}) - (a^k, \phi^k)
\end{cases}
$$

The critical observation is that the variational problems above are well-posed and easy to solve. In what follows we discuss in details each of the updates.

The updates for (ρ, m)**.** We have that

$$
\frac{\delta\mathcal{L}}{\delta\rho} = -\phi_t - L\left(x, \frac{m}{\rho}\right) + \nabla_v L\left(x, \frac{m}{\rho}\right) \cdot \frac{m}{\rho} - \sum_{i=1}^{r} a_i(t) f_i(x)
$$

$$
\frac{\delta\mathcal{L}}{\delta m} = -\nabla\phi - \nabla_v L\left(x, \frac{m}{\rho}\right)
$$

Therefore, for updating (ρ, m) we must solve the following system

$$
\begin{cases}
\nabla_v L\left(x, \frac{m}{\rho}\right) \cdot \frac{m}{\rho} - L\left(x, \frac{m}{\rho}\right) - \frac{\rho - \rho^k}{\tau_\rho} = \bar{\phi}^k_t + \sum_{i=1}^{r} \bar{a}^k_i(t) f_i(x) \\[2mm]
\nabla_v L\left(x, \frac{m}{\rho}\right) + \frac{m - m^k}{\tau_m} = \nabla\bar{\phi}^k
\end{cases} \tag{2.3.3}
$$

Remark 3. *Once discretized, system (2.3.3) yields decoupled one-dimensional convex optimization problems at the grid-points. Therefore the proximal update for (ρ, m) can de performed efficiently in parallel. This feature is one of the most appealing properties of ADMM [BB00, BC15a, BCS17] and PDHG [AKS18, AKK19, JLL19, LRO18] algorithms for MFG systems and related problems for local couplings. However, direct extensions of*

aforementioned methods to nonlocal MFG systems do not preserve this property. One of the

critical features of our approach is that we preserve this property. We refer to Section 2.3.3

for details.

For some Lagrangians, (2.3.3) simplifies greatly. For instance, for $L(x, v) = \frac{|v|^2}{2} + Q(x, t)$
we have that $\nabla_v L(x, v) = v$, and (2.3.3) becomes

$$
\begin{cases}
\frac{|m|^2}{2\rho^2} - \frac{\rho - \rho^k}{\tau_\rho} = Q(x, t) + \bar{\phi}_t^k + \sum_{i=1}^r \bar{a}_i^k(t) f_i(x) \\
\frac{m}{\rho} + \frac{m - m^k}{\tau_m} = \nabla \bar{\phi}^k
\end{cases}
$$

Furthermore, eliminating m from the second equation, we obtain

$$
\begin{cases}
\frac{|m^k + \tau_m \nabla \bar{\phi}^k|^2}{2(\tau_m + \rho)^2} - \frac{\rho - \rho^k}{\tau_\rho} = Q(x, t) + \bar{\phi}_t^k + \sum_{i=1}^r \bar{a}_i^k(t) f_i(x) \\
m = \rho \frac{m^k + \tau_m \nabla \bar{\phi}^k}{\tau_m + \rho}
\end{cases}
$$

Therefore, we just need to solve a cubic equation for ρ and update m by an explicit formula.

Remark 4. *As mentioned before, we must add a constraint $\rho \geq 0$ in (2.3.2). Therefore, equations above must be complemented by the condition $\rho \geq 0$. The function $\gamma(\rho) = \frac{|m^k + \tau_m \nabla \bar{\phi}^k|^2}{2(\tau_m + \rho)^2} - \frac{\rho - \rho^k}{\tau_\rho}$, $\rho \geq 0$ is strictly decreasing. Therefore, either $\gamma(0) \geq Q(x, t) + \bar{\phi}_t^k + \sum_{i=1}^r \bar{a}_i^k(t) f_i(x)$ or $\gamma(0) < Q(x, t) + \bar{\phi}_t^k + \sum_{i=1}^r \bar{a}_i^k(t) f_i(x)$. In the former case, there exists a unique $\rho^{k+1}(x, t) \geq 0$ such that $\gamma(\rho^{k+1}(x, t)) = Q(x, t) + \bar{\phi}_t^k(x, t) + \sum_{i=1}^r \bar{a}_i^k(t) f_i(x)$. In the latter case, we set $\rho^{k+1}(x, t) = 0$. In both cases, we update m accordingly.*

The updates for (a, ϕ). We have that

$$
\begin{aligned}
\frac{\partial \mathcal{L}}{\partial a} &= \mathbf{K}^{-1} a - \left(\int_\Omega f_i(x) \rho(x, t) dx \right)_{i=1}^r \\
\frac{\partial \mathcal{L}}{\partial \phi} &= \rho_t + \nabla \cdot m + (\rho - \rho_0) \, dx \times \delta_{t=0} - m \cdot \nu \, d_{\partial\Omega} x \times dt
\end{aligned}
$$

where ν is the outward normal of Ω, and $d_{\partial\Omega}$ is the surface measure of $\partial\Omega$. Note that we
only consider variations that preserve the boundary condition $\phi(x, 1) = g(x)$. Therefore, to

19

update (a, ϕ) we must solve the system

$$
\begin{cases}
\mathbf{K}^{-1}a - \left(\int_\Omega f_i(x)\rho^{k+1}(x,t)dx\right)_{i=1}^r + \frac{a-a^k}{\tau_a} = 0 \\[2mm]
\rho_t^{k+1} + \nabla \cdot m^{k+1} - \frac{\phi_{tt}-\phi_{tt}^k}{\tau_{\phi_t}} - \frac{\Delta\phi - \Delta\phi^k}{\tau_{\nabla\phi}} = 0 \\[2mm]
\rho^{k+1}(x,0) - \rho_0(x) - \frac{\phi_t(x,0)-\phi_t^k(x,0)}{\tau_{\phi_t}} + \frac{\phi(x,0)-\phi^k(x,0)}{\tau_{\phi(0)}} = 0 \\[2mm]
\phi(x,1) = g(x) \\[2mm]
\left(-m^{k+1} + \frac{\nabla\phi - \nabla\phi^k}{\tau_{\nabla\phi}}\right)\cdot\nu = 0
\end{cases}
$$

Note that the equations for a and ϕ are decoupled. Furthermore, we obtain explicit updates for a:

$$
a^{k+1} = (\tau_a\mathbf{K}^{-1} + \mathbf{I})^{-1}\left(a^k + \tau_a\left(\int_\Omega f_i(x)\rho^{k+1}(x,t)dx\right)_{i=1}^r\right) \tag{2.3.4}
$$

Finally, to update ϕ we must solve the space-time elliptic equation

$$
\begin{cases}
\frac{\phi_{tt}}{\tau_{\phi_t}} + \frac{\Delta\phi}{\tau_{\nabla\phi}} = \rho_t^{k+1} + \nabla\cdot m^{k+1} + \frac{\phi_{tt}^k}{\tau_{\phi_t}} + \frac{\Delta\phi^k}{\tau_{\nabla\phi}} & \text{in} \quad \Omega \times (0,1) \\[2mm]
\frac{\phi_t(x,0)}{\tau_{\phi_t}} - \frac{\phi(x,0)}{\tau_{\phi(0)}} = \rho^{k+1}(x,0) - \rho_0(x) + \frac{\phi_t^k(x,0)}{\tau_{\phi_t}} - \frac{\phi^k(x,0)}{\tau_{\phi(0)}} & \text{in} \quad \Omega \\[2mm]
\phi(x,1) = g(x) & \text{in} \quad \Omega \\[2mm]
\frac{\partial\phi(x,t)}{\partial\nu} = \frac{\partial\phi^k(x,t)}{\partial\nu} + \tau_{\nabla\phi}m^{k+1}\cdot\nu & \text{in} \quad \partial\Omega \times (0,1)
\end{cases}
$$

Once discretized, this step can be efficiently performed by the Fast Fourier Transform (FFT).

2.3.3 Dimension reduction

Here, we illustrate the dimension reduction and computational efficiency obtained with our method. Assume that Ω is bounded, and K_r, S_r are approximations of K, S in the C^2 norm [NS18, Section 4]. Then we have that

$$
\left\|\int_\Omega K(\cdot,y)\rho(y)dy - \int_\Omega K_r(\cdot,y)\rho(y)dy\right\|_{C^2} \leq \|K - K_r\|_{C^2},
$$

$$
\left\|\int_\Omega S(\cdot,y)\rho(y)dy - \int_\Omega S_r(\cdot,y)\rho(y)dy\right\|_{C^2} \leq \|S - S_r\|_{C^2},
$$

for all $\rho \in \mathcal{P}(\Omega)$. Therefore, if we approximate f, g by f_r, g_r in the C^2 norm, we obtain C^2 approximations of the terms

$$f\left(x, \int_\Omega K(x,y)\rho(y,t)dy\right), \quad g\left(x, \int_\Omega S(x,y)\rho(y,1)dy\right)$$

that are uniform in ρ.

In the periodic case, from the stability theory of (2.1.1) [LL07, Car13a], we have that solutions of (2.1.1) corresponding to f_r, g_r, K_r, S_r are precompact in $C(\Omega \times [0,1]) \times C([0,1], \mathcal{P}(\Omega))$, and all accumulation points are solutions corresponding to f, g, K, S. Additionally, if the operators

$$\rho \mapsto f\left(x, \int_\Omega K(x,y)\rho(y)dy\right), \quad \rho \mapsto g\left(x, \int_\Omega S(x,y)\rho(y)dy\right) \tag{2.3.5}$$

are monotone, (2.1.1) admits a unique solution, (ϕ, ρ), and

$$\lim_{r \to \infty} \|\phi_r - \phi\|_{L^\infty} = 0, \quad \lim_{r \to \infty} \sup_{t \in [0,1]} W_1(\rho_r(\cdot, t), \rho(\cdot, t)) = 0,$$

if $\lim_{r \to \infty} \|\xi - \xi_r\|_{C^2} = 0$, $\xi \in \{f, g, K, S\}$, where W_1 is the 1-Wasserstein or Monge-Kantorovich distance in $\mathcal{P}(\Omega)$.

Thus, if we discretize (2.1.1) the *approximation error of the interaction functionals* introduced by replacing f, g, K, S by f_r, g_r, K_r, S_r will be independent of the discretization. Therefore, once we fix r, we can solve the r-problem as accurately as we wish without extra cost for approximating the interactions on fine grids. Additionally, as we show below, for fixed r, the computational cost is on par with those of existing algorithms for local couplings. Of course, the smaller r the better, and the size of r depends on how well $\{f_i\}$ approximate f, g, K, S.

Remark 5. *To the best of our knowledge, the stability of (2.1.1) with respect to the data in the non-periodic is not explicitly discussed in the literature. Nevertheless, results in [CC18, CCC19, CCC21] indicate that such stability should be valid. In this case, (2.3.5) guarantees the uniqueness of ϕ only [CC18, Theorem 4.1].*

We now compare the computational complexity of our method versus direct applications of primal-dual optimization algorithms to solve (2.1.1) on the example of (2.2.1). The starting point for these methods is to write (2.2.1) as a convex optimization problem introduced in [LL07]. More precisely, when K is symmetric, one has that (2.2.1) is equivalent to

$$
\inf_{\substack{\phi(x,1)\leq g}} \sup_{\rho\geq 0,m} \left\{ -\int_\Omega \phi(x,0)\rho_0(x)dx - \int_\Omega \int_0^1 (\rho\phi_t + m\cdot\nabla\phi)\,dxdt \right.
$$
$$
\left. -\int_0^1 \left\{ \int_\Omega \rho L\left(x,\frac{m}{\rho}\right)dx + \mathcal{F}(\rho(\cdot,t)) \right\} dt \right\} \tag{2.3.6}
$$
$$
= \inf_{\substack{\phi(x,1)\leq g \\ \alpha}} \sup_{\rho\geq 0,m} \mathcal{L}_1(\phi,\rho,m)
$$

where

$$
\mathcal{F}(\rho) = \frac{1}{2}\int_{\Omega^2} K(x,y)\rho(x)\rho(y)dxdy, \quad \rho\in\mathcal{P}(\Omega). \tag{2.3.7}
$$

One can also work with the convex dual $\mathcal{F}^*$ of $\mathcal{F}$ by introducing a dual variable α:

$$
\inf_{\substack{\phi(x,1)\leq g \\ \alpha}} \sup_{\rho\geq 0,m} \left\{ \int_0^1 \mathcal{F}^*(\alpha(\cdot,t))dt - \int_\Omega \phi(x,0)\rho_0(x)dx - \int_\Omega \int_0^1 (\rho\phi_t + m\cdot\nabla\phi)\,dxdt \right.
$$
$$
\left. -\int_\Omega\int_0^1 \rho\left(L\left(x,\frac{m}{\rho}\right)+\alpha\right)dxdt \right\} \tag{2.3.8}
$$
$$
= \inf_{\substack{\phi(x,1)\leq g \\ \alpha}} \sup_{\rho\geq 0,m} \mathcal{L}_2(\phi,\alpha,\rho,m),
$$

where $\mathcal{F}^*(\alpha) = \sup_\rho \int_\Omega \alpha(x)\rho(x)dx - \mathcal{F}(\rho)$. Therefore, there are two options for solving (2.2.1): (i) work directly with $\mathcal{F}$ and solve (2.3.6) or its variants [AKS18, AKK19], (ii) work with the dual $\mathcal{F}^*$ and solve (2.3.8) or its variants [BC15a, BCS17]. We illustrate that direct applications of both approaches to nonlocal problems lead to computationally expensive updates.

For concreteness, we estimate the computational complexity of the PDHG algorithm proposed here, with and without applying the coefficients method. The analysis of other primal-dual algorithms is analogous. First, we discuss the option of working directly with $\mathcal{F}$

and solving (2.3.6). In this case, the proximal update for (ρ, m) would be

$$
\sup_{\rho \geq 0, m} \left\{ - \int_\Omega \bar{\phi}^k(x, 0) \rho_0(x) dx - \int_\Omega \int_0^1 \left(\rho \bar{\phi}_t^k + m \cdot \nabla \bar{\phi}^k \right) dx dt \right.
$$
$$
- \int_0^1 \left\{ \int_\Omega \rho L \left(x, \frac{m}{\rho} \right) dx + \mathcal{F}(\rho(\cdot, t)) \right\} dt \right\}
$$
$$
- \frac{1}{2\tau_\rho} \| \rho - \rho^k \|_{L_{x,t}^2}^2 - \frac{1}{2\tau_m} \| m - m^k \|_{L_{x,t}^2}^2
$$

Therefore, we must solve the following system

$$
\begin{cases}
L \left(x, \frac{m}{\rho} \right) - \nabla_v L \left(x, \frac{m}{\rho} \right) \cdot \frac{m}{\rho} + \bar{\phi}_t^k + \frac{\rho - \rho^k}{\tau_\rho} + \delta_\rho \mathcal{F}(\rho) = 0 \\
\nabla_v L \left(x, \frac{m}{\rho} \right) + \frac{m - m^k}{\tau_m} = \nabla \bar{\phi}^k
\end{cases}
\tag{2.3.9}
$$

For local interactions, one has that $\mathcal{F}(\rho) = \int_\Omega F(\rho(x)) dx$ for some F, and (2.3.9) becomes

$$
\begin{cases}
L \left(x, \frac{m}{\rho} \right) - \nabla_v L \left(x, \frac{m}{\rho} \right) \cdot \frac{m}{\rho} + \frac{\rho - \rho^k}{\tau_\rho} + F'(\rho) = 0 \\
\nabla_v L \left(x, \frac{m}{\rho} \right) + \frac{m - m^k}{\tau_m} = \nabla \bar{\phi}^k,
\end{cases}
$$

which is a decoupled system of one-dimensional equations that can be solved efficiently at each node. Therefore, the computational complexity of solving this system for local problems is linear in the number of grid-points. However, for nonlocal interactions such as in (2.3.7) we have that $\delta_\rho \mathcal{F} = \int_\Omega K(x, y) \rho(y) dy$, and (2.3.9) is now a fully coupled (in space) system of nonlinear equations. Additionally, the complexity of the system grows with the mesh-size. One could approximate the term by $\delta_\rho \mathcal{F}(\rho)$ by $\delta_\rho \mathcal{F}(\rho^k)$ and decouple the system. Nevertheless, this would require a matrix multiplication that yields a superlinear computational cost. Moreover, the proximal step could not be parallelized.

On the other hand, our method yields fully parallel proximal updates for (ρ, m) (2.3.3) at the expense of solving an $r \times r$ system of equations to update the coefficients (a_i). To assemble the system for (a_i), we need to evaluate terms $\int_\Omega f_i(x) \rho^{k+1}(x, t) dx$ that yields a linear cost in the number of grid-points. Therefore, once r is fixed, we obtain an overall linear cost for updating (ρ, m) and (a_i) which is the case for local interactions.

Next, we discuss the option of working with $\mathcal{F}^*$ and solving (2.3.8). In this case, the proximal update for α would be

$$\inf_\alpha \int_0^1 \mathcal{F}^*(\alpha(\cdot,t))dt - \int_\Omega \int_0^1 \rho^{k+1}\alpha \, dx \, dt + \frac{1}{2\tau_\alpha}\|\alpha - \alpha^k\|_{L^2_{x,t}}^2$$

Therefore, we must solve the following system

$$\delta_\alpha \mathcal{F}^*(\alpha)(x,t) - \rho^{k+1}(x,t) + \frac{\alpha(x,t) - \alpha^k(x,t)}{\tau_\alpha} = 0 \qquad (2.3.10)$$

For local interactions, $\mathcal{F}(\rho) = \int_\Omega F(\rho(x))dx$, we can calculate $\mathcal{F}^*(\alpha)$ on the continuum level by an explicit formula

$$\mathcal{F}^*(\alpha) = \int_\Omega F^*(\alpha(x))dx,$$

where F^* is the convex dual of F. Therefore, $\delta_\alpha \mathcal{F}(\alpha)(x) = (F^*)'(\alpha(x))$, and (2.3.10) becomes

$$(F^*)'(\alpha(x,t)) - \rho^{k+1}(x,t) + \frac{\alpha(x,t) - \alpha^k(x,t)}{\tau_\alpha} = 0$$

As before, we obtain one-dimensional decoupled equations that can be solved in parallel at grid-points.

In the nonlocal case though, the first issue is that we cannot calculate $\mathcal{F}^*$ analytically on the continuum level unless K is special. However, one can calculate $\mathcal{F}^*$ on the discrete level. Assume that $\{x_i\}_{i=1}^N$ is some space-discretization. Then we have that

$$\mathcal{F}(\rho) = \frac{1}{2}\sum_{i,j} K(x_i, x_j)\rho_i \rho_j, \quad \mathcal{F}^*(\alpha) = \frac{1}{2}\sum_{i,j} Q_{ij}\alpha_i \alpha_j, \quad \delta_\alpha \mathcal{F}^*(\alpha)_i = \sum_j Q_{ij}\alpha_j$$

where $\rho_i = \rho(x_i)$, $\alpha_i = \alpha(x_i)$, and $Q = (Q_{ij}) = (K(x_i, x_j))^{-1}$. Therefore, (2.3.10) becomes an $N \times N$ system of linear equations

$$\sum_j Q_{ij}\alpha_j(t) - \rho_i^{k+1}(t) + \frac{\alpha_i(t) - \alpha_i^k(t)}{\tau_\alpha} = 0, \quad i \in \{1, 2, \cdots, N\}. \qquad (2.3.11)$$

As before, we obtain a coupled system in the nonlocal case. The solution of this system yields a polynomial computational complexity unless $(K(x_i, x_j))$ is special. For instance, if

$(K(x_i, x_j))$ is diagonalizable in a Fourier basis the computational cost is of order $N \log N$ via FFT.

In our method, on the other hand, we replace dual variables $(\alpha_i(t))_{i=1}^N$ by coefficients $(a_i(t))_{i=1}^r$, and (2.3.11) is replaced by an $r \times r$ system (2.3.4). Therefore, we have to store much less variables and, as mentioned before, obtain a linear computational cost. Additionally, we can calculate the $r \times r$ matrix $(\tau_a \mathbf{K}^{-1} + \mathbf{I})^{-1}$ prior to optimization and use it afterward. Moreover, since the size of this matrix is independent of the mesh-size, we do not have to deal with conditioning issues for every mesh-size separately: we can do it once and for all before optimization.

Finally, as we will see in Section 2.4, a smart choice of basis functions $\{f_i\}$ yields $\mathbf{K} = \mathbf{I}$. Therefore, the updates for $(a_i(t))_{i=1}^r$ are trivial and there is no need to solve linear systems at all!

2.4 Modeling interactions with kernels

Here, we discuss modeling aspects of nonlocal MFG systems. In particular, we show how to build kernels to enforce suitable behavior of agents. For that, we draw inspiration from kernel methods in machine learning [MRT18, Chapter 6].

As mentioned before, (2.2.1) is well posed when $\rho \mapsto \int_\Omega K(x,y)\rho(y)dy$ is monotone. This condition means that agents repel one another and try to minimize the cost

$$\phi(x,t) = \inf_{z(t)=x} \int_t^1 \left\{ L(z(s), \dot{z}(s)) + \int_\Omega K(z(s), y)\rho(y,t)dy \right\} ds + g(z(T))$$

Therefore, $K(x,y)$ is a *similarity measure* between positions x and y that agents try to minimize. Kernel methods in ML study exactly this type of K for data separation. Different choices of K lead to different separations.

The simplest example of K is the inner product, $K(x,y) = x \cdot y$, which is amenable to rigorous mathematical analysis. Natural extensions of the inner product are *positive definite*

25

symmetric (PDS) kernels.

Definition 1 ([MRT18]). $K : (x, y) \mapsto K(x, y)$ *is a PDS kernel if* $(K(x^i, x^j))_{i,j=1}^m$ *is symmetric positive semidefinite matrix for all* $\{x^i\}_{i=1}^m \subset \mathbb{R}^d$.

Assume K is a continuous PDS kernel. Thus, its symmetric, and for arbitrary $\rho_k = \frac{1}{N} \sum_i w_k^i \delta_{x^i}$, $k = 1, 2$ we have that

$$\int_{\Omega^2} K(x, y)(\rho_2(x) - \rho_1(x))(\rho_2(y) - \rho_1(y))dxdy$$
$$= \sum_{i,j} K(x^i, x^j)(w_2^i - w_1^i)(w_2^j - w_1^j) \geq 0,$$

and hence $\rho \mapsto \int_\Omega K(x, y)\rho(y)dy$ is monotone.

The discussion above shows that *PDS kernels suit MFG models extremely well.* Thus, we will build various MFG models by choosing suitable PDS kernels. In this context, as we shall see below, the basis $\{f_i\}$ corresponds to feature vectors.

The remarkable fact about PDS kernels is that all of them are inner products. More precisely, K is PDS iff there exists a Hilbert space $\mathcal{H}$ and a mapping $x \mapsto f(x) \in \mathcal{H}$ such that

$$K(x, y) = \langle f(x), f(y) \rangle_{\mathcal{H}}, \quad \forall x, y$$

In other words, one can associate points $\{x\}$ in the input space with vectors $\{f(x)\}$ in a Hilbert space so that $K(x, y)$ is precisely the inner product of $f(x)$ and $f(y)$ in $\mathcal{H}$ [MRT18, Theorem 6.8]. The vector $f(x)$ is called the *feature vector* of x. If $\mathcal{H}$ is separable we can write $f(x) = (f_1(x), f_2(x), \cdots, f_n(x), \cdots)$ in some basis of $\mathcal{H}$ and $f_1(x), f_2(x), \cdots, f_n(x), \cdots$ will be the *features* of x. $\mathcal{H}$ is called a *reproducing kernel Hilbert space (RKHS)*. For $K(x, y) = x \cdot y = \sum x_i y_i$ the features are simply the coordinates.

The RKHS theory blends very well with our coefficients method by providing the basis we need in the form of feature vectors. Indeed, assume that K is a PDS kernel and $\mathcal{H}$ is its

RKHS with a basis $\{e_i\}$. Then, we obtain that

$$K(x,y) = \langle f(x), f(y) \rangle_{\mathcal{H}} = \Big\langle \sum_i f_i(x)e_i, \sum_i f_i(y)e_i \Big\rangle_{\mathcal{H}}$$

$$= \sum_{i,j} \langle e_i, e_j \rangle_{\mathcal{H}} f_i(x) f_j(y) = \sum_{i,j} k_{ij} f_i(x) f_j(y),$$

which is the representation we need. In this case, $\mathbf{K} = (\langle e_i, e_j \rangle_{\mathcal{H}})$ is the Gram matrix associated to the basis $\{e_i\}$ in $\mathcal{H}$. Below, we present several common choices for K and provide the basis $\{f_i\}$ and the matrix $\mathbf{K}$.

2.4.1 Maximal spread

Assume that we want to enforce a maximal spread of the population by penalizing individual agents for being close to the average position of the population. This means that an individual agent faces an optimal control problem

$$\inf_{z(t)=x} \int_0^1 \ell(z(s), \dot{z}(s)) - \sum_{i=1}^d \lambda_i \left| z_i(s) - \int_\Omega y_i \rho(y, s) dy \right|^2 ds + g(z(1))$$

$$= \inf_{z(t)=x} \int_0^1 \left[\ell(z(s), \dot{z}(s)) - \sum_{i=1}^d \lambda_i |z_i(s)|^2 + 2 \sum_{i=1}^d \lambda_i \left\{ \int_\Omega z_i(s) \cdot y_i \rho(y, s) dy \right\} \right.$$

$$\left. - \sum_{i=1}^d \lambda_i \left| \int_\Omega y_i \rho(y, s) dy \right|^2 \right] ds + g(z(1))$$

Above, $\lambda_1, \lambda_2, \cdots, \lambda_d \geq 0$ signify how much we enforce spreading in each coordinate direction. Additionally, $\ell(x, u)$ is some intrinsic running cost.

Since the term $-\sum_{i=1}^d \lambda_i \left| \int_{\mathbb{R}^d} y_i \rho(y, s) dy \right|^2$ does not depend on the trajectory z, the problem above is equivalent to

$$\inf_{z(t)=x} \int_0^1 \ell(z(s), \dot{z}(s)) - \sum_{i=1}^d \lambda_i |z_i(s)|^2 + \int_\Omega \left\{ 2 \sum_{i=1}^d \lambda_i z_i(s) \cdot y_i \right\} \rho(y, s) dy dt$$

$$+ g(z(1))$$

Therefore, we obtain an MFG system (2.2.1) where

$$L(x,v) = \ell(x,v) - \sum_{i=1}^{d} \lambda_i |x_i|^2$$

$$K(x,y) = 2 \sum_{i=1}^{d} \lambda_i x_i y_i$$

$$H(x,p) = \sup_{v} \{-p \cdot v - L(x,v)\}$$

The key point is that $\mathbb{R}^d$ is an RKHS for this K, and

$$K(x,y) = \sum_{i=1}^{d} f_i(x) f_i(y)$$

where $f_i(x) = \sqrt{2\lambda_i} x_i$, $1 \le i \le d$. Thus, we use these $\{f_i\}$ as the basis in our method. An excellent feature of this choice is that we obtain $\mathbf{K} = \mathbf{K}^{-1} = \mathbf{I}$ which yields a trivial update rule (2.3.4) for a that reads

$$a_i^{k+1}(t) = \frac{\tau_a \int_\Omega f_i(x) \rho^{k+1}(x,t) dx + a_i^k(t)}{\tau_a + 1}$$

2.4.2 Gaussian repulsion

Another common choice for PDS kernels are Gaussians

$$K(x,y) = \mu \prod_{i=1}^{d} \exp\left(-\frac{|x_i - y_i|^2}{2\sigma_i^2}\right),$$

for some $\mu, \sigma_1, \sigma_2, \cdots, \sigma_d > 0$. The parameter σ_i signifies how repulsive are the agents in i-th coordinate direction.

As before, we will try to find a suitable expansion of K. Using the power series expansion of e^x one can show that

$$K(x,y) = \sum_{\alpha_1,\alpha_2,\cdots,\alpha_d \ge 0} \left\{ \sqrt{\mu} e^{-\sum_{i=1}^{d} \frac{|x_i|^2}{2\sigma_i^2}} \prod_{i=1}^{d} \frac{x_i^{\alpha_i}}{\sigma_i^{\alpha_i} \sqrt{\alpha_i!}} \right\} \cdot \left\{ \sqrt{\mu} e^{-\sum_{i=1}^{d} \frac{|y_i|^2}{2\sigma_i^2}} \prod_{i=1}^{d} \frac{y_i^{\alpha_i}}{\sigma_i^{\alpha_i} \sqrt{\alpha_i!}} \right\}$$

$$= \sum_{\alpha_1,\alpha_2,\cdots,\alpha_d \ge 0} f_{\alpha_1,\alpha_2,\cdots,\alpha_d}(x) f_{\alpha_1,\alpha_2,\cdots,\alpha_d}(y),$$

where

$$f_{\alpha_1,\alpha_2,\cdots,\alpha_d}(x) = \sqrt{\mu}e^{-\sum_{i=1}^{d}\frac{|x_i|^2}{2\sigma_i^2}}\prod_{i=1}^{d}\frac{x_i^{\alpha_i}}{\sigma_i^{\alpha_i}\sqrt{\alpha_i!}}, \quad \alpha_1,\alpha_2,\cdots,\alpha_d \geq 0.$$

Hence, we choose $\{f_{\alpha_1,\alpha_2,\cdots,\alpha_d}\}$ as the basis for our coefficients method and choose n to approximate K with functions of order $\sum_{i=1}^{d}\alpha_i \leq n$. As before, an excellent feature of this basis is that $\mathbf{K} = \mathbf{K}^{-1} = \mathbf{I}$.

Interactions in sub-regions

Methods described above also provide flexible framework to model interactions within sub-regions. Assume that Ω_1, Ω_2 are complementary in Ω. Furthermore, assume that agents in Ω_i interact only with those in Ω_i for $i = 1, 2$. There is a straightforward way of extending the framework above to this setting.

Suppose that kernels modeling the interaction in Ω_1, Ω_2 are K_1, K_2, respectively. Additionally, assume that the basis for K_1 is $\{f_i^1\}$, and the one for K_2 is $\{f_i^2\}$ that can be of a different size. Thus, we want to construct K such that

$$K(x,y) = \begin{cases} K_i(x,y), & (x,y) \in \Omega_i \times \Omega_i \\ 0, & \text{otherwise} \end{cases}$$

Furthermore, we want to construct a basis for K out of $\{f_i^1\}$ and $\{f_i^2\}$. These can be done as follows:

$$\begin{aligned} K(x,y) =& K_1(x,y)\cdot\chi_{\Omega_1}(x)\chi_{\Omega_1}(y) + K_2(x,y)\cdot\chi_{\Omega_2}(x)\chi_{\Omega_2}(y) = \\ =& \sum_{ij}k_{ij}^1 f_i^1(x)f_j^1(y)\chi_{\Omega_1}(x)\chi_{\Omega_1}(y) + \sum_{ij}k_{ij}^2 f_i^2(x)f_j^1(y)\chi_{\Omega_2}(x)\chi_{\Omega_2}(y) \\ =& \sum_{ij}k_{ij}^1 f_i^1(x)\chi_{\Omega_1}(x)f_j^1(y)\chi_{\Omega_1}(y) + \sum_{ij}k_{ij}^2 f_i^2(x)\chi_{\Omega_2}(x)f_j^2(y)\chi_{\Omega_2}(y), \end{aligned}$$

where χ_A is the characteristic function of A. Therefore, the basis for K can be obtained from the ones of K_1, K_2 by simply restricting them into subdomains and combining:

$$\{f_i^1(x)\chi_{\Omega_1}(x),\ f_i^2(x)\chi_{\Omega_2}(x)\}$$

Furthermore, we have that

$$\mathbf{K} = \begin{pmatrix} \mathbf{K}_1 & \mathbf{0} \\ \mathbf{0} & \mathbf{K}_2 \end{pmatrix}, \quad \mathbf{K}^{-1} = \begin{pmatrix} \mathbf{K}_1^{-1} & \mathbf{0} \\ \mathbf{0} & \mathbf{K}_2^{-1} \end{pmatrix},$$

where $\mathbf{K}_i = (k_{ij}^i)$, $i = 1, 2$. Therefore, low complexity matrices for K_1, K_2 yield a low complexity matrix for K.

In case we have multiple regions $\Omega_1, \Omega_2, \cdots, \Omega_N$ with kernels $K_1, K_2, \cdots, K_N$ and bases $\{f_i^1\}, \{f_i^2\}, \cdots \{f_i^N\}$ we obtain a basis

$$\big\{ f_i^1(x)\chi_{\Omega_1}(x), \; f_i^2(x)\chi_{\Omega_2}(x), \; \cdots, f_i^N(x)\chi_{\Omega_N}(x) \big\},$$

and

$$\mathbf{K} = \begin{pmatrix} \mathbf{K}_1 & \mathbf{0} & \cdots & \mathbf{0} \\ \mathbf{0} & \mathbf{K}_2 & \cdots & \mathbf{0} \\ \vdots & \vdots & \vdots & \vdots \\ \mathbf{0} & \cdots & \mathbf{K}_{N-1} & \mathbf{0} \\ \mathbf{0} & \cdots & \mathbf{0} & \mathbf{K}_N \end{pmatrix}, \quad \mathbf{K}^{-1} = \begin{pmatrix} \mathbf{K}_1^{-1} & \mathbf{0} & \cdots & \mathbf{0} \\ \mathbf{0} & \mathbf{K}_2^{-1} & \cdots & \mathbf{0} \\ \vdots & \vdots & \vdots & \vdots \\ \mathbf{0} & \cdots & \mathbf{K}_{N-1}^{-1} & \mathbf{0} \\ \mathbf{0} & \cdots & \mathbf{0} & \mathbf{K}_N^{-1} \end{pmatrix},$$

where $\mathbf{K}_i$ is the matrix corresponding to K_i.

Formally, using restrictions violates the smoothness assumption on kernels and bases. Thus, we can use smooth cutoff functions instead of characteristic ones. In practice though, we obtain solid results with the latter choice.

2.4.3   Interactions given by differential operators

Finally, we demonstrate how our methods work for interactions given by differential operators. In a seminal paper on numerical methods for MFG [AC10], the authors consider an interaction term

$$V[\rho] = \mu(I - \Delta)^{-2}\rho,$$

where $\mu > 0$, Δ is the Laplacian operator, and the problem is set on a flat torus $\mathbb{T}^d$. We have that

$$V[\rho] = \int_{\mathbb{T}^d} \Gamma(x - y)\rho(y)dy,$$

where Γ is the fundamental solution; that is,

$$(I - \Delta)^2 \Gamma = \mu\delta_0. \tag{2.4.1}$$

Thus, we have that $K(x, y) = \Gamma(x - y)$. As pointed out in [NS18], for convolutions on a torus, the appropriate basis is the trigonometric one. Thus, we need to expand Γ into Fourier series with respect to functions $\{\cos(2\pi\alpha \cdot x), \sin(2\pi\alpha \cdot x)\}$ where $\alpha = (\alpha_1, \alpha_2, \cdots, \alpha_d)$. Furthermore, by the symmetry we have that $\Gamma(x) = \Gamma(-x)$. Therefore, the expansion of Γ contains only even functions; that is,

$$\Gamma(x) = \sum_{\alpha \geq 0} \gamma_\alpha \cos(2\pi\alpha \cdot x)$$

Next, solving (2.4.1) in a Fourier space yields

$$\gamma_0 = \mu, \quad \gamma_\alpha = \frac{2\mu}{1 + 8\pi^2|\alpha|^2 + 16\pi^4|\alpha|^4}, \quad \alpha > 0,$$

where $|\alpha|^2 = \sum_{i=1}^d \alpha_i^2$. Furthermore, we have that

$$
\begin{aligned}
K(x, y) =& \Gamma(x - y) = \sum_{\alpha \geq 0} \gamma_\alpha \cos(2\pi\alpha \cdot (x - y)) \\
=& \sum_{\alpha \geq 0} \left(\gamma_\alpha \cos(2\pi\alpha \cdot x) \cos(2\pi\alpha \cdot y) + \gamma_\alpha \sin(2\pi\alpha \cdot x) \sin(2\pi\alpha \cdot y) \right) \\
=& \sum_{\alpha \geq 0} f_\alpha^{\cos}(x) f_\alpha^{\cos}(y) + \sum_{\alpha > 0} f_\alpha^{\sin}(x) f_\alpha^{\sin}(y),
\end{aligned}
$$

where

$$f_\alpha^{\cos}(x) = \sqrt{\gamma_\alpha} \cos(2\pi\alpha \cdot x), \quad f_\alpha^{\sin}(x) = \sqrt{\gamma_\alpha} \sin(2\pi\alpha \cdot x), \quad \alpha \geq 0.$$

Therefore, we choose $\{f_\alpha^{\cos}, f_\alpha^{\sin}\}$ as the basis for our coefficients method and choose n to approximate K with functions of order $\sum_{i=1}^d \alpha_i \leq n$. Again, this choice renders $\mathbf{K} = \mathbf{K}^{-1} = \mathbf{I}$.

31

2.5 Potential applications to multi-agent trajectory planning problems

Here, we discuss potential applications of our methods to multi-agent trajectory planning problems. To provide a self contained discussion and for the convenience of readership unfamiliar with MFG, we start by a brief derivation of (2.1.1) and (2.2.1) that can be found in [LL07, Car13a]. Assume that we have a swarm of agents where agent $i \in \{1, 2, \cdots, N\}$ aims at minimizing a cost

$$\inf_{u_i} \int_t^1 L(z_i(s), u_i(s), s) + f_i(z_i(s), z_{-i}(s))ds + g_i(z_i(1), z_{-i}(1))$$

$$\text{s.t. } \dot{z}_i(s) = c(z_i(s), u_i(s)), \quad z_i(t) = x_i$$

(2.5.1)

Above, $z_{-i} = (z_j)_{j \neq i}$, and f, g model interactions between the agents. This problem leads to a system of N coupled HJBs that is extremely challenging to solve, especially in high-dimensions and for many agents.

The MFG framework provides a solution to this problem by assuming symmetric interactions and considering the continuum limit $N = \infty$. More precisely, if we suppose that

$$f_i(z_i, z_{-i}) = f\left(z_i, \frac{1}{N-1}\sum_{j \neq i}\delta_{z_j}\right), \quad g_i(z_i, z_{-i}) = g\left(z_i, \frac{1}{N-1}\sum_{j \neq i}\delta_{z_j}\right),$$

and formally pass to the limit when $N \to \infty$ we obtain a system where a generic agent solves an optimal control problem

$$\phi(x, t) = \inf_u \int_t^1 L(z(s), u(s), s) + f(z(s), \rho(\cdot, s))ds + g(z(1), \rho(\cdot, 1))$$

$$\text{s.t. } \dot{z}(s) = c(z(s), u(s)), \quad z(t) = x,$$

where $\rho(\cdot, s)$ is the distribution of population at time s. We have that ϕ solves the HJB equation

$$\begin{cases} -\phi_t + \sup_u \{-\nabla\phi(x, t) \cdot c(x, u) - L(x, u, t)\} = f(x, \rho(x, t)) \\ \phi(x, 1) = g(x, \rho(x, 1)), \end{cases}$$

and the optimal control, u^*, is given by the Pontryagin Maximum Principle:

$$u^*(x,t) \in \operatorname{argmax}_u \{-\nabla \phi(x,t) \cdot c(x,u) - L(x,u,t)\}$$

Furthermore, ρ satisfies the continuity equation

$$\begin{cases} \rho_t(x,t) + \nabla \cdot (\rho(x,t)c(x,u^*(x,t))) = 0 \\ \rho(x,0) = \rho_0(x), \end{cases}$$

where ρ_0 is the initial distribution of the agents. Collecting all equations together we obtain the MFG system

$$\begin{cases} -\phi_t + \sup_u \{-\nabla \phi \cdot c(x,u) - L(x,u,t)\} = f(x,\rho(x,t)) \\ \rho_t(x,t) + \nabla \cdot (\rho(x,t)c(x,u^*(x,t))) = 0 \\ u^*(x,t) \in \operatorname{argmax}_u \{-\nabla \phi(x,t) \cdot c(x,u) - L(x,u)\} \\ \rho(x,0) = \rho_0(x), \ \phi(x,1) = g(x,\rho(x,1)) \end{cases} \qquad (2.5.2)$$

Remark 6. *Equations* (2.1.1), (2.2.1) *correspond to the case* $c(x,u) = u$, *and* $u \mapsto L(x,u)$ *convex, for which we have a rigorous mathematical analysis [LL07].*

The appealing feature of MFG systems is that instead of solving a highly coupled system of N HJBs in $d \times N$ dimensions we have to solve a single HJB coupled with a continuity equation in d dimensions. More importantly, the MFG optimal control, u^*, yields *near optimal* controls for the N agent problem (2.5.1).

Of course, the performance of the MFG control in (2.5.1) depends on N and gets better as N grows. Nevertheless, it still makes sense to apply MFG controls because they are faster to generate and provide appealing properties such as no-collision trajectories. For instance, if $c(x,u) = u$, and $L(x,u) = \frac{|u^2|}{2} + Q(x,t)$ for some smooth Q, one can show that trajectories corresponding to $u^*(x,t)$ do not intersect [Car13a, Lemma 4.13].

In the context above, our method may provide a flexible way of augmenting existing solution methods for single-agent trajectory planning problems to generate MFG optimal controls for multi-agent problems.

Indeed, Theorem 2.2.2 asserts that, under the settings of Section 2.2, we have that (2.5.2) is equivalent to the optimization problem

$$\inf_{a \in C([0,1];\mathbb{R}^r)} \frac{\langle \mathbf{K}^{-1}a, a \rangle}{2} - \int_{\Omega} \phi_a(x, 0) \rho_0(x) dx \tag{2.5.3}$$

where ϕ_a solves the HJB

$$\begin{cases} -\phi_t + \sup_u \{-\nabla \phi(x, t) \cdot c(x, u) - L(x, u, t)\} = \sum_{i=1}^r a_i(t) f_i(x) \\ \phi(x, 1) = g(x), \end{cases} \tag{2.5.4}$$

In Section 2.3, we showed how to apply a PDHG algorithm to solve (2.5.3). Here, we argue that virtually any HJB solver (single-agent trajectory-planner) can be augmented to solve (2.5.3).

We propose solving (2.5.3) by some type of gradient descent on $a = (a_i)$. For that, we fix an iterate $a^{current}$ and run any single-agent trajectory planning algorithm to solve (2.5.4) for $a = a^{current}$ and generate an optimal control $u^{current}$. Then we solve the forward continuity equation

$$\begin{cases} \rho_t(x, t) + \nabla \cdot (\rho(x, t) c(x, u^{current}(x, t))) = 0 \\ \rho(x, 0) = \rho_0(x), \end{cases}$$

and generate $\rho^{current}$. Finally, we update $a = (a_i)$ by a gradient descent step using (2.2.6):

$$a_i^{new}(t) = a_i^{current}(t) - h \sum_{j=1}^r k_{ij} a_j^{current}(t) + h \int_{\Omega} f_i(x) \rho^{current}(x, t) dx,$$

where $h > 0$ is the descent step-sizes.

Remark 7. *Several remarks are in order.*

1. *Explicit gradient descent steps and exact solutions $u^{current}$ can be replaced by implicit (proximal) steps and approximate solutions as in the PDHG here and [NS18].*

2. *The approach above works for both Eulerian and Lagrangian solvers. For latter, the terms $\int_{\Omega} f_i(x) \rho^{current}(x, t)$ are simply averages of f_i-s on the trajectories of particles [NS18].*

3. The number of coefficients, r, does not depend on the number of agents, and we always need to (approximately) solve one decoupled HJB at each iteration.

Finally, we observe that the methods discussed here also work the other way around; that is, optimal control solvers can be easily adapted to solve MFG problems.

2.6 Numerical experiments

Here, we present several numerical experiments in a two-dimensional case for kernels and bases discussed in Section 2.4.

2.6.1 The finite difference scheme and the discrete variational problem

We consider rectangular domains $\Omega \times [0, T] = [b_1, b_2]^2 \times [0, 1]$ and choose a regular space-time grid with $N_x = N_{x_1} \times N_{x_2} = 64 \times 64$ points in space and $N_t = 32$ points in time.

We employ the finite difference scheme introduced in [AKK19] (see also [AC10, AKS18]). Given N_{x_1}, N_{x_2}, N_t, we have $\Delta x_1 = \frac{b_2 - b_1}{N_{x_1}}$, $\Delta x_2 = \frac{b_2 - b_1}{N_{x_2}}$, $\Delta t = \frac{1}{N_t}$. For $x_1 = i\Delta x_1, x_2 =$

$j\Delta x_2, t_l = l\Delta t$, define

$$\rho_{i,j}^l = \rho(x_i, x_j, t_l) \quad 1 \le i \le N_{x_1}, 1 \le j \le N_{x_2}, 0 \le l \le N_t$$

$$m_{1,i,j}^l = (m_{x_1}(x_i, x_j, t_l))^+ \quad 1 \le i \le N_{x_1}, 1 \le j \le N_{x_2}, 1 \le l \le N_t$$

$$m_{2,i,j}^l = -(m_{x_1}(x_i, x_j, t_l))^- \quad 1 \le i \le N_{x_1}, 1 \le j \le N_{x_2}, 1 \le l \le N_t$$

$$m_{3,i,j}^l = (m_{x_2}(x_i, x_j, t_l))^+ \quad 1 \le i \le N_{x_1}, 1 \le j \le N_{x_2}, 1 \le l \le N_t$$

$$m_{4,i,j}^l = -(m_{x_2}(x_i, x_j, t_l))^- \quad 1 \le i \le N_{x_1}, 1 \le j \le N_{x_2}, 1 \le l \le N_t$$

$$\phi_{i,j}^l = \phi(x_i, x_j, t_l) \quad 1 \le i \le N_{x_1}, 1 \le j \le N_{x_2}, 1 \le l \le N_t$$

$$a_k^l = a_i(t_l) \quad 1 \le l \le N_t, 1 \le k \le r$$

$$f_{k,i,j} = f_k(x_i, x_j) \quad 1 \le i \le N_{x_1}, 1 \le j \le N_{x_2}, 1 \le k \le r$$

$$\rho_{i,j}^0 = \rho_0(x_i, x_j) \quad 1 \le i \le N_{x_1}, 1 \le j \le N_{x_2}$$

$$g_{i,j} = g(x_i, x_j) \quad 1 \le i \le N_{x_1}, 1 \le j \le N_{x_2}$$

where $u^+ := \max(u, 0)$ and $u^- = u^+ - u$.

We define the first order finite difference operators

$$(D_1 u)_{i,j} := \frac{u_{i+1,j} - u_{i,j}}{\Delta x_1}, \text{ and } (D_2 u)_{i,j} := \frac{u_{i,j+1} - u_{i,j}}{\Delta x_2}$$

$$[Du]_{i,j} := \left((D_1 u)_{i,j}, (D_1 u)_{i-1,j}, (D_2 u)_{i,j}, (D_2 u)_{i,j-1} \right)$$

$$\widehat{[Du]}_{i,j} = \left((D_1 u)_{i,j}^-, -(D_1 u)_{i-1,j}^+, (D_2 u)_{i,j}^-, -(D_2 u)_{i,j-1}^+ \right)$$

To satisfy the Neumann boundary condition, we set

$$(D_1 m_1)_{i-1,j}^l = \frac{m_{1,i,j}^l - 0}{\Delta x_1} \quad i = 1, \ 1 \le j \le N_{x_2}, 1 \le l \le N_t$$

$$(D_1 m_2)_{i,j}^l = \frac{0 - m_{2,i,j}^l}{\Delta x_1} \quad i = N_{x_1}, \ 1 \le j \le N_{x_2}, 1 \le l \le N_t$$

$$(D_2 m_3)_{i,j-1}^l = \frac{m_{3,i,j}^l - 0}{\Delta x_2} \quad 1 \le i \le N_{x_1}, \ j = 1, 1 \le l \le N_t$$

$$(D_2 m_4)_{i,j}^l = \frac{0 - m_{4,i,j}^l}{\Delta x_2} \quad 1 \le i \le N_{x_1}, j = N_{x_2}, 1 \le l \le N_t$$

The Fokker-Planck equation discretized with forward difference in time as follows:

$$\frac{1}{\Delta t} \left(\rho_{i,j}^{l+1} - \rho_{i,j}^l \right) + (D_1 m)_{1,i-1,j}^l + (D_1 m)_{1,i,j}^l + (D_2 m)_{3,i,j-1}^l + (D_2 m)_{4,i,j}^l = 0.$$

The HJB equation is discretized with backward difference in time as follows:

$$-\frac{1}{\Delta t}\left(\phi_j^l - \phi_j^{l-1}\right) + H\left(x_j, \widehat{[D\phi]}_{i,j}^l\right) = \sum_{k=1}^{r} a_{k,l} f_{k,i,j},$$

With above finite difference scheme, we are ready to define the objective function of our min-max problem $\mathcal{L}(\phi, a, \rho, m)$ in discrete form:

$$\mathcal{L}(\phi, a, \rho, m) = \frac{\Delta t}{2} \sum_{l=1}^{N_t} \sum_{k_1,k_2=1}^{r} a_{k_1}^l a_{k_2}^l q_{k_1 k_2} - \Delta x_1 \Delta x_2 \sum_{i,j=1}^{N_{x_1},N_{x_2}} \phi_{i,j}^l \rho_{i,j}^0$$
$$- \Delta x_1 \Delta x_2 \Delta t \sum_{i,j=1}^{N_{x_1},N_{x_2}} \sum_{l=1}^{N_t} \left\{ \left(\rho_{i,j}^l \frac{\left(\phi_j^{l+1} - \phi_j^l\right)}{\Delta t} + m_{i,j}^l \cdot \widehat{[D\phi]}_{i,j}^l \right) \right.$$
$$\left. + \rho_{i,j}^l \left(L(x, \frac{m_{i,j}^l}{\rho_{i,j}^l}) + \sum_{k=1}^{r} \left(a_k^l f_{k,i,j}\right) \right) \right\},$$

where $(q_{k_1 k_2}) = \mathbf{K}^{-1}$, $m_{i,j}^l = \left[m_{1,i,j}^l, m_{2,i,j}^l, m_{3,i,j}^l, m_{4,i,j}^l\right]^T$.

For discretized ρ, m, a, the updates are straightforward. For ϕ, we provide details here. For the following discretized system,

$$\left(\frac{1}{\tau_{\phi_t}}\Delta_t + \frac{1}{\tau_{\nabla\phi}}\Delta_x\right)\phi_{i,j}^l = \nabla_t \rho_{i,j}^{l,k+1} + \nabla_x \cdot m_{i,j}^{l,k+1} + \left(\frac{1}{\tau_{\phi_t}}\Delta_t + \frac{1}{\tau_{\nabla\phi}}\Delta_x\right)\phi_{i,j}^{l,k},$$

where the $\Delta_x, \Delta_t, \nabla_x, \nabla_t$ are finite difference Laplace and finite-difference operators in space and time, respectively. Next, we apply Discrete Fourier Transform (in space) to the system. Specifically, we use Discrete Cosine Transform, due to the Neumann type boundary condition. For each Fourier mode μ, we have the following:

$$\left(\frac{1}{\tau_{\phi_t}}\Delta_t + \frac{c(\mu)}{\tau_{\nabla\phi}}\right)\mathcal{F}(\phi)_\mu^l = \mathcal{F}(h)_\mu^l,$$

where $h_{i,j}^l$ represents the right hand side of the previous equation and $c(\mu) = \mathcal{F}(\Delta_x)_\mu$ is the Discrete Cosine transform of the finite difference Laplace operator. This is a tridiagonal system that can be solved easily. Note that at the $t = 0, T$, the equation can be modified accordingly. Finally, we apply an inverse cosine transform to get the $\phi_{i,j}^{l,k+1}$ at the $(k+1)$th iteration.

For the rest of this section, we present four sets of numerical results of nonlocal MFG models presented in section 2.4. For each example, we run the algorithm for $5,000$ iterations using MATLAB, which takes around 3 minutes.

2.6.2 Maximal spread

We consider a maximal spread model on from Section 2.4.1 in the domain $\Omega \times [0, T] = [0,1]^2 \times [0,1]$. We denote by $\rho_G(c_1, c_2, \sigma_G^2)$ the density of a homogeneous normal distribution centered at (c_1, c_2) with variance σ_G^2. We set the initial-terminal conditions for our MFG system to be

$$\rho_0 = \rho_G(0.5, 0.9, 0.04^2)$$
$$g(x_1, x_2) = 2 \exp\left(-10\left(x_1 - 0.5\right)^2 - (x_2 - 0.1)^2\right)\left((x_2 - 0.1)^2 - 1\right).$$

Furthermore, we set

$$L(x, v) = \frac{1}{2}\|v\|^2 + 10^3 \left(\max\left(|x_1 - 0.5|, |x_2 - 0.5|\right)\right)^8 - \sum_{i=1}^{2} \lambda_i |x_i|^2$$

We have computed the MFG solutions for four choices of parameters

$$(\lambda_1, \lambda_2) \in \{(0.1, 0.1), (0.1, 4), (4, 0.1), (4, 4)\}$$

The results are shown in Figure 2.1. We can see that, in accordance to theory, larger λ_i prompt larger spread in x_i directions. Additionally, we see the flexibility of our method for modeling interactions that are heterogeneous in different directions. We provide a 3 D view of the solutions in Figure2.2.

(a) $\lambda_1 = 0.1, \lambda_2 = 0.1$

(b) $\lambda_1 = 0.1, \lambda_2 = 4$

(c) $\lambda_1 = 4, \lambda_2 = 0.1$

(d) $\lambda_1 = 4, \lambda_2 = 4$
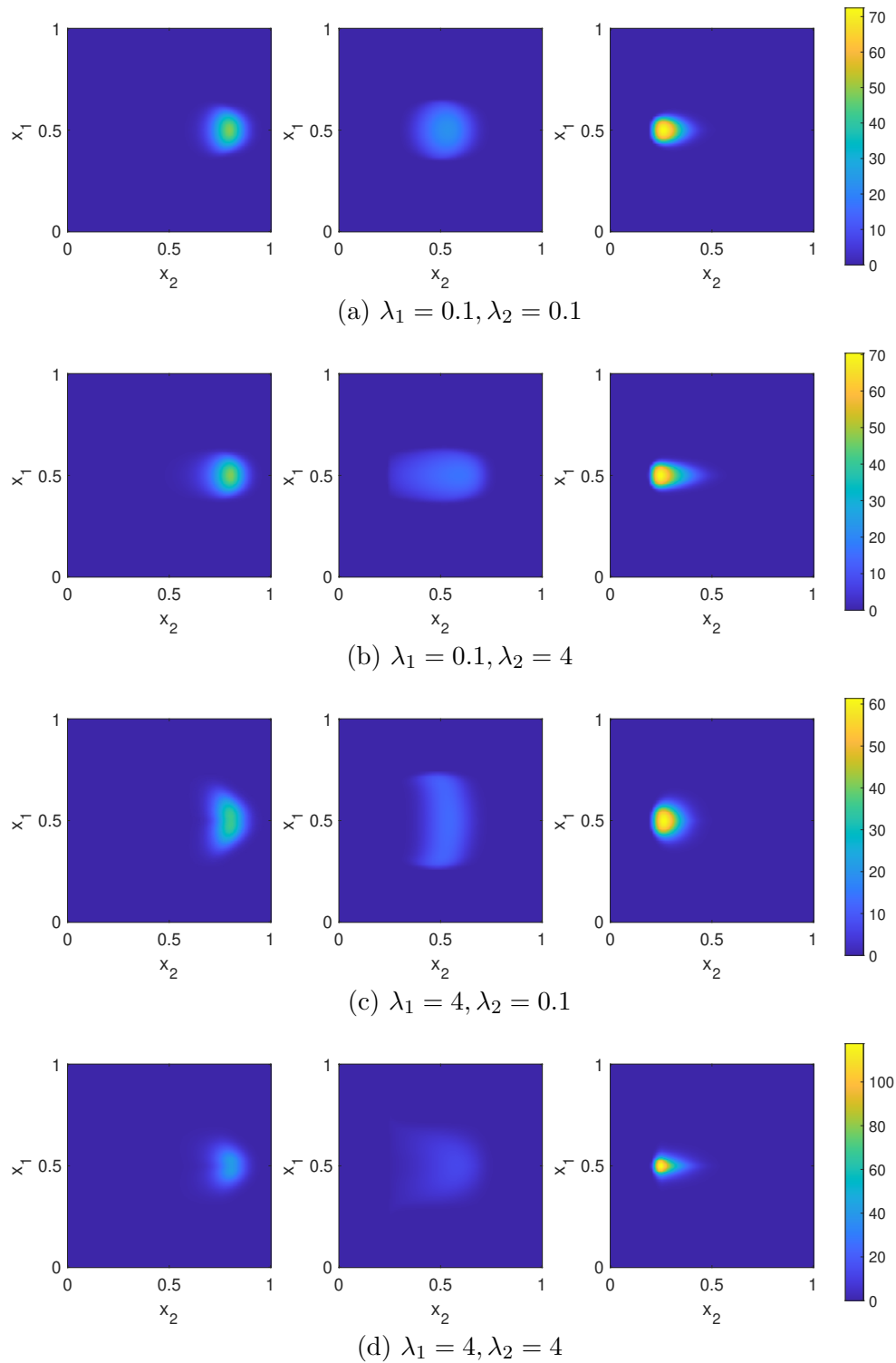
Figure 2.1: Example of maximal spread. MFG solution $\rho(x, t)$ at $t = 0.1, 0.5, 0.9$ with different choices of λ_i along x_1, x_2 directions.
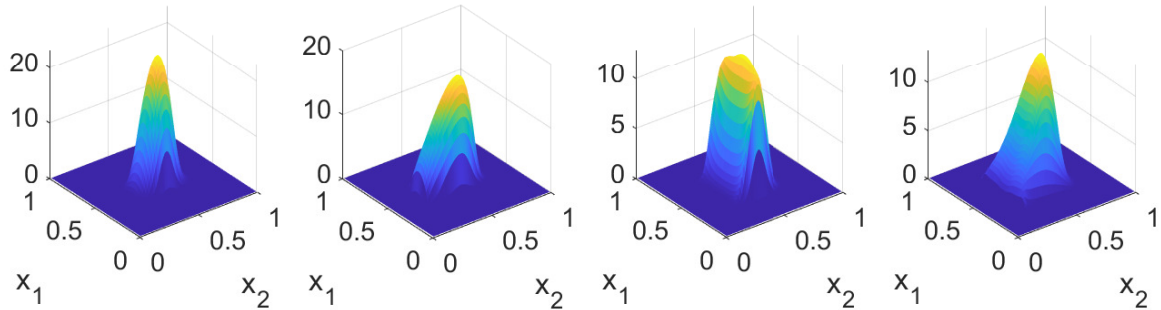
Figure 2.2: The 3D view of MFG solutions $\rho(x, 0.5)$ for different choice of λ_i. From left to right : case a,b,c, and d.

2.6.3 Gaussian repulsion with static obstacles

We consider a MFG model with Gaussian repulsion from Section 2.4.2 on the domain $\Omega \times [0, T] = [-1, 1]^2 \times [0, 1]$. We set the initial-terminal conditions for our MFG system to be

$$\rho_0 = \rho_G(0, -0.9, 0.04^2)$$

$$g(x_1, x_2) = 2 \exp\left(-5x_1^2 - 0.25(x_2 - 0.9)^2\right)\left((x_2 - 0.9)^2 - 1\right) + x_1^2$$

We fix this g for all examples with Gaussian repulsion. Furthermore, we set

$$L(x, v) = \frac{1}{2}\|v\|^2 + Q(x)$$

where $Q(x)$ takes on extremely high values on the four rectangular regions in Figure 2.3 and 0 elsewhere. Thus, Q models four static rectangular obstacles. Finally, we choose $n = 3$ to approximate the Gaussian kernel in later examples. Larger n will give a more accurate approximation of the Gaussian repulsion kernel. Here we choose $n = 3$ such that, when varying the kernel parameters σ_1, σ_2, μ, we can observe quantitatively different behavior in our numerical examples.

We have computed the MFG solutions for four choices of parameters

$$(\sigma_1, \sigma_2, \mu) \in \{(0.8, 0.8, 0.1), (0.2, 0.2, 5), (0.5, 0.2, 5), (0.2, 0.5, 5)\}$$

40

(a) $\sigma_1 = 0.8, \sigma_2 = 0.8, \mu = 0.1$

(b) $\sigma_1 = 0.2, \sigma_2 = 0.2, \mu = 5$

(c) $\sigma_1 = 0.5, \sigma_2 = 0.2, \mu = 5$

(d) $\sigma_1 = 0.2, \sigma_2 = 0.5, \mu = 5$
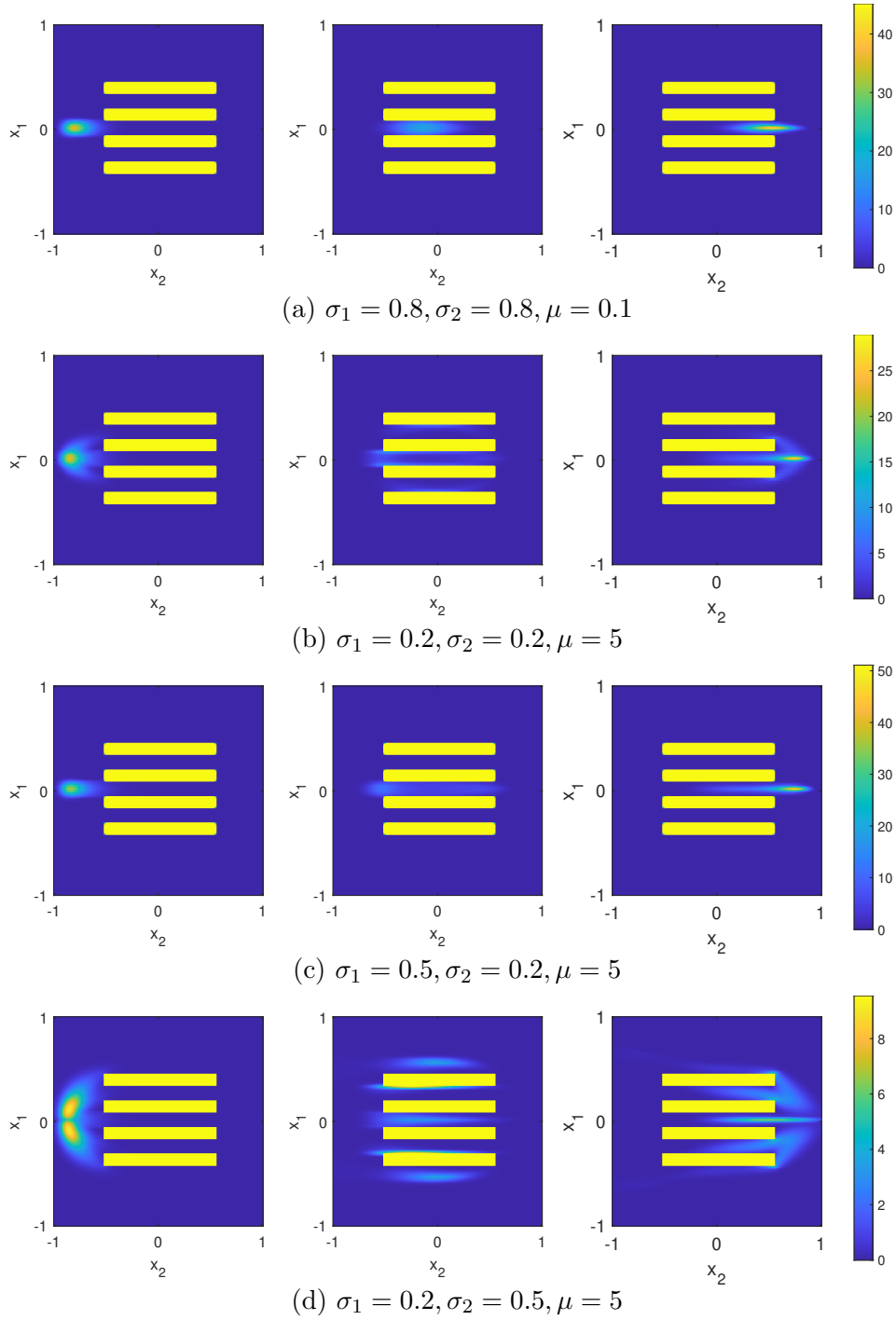
Figure 2.3: Example of Gaussian repulsion with static obstacles. MFG solution $\rho(x, t)$ at $t = 0.1, 0.5, 0.9$ with different Gaussian parameters $(\sigma_1, \sigma_2, \mu)$, where bright yellow rectangles represents static obstacles.

The results are shown in Figure 2.3. As we can see, agents travel through the channels created by $Q(x)$ to avoid high cost. Recall that small σ_i yields strong repulsion in x_i direction, which results in different behavior by agents. For instance, in Figure 2.3 (C) we impose a strong repulsion in x_2 direction and see horizontally elongated density evolution.

2.6.4   Gaussian repulsion with dynamic obstacles

Next we consider a MFG model with Gaussian repulsion on $\Omega \times [0, T] = [-1, 1]^2 \times [0, 1]$ with dynamic obstacles. We set

$$\rho_0 = \frac{1}{5} \sum_{j=1}^{5} \rho_G(c_j, -0.9, 0.04^2), \quad c_j = -1.2 + 0.4j, \ 1 \le j \le 5.$$

To model dynamic obstacles, we set

$$L(t, x, v) = \frac{1}{2}\|v\|^2 + Q(x, t)$$

where Q now represents time-dependent rectangular obstacles that move vertically. The center of each obstacles (from left to right) are moving with position $z(t) = [1.5t - 0.7, 1.5t - 0.7, -1.5t + 0.6, -t + 0.5]$ along x_1 direction. The rest of the parameters are the same as in the previous section. The results are shown in Figure 2.4. Again, values of σ_1, σ_2 control how spread is the solution in x_1, x_2 directions.

We also note that the computational cost for the static obstacles and dynamic obstacles models is the same.

2.6.5   Interactions in sub-regions

Next, we consider a MFG model with a Gaussian repulsion on $\Omega \times [0, T] = [-1, 1]^2 \times [0, 1]$ where agents interact only within domains $\Omega_1 = \{(x_1, x_2) : x_1 \le 0\}$ and $\Omega_2 = \{(x_1, x_2) : x_1 > 0\}$.

(a) $\sigma_1 = 0.8, \sigma_2 = 0.8, \mu = 0.1$

(b) $\sigma_1 = 0.2, \sigma_2 = 0.2, \mu = 5$

(c) $\sigma_1 = 0.5, \sigma_2 = 0.2, \mu = 5$

(d) $\sigma_1 = 0.2, \sigma_2 = 0.5, \mu = 5$
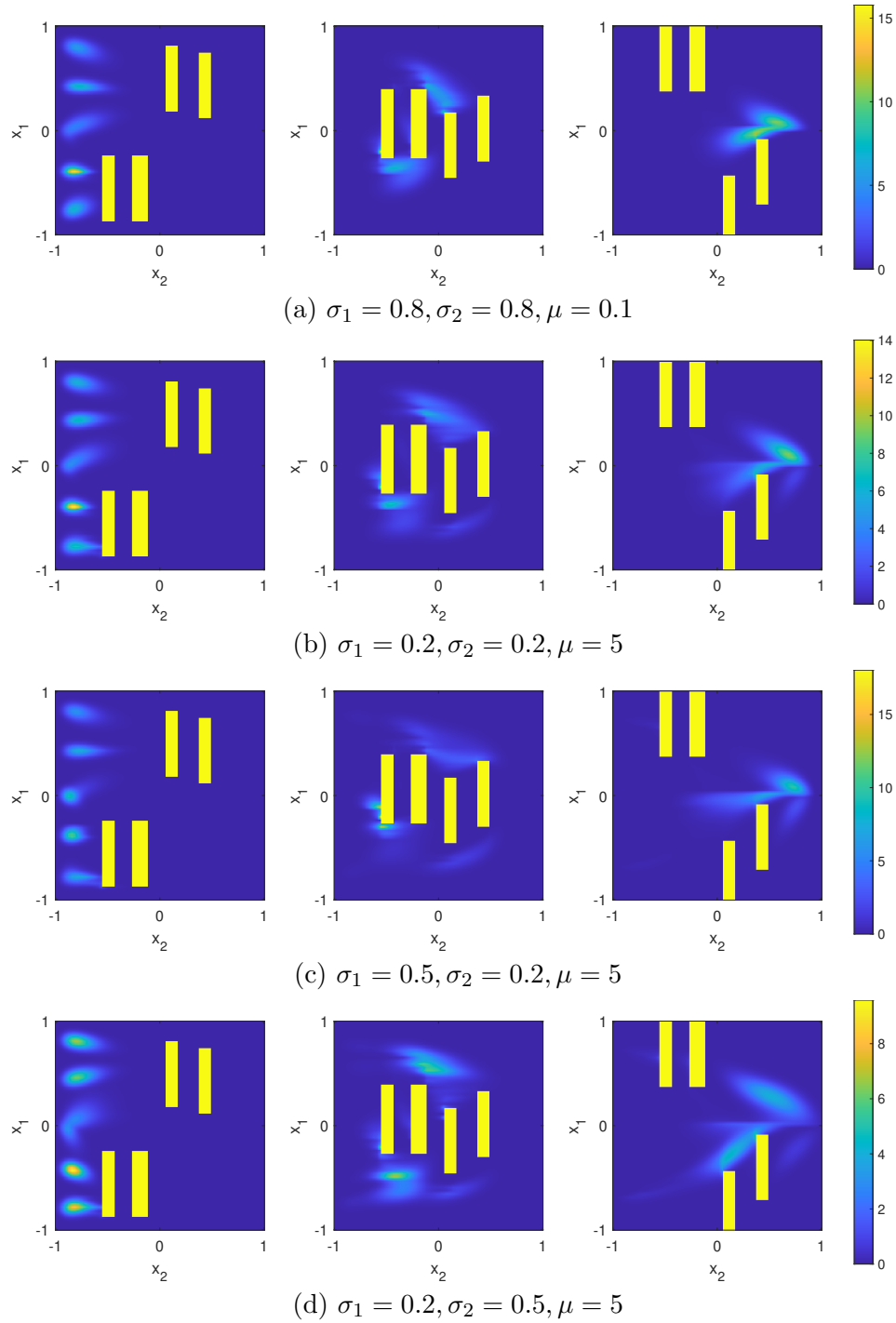
Figure 2.4: Example of Gaussian repulsion with dynamic obstacles. MFG solution $\rho(x, t)$ at $t = 0.1, 0.5, 0.9$ with different Gaussian parameters σ_1, σ_2, μ, where bright yellow rectangles represent obstacles moving along x_1 direction.

This means that agents in Ω_i interact only with those in Ω_i. We set

$$\rho_0 = \frac{1}{2}\rho_G(0.2, -0.9, 0.1^2) + \frac{1}{2}\rho_G(-0.2, -0.9, 0.1^2)$$

$$g(x_1, x_2) = -4\exp\left(-5\left(x_1 - 0.0\right)^2 - 2.5(x_2 - 0.5)^2\right)$$

The rest of the parameters are the same as for previous examples with Gaussian repulsion. We apply the basis modification explained in Section 2.4.2 to compute the solution. The
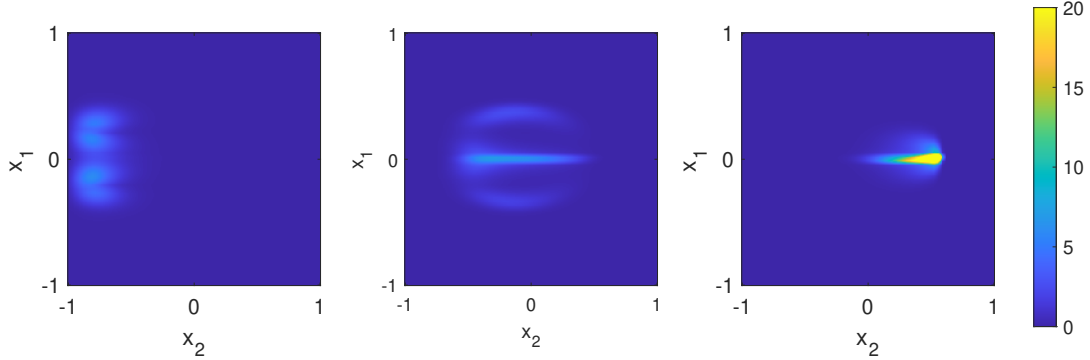
(a) Kernel with sub-region interactions.
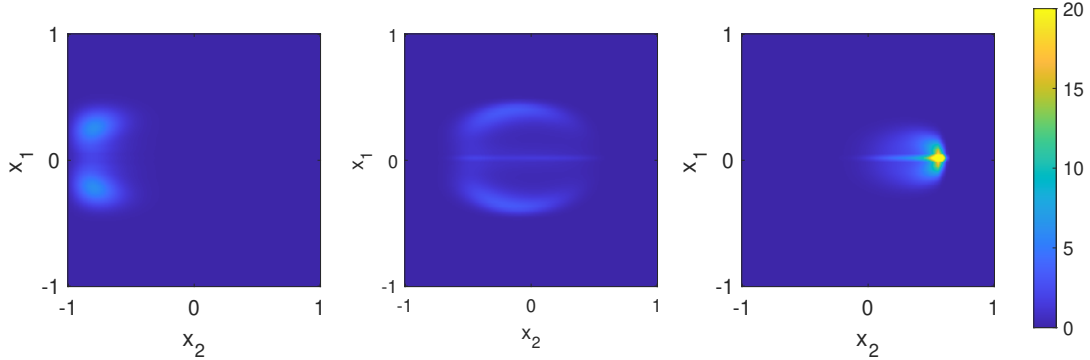
(b) Kernel with global interactions.

Figure 2.5: Example of sub-region interactions. MFG solution $\rho(x, t)$ at $t = 0.1, 0.5, 0.9$ for sub-region and global interactions kernels. Parameters are set as follows: $\sigma_1 = \sigma_2 = 0.2$, $\mu = 5$.

results are shown in Figure 2.5 where we have also included the solution with same data but full interaction. In both cases, densities spread before concentrating at the desired location. However, in the sub-region interaction case, Figure 2.5 (A), there is a concentration of agents along the common boundary of Ω_1, Ω_2. The reason is that agents on different sides of this boundary do not interact with each other, so they do not mind congestion.

2.6.6 Differential-operator interactions

Throughout this section, we set $V = \mu(I - \Delta)^{-2}$, $\mu > 0$ and $\Omega = \mathbb{T}^d$. In [AC10], the authors solve a stationary MFG system

$$
\begin{cases}
H(x, \nabla\phi) = V[\rho] + \lambda \\
-\nabla \cdot (\rho \nabla_p H(x, \nabla\phi)) = 0 \\
\int \rho = 1, \ \rho \geq 0, \quad \lambda \in \mathbb{R}
\end{cases}
\tag{2.6.1}
$$

by approximating it with its second-order version

$$
\begin{cases}
-\sigma\Delta\phi + H(x, \nabla\phi) = V[\rho] + \lambda \\
-\sigma\Delta\rho - \nabla \cdot (\rho \nabla_p H(x, \nabla\phi)) = 0 \\
\int \rho = 1, \ \rho \geq 0, \quad \lambda \in \mathbb{R}
\end{cases}
$$

for small $\sigma > 0$. Here, we recover the results in [AC10] using our method. Since we consider first-order time-dependent systems instead of second-order stationary ones, we apply a different approximation procedure for (2.6.1).

To approximate (2.6.1) we use the long-time convergence, or the turnpike property, of MFG systems discussed in [Car13b]. More precisely, we approximate (2.6.1) by

$$
\begin{cases}
-\psi_t + H(x, \nabla\psi) = V[\nu] \\
\nu_t - \nabla \cdot (\nu \nabla_p H(x, \nabla\psi)) = 0 \\
\nu(x, 0) = \rho_0(x), \ \psi(x, T) = g(x)
\end{cases}
\tag{2.6.2}
$$

where $\rho_0 \in L^\infty(\mathbb{T}^d)$, $g \in C^2(\mathbb{T}^d)$ and $T > 0$ is large. To formulate the convergence results, we need to scale the time variable in (2.6.2) and obtain a problem on a time-interval $[0, 1]$. For that, we write $\psi(x, t) = \phi(x, \frac{t}{T})$, $\nu(x, t) = \rho(x, \frac{t}{T})$, and (2.6.2) becomes

$$
\begin{cases}
-\phi_t + T \cdot H(x, \nabla\phi) = TV[\rho] \\
\rho_t - \nabla \cdot \big(\rho \nabla_p (T \cdot H(x, \nabla\phi))\big) = 0 \\
\rho(x, 0) = \rho_0(x), \ \phi(x, 1) = g(x)
\end{cases}
\tag{2.6.3}
$$

Furthermore, a triple $(\bar{\phi}, \bar{\rho}, \bar{\lambda})$ is solution of (2.6.1) if $\bar{\phi}$ is a Lipschitz viscosity solution of the HJB in (2.6.1), $\bar{\phi}$ is differentiable $\bar{\rho}$ a.e., and the continuity equation in (2.6.1) is satisfied in the sense of distributions. We summarize the results from [Car13b] in the following theorem. We omit assumptions and technicalities and refer to the original paper for details.

Theorem 2.6.1 ([Car13b])**.** *Under suitable assumptions,*

1. *system (2.6.1) has at least one solution. Moreover, if $(\bar{\phi}_1, \bar{\rho}_1, \bar{\lambda}_1)$ and $(\bar{\phi}_2, \bar{\rho}_2, \bar{\lambda}_2)$ are solutions, then $\bar{\lambda}_1 = \bar{\lambda}_2$, and $V[\bar{\rho}_1] = V[\bar{\rho}_2]$.*

2. *for a solution $(\bar{\phi}, \bar{\rho}, \bar{\lambda})$ of (2.6.1) one has that*

$$\sup_{t \in [0,1]} \left\| \frac{\phi_T(\cdot, t)}{T} - \bar{\lambda}(1 - t) \right\|_{L^\infty(\mathbb{T}^d)} \le \frac{C}{T^{\frac{1}{2}}},$$

and

$$\int_0^1 \|V[\rho_T(\cdot, t)] - V[\bar{\rho}]\|_{L^\infty(\mathbb{T}^d)} dt \le \frac{C}{T^{\frac{1}{2}}},$$

where (ϕ_T, ρ_T) is the solution of (2.6.3).

Therefore, to approximate solutions of (2.6.1) we need to solve (2.6.3). We take $H(x, p) = \frac{|p|^2}{2} - Q(x)$ where Q is a smooth periodic function. In this case, one can easily verify that assumptions in [Car13b] are fulfilled.

As mentioned in the theorem above, a solution $\bar{\phi}$ in (2.6.1) is not necessarily unique even up to constants, whereas $\bar{\lambda}$ and $V[\bar{\rho}]$ are. However, for $V = \mu(I - \Delta)^{-2}$ the uniqueness of $V[\bar{\rho}]$ implies that of $\bar{\rho}$. Furthermore, $\lim_{T \to \infty} \|V[\rho_T(\cdot, t)] - V[\hat{\rho}]\|_{L^\infty(\mathbb{T}^d)} = 0$ implies a weak convergence $\rho_T(\cdot, t) \rightharpoonup \bar{\rho}$. Hence Theorem 2.6.1 guarantees that for a large set of times $t \in [0, 1]$ the solution $\rho_T(\cdot, t)$ of (2.6.3) converges weakly to a well defined limit $\bar{\rho}$.

As in [AC10] we take $d = 2, \mu = 200$, and

$$Q(x_1, x_2) = -\sin(2\pi x_2) - \sin(2\pi x_1) - \cos(4\pi x_1)$$

We approximate V as in Section 2.4.3 using trigonometric polynomials up to order $n = 2$. Additionally, we set $T = 10$, $\rho_0(x) = 1$, $g(x) = 0$. The results are shown in Figure 2.6

46

where we plot $\rho_T(x,t)$. We also plot $\phi_T(x,t) - \int_{\mathbb{T}^d} \phi_T(y,t)dy$ to test whether it approximates a solution $\bar{\phi}$ of (2.6.1). Latter holds for second-order problems but not the first-order ones.

As we can see, we obtain accurate reconstructions of Tests 5, 6 in [AC10]. Our solutions are slightly less diffused because we consider first-order equations as opposed to second-order ones in [AC10]. Additionally, we use $H(x,p) = \frac{|p|^2}{2} - Q(x)$ whereas the examples in [AC10] are computed for $H(x,p) = |p|^{\frac{3}{2}} - Q(x)$. Nevertheless, we believe that qualitative properties and shapes of the solutions do not alter much due to this difference.
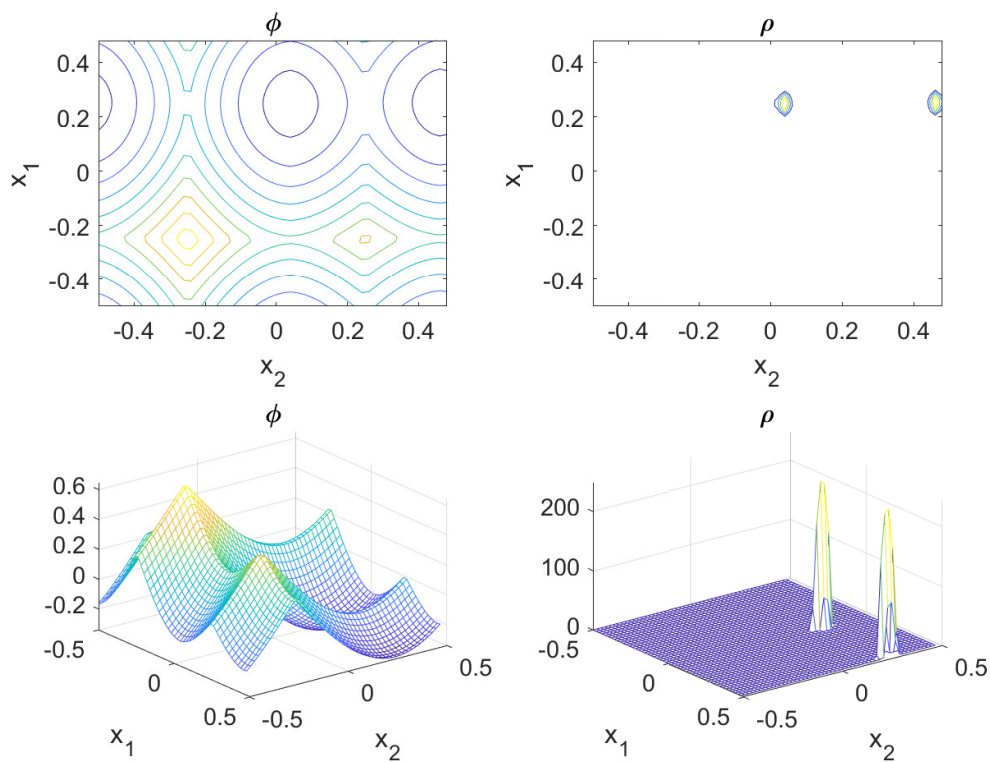
Figure 2.6: The contours and graphs of $\phi_T(x,t) - \int_{\mathbb{T}^d} \phi_T(y,t)dy$ and $\rho_T(x,t)$ for $T = 10$ and $t = 0.4$.

CHAPTER 3

Splitting Methods for a Class of Non-potential Mean-field Games

We extend the methods from Chapter1 to a class of *non-potential* mean-field game (MFG) systems with mixed couplings. Up to now, splitting methods have been applied to *potential* MFG systems that can be cast as convex-concave saddle-point problems. Here, we show that a class of non-potential MFG can be cast as primal-dual pairs of monotone inclusions and solved via extensions of convex optimization algorithms such as the primal-dual hybrid gradient algorithm. A critical feature of our approach is in considering dual variables of nonlocal couplings in *Fourier* or *feature spaces*.

This chapter is organized as follows. In Section3.1, we review computational methods for potential mean-field games and introduce a class of non-potential MFGs with mixed couplings in form of 3.1.1. In Section 3.2, we present our approach and derive the monotone-inclusion formulation of (3.1.1) with formal derivations. In Section 3.3, we propose a primal-dual algorithm based on this formulation. Furthermore, in Section 2.4, we consider a concrete class of non-potential models with density constraints. Finally, in Section 3.5, we provide numerical examples.

The contributions in this chapter were first presented in the joint work with Levon Nurbekyan in [LN21].

3.1 Introduction

Our goal is to develop computational methods for the mean-field games (MFG) systems of the form

$$
\begin{cases}
-\phi_t + H(t, x, \nabla\phi) = f_0(t, x, \rho(x,t)) + f_1\left(t, x, \int_\Omega K(x,y)\rho(y,t)dy\right) \\
\rho_t - \nabla \cdot (\rho \nabla_p H(t, x, \nabla\phi(x,t))) = 0 \\
\rho(x, 0) = \rho_0(x), \ \phi(x, 1) = g_0(x, \rho(x, 1)) + g_1\left(x, \int_\Omega S(x,y)\rho(y,1)dy\right)
\end{cases}
\tag{3.1.1}
$$

This system characterizes Nash equilibria of a differential game with a continuum of agents. For a detailed introduction and description of these models we refer to seminal papers [LL06a, LL06b, LL07, HMC06, HCM07], manuscripts [GLL11, Car13a, GS14], and references therein.

In (3.1.1), $x \in \Omega$ represents the state of a generic agent, and $t \in [0, 1]$ represents the time. We assume that $\Omega \subset \mathbb{R}^d$ is a smooth bounded domain. Furthermore, ϕ is the value function of a generic agent, ρ is the distribution of the agents in the state-space, H is the Hamiltonian of a single agent, and f_0, f_1, g_0, g_1 are the terms that model interactions between a single agent and the population. These interactions can be either local, f_0, g_0 terms, or nonlocal, f_1, g_1 terms. In the latter case, one needs to assemble information across the whole population using interaction kernels K, S. More specifically, $K(x, y), S(x, y)$ signify how agents located at y affect the decision-making of an agent at x. Finally, we impose a no-flux condition on the boundary

$$
\nu(x) \cdot (\rho \nabla_p H(t, x, \nabla\phi(x,t))) = 0 \quad (t, x) \in [0, 1] \times \partial\Omega,
\tag{3.1.2}
$$

where $\nu(x)$ is the outer normal to $\partial\Omega$ at x. This assumption ensures that agents do not leave Ω. Throughout the chapter, we assume (3.1.2) and often do not write it explicitly.

Computational methods for (3.1.1) can be roughly divided into two groups. The first group of methods applies to a specific class of MFG systems that are called *potential* and can be cast as convex-concave saddle-point problems. In this case, (3.1.1) can be efficiently

solved via splitting methods such as alternating direction method of multipliers (ADMM) [BC15a, BCS17] and primal-dual hybrid gradient (PDHG) algorithm [AKS18, AKK19]. These methods are mostly applicable to systems with only local couplings because only a limited class of problems with nonlocal ones are potential: see Section 1.2 in [CH17].

The second group of methods are general purpose and do not rely on a specific structure of (3.1.1). We refer to [AC10, Ach13, ACC13] for finite-difference, [CS12, CS14, CS15, CS18] for semi-Lagrangian, [AFG17, GS21] for monotone flow, and [CH17, Had17, HS19] for game-theoretic learning methods.

Systems considered in Chapter 1([NS18, LJL21]) have only nonlocal interactions and are potential. Here, we extend these results to systems of the form (3.1.1) that are non-potential in general and contain both local and nonlocal interactions. Our method relies on a monotone-inclusion formulation of (3.1.1) where inputs from different interaction terms are split via dual variables. In this context, our approach is analogous to [BC13] where the authors find Nash equilibria for non-potential games with finitely many players. A critical feature of our method is that dual variables corresponding to nonlocal terms are set up in Fourier spaces.

We list a number of advantages of our method. Firstly, the Fourier approach yields a dimension reduction: see Chapter 1 Section 2.3.3 for a detailed discussion. Secondly, any number of local and nonlocal interactions can be added to the system bearing minimal and straightforward changes on the algorithm. Furthermore, the algorithm is highly modular and parallelizable. Indeed, the updates of dual variables corresponding to different interactions are decoupled. Finally, the monotone inclusion formulation readily provides the convergence guarantees for the algorithm.

Here, we do not concentrate on theoretical aspects of (3.1.1) and our derivations are mostly formal. For purely nonlocal interactions; that is, $f_0, g_0 = 0$, existence and uniqueness of suitable weak solutions was established in [LL07] (see also [Car13a, Car13b]). For purely local interactions; that is, $f_1 = g_1 = 0$, we refer to [GM18] for a detailed exposition on the subject and higher-order regularity of solutions. To the best of our knowledge, the regularity

theory for (3.1.1) in the presence of both local and nonlocal interactions is not explicitly discussed in the literature. However, nonlocal terms in (3.1.1) are regularizing and separated from local ones. In this context, (3.1.1) can be considered as a smooth perturbation of purely local system with an analogous regularity theory. For an analysis of second order problems with mixed and not necessarily separated interactions we refer to [FGT21]. See Remark 10 for further comments.

3.2 MFG via monotone inclusions

We solve (3.1.1) in two steps. Firstly, we approximate (3.1.1) by a lower-dimensional system via orthogonal projections of nonlocal terms. Next, we formulate the lower-dimensional system as a monotone inclusion problem.

Assume that $\{\zeta_i\}_{i=1}^r \subset C^2(\Omega)$ is an orthonormal system with respect to the $L^2(\Omega)$ inner product. Then the system of functions $\{\zeta_i \otimes \zeta_j\}_{i,j=1}^r$ is also orthonormal, where $\zeta_i \otimes \zeta_j(x,y) = \zeta_i(x)\zeta_j(y)$. Furthermore, denote by $\mathbb{P}_r$ and $\mathbb{P}_{r,r}$ the orthogonal projection operators in $L^2(\Omega)$ and $L^2(\Omega^2)$ onto $\mathrm{span}\{\zeta_i\}_{i=1}^r$ and $\mathrm{span}\{\zeta_i \otimes \zeta_j\}_{i,j=1}^r$, respectively. Now consider the following approximation of (3.1.1)

$$
\begin{cases}
-\phi_t + H(t,x,\nabla\phi) = f_0(t,x,\rho(x,t)) + \mathbb{P}_r\left(f_1\left(t,\cdot,\int_\Omega K_r(\cdot,y)\rho(y,t)dy\right)\right)(x), \\
\rho_t - \nabla \cdot (\rho\nabla_p H(t,x,\nabla\phi(x,t))) = 0, \\
\rho(x,0) = \rho_0(x), \ \phi(x,1) = g_0(x,\rho(x,1)) + \mathbb{P}_r\left(g_1\left(\cdot,\int_\Omega S_r(\cdot,y)\rho(y,1)dy\right)\right)(x),
\end{cases}
\tag{3.2.1}
$$

where $K_r = \mathbb{P}_{r,r}(K)$, $S_r = \mathbb{P}_{r,r}(S)$. For smooth K, S, f_1, g_1 and a suitable choice of $\{\zeta_i\}_{i=1}^r$, solutions of (3.2.1) approximate those of (3.1.1): see Remark 12. Furthermore, we solve (3.2.1) by the *coefficients method* proposed in [Nur18, NS18, LJL21]. The key observation is

that for any ρ we a priori have that

$$\mathbb{P}_r \left(f_1 \left(t, \cdot, \int_\Omega K_r(\cdot, y)\rho(y, t)dy \right) \right)(x) = \sum_{i=1}^r a_i(t)\zeta_i(x)$$

$$\mathbb{P}_r \left(g_1 \left(\cdot, \int_\Omega S_r(\cdot, y)\rho(y, 1)dy \right) \right)(x) = \sum_{i=1}^r b_i\zeta_i(x),$$

where

$$a_i(t) = \int_\Omega f_1 \left(t, x, \int_\Omega K_r(x, y)\rho(y, t)dy \right) \zeta_i(x)dx,$$

$$b_i = \int_\Omega g_1 \left(x, \int_\Omega S_r(x, y)\rho(y, 1)dy \right) \zeta_i(x)dx.$$

Therefore, introducing variables

$$\alpha(x, t) = f_0(t, x, \rho(x, t)), \quad \beta(x) = g_0(x, \rho(x, 1)), \quad m(x, t) = -\rho\nabla_p H(t, x, \nabla\phi),$$

we obtain that (3.2.1) is equivalent to

$$\begin{cases} -\phi_t + H(t, x, \nabla\phi) = \alpha(x, t) + \sum_{i=1}^r a_i(t)\zeta_i(x), \\ m(x, t) = -\rho\nabla_p H(t, x, \nabla\phi), \\ \rho(x, 0) = \rho_0(x), \ \phi(x, 1) = \beta(x) + \sum_{i=1}^r b_i\zeta_i(x), \end{cases} \tag{3.2.2}$$

supplemented with compatibility conditions

$$\begin{cases} a_i(t) = \int_\Omega f_1 \left(t, x, \int_\Omega \mathbb{P}_{r,r}(K)(x, y)\rho(y, t)dy \right) \zeta_i(x)dx, \ \forall i \\ b_i = \int_\Omega g_1 \left(x, \int_\Omega \mathbb{P}_{r,r}(S)(x, y)\rho(y, 1)dy \right) \zeta_i(x)dx, \ \forall i \\ \alpha(x, t) = f_0(t, x, \rho(x, t)) \\ \beta(x) = g_0(x, \rho(x, 1)) \\ \rho_t(t, x) + \nabla \cdot m(t, x) = 0 \\ m(t, x) \cdot \nu(x) = 0, \ x \in \partial\Omega \end{cases} \tag{3.2.3}$$

Thus, our goal is to formulate (3.2.2)-(3.2.3) as a monotone inclusion problem. For that, we start by casting (3.2.2) as a convex duality relation between variables $(a, b, \alpha, \beta, \phi)$ and

(ρ, m). We omit the domains in the notation of Lebesgue and Sobolev spaces when there is no ambiguity. Recall that

$$L(t, x, v) = \sup_p -v \cdot p - H(t, x, p)$$

is the convex dual of H. The indicator function of a convex set A is defined as

$$\mathbf{1}_A(x) := \begin{cases} 0 & \text{if } x \in A \\ +\infty & \text{if } x \notin A \end{cases}$$

We assume that $p \mapsto H(t, x, p)$ is convex and lower-semicontinuous. For detailed assumptions on H for various instances of (3.1.1) we refer to [Car13b, GM18].

Proposition 1. *For* $(a, b, \alpha, \beta, \phi) \in L_t^2 \times l^2 \times L_{x,t}^2 \times L_x^2 \times H_{x,t}^1$ *define*

$$
\begin{aligned}
\Psi(a, b, \alpha, \beta, \phi) = \inf_{\rho, m} \Xi(\rho, m) &+ \int_0^1 \int_\Omega \left(\alpha(x, t) + \sum_{i=1}^r a_i(t)\zeta_i(x) \right) \rho(x, t) dx dt \\
&+ \int_\Omega \left(\beta(x) + \sum_{i=1}^r b_i \zeta_i(x) \right) \rho(x, 1) dx \\
&+ \int_0^1 \int_\Omega \phi_t \rho + \nabla\phi \cdot m \, dx dt - \int_\Omega \phi(x, 1)\rho(x, 1) dx \\
&+ \int_\Omega \phi(x, 0)\rho(x, 0) dx,
\end{aligned}
\tag{3.2.4}
$$

where

$$\Xi(\rho, m) = \int_0^1 \int_\Omega \rho L\left(t, x, \frac{m}{\rho}\right) dx dt + \mathbf{1}_{\rho(x,0)=\rho_0(x)}(\rho) + \mathbf{1}_{\rho \geq 0}(\rho) + \mathbf{1}_{m << \rho}(\rho, m)$$

Then (ϕ, ρ) *satisfy (3.2.2) if and only if* (ρ, m) *is a solution of the optimization problem in (3.2.4). Furthermore,*

$$\Psi(a, b, \alpha, \beta, \phi) = -\Xi^* \left(C(a, b, \alpha, \beta, \phi) \right),$$

where

$$
C(a, b, \alpha, \beta, \phi) = \begin{pmatrix} -\sum_i a_i(t)\zeta_i(x) - \alpha(x, t) - \phi_t \\ -\nabla\phi \\ -\phi(x, 0) \\ -\sum_i b_i\zeta_i(x) - \beta(x) + \phi(x, 1) \end{pmatrix},
\tag{3.2.5}
$$

53

and Ξ^* is the convex dual of Ξ; that is,

$$\Xi^*(\hat{\rho}, \hat{m}, \hat{\rho}(\cdot, 0), \hat{\rho}(\cdot, 1)) = \sup_{\rho, m} \int_0^1 \int_\Omega \hat{\rho}\rho + \hat{m} \cdot m \, dx dt + \int_\Omega \hat{\rho}(x, 0)\rho(x, 0)dx$$
$$+ \int_\Omega \hat{\rho}(x, 1)\rho(x, 1)dx - \Xi(\rho, m).$$

In particular, (ρ, m) is a solution of the optimization problem (3.2.4) if and only if

$$C(a, b, \alpha, \beta, \phi) \in \partial\Xi(\rho, m), \quad or \quad (\rho, m) \in \partial\Xi^* \left(C(a, b, \alpha, \beta, \phi)\right)$$

Proof. Calculating the first variation with respect to ρ, m in (3.2.4), we obtain

$$\begin{cases} L\left(t, x, \frac{m}{\rho}\right) - \frac{m}{\rho}\nabla_v L\left(t, x, \frac{m}{\rho}\right) + \alpha(x, t) + \sum_{i=1}^r a_i(t)\zeta_i(x) + \phi_t = 0 \\ \nabla_v L\left(t, x, \frac{m}{\rho}\right) + \nabla\phi = 0 \\ \beta(x) + \sum_{i=1}^r b_i\zeta_i(x) - \phi(x, 1) = 0 \end{cases}$$

Additionally, $\rho(x, 0) = \rho_0(x)$ as $\Xi(\rho, m) < \infty$. From the properties of the Legendre transform, we obtain that

$$\begin{cases} \frac{m}{\rho} = -\nabla_p H(t, x, \nabla\phi) \\ H(t, x, \nabla\phi) = \frac{m}{\rho}\nabla_v L\left(t, x, \frac{m}{\rho}\right) - L\left(t, x, \frac{m}{\rho}\right) \end{cases}$$

which yields (3.2.2). Rest of the proof readily follows from the convex duality relation between Ξ and Ξ^*. ∎

Next step is to find a map M such that the relation (3.2.3) can be written as

$$-\left(C^*(\rho, m, \rho(\cdot, 0), \rho(\cdot, 1))\right) \in M(a, b, \alpha, \beta, \phi),$$

where C^* is the adjoint operator of C, and M is a maximally monotone map. We have that

$$K_r(x, y) = \sum_{p,q=1}^r k_{pq}\zeta_p(x)\zeta_q(y), \quad k_{pq} = \int_{\Omega^2} K(x, y)\zeta_p(x)\zeta_q(y)dxdy,$$

$$S_r(x, y) = \sum_{p,q=1}^r s_{pq}\zeta_p(x)\zeta_q(y), \quad s_{pq} = \int_{\Omega^2} S(x, y)\zeta_p(x)\zeta_q(y)dxdy,$$

and we denote by $\mathbf{K} = (k_{pq})$, $\mathbf{S} = (s_{pq})$. Without loss of generality, we assume that $\mathbf{K}$, $\mathbf{S}$ are invertible.

Additionally, assume that $f_0(t, x, \cdot)$, $g_0(x, \cdot)$, $f_1(t, x, \cdot)$, $g_1(x, \cdot)$ are increasing. This assumption means that agents are crowd averse that leads to a well posed system (3.1.1) [LL07]. Furthermore, denote by

$$U_0(\rho) = \int_0^1 \int_\Omega F_0(t, x, \rho(x, t)) dx dt, \quad V_0(\mu) = \int_\Omega G_0(x, \mu(x)) dx$$

$$U_1(c) = \int_0^1 \int_\Omega F_1\left(t, x, \sum_p c_p(t)\zeta_p(x)\right) dx dt, \quad V_1(w) = \int_\Omega G_1\left(x, \sum_p w_p\zeta_p(x)\right) dx,$$

(3.2.6)

where $\partial_z \Diamond_i(t, x, z) = \Diamond_i$ for $\Diamond \in \{f, g\}$ and $i \in \{0, 1\}$. Then we have that U_i, V_i are convex, and we can consider their dual functions

$$U_1^*(a) = \sup_c \int_0^1 \sum_p a_p(t) c_p(t) dt - U_1(c), \quad V_1^*(b) = \sup_w b \cdot w - V_1(w),$$

$$U_0^*(\alpha) = \sup_\rho \int_0^1 \int_\Omega \alpha \rho \, dx dt - U_0(\rho), \quad V_0^*(\beta) = \sup_\mu \int_\Omega \beta \mu \, dx - V_0(\mu).$$

Proposition 2. *Assume that C is defined as in (3.2.5). Then we have that*

$$C^*(\rho, m, \rho(\cdot, 0), \rho(\cdot, 1)) = \begin{pmatrix} (-\int_\Omega \rho(x, t)\zeta_i(x) dx)_i \\ (-\int_\Omega \rho(x, 1)\zeta_i(x) dx)_i \\ -\rho(x, t) \\ -\rho(x, 1) \\ -\mathcal{L}^{-1}(\rho_t + \nabla \cdot m, \ m \cdot \nu, \ 0, 0) \end{pmatrix}, \quad (3.2.7)$$

where $\mathcal{L} = \left(\Delta_{t,x}, \partial_\nu \lfloor_{[0,1] \times \partial\Omega}, (\mathrm{Id} - \partial_t) \lfloor_{\Omega \times \{0\}}, (\mathrm{Id} + \partial_t) \lfloor_{\Omega \times \{1\}}\right)$. Furthermore, (3.2.3) is equivalent to

$$- (C^*(\rho, m, \rho(\cdot, 0), \rho(\cdot, 1))) \in M(a, b, \alpha, \beta, \phi), \quad (3.2.8)$$

55

where

$$M(a, b, \alpha, \beta, \phi) = \begin{pmatrix} \mathbf{K}^{-1} \ \partial_a U_1^*(a) \\ \mathbf{S}^{-1} \ \partial_b V_1^*(b) \\ \partial_\alpha U_0^*(\alpha) \\ \partial_\beta V_0^*(\beta) \\ 0 \end{pmatrix}$$

Proof. The components of C^* corresponding to variables a, b, α, β are straightforward to calculate as they are in L^2 spaces. As for the component corresponding to ϕ, we have to find $h = h(\rho, m)$ such that for all ϕ one has that

$$\langle h, \phi \rangle_{H^1} = -\int_0^1 \int_\Omega \phi_t \rho + \nabla \phi \cdot m \, dx dt + \int_\Omega \phi(x, 1) \rho(x, 1) dx - \int_\Omega \phi(x, 0) \rho(x, 0) dx$$
$$= \int_0^1 \int_\Omega \phi \left(\rho_t + \nabla \cdot m \right) dx dt - \int_0^1 \int_{\partial\Omega} \phi \ m \cdot \nu \ dx dt$$

We have that

$$\langle h, \phi \rangle_{H^1} = \int_\Omega \phi(x, 0) h(x, 0) dx + \int_\Omega \phi(x, 1) h(x, 1) dx + \int_0^1 \int_\Omega \nabla_{t,x} \phi \cdot \nabla_{t,x} h \, dx dt$$
$$= -\int_0^1 \int_\Omega \phi \Delta_{t,x} h \, dx dt + \int_0^1 \int_{\partial\Omega} \phi \ \partial_\nu h \ dx dt$$
$$+ \int_\Omega \phi(x, 1) \left(h(x, 1) + h_t(x, 1) \right) dx + \int_\Omega \phi(x, 0) \left(h(x, 0) - h_t(x, 0) \right) dx$$

Therefore h must satisfy the conditions

$$\begin{cases} \Delta_{t,x} h = -\left(\rho_t + \nabla \cdot m \right) \\ \partial_\nu h = -m \cdot \nu \\ h(x, 0) - h_t(x, 0) = 0 \\ h(x, 1) + h_t(x, 1) = 0 \end{cases} \tag{3.2.9}$$

and we obtain (3.2.7). Next, we prove (3.2.8). We have that

$$U_0^*(\alpha) = \int_0^1 \int_\Omega F_0^*(t, x, \alpha(x, t)) dx dt, \quad \partial_\alpha U_0^*(\alpha(x, t)) = \partial_\alpha F_0^*(t, x, \alpha(x, t)),$$

56

where $F_0^*(t, x, \alpha) = \sup_\rho \alpha\rho - F_0(t, x, \rho)$. Therefore, the α-entry inclusion in (3.2.8) is equivalent to

$$\rho(x, t) \in \partial_\alpha F_0^*(t, x, \alpha(x, t)) \iff \alpha(x, t) \in \partial_\rho F_0(t, x, \rho) = f_0(t, x, \rho)$$

Similarly, the β-entry inclusion is equivalent to

$$\rho(x, 1) \in \partial_\alpha G_0^*(x, \beta(x)) \iff \beta(x) \in \partial_\rho G_0(x, \rho(x, 1)) = g_0(x, \rho(x, 1))$$

Next, the ϕ-entry inclusion means that $h = 0$ in (3.2.9) that is equivalent to

$$\rho_t + \nabla \cdot m = 0$$

The a-entry inclusion in (3.2.8) is

$$\left(\int_\Omega \rho(x, t)\zeta_i(x)dx\right)_{i=1}^r \in \mathbf{K}^{-1}\partial_a U_1^*(a) \iff \mathbf{K}\left(\int_\Omega \rho(x, t)\zeta_i(x)dx\right)_{i=1}^r \in \partial_a U_1^*(a)$$

Applying the properties of the Legendre transform again, we obtain that this previous inclusion is equivalent to

$$a \in \partial_c U_1\left(\mathbf{K}\left(\int_\Omega \rho(x, t)\zeta_i(x)\right)_{i=1}^r\right) \tag{3.2.10}$$

On the other hand, we have that

$$\partial_{c_i} U_1(c) = \int_0^1 \int_\Omega f_1\left(t, x, \sum_{p=1}^r c_p(t)\zeta_p(x)\right)\zeta_i(x)dxdt$$

and therefore

$$\partial_{c_i} U_1\left(\mathbf{K}\left(\rho(x, t)\zeta_i(x)\right)_{i=1}^r\right)$$
$$= \int_0^1 \int_\Omega f_1\left(t, x, \sum_{p=1}^r \sum_{q=1}^r k_{pq}\int_\Omega \rho(y, t)\zeta_q(y)dy\zeta_p(x)\right)\zeta_i(x)dxdt$$
$$= \int_0^1 \int_\Omega f_1\left(t, x, \int_\Omega K_r(x, y)\rho(y, t)dy\right)\zeta_i(x)dxdt$$

Hence, (3.2.10) is equivalent to the first equation in (3.2.3). The derivation for the b-entry in (3.2.8) is similar. ■

Remark 8. *The inverse Laplacian operator appears in C^* because we consider ϕ as an element of H^1 space rather than L^2. As an inner product in H^1 we set*

$$\langle \phi, h \rangle_{H^1} = \int_\Omega \phi(x, 0) h(x, 0) dx + \int_\Omega \phi(x, 1) h(x, 1) dx + \int_0^1 \int_\Omega \nabla_{t,x} \phi \cdot \nabla_{t,x} h \, dx \, dt$$

where we slightly abuse notation by using dx for the surface measure of $\partial\Omega$. As pointed out in [JLL19, JL20], the choice of spaces is crucial for grid-independent convergence of primal-dual algorithms. We come back to this point below when we discuss the algorithms: Remark 13.

Combining Propositions 1, 2 we obtain the following theorem.

Theorem 3.2.1. *The pair of systems (3.2.2)-(3.2.3), and so (3.2.1), can be written as a primal-dual pair of inclusions*

$$0 \in M(a, b, \alpha, \beta, \phi) + C^*(N(C(a, b, \alpha, \beta, \phi))) \quad (P)$$

$$\begin{cases} (\rho, m, \rho(\cdot, 0), \rho(\cdot, 1)) \in N(C(a, b, \alpha, \beta, \phi)) \\ -C^*(\rho, m, \rho(\cdot, 0), \rho(\cdot, 1)) \in M(a, b, \alpha, \beta, \phi) \end{cases} \quad (D) \qquad (3.2.11)$$

where $N = \partial\Xi^*$. Furthermore, if $c \mapsto \partial_c U_1(\mathbf{K}c)$ and $w \mapsto \partial_w V_1(\mathbf{S}w)$ are maximally monotone, then M is maximally monotone, and (3.2.11) is a primal-dual pair of monotone inclusions.

Proof. The equivalence of (3.2.11) and (3.2.2)-(3.2.3) is simply a combination of assertions in Propositions 1 and 2. Furthermore, assume that $c \mapsto \partial_c U_1(\mathbf{K}c)$ and $w \mapsto \partial_w V_1(\mathbf{S}w)$ are maximally monotone. We have that

$$(\partial_c U_1 (\mathbf{K}c))^{-1} = \mathbf{K}^{-1} \partial_a U_1^*(a), \quad (\partial_w V_1 (\mathbf{S}w))^{-1} = \mathbf{S}^{-1} \partial_b V_1^*(b)$$

Therefore $a \mapsto \mathbf{K}^{-1}\partial_a U_1^*(a)$ and $b \mapsto \mathbf{S}^{-1}\partial_b V_1^*(b)$ are maximally monotone. Next, $\alpha \mapsto \partial_\alpha U_0^*(\alpha)$ and $\beta \mapsto \partial_\beta V_0^*(\beta)$ are maximally monotone by the convexity of U_0^*, V_0^*. Hence, M is maximally monotone. ∎

Remark 9. *The monotonicity of $c \mapsto \partial_c U_1(\mathbf{K}c)$ and $w \mapsto \partial_w V_1(\mathbf{S}w)$ yields that the mean-field coupling in (3.2.1) satisfies the Lasry-Lions monotonicity condition [LL07, Theorems 2.4, 2.5], and hence (3.2.1) is well-posed.*

Remark 10. *Throughout the chapter, we embed $a, b, \alpha, \beta, \phi, \rho, m$ in suitable Hilbert spaces. In general, (3.2.1) and (3.1.1) do not admit smooth solutions, and a suitable notion of a weak solution is necessary. Thus, a natural question arises whether (3.2.11) admits solutions in these Hilbert spaces and can be regarded as a weak formulation of (3.2.1). This question is a subject of our subsequent work, and we do not address it here. Nevertheless, we provide some comments on possible methods and expected results below.*

When (3.2.1) has only nonlocal smoothing interactions; that is, $f_0, g_0 = 0$, and $f_1, g_1, K, S, \zeta_i \in C^2$, one can prove that (3.2.1) admit weak solutions $(\phi, \rho) \in W^{1,\infty} \times L^\infty$ if $\rho_0 \in L^\infty$ [LL07, Car13b]. Here, weak solutions are understood in the viscosity sense for ϕ and distributional sense for ρ. In this case, we solutions of (3.2.1) and (3.2.11) coincide [NS18, Theorem 3.1].

In the presence of local interactions, the theory of weak solutions is more peculiar and depends on the growth of $p \mapsto H(t, x, p)$, $\rho \mapsto f_0(t, x, \rho)$, $\rho \mapsto g_0(t, x, \rho)$ and the variational structure of the problem. Typically, one obtains suitably defined weak solutions $(\phi, \rho) \in W^{1,q} \times L^r$ for some q, r related to these previous growth rates. We refer to [GM18, GMS19] for a thorough discussion on the topic. In this case, rigorous connections between (3.2.11) and weak solutions of (3.2.1) is an interesting question remaining to be understood. For related analyses of monotone inclusions methods for non-potential MFG systems see [FG18, FGT21].

Remark 11. *On the discrete level, there is no obstruction to Hilbert-space embedding caused by the lack of regularity, which is then relevant for the convergence-rate analysis of the discrete solution to the continuous one. In this context, the choice of Hilbert spaces corresponds to metric chosen for discrete variables which can affect the convergence rate of primal-dual algorithms: see Remarks 8, 13 and [JLL19, JL20]. Rigorous analysis of discrete versions of (3.2.1), (3.2.11) and their convergence to continuous counterparts is a subject of our future studies.*

Remark 12. *Another important question is whether solutions of (3.2.1), and consequently of (3.2.11), converge to those of (3.1.1). This question reduces to the stability of solutions*

under smooth, C^2, perturbations of the nonlocal smoothing coupling. In the absence of local interactions, solutions are indeed stable under such perturbations: see [Car13a, Section 4.3] and the discussion in [NS18, Sections 2, 4]. As before, systems that involve local interactions remain to be analyzed. Nevertheless, stability results in [CGP15, Section 6] and the fact that perturbations are only in the nonlocal smoothing terms suggest that solutions will be stable.

3.3 A monotone primal-dual algorithm

We apply the monotone primal-dual algorithm in [V 13] to solve (3.2.11) (and thus (3.2.1)). We start by an abstract discussion of the algorithm. Following [V 13], assume that $\mathcal{H}, \mathcal{G}$ are real Hilbert spaces, $M : \mathcal{H} \to 2^{\mathcal{H}}$, $N : \mathcal{G} \to 2^{\mathcal{G}}$ are maximally monotone operators, and $C : \mathcal{H} \to \mathcal{G}$ is a nonzero bounded linear operator. Furthermore, consider the following pair of monotone inclusion problems

$$\text{find } s \text{ s.t. } 0 \in Ms + C^*(N(Cs)) \quad \text{(P)}$$
$$\text{find } q \text{ s.t. } q \in N(Cs), \quad -C^*q \in Ms, \text{ for some } s \quad \text{(D)}$$

$$(3.3.1)$$

When $M = \partial f$, $N = \partial g$ (3.3.1) reduces to a convex-concave saddle-point problem

$$\inf_s f(s) + g(Cs) = \inf_s \sup_q f(s) + \langle Cs, q \rangle - g^*(q)$$

Accordingly, one can solve (3.3.1) by a monotone-inclusion version of the celebrated primal-dual hybrid gradient (PDHG) method [CP11, CP16]. In its simplest form, the algorithm in [V 13] reads as follows

$$\begin{cases} s^{n+1} = J_{\tau_s M}(s^n - \tau_s C^* q^n) \\ \tilde{s}^{n+1} = 2s^{n+1} - s^n \\ q^{n+1} = J_{\tau_q N^{-1}}(q^n + \tau_q C \tilde{s}^{n+1}), \end{cases} \quad (3.3.2)$$

where $J_{\tau F} = (I + \tau F)^{-1}$ is the resolvent operator, and $\tau_s, \tau_q > 0$ are such that $\tau_s \tau_q \|C\|^2 < 1$. Note that when $M = \partial f$, $N = \partial g$ (3.3.2) reduces to the standard PDHG [CP11, CP16].

60

3.3.1 A primal-dual algorithm

Applying (3.3.2) to (3.2.11) we obtain the following algorithm to solve the MFG system (3.2.1):

$$
\begin{cases}
(a^{n+1}, b^{n+1}, \alpha^{n+1}, \beta^{n+1}, \phi^{n+1}) \\
= J_{\tau M}\left((a^n, b^n, \alpha^n, \beta^n, \phi^n) - \tau C^*(\rho^n, m^n, \rho^n(\cdot, 0), \rho^n(\cdot, 1)) \right) \\
(\tilde{a}^{n+1}, \tilde{b}^{n+1}, \tilde{\alpha}^{n+1}, \tilde{\beta}^{n+1}, \tilde{\phi}^{n+1}) \\
= 2(a^{n+1}, b^{n+1}, \alpha^{n+1}, \beta^{n+1}, \phi^{n+1}) - (a^n, b^n, \alpha^n, \beta^n, \phi^n) \\
(\rho^{n+1}, m^{n+1}, \rho^{n+1}(\cdot, 0), \rho^{n+1}(\cdot, 1)) \\
= J_{\sigma \partial \Xi}\left((\rho^n, m^n, \rho^n(\cdot, 0), \rho^n(\cdot, 1)) + \sigma C(\tilde{a}^{n+1}, \tilde{b}^{n+1}, \tilde{\alpha}^{n+1}, \tilde{\beta}^{n+1}, \tilde{\phi}^{n+1}) \right)
\end{cases}
\tag{3.3.3}
$$

Remark 13. *The time-steps in* (3.3.3) *must satisfy the condition* $\tau\sigma\|C\|^2 < 1$. *Note that*

$$
|\langle C(a, b, \alpha, \beta, \phi), (\rho, m, \rho(\cdot, 0), \rho(\cdot, 1))\rangle| \leq \left(\|a\|_{L_t^2} + \|b\|_2 + \|\alpha\|_{L_{x,t}^2} + \|\beta\|_{L_x^2} + \|\phi\|_{H^1} \right)
$$
$$
\left(\|\rho\|_{L_{x,t}^2} + \|m\|_{L_{x,t}^2} + \|\rho(\cdot, 0)\|_{L_x^2} + \|\rho(\cdot, 1)\|_{L_x^2} \right)
$$

Therefore, $\|C\|$ *is finite, and independent of the grid-size.*

The updates for $(a, b, \alpha, \beta, \phi)$. Note that the updates for $a, b, \alpha, \beta, \phi$ are decoupled. Indeed, (3.3.3) yields

$$
\begin{cases}
a^n(t) + \tau \left(\int_\Omega \rho^n(x, t)\zeta_i(x)dx \right)_i \in a^{n+1}(t) + \tau \mathbf{K}^{-1}\partial_a U_1^*(a^{n+1}(t)) \\
b^n + \tau \left(\int_\Omega \rho^n(x, 1)\zeta_i(x)dx \right)_i \in b^{n+1} + \tau \mathbf{S}^{-1}\partial_b V_1^*(b^{n+1}) \\
\alpha^n(x, t) + \tau \rho^n(x, t) \in \alpha^{n+1}(x, t) + \tau \partial_\alpha U_0^*(\alpha^{n+1}(x, t)) \\
\beta^n(x) + \tau \rho^n(x, 1) \in \beta^{n+1}(x) + \tau \partial_\beta V_0^*(\beta^{n+1}(x)) \\
\phi^n(x, t) + \tau \mathcal{L}^{-1}(\rho_t^n + \nabla \cdot m^n, 0, 0) = \phi^{n+1}(x, t)
\end{cases}
$$

To update a, we need to solve an $r \times r$ system for every fixed t. Next, to update b we need to solve an $r \times r$ system. Once r is fixed the sizes of these systems do not depend on the mesh.

Next, we observe that

$$U_0^*(\alpha) = \int_0^1 \int_\Omega F_0^*(t, x, \alpha(x, t)) dx dt, \quad \partial_\alpha U_0^*(\alpha(x, t)) = \partial_\alpha F_0^*(t, x, \alpha(x, t)),$$

$$V_0^*(\beta) = \int_\Omega G_0^*(x, \beta(x)) dx, \quad \partial_\beta V_0^*(\beta(x)) = \partial_\beta G_0^*(x, \beta(x)),$$

where

$$F_0^*(t, x, \alpha) = \sup_\rho \alpha\rho - F_0(t, x, \rho), \quad G_0^*(x, \beta) = \sup_\rho \beta\rho - G_0(x, \rho).$$

Therefore, the updates for α, β correspond to decoupled one-dimensional proximal steps; that is,

$$\begin{cases} \alpha^{n+1}(x, t) \in \arg\min_\alpha F_0^*(t, x, \alpha) + \frac{|\alpha - \alpha^n(x,t) - \tau\rho^n(x,t)|^2}{2\tau} \\ \beta^{n+1} \in \arg\min_\beta G_0^*(x, \beta) + \frac{|\beta - \beta^n(x) - \tau\rho^n(x,1)|^2}{2\tau} \end{cases}$$

Therefore, the updates for α, β can be efficiently performed in parallel yielding linear-in-grid computational cost. Finally, recalling the definition of $\mathcal{L}$, we obtain that to update ϕ we need to solve a space-time elliptic equation

$$\begin{cases} \Delta_{t,x}\phi = \Delta_{t,x}\phi^n + \tau(\rho_t^n + \nabla \cdot m^n) \\ \phi(x, 0) - \phi_t(x, 0) = \phi^n(x, 0) - \phi_t^n(x, 0) \\ \phi(x, 1) + \phi_t(x, 1) = \phi^n(x, 1) + \phi_t^n(x, 1) \end{cases}$$

This step can be efficiently performed via Fast Fourier Transform (FFT).

The updates for (ρ, m). The resolvent operator $J_{\sigma\partial\Xi}$ is the proximal operator $\text{prox}_{\sigma\Xi}$.

Therefore, (ρ, m) updates reduce to an optimization problem

$$\inf_{\rho,m} \int_0^1 \int_\Omega \rho L\left(t, x, \frac{m}{\rho}\right) dxdt + \mathbf{1}_{\rho(x,0)=\rho_0(x)} + \mathbf{1}_{\rho \geq 0} + \mathbf{1}_{m <<\rho}$$

$$+ \frac{1}{2\sigma} \int_\Omega \left(\rho(x,0) - \rho^n(x,0) + \sigma\tilde{\phi}^{n+1}(x,0)\right)^2 dx$$

$$+ \frac{1}{2\sigma} \int_\Omega \left(\rho(x,1) - \rho^n(x,1) + \sigma\sum_i \tilde{b}_i^{n+1}\zeta_i(x) + \sigma\tilde{\beta}^{n+1}(x) - \sigma\tilde{\phi}^{n+1}(x,1)\right)^2 dx$$

$$+ \frac{1}{2\sigma} \int_0^1 \int_\Omega \left(\rho(x,t) - \rho^n(x,t) + \sigma\sum_i \tilde{a}^{n+1}(t)\zeta_i(x) + \sigma\tilde{\alpha}^{n+1}(x,t) + \sigma\tilde{\phi}_t^{n+1}(x,t)\right)^2 dxdt$$

$$+ \frac{1}{2\sigma} \int_0^1 \int_\Omega \left|m(x,t) - m^n(x,t) + \sigma\nabla\tilde{\phi}^{n+1}(x,t)\right|^2 dxdt$$

Again, we obtain decoupled one-dimensional optimization problems

$$\begin{cases} (\rho^{n+1}(x,t), m^{n+1}(x,t)) \in \arg\min_{\rho,m} \rho L\left(t, x, \frac{m}{\rho}\right) + \mathbf{1}_{\rho \geq 0} + \mathbf{1}_{m <<\rho} \\ + \dfrac{\left|\rho - \rho^n(x,t) + \sigma\sum_i \tilde{a}^{n+1}(t)\zeta_i(x) + \sigma\tilde{\alpha}^{n+1}(x,t) + \sigma\tilde{\phi}_t^{n+1}(x,t)\right|^2}{2\sigma} \\ + \dfrac{\left|m - m^n(x,t) + \sigma\nabla\tilde{\phi}^{n+1}(x,t)\right|^2}{2\sigma} \\ \rho^{n+1}(x,0) \in \arg\min_{\rho} \mathbf{1}_{\rho=\rho_0(x)} + \dfrac{\left|\rho - \rho^n(x,0) + \sigma\tilde{\phi}^{n+1}(x,0)\right|^2}{2\sigma} \\ \rho^{n+1}(x,1) \in \arg\min_{\rho} \dfrac{\left|\rho - \rho^n(x,1) + \sigma\sum_i \tilde{b}_i^{n+1}\zeta_i(x) + \sigma\tilde{\beta}^{n+1}(x) - \sigma\tilde{\phi}^{n+1}(x,1)\right|^2}{2\sigma} + \mathbf{1}_{\rho \geq 0} \end{cases}$$

3.4 A class of non-potential MFG with density constraints

Here discuss an instance of (3.1.1) that is non-potential and incorporates pointwise density constraints for the agents. We illustrate that our method handles mixed couplings in an efficient manner. Assume that

$$f_1(t,x,z) = z, \quad f_0(t,x,z) = \partial_z \mathbf{1}_{\underline{h}(x,t) \leq z \leq \bar{h}(x,t)}$$

$$g_1(x,z) = 0, \quad g_0(x,z) = \partial_z \mathbf{1}_{\underline{e}(x) \leq z \leq \bar{e}(x)} + g(x)$$

Functions $\underline{h}$, $\bar{h} \geq 0$ and $\underline{e}, \bar{e} \geq 0$ are density constraints; that is, the solution to the MFG problem must satisfy the hard constraints $\underline{h}(x,t) \leq \rho(x,t) \leq \bar{h}(x,t)$, $(x,t) \in \Omega \times (0,1)$ and $\underline{e}(x) \leq \rho(x,1) \leq \bar{e}(x)$, $x \in \Omega$. Next, g is a terminal cost function.

Remark 14. *We can model static and dynamic obstacles in this framework. Indeed, assume that $\Omega_t \subset \Omega$ is a dynamic obstacle and set $\underline{h}(x,t) = \bar{h}(x,t) = \chi_{\Omega_t}(x)$. Then the hard constraint $\underline{h}(x,t) \leq \rho(x,t) \leq \bar{h}(x,t)$ is equivalent to $\mathrm{supp}\rho(\cdot,t) \cap \Omega_t = \emptyset$, which means that there are no agents in Ω_t. One can also use the lower bounds on ρ to maintain a minimal fraction of agents at specific locations.*

From (3.2.6), we obtain

$$U_1(c) = \int_0^1 \int_\Omega \frac{\left(\sum_{j=1}^r c_j(t)\zeta_j(x)\right)^2}{2}\,dxdt = \frac{1}{2}\int_0^1 \sum_{j=1}^r c_j^2(t)dt$$

$$U_0(\rho) = \int_0^1 \int_\Omega \mathbf{1}_{\underline{h}(x,t)\leq\rho(x,t)\leq\bar{h}(x,t)}dxdt$$

$$V_0(\mu) = \int_\Omega \mathbf{1}_{\underline{e}(x)\leq\mu(x)\leq\bar{e}(x)} + g(x)\mu(x)dx$$

Note that we do not need V_1 and b since $g_1 = 0$. Furthermore, the dual functions are

$$U_1^*(a) = \frac{1}{2}\int_0^1 \sum_{j=1}^r a_j^2(t)dt,$$

$$U_0^*(\alpha) = \int_0^1 \int_\Omega \max\left\{\alpha(x,t)\underline{h}(x,t), \alpha(x,t)\bar{h}(x,t)\right\}dxdt$$

$$V_0^*(\beta) = \int_\Omega \max\left\{(\beta(x) - g(x))\,\underline{e}(x), (\beta(x) - g(x))\,\bar{e}(x)\right\}dx$$

Accordingly, the algorithm (3.3.3) reduces to

$$
\begin{cases}
a^{n+1} = (\mathbf{I} + \tau \mathbf{K}^{-1})^{-1} \left(a^n + \tau \left(\rho^n(x,t)\zeta_j(x) \right)_j \right) \\[2mm]
\alpha^{n+1}(x,t) = \min \left\{ \max \left\{ 0, \alpha^n(x,t) + \tau\rho^n(x,t) - \tau\bar{h}(x,t) \right\}, \alpha^n(x,t) + \tau\rho^n(x,t) - \tau\underline{h}(x,t) \right\} \\[2mm]
\beta^{n+1}(x) = \min \left\{ \max \left\{ g(x), \beta^n(x) + \tau\rho^n(x,1) - \tau\bar{e}(x) \right\}, \beta^n(x) + \tau\rho^n(x,1) - \tau\underline{e}(x) \right\} \\[2mm]
\Delta_{t,x}\phi^{n+1} = \Delta_{t,x}\phi^n + \tau(\rho_t^n + \nabla \cdot m^n) \\[2mm]
\phi^{n+1}(x,0) - \phi_t^{n+1}(x,0) = \phi^n(x,0) - \phi_t^n(x,0) \\[2mm]
\phi^{n+1}(x,1) + \phi_t^{n+1}(x,1) = \phi^n(x,1) + \phi_t^n(x,1) \\[2mm]
\left(\tilde{a}^{n+1}, \tilde{\alpha}^{n+1}, \tilde{\beta}^{n+1}, \tilde{\phi}^{n+1} \right) = 2\left(a^{n+1}, \alpha^{n+1}, \beta^{n+1}, \phi^{n+1} \right) - \left(a^n, \alpha^n, \beta^n, \phi^n \right) \\[2mm]
\left(\rho^{n+1}(x,t), m^{n+1}(x,t) \right) \in \arg\min_{\rho,m} \rho L\left(t, x, \frac{m}{\rho} \right) + \mathbf{1}_{\rho \geq 0} + \mathbf{1}_{m \ll \rho} \\[2mm]
\quad + \dfrac{\left| \rho - \rho^n(x,t) + \sigma \sum_i \tilde{a}^{n+1}(t)\zeta_i(x) + \sigma\tilde{\alpha}_1^{n+1}(x,t) + \sigma\tilde{\alpha}_2^{n+1}(x,t) + \sigma\tilde{\phi}_t^{n+1}(x,t) \right|^2}{2\sigma} \\[2mm]
\quad + \dfrac{\left| m - m^n(x,t) + \sigma\nabla\tilde{\phi}^{n+1}(x,t) \right|^2}{2\sigma} \\[2mm]
\rho^{n+1}(x,0) = \rho_0(x) \\[2mm]
\rho^{n+1}(x,1) = \max\{ \rho^n(x,1) - \sigma\tilde{\beta}^{n+1}(x) + \sigma\tilde{\phi}^{n+1}(x,1), 0 \}
\end{cases}
$$

We have that $\mathbf{K} = (k_{pq})$ where $k_{pq} = \int_{\Omega^2} K(x,y)\zeta_p(x)\zeta_q(y)dxdy$. Therefore, $\mathbf{K}$ may not be symmetric if K is not. In this case, (3.1.1) is non-potential. Nevertheless, if K is monotone then such is $\mathbf{K}$, and our methods apply. Below we discuss a class of non-symmetric interactions that are monotone but non-symmetric. For $\delta_-, \delta_+ > 0$ consider

$$
\gamma_{\delta_-,\delta_+}(x) = e^{-\frac{x^2}{2\delta_-^2}} \chi_{x<0} + e^{-\frac{x^2}{2\delta_+^2}} \chi_{x\geq 0}, \quad x \in \mathbb{R}
$$

The cosine transform of γ is

$$
\int_{\mathbb{R}} \cos\left(2i\pi\zeta x\right) \gamma(x)dx = \sqrt{\frac{\pi}{2}} \left(\delta_- e^{-2\pi^2\zeta^2\delta_-^2} + \delta_+ e^{-2\pi^2\zeta^2\delta_+^2} \right) > 0, \quad \zeta \in \mathbb{R}.
$$

Therefore, $K(x,y) = \gamma(y-x)$ is a monotone kernel. Therefore, for $\delta_-, \delta_+ \in \mathbb{R}_+^d$

$$
K_{\delta_-,\delta_+}(x,y) = \prod_{i=1}^{d} \gamma_{\delta_{i,-},\delta_{i,+}}(y_i - x_i)
$$

65

is a monotone kernel. Furthermore, for any non-singular linear transformation Q we have that $K_{\delta_-,\delta_+}(Q^{-1}x, Q^{-1}y)$ is a monotone kernel. Therefore, for a basis $\nu = \{\nu_1, \nu_2, \cdots, \nu_d\} \subset \mathbb{R}^d$ we have that

$$K_{\nu,\delta_-,\delta_+}(x, y) = K_{\delta_-,\delta_+}(Q^{-1}x, Q^{-1}y) = \prod_{i=1}^{d} \gamma_{\delta_{i,-},\delta_{i,+}}(y_i' - x_i') \tag{3.4.1}$$

is a monotone kernel, where $Q = (\nu_1\ \nu_2\ \cdots\ \nu_d)$ is the coordinates transformation matrix and $x' = Q^{-1}x$ are the coordinates in ν.

Kernels in (3.4.1) model interactions that have different strengths of repulsion along lines parallel to ν_i. Moreover, these interactions are not symmetric as they depend on the sign of $y_i' - x_i'$ that tells us whether y is in the front or back of x relative to ν_i. We can think of crowd motion models where people mostly pay attention to the crowd in front of them.

3.5 Numerical experiments

In this section, we present three sets of numerical examples for MFG with mixed couplings using Algorithm (3.3.3). In these MFG systems, we have the running cost $L(t, x, v) = \frac{|v|^2}{2}$ which leads to

$$\rho L\left(t, x, \frac{m}{\rho}\right) = \begin{cases} \frac{|m|^2}{2\rho} & \text{if } \rho > 0 \\ 0 & \text{if } (\rho, m) = (0, 0) \\ +\infty & \text{otherwise.} \end{cases}$$

We take $\Omega \times [0, T] = [-1, 1]^2 \times [0, 1]$, with a uniform space-grid $N_x = 64$ and a uniform time-grid $N_t = 32$ in all examples. The finite difference scheme follows [AC10]. As for the orthonormal system, we use the Legendre polynomials and set the number of coefficients $r = 15^2$ to get a suitable approximation of the kernel. Figure 3.1 shows the quality of approximated kernels.
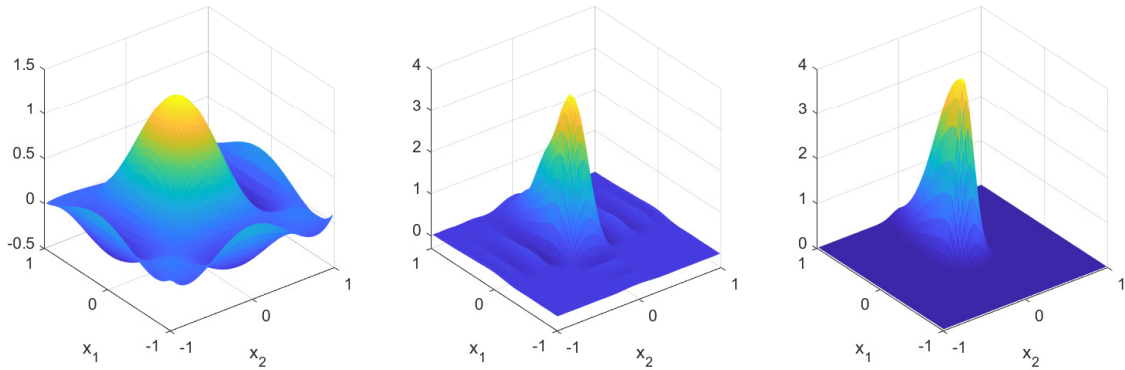
Figure 3.1: Plot of approximated kernels for example 5.1 case B. From left to right: approximated kernel with $r = 5^2$; approximated kernel with $r = 15^2$; the exact kernel.

3.5.1 Density Splitting with Asymmetric Kernel

We consider a MFG problem where the density splits into 8 parts at final time. For this non-potential MFG with density constraints (3.5.3), we set

$$\rho_0(x) = \mathcal{N}([0,0], 0.1^2)$$

$$g(x) = \frac{1}{2} \sum_{j=1}^{8} \left(1 - \exp\left(20\|x - x_j\|^2\right)\right), \quad \text{where } x_j = 0.75 \left[\sin\frac{2\pi j}{8}, \cos\frac{2\pi j}{8}\right]$$

$$\bar{e}(x) = 4,$$

where $\mathcal{N}(x, \sigma_G)$ is the density of a homogeneous normal distribution centered at x with variance σ_G^2. As for the Gaussian type Kernel $K(x, y)$ in (3.4.1), we choose the three following set-up:

- Case A, symmetric kernel

$$K(x, y) = 4 \exp\left(-\frac{\|x - y\|^2}{2\delta^2}\right)$$

$$\delta = \delta_{i,-} = \delta_{i,+} = 0.1 \text{ for } i = 1, 2$$

- Case B, asymmetric kernel

$$K(x, y) = 4\gamma_{\delta_-, \delta}(x_1 - y_1)\gamma_{\delta, \delta}(x_2 - y_2)$$

$$\delta = 0.1, \delta_- = 0.4.$$

- Case C, asymmetric kernel (coordination transform)

$$K(x, y) = 4\exp\left(-\frac{(x-y)^T Q(x-y)}{2\delta^2}\right)$$

$$Q = \begin{pmatrix} \frac{1}{\delta^2} & \frac{c}{\delta^2} \\ \frac{c}{\delta^2} & \frac{1}{\delta^2} \end{pmatrix}, c = 0.95, \delta = 0.2$$

The results are shown in Figure 3.2. As we can see nonlocal kernel affect how the density moves and have different final distributions. In case A, a symmetric kernel leads to an even splitting of the initial density. Comparing case A and B, we see that the large $\delta_{1,-}$ causes density to favor a motion towards $x_{1,-}$ direction. As a result, the final density has more concentration in $x_{1,-}$ domain. As for a comparison between A and C, we see that agents in case C have a preference to move along $x_1 = x_2$ direction, which is consistent with the shape of the kernel $K(x, 0)$.

3.5.2 Static Obstacles Modeled with Density Constraint

Here we provide a MFG problem where the the density moves while avoiding the obstacles, which is modeled using density constraint. We also include a small local interaction term in this example:

$$f_0(t, x, z) = \partial_z \mathbf{1}_{\underline{h}(x,t) \leq z \leq \bar{h}(x,t)} + \epsilon \log z, \quad \epsilon = 0.01,$$

$$\bar{h}(x, t) = 0, \bar{e}(x) = 0 \text{ for } x \in \Omega_{obs},$$

$$K(x, y) = 4\gamma_{\delta_-, \delta}(x_1 - y_1)\gamma_{\delta, \delta}(x_2 - y_2), \quad \delta = 0.1, \delta_- = 0.4$$

As for the initial-terminal conditions, we have

$$\rho_0(x) = \frac{1}{2}\mathcal{N}([-0.8, 0.5], 0.1^2) + \frac{1}{2}\mathcal{N}([-0.8, 0.5], 0.1^2)$$

$$g(x) = x_1^2 + (x_2 - 0.85)^2 - 2e^{-10(x_2 - 0.75)^2}.$$

68
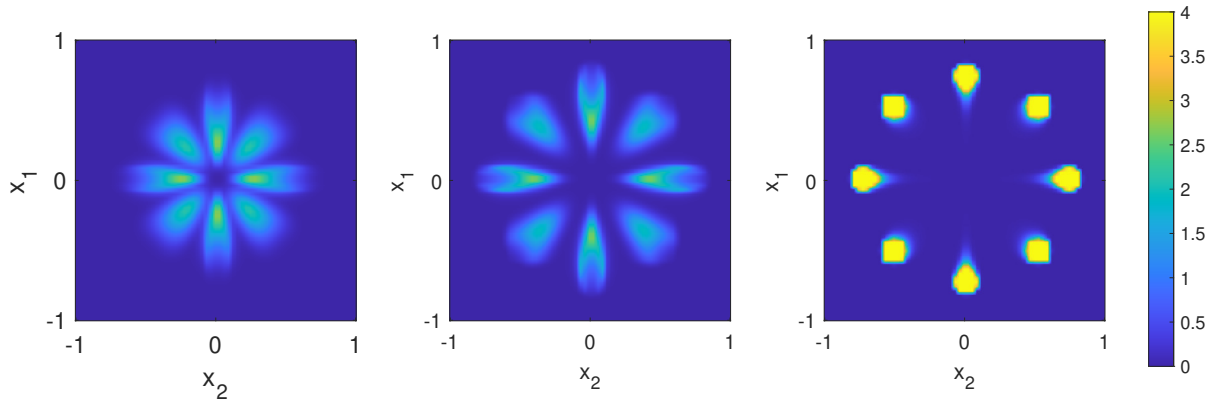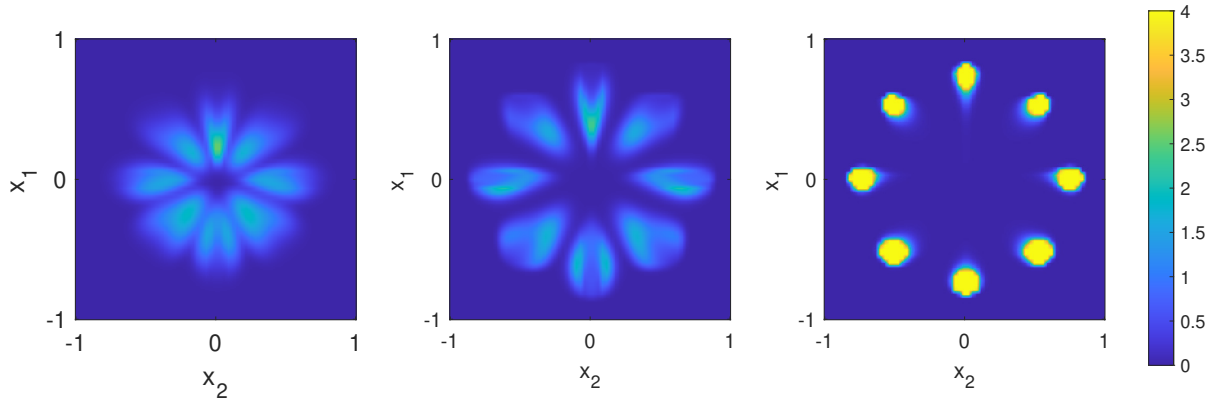
(a) Symmetric kernel

(b) Asymmetric kernel
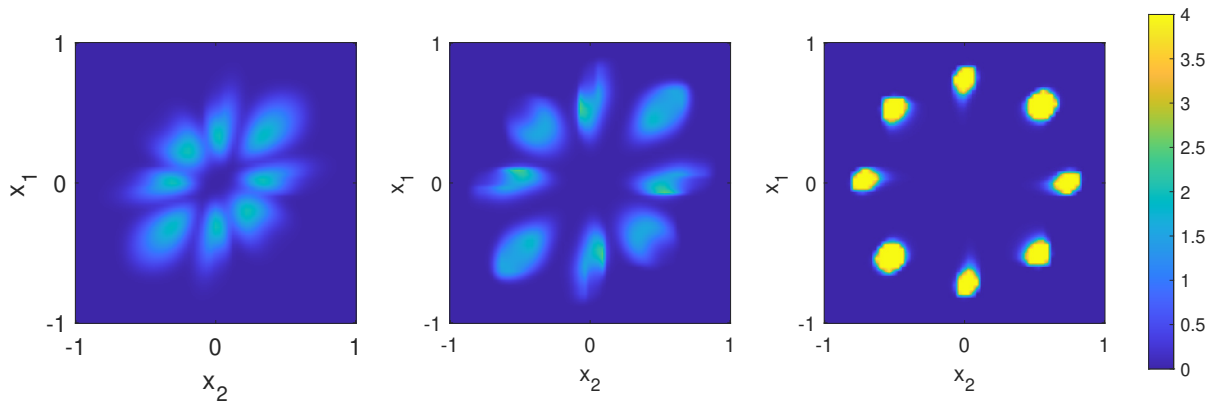
(c) Asymmetric kernel (coordination transform)

Figure 3.2: MFG solution $\rho(x, 0.3), \rho(x, 0.6), \rho(x, 1)$ for density splitting examples.

Under above setup, we consider the following 2 cases: case A, $\bar{h}(x,t) = 20$; case B, $\bar{h}(x,t) = 10$ for all $(x,t), x \notin \Omega_{obs}$.
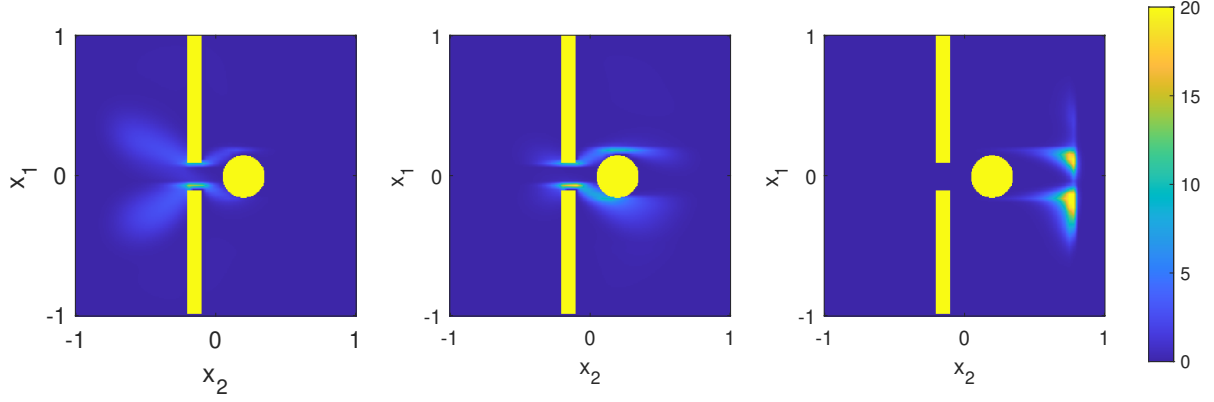
(a) $\bar{h}(x,t) = 20$
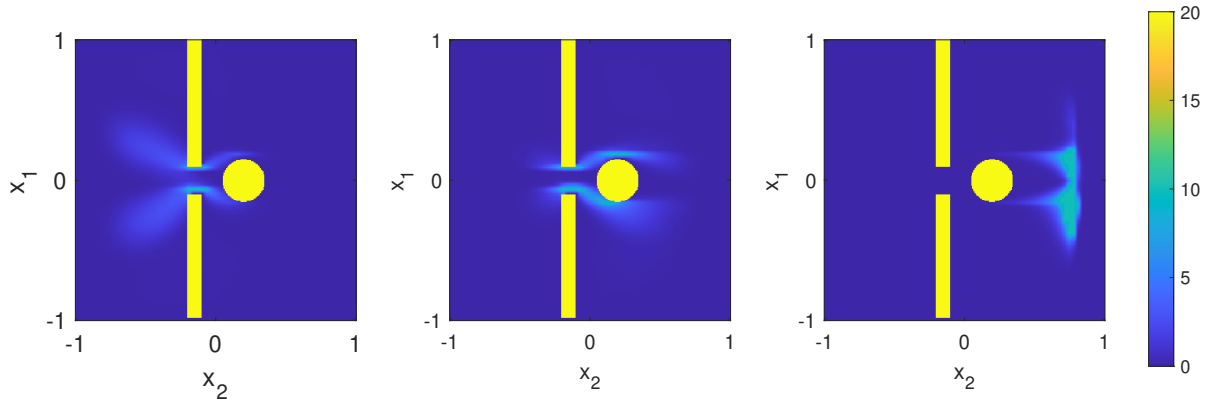
(b) $\bar{h}(x,t) = 10$

Figure 3.3: MFG solution $\rho(x,0.3), \rho(x,0.6), \rho(x,1)$ for static obstacles examples, where the obstacle (yellow) is located at $\Omega_{obs} = \{\|x - [0,0.2]\|^2 \leq 0.15^2\} \cup \{|x_1| \geq 0.1, |x_2 + 0.15| \leq 0.05\}$

The numerical results are shown in Figure 3.3. As we see the density moves from left to the right and avoids both the rectangle and round obstacles. It avoids the round obstacles via an uneven splitting, which is caused by the asymmetric kernel. Comparing Case A and B, we see that the density constraint make the agents spread more. We present 3D plots of final density distribution for both cases in Figure 3.4

70
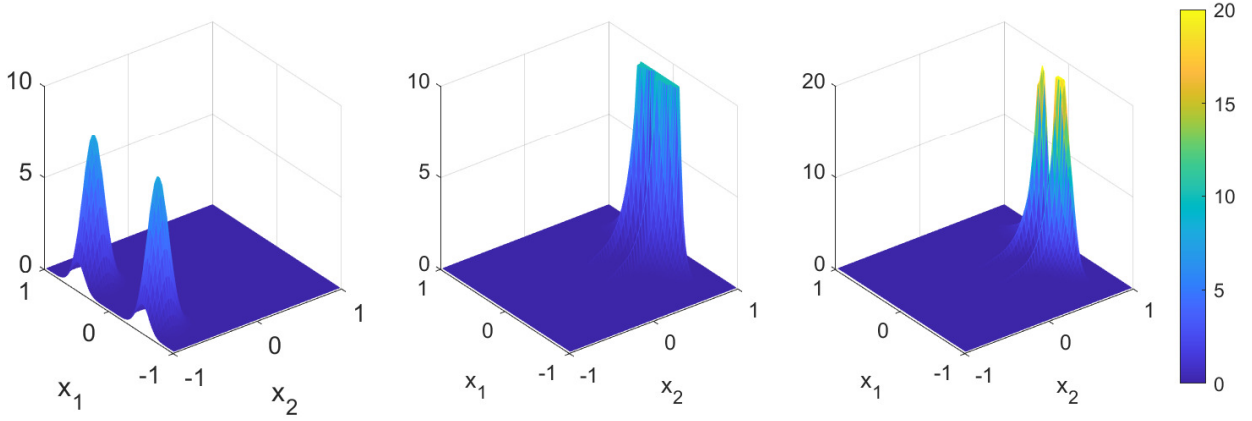
Figure 3.4: 3D plots of example 5.2. From left to right: initial density distribution; final density distribution for Case A; final density distribution for Case B

3.5.3 Dynamic Obstacles Modeled with Density constraint

In the last example, we model an Optimal-Transport-like problem with dynamic obstacles via density constraint. Our mean field game system is as follows:

$$K(x, y) = \exp\left(-\frac{\|x - y\|^2}{2\delta^2}\right), \quad \delta = 0.1$$

$$\rho_0(x) = \sum_{j=1}^{5} \frac{1}{5}\mathcal{N}(x_j, 0.1^2), \text{for } x_j = [-0.9 + 0.3j, -0.85]$$

$$g(x) = x_1^2 + 5|x_2 - 0.85|^{1.5}.$$

We use the density constraint $\bar{h}(x, t)$ to model 4 rectangles moving vertically. As for the density constraint at final time, we choose $\underline{e}(x)$ to be exactly a density distribution. Specifically,

$$\underline{e}(x) = c_e, \text{ for } \|x - x_j\| \leq 0.08, \text{ for } x_j = [-0.9 + 0.3j, 0.85], j = 1...5,$$

where c_e is a constant that normalized $\underline{e}(x)$. This setup is equivalent to specifying the final density distribution $\rho(x, 1) = \underline{e}(x)$. This is case A that is shown in Figure 3.5.

We also relax the density constraint at $t = 1$, by setting

$$\underline{e}(x) = \frac{1}{2}c_e, \text{ for } \|x - x_j\| \leq 0.08, \text{ for } x_j = [-0.9 + 0.3j, 0.85], j = 1...5.$$

71
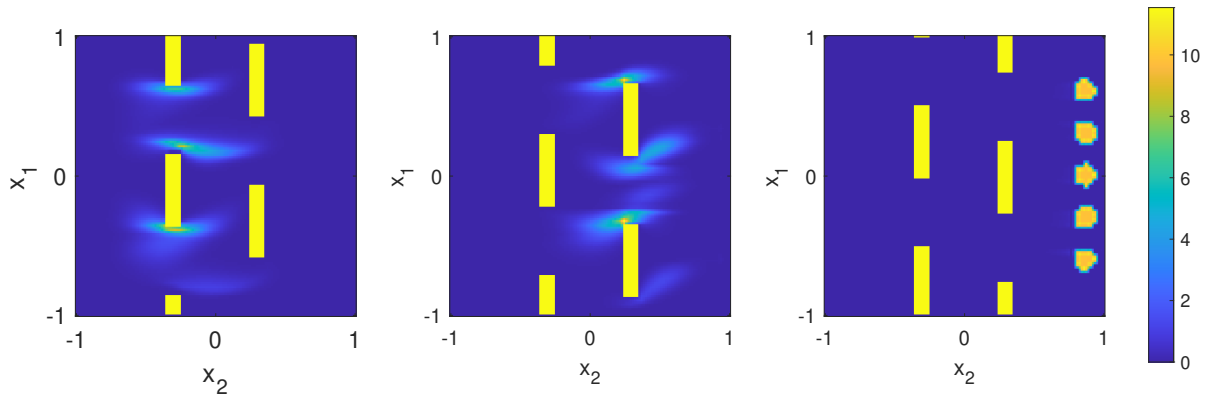
(a) $\underline{e}(x) = c_e$
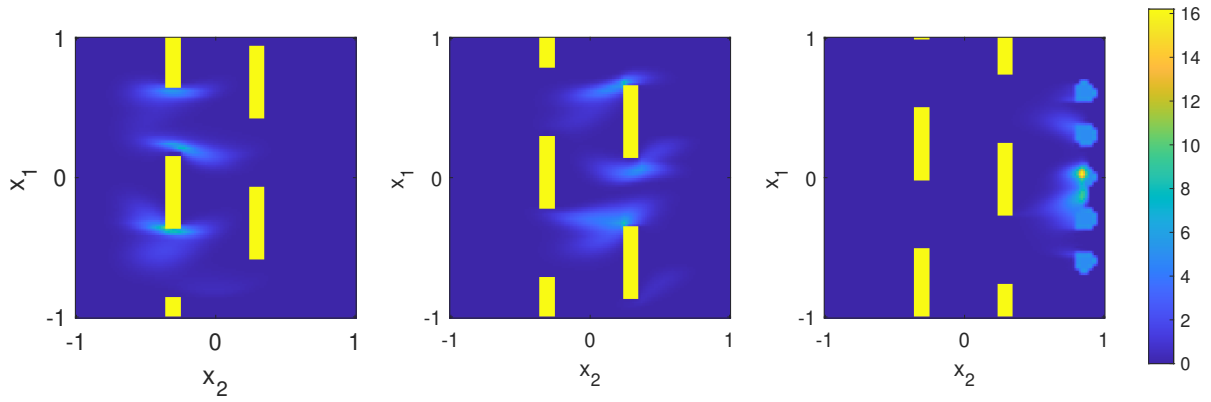
(b) $\underline{e}(x) = \frac{1}{2} c_e$

Figure 3.5: MFG solution $\rho(x, 0.3), \rho(x, 0.6), \rho(x, 1)$ for dynamic obstacles examples.

That is, we decrease the lower bound of $\rho(x, 1)$ by half. This is Case B shown in Figure 3.5. As we can see, unlike case A, the agents do not completely fill the support of $\underline{e}(x)$. The aspect of modeling dynamic obstacles also works well as agents avoid the prohibited regions.

3.5.4 Acceleration of PDHG

To accelerate the convergence of PDHG, we have modified the algorithm following the idea of balance residual and the adaptive PDHG from [GLY13]. To show the improvement, we conduct the following experiment. We initiate a pair of stepsizes (τ_0, σ_0) that guarantee the convergence of the algorithm. During the PDHG iteration, we update the step sizes by (τ_k, σ_k) according to Algorithm 2 in [GLY13]. We obtain faster convergence in terms of primal-dual residuals p_k, d_k as defined in [GLY13]. In Table 3.1, we present the number of iterations required to satisfy the stopping criteria $p_k, d_k < \epsilon$. We run examples for a set of (τ_0, σ_0) values and report the best number of iterations achieved. We see that the adaptive PDHG shows better performance than the PDHG with constant stepsizes.

Table 3.1: Comparison of adaptive PDHG and PDHG

ϵ	1.00e-3	1.00e-4	1.00e-5	1.00e-6	1.00e-7
PDHG	393	955	3030	9108	>2e4
adaptive PDHG	295	701	2033	6200	17842

CHAPTER 4

Controlling Propagation of Epidemics via Mean-field Controls

In this chapter, we focus on modeling perspective of mean field controls. We introduce a mean-field control model in controlling the propagation of epidemics on a spatial domain. The control variable, the spatial velocity, is first introduced for the classical disease models, such as the SIR model. For this proposed model, we provide fast numerical algorithms based on proximal primal-dual methods. Numerical experiments demonstrate that the proposed model illustrates how to separate infected patients in a spatial domain effectively.

This chapter is organized as follows. We review studies on epidemic models, especially recent ones on COVID-19 in Section 4.1. In Section 4.2, we introduce the mean field control model for propagation of epidemics. We introduce a primal-dual hybrid gradient algorithm for this model in Section 4.3. In Section 4.4, several numerical examples are demonstrated. We discuss some potential directions in Section 4.5.

The contributions in this chapter were presented in the joint work with Wonjun Lee, Hamidou Tembine, Wuchen Li, and Stanley Osher in[LLT21].

4.1 Introduction

The outbreak of COVID-19 epidemic has resulted in over millions of confirmed cases and hundred thousands of deaths globally. It has a huge impact on global economy as well as everyone's daily life. There has been a lot of interest in modeling the dynamics and

propagation of the epidemic. One of the well-known and basic models in epidemiology is the SIR model proposed by Kermack and McKendrick [KM27] in 1927. Here, S, I, R represent the number of susceptible, infected and recovered people respectively. They use an ODE system to describe the transmission dynamics of infectious diseases among the population. As the propagation of COVID-19 has significant spatial characteristic, actions such as travel restrictions, physical distancing and self-quarantine are taken to slow down the spread of the epidemic. It is important to have a spatial-type SIR model to study the spread of the infectious disease and movement of individuals [Ken65, Kal84, HI95].

Since the epidemic has affected the society and individuals significantly, mean-field controls (MFC) provide a perspective to study and understand the underlying population dynamics.

In this chapter, we combine the above ideas of spatial SIR model and MFG. In other words, we introduce a mean-field control model for controlling the virus spreading within a spatial domain. Here the goal is to minimize the number of infectious agents and the amount of movement of the population. In short, we formalize the following constrained optimization problem

$$\inf_{(\rho_i, v_i)_{i \in \{S,I,R\}}} \quad E(\rho_I(T, \cdot)) + \int_0^T \int_\Omega \sum_{i \in \{S,I,R\}} \frac{\alpha_i}{2} \rho_i \|v_i\|^2 + \frac{c}{2}(\rho_S + \rho_I + \rho_R)^2 dx dt$$

subject to

$$\begin{cases} \partial_t \rho_S + \nabla \cdot (\rho_S v_S) + \beta \rho_S \rho_I - \frac{\eta_S^2}{2} \Delta \rho_S = 0 \\[2mm] \partial_t \rho_I + \nabla \cdot (\rho_I v_I) - \beta \rho_S \rho_I + \gamma \rho_I - \frac{\eta_I^2}{2} \Delta \rho_I = 0 \\[2mm] \partial_t \rho_R + \nabla \cdot (\rho_R v_R) - \gamma \rho_I - \frac{\eta_R^2}{2} \Delta \rho_R = 0 \\[2mm] \rho_S(0, \cdot), \rho_I(0, \cdot), \rho_R(0, \cdot) \text{ are given.} \end{cases}$$

Here ρ_i represents population density and v_i describes the movement, with $i \in \{S, I, R\}$ corresponding to the susceptible, infected and recovered compartmental state or class. We consider the spatial SIR model with nonlocal spreading modeled by an integration kernel K representing the physical distancing and a spatial diffusion of population, and set it as dynamic

to our mean-field control problem, which is the constraint to the minimization problem. The minimization objective include both the movement and the congestion of the population. The kinetic energy terms describes the situation that, if population (the susceptible, infected or recovered) needs to be moved to alleviate local medical shortage, there is a cost behind it. The congestion term models the fact that government don't want the population gets too concentrated in one place. This might increase the risk of disease outbreaks and their faster and wider spread. Note that Kendall [Ken65] introduced this kernel for modeling pandemic dynamics and took the nonlocal exposure to infectious agents into consideration. Due to the multiplicative nature of the interaction term between susceptible and infectious agents $\beta \rho_S \rho_I$, the mean-field control problem is a non-convex problem. With Lagrange multipliers, we formalize the mean-field control problem as an unconstrained optimization problem. Fast numerical algorithms are designed to solve the non-convex optimization problem in $2D$ with $G - prox$ preconditioning [JLL19].

In the literature, spatial SIR models in the form of a nonlinear integro-differential [Aro77, Die79, Thi77] and reaction-diffusion system [Kal84, HI95] have been studied. Traveling waves are studied to understand the propagation of various type of epidemics, such as Lyme disease, measles etc, and recently, COVID-19 [CGC02, GBK01, WW10, BRR20]. In [BRR20], they introduce a SIRT model to study the effects of the presence of a road on the spatial propagation of the epidemic. For surveys, see [Mur01, Rua07]. As for numerical modelling of epidemic model concerning spatial effect, finite-difference methods are used to discretize the reaction-diffusion system and solve the spatial SIR model and its various extensions [CC10, JC14, FH16]. Epidemic models have been treated using optimal control theory, with major control measures on medicare (vaccination) [SS78, LES18, JKL20]. In [JKL20], a feedback control problem of SIR model is studied to help determine the vaccine policy, with the goal to minimize the number of infected people. In [LZM19], they introduce a nonlinear SIQS epidemic model on complex networks and study the optimal quarantine control. Compared to previous works, our model is the first to consider an optimal control

problem for SIR on a spatial domain. In particular, we formulate velocity fields among S, I, R, populations as control variables.

4.2 Models

In this section, we briefly review the classical epidemics models, e.g. SIR dynamics. We then introduce a mean field control model for SIR dynamics on a spatial domain. We derive a system to find the minimizer of the proposed model.

4.2.1 Review

We first review the classical SIR model.

$$\begin{cases} \dfrac{dS}{dt} = -\beta SI \\ \dfrac{dI}{dt} = \beta SI - \gamma I \\ \dfrac{dR}{dt} = \gamma I \end{cases}$$

where S, I,$R :\ [0,T] \to [0,1]$ represent the proportion of the susceptible population, infected population, and recovered population, respectively, given time t. The nonnegative constants β and γ represent the rates of susceptible becoming infected and infected becoming recovered. SIR has an interpretation in terms of stochastic processes of agent-based models. The SIR model can be obtained as a motion of the law of a three-state Markov chain with the transition from S to I and I to R. The simplicity of this model allows people to predict an infectious disease epidemic by only estimating a few parameters. However, it has limitations by assuming the population is homogeneous-mixing, which means that every individual has an equal probability of disease-causing contact. As a result, the predictions will lack spatial information and may not help the (local) governments make policies or relocate medical resources. Therefore, we are motivated to study the spatial SIR model. On the other hand, the SIR model does not consider the latent period between when a person is exposed to

a disease and when they become infected. This leads to the extension of the SIR model, such as the SEIR model. Our proposed model has a flexible structure and can naturally be generalized to such epidemiological models.

4.2.2 Spatial SIR variational problem

We then consider the spatial dimension of the S, I, R functions. Let $\Omega \subset \mathbb{R}^d$ be a bounded domain. Consider the following functions

$$\rho_S, \rho_I, \rho_R : \ [0,T] \times \Omega \to \mathbb{R}_+, \quad (i \in \{S, I, R\})$$

Here, ρ_S, ρ_I, and ρ_R represent susceptible, infected, and recovered populations, respectively. We assume ρ_i for each $i \in \{S, I, R\}$ moves on a spatial domain with velocities v_i. We can describe these movements by continuity equations.

$$\begin{cases} \partial_t \rho_S + \nabla \cdot (\rho_S v_S) + \beta \rho_S \rho_I - \dfrac{\eta_S^2}{2} \Delta \rho_S = 0 \\[2mm] \partial_t \rho_I + \nabla \cdot (\rho_I v_I) - \beta \rho_S \rho_I + \gamma \rho_I - \dfrac{\eta_I^2}{2} \Delta \rho_I = 0 \\[2mm] \partial_t \rho_R + \nabla \cdot (\rho_R v_R) - \gamma \rho_I - \dfrac{\eta_R^2}{2} \Delta \rho_R = 0 \\[2mm] \rho_S(0, \cdot), \rho_I(0, \cdot), \rho_R(0, \cdot) \text{ are given.} \end{cases} \quad (4.2.1)$$

where $v_i : [0,T] \times \Omega \to \mathbb{R}^d \ (i \in \{S, I, R\})$ are vector fields that represent the velocity fields for $\rho_i \ (i \in \{S, I, R\})$ and nonnegative constants $\eta_i \ (i \in \{S, I, R\})$ are coefficients representing for viscosity terms. In addition, we will assume zero flux conditions by the Neumann boundary conditions. These systems of continuity equations satisfy the following equality:

$$\frac{\partial}{\partial t} \int_\Omega \rho_S(t, x) + \rho_I(t, x) + \rho_R(t, x) dx = 0,$$

i.e., the total mass of the populations will be conserved for all time.

Lastly, we introduce the proposed mean field control models. Consider the following

variational problem:

$$\inf_{(\rho_i, v_i)_{i \in \{S,I,R\}}} \quad E(\rho_I(T, \cdot)) + \int_0^T \int_\Omega \sum_{i \in \{S,I,R\}} \frac{\alpha_i}{2} \rho_i \|v_i\|^2 + \frac{c}{2}(\rho_S + \rho_I + \rho_R)^2 dx dt$$

subject to (4.2.1) with fixed initial densities.

Here E is a convex functional and α_i ($i \in \{S, I, R\}$) and c are nonnegative constants. The minimizers of the above variational problem will provide the optimal movements for each population while minimizing the terminal cost functional with respect to the infected population ρ_I. The last term in the running cost, $\frac{c}{2}(\rho_S + \rho_I + \rho_R)^2$, penalizes congestion of the total population.

We note that the function $(\rho_i, v_i) \mapsto \rho_i \|v_i\|^2$ is not convex. By introducing new variables $m_i := \rho_i v_i$, we convert the cost function to be convex.

$$\min_{\rho_i, v_i} \quad P(\rho_i, m_i)_{i \in \{S,I,R\}}$$

subject to

$$\begin{cases} \partial_t \rho_S + \nabla \cdot m_S + \beta \rho_S \rho_I - \dfrac{\eta_S^2}{2} \Delta \rho_S = 0 \\[2mm] \partial_t \rho_I + \nabla \cdot m_I - \beta \rho_S \rho_I + \gamma \rho_I - \dfrac{\eta_I^2}{2} \Delta \rho_I = 0 \\[2mm] \partial_t \rho_R + \nabla \cdot m_R - \gamma \rho_I - \dfrac{\eta_R^2}{2} \Delta \rho_R = 0 \\[2mm] \rho_S(0, \cdot), \rho_I(0, \cdot), \rho_R(0, \cdot) \text{ are given.} \end{cases}$$

Here

$$P(\rho_i, m_i)_{i \in \{S,I,R\}} = E(\rho_I(T, \cdot)) + \int_0^T \int_\Omega F(\rho_i, m_i)_{i \in \{S,I,R\}} dx dt$$

$$F(\rho_i, m_i)_{i \in \{S,I,R\}} = \frac{\alpha_S \|m_S\|^2}{2\rho_S} + \frac{\alpha_I \|m_I\|^2}{2\rho_I} + \frac{\alpha_R \|m_R\|^2}{2\rho_R} + \frac{c}{2}(\rho_S + \rho_I + \rho_R)^2.$$

From an optimization viewpoint, we note that the minimization problem is not a convex problem since the coupling terms, $\beta \rho_S \rho_I$, in constraints make the feasible set nonconvex. To regularize the nonconvex coupling term $\beta \rho_S \rho_I$, we replace products by convolutions.

$$\min_{(\rho_i, v_i)_{i \in \{S,I,R\}}} \quad P(\rho_i, m_i)_{i \in \{S,I,R\}}$$

subject to

$$
\begin{cases}
\partial_t \rho_S(t,x) + \nabla \cdot m_S(t,x) + \beta \rho_S(t,x) \int_\Omega K(x,y)\rho_I(t,y)dy - \dfrac{\eta_S^2}{2}\Delta\rho_S(t,x) = 0 \\[2mm]
\partial_t \rho_I(t,x) + \nabla \cdot m_I(t,x) - \beta \rho_I(x) \int_\Omega K(x,y)\rho_S(t,y)dy + \gamma\rho_I(t,x) - \dfrac{\eta_I^2}{2}\Delta\rho_I(t,x) = 0 \\[2mm]
\partial_t \rho_R(t,x) + \nabla \cdot m_R(t,x) - \gamma\rho_I(t,x) - \dfrac{\eta_R^2}{2}\Delta\rho_R(t,x) = 0 \\[2mm]
\rho_S(0,\cdot), \rho_I(0,\cdot), \rho_R(0,\cdot) \text{ given.}
\end{cases}
$$

Here $K(x,y)$ is a symmetric positive definite kernel representing the physical distancing between a susceptible agent located at position x and infectious agent at position y, and $\int_\Omega K(x,y)\rho_I(t,y)dy$ is the exposure of a susceptible located at x to infectious agents. Here, we focus on a Gaussian kernel

$$
K(x,y) = \frac{1}{\sqrt{(2\pi)^d}} \prod_{k=1}^{d} \frac{1}{\sigma_k} \exp\left(-\frac{|x_k - y_k|^2}{2\sigma_k^2} \right).
$$

In modeling, the variance σ of Gaussian kernel can be viewed as a parameter for modeling the spatial spreading effect of virus.

Remark 15. *The formulation is not limited to the SIR model. It can be used to solve any types of spatial epidemiological models.*

4.2.3 Properties

We next derive the mean field game system, i.e. the minimizer system associated with spatial SIR variational problem (4.2.3).

Define the Lagrangian functional

$$
\begin{aligned}
&\mathcal{L}((\rho_i, m_i, \phi_i)_{i\in\{S,I,R\}}) \\
&= P(\rho_i, m_i)_{i\in\{S,I,R\}} - \int_0^T \int_\Omega \sum_{i\in\{S,I,R\}} \phi_i\left(\partial_t\rho_i + \nabla\cdot m_i - \frac{\eta_i^2}{2}\Delta\rho_i\right)dxdt \\
&\quad + \int_0^T \int_\Omega \beta\phi_I\rho_I K * \rho_S - \beta\phi_S\rho_S K * \rho_I + \gamma\rho_I(\phi_R - \phi_I)dxdt.
\end{aligned}
$$

80

Using this Lagrangian functional, we convert the minimization problem into a saddle problem.

$$\inf_{(\rho_i, m_i)_{i \in \{S, I, R\}}} \sup_{(\phi_i)_{i \in \{S, I, R\}}} \mathcal{L}((\rho_i, m_i, \phi_i)_{i \in \{S, I, R\}}). \tag{4.2.4}$$

Because of the nonconvex functional $(\rho_S, \rho_I) \mapsto \rho_S \rho_I$, the feasible set here is nonconvex. Thus, we cannot guarantee that the dual gap is zero for this problem. Swapping infimum and supremum will only provide us a lower bound for the minimization problem. Here we hope that we can gain good information from the bound.

$$\inf_{(\rho_i, m_i)_{i \in \{S, I, R\}}} \sup_{(\phi_i)_{i \in \{S, I, R\}}} \mathcal{L}((\rho_i, m_i, \phi_i)_{i \in \{S, I, R\}}) \geq \sup_{\phi_i} \inf_{(\rho_i, m_i)_{i \in \{S, I, R\}}} \mathcal{L}((\rho_i, m_i, \phi_i)_{i \in \{S, I, R\}}).$$

The following propositions are the properties of the saddle point problem derived from optimality conditions (Karush-Kuhn-Tucker (KKT) conditions).

Proposition 3 (Mean field game SIR system). *By KKT conditions, the saddle problem (4.2.4) satisfies the following equations.*

$$\begin{cases}
\partial_t \phi_S - \dfrac{\alpha_S}{2}|\nabla \phi_S|^2 + \dfrac{\eta_S^2}{2}\Delta \phi_S + c(\rho_S + \rho_I + \rho_R) + \beta\left(K * (\phi_I \rho_I) - \phi_S K * \rho_I\right) = 0 \\[2mm]
\partial_t \phi_I - \dfrac{\alpha_I}{2}|\nabla \phi_I|^2 + \dfrac{\eta_I^2}{2}\Delta \phi_I + c(\rho_S + \rho_I + \rho_R) \\[2mm]
\qquad\qquad\qquad + \beta\left(\phi_I K * \rho_S - K * (\phi_S \rho_S)\right) + \gamma \rho(\phi_R - \phi_I) = 0 \\[2mm]
\partial_t \phi_R - \dfrac{\alpha_R}{2}|\nabla \phi_R|^2 + \dfrac{\eta_R^2}{2}\Delta \phi_R + c(\rho_S + \rho_I + \rho_R) = 0 \\[2mm]
\partial_t \rho_S - \dfrac{1}{\alpha_S}\nabla \cdot (\rho_S \nabla \phi_S) + \beta \rho_S K * \rho_I - \dfrac{\eta_S^2}{2}\Delta \rho_S = 0 \\[2mm]
\partial_t \rho_I - \dfrac{1}{\alpha_I}\nabla \cdot (\rho \nabla \phi_I) - \beta \rho_I K * \rho_S + \gamma \rho_I - \dfrac{\eta_I^2}{2}\Delta \rho_I = 0 \\[2mm]
\partial_t \rho_R - \dfrac{1}{\alpha_R}\nabla \cdot (\rho \nabla \phi_R) - \gamma \rho_I - \dfrac{\eta_R^2}{2}\Delta \rho_R = 0.
\end{cases} \tag{4.2.5}$$

where $\rho_S(0, \cdot), \rho_I(0, \cdot), \rho_R(0, \cdot)$ are given and

$$\phi_I(T, x) = \delta E(\rho_I(T, x)).$$

Proof. Via integration by parts, we reformulate the Lagrangian function (4.2.4) as follows.

$$L((\rho_i, m_i, \phi_i)_{i \in \{S,I,R\}})$$

$$= E(\rho_I(T, \cdot)) + \int_0^T \int_\Omega \beta \phi_I \rho_I K * \rho_S - \beta \phi_S \rho_S K * \rho_I + \gamma \rho_I (\phi_R - \phi_I) dxdt$$

$$+ \sum_{i \in \{S,I,R\}} \int_0^T \int_\Omega \frac{\alpha_i \|m_i\|^2}{2\rho_i} + \rho_i \partial_t \phi_i + m_i \cdot \nabla \phi_i + \frac{\eta_i^2}{2} \rho_i \Delta \phi_i + \frac{c}{2}(\rho_S + \rho_I + \rho_R)^2 dxdt$$

$$+ \sum_{i \in \{S,I,R\}} \int_\Omega \rho_i(0, x) \phi_i(0, x) - \rho_i(T, x) \phi_i(T, x) dx$$

Let the differential of Lagrangian with respect to ρ_i, m_i, ϕ_i ($i \in \{S, I, R\}$), $\rho_I(T, \cdot)$, equal to zero. We have

$$\begin{cases} \dfrac{\delta}{\delta \rho_i} L = 0 \\ \dfrac{\delta}{\delta m_i} L = 0 \\ \dfrac{\delta}{\delta \phi_i} L = 0. \end{cases}$$

Hence $-\nabla \phi_i = \alpha_i \frac{m_i}{\rho_i}$. And we derive the result. ∎

We note that dynamical system (4.2.5) models the optimal vector field strategies for S,I,R populations. It combines both strategies from mean field games and SIR models. For this reason, we call (4.2.5) *Mean field game SIR system.*

4.3 Algorithm

In this section, we implement optimization methods to solve the proposed SIR variational problems. Specifically, we use G-Prox Primal Dual Hybrid Gradient (G-Prox PDHG) method [JLL19]. This is a variation of Chambolle-Pock primal-dual algorithm [CP11, CP16].

4.3.1 Review of primal-dual algorithms

The PDHG method solves the minimization problem

$$\min_x f(Ax) + g(x)$$

by converting it into a saddle point problem

$$\min_x \sup_y \left\{ L(x,y) := \langle Ax, y \rangle + g(x) - f^*(y) \right\}.$$

Here, f and g are convex functions with respect to a variable x, A is a continuous linear operator, and

$$f^*(y) = \sup_x x \cdot y - f(x)$$

is a Legendre transform of f. For each iteration, the algorithm finds the minimizer x_* by gradient descent method and the maximizer y_* by gradient ascent method. Thus, the minimizer and maximizer are calculated by iterating

$$\begin{cases} x^{k+1} &= \operatorname{argmin}_x L(x, y^k) + \frac{1}{2\tau} \|x - x^k\|^2 \\ y^{k+1} &= \operatorname{argmax}_y L(x^{k+1}, y) + \frac{1}{2\sigma} \|y - y^k\|^2 \end{cases}$$

where τ and σ are step sizes for the algorithm.

Here G-Prox PDHG is a modified version of PDHG that solves the minimization problem by choosing the most appropriate norms for updating x and y. Choosing the appropriate norms allows us to choose larger step sizes. Hence, we get a faster convergence rate. In details,

$$\begin{cases} x^{k+1} &= \operatorname{argmin}_x L(x, y^k) + \frac{1}{2\tau} \|x - x^k\|_{\mathcal{H}}^2 \\ y^{k+1} &= \operatorname{argmax}_y L(x^{k+1}, y) + \frac{1}{2\sigma} \|y - y^k\|_{\mathcal{G}}^2 \end{cases}$$

where $\mathcal{H}$ and $\mathcal{G}$ are some Hilbert spaces with the inner product

$$(u_1, u_2)_{\mathcal{G}} = (Au_1, Au_2)_{\mathcal{H}}.$$

In particular, we use G-Prox PDHG to solve the minimization problem (4.2.3) by setting

$$x = (\rho_S, \rho_I, \rho_R, m_S, m_I, m_R), \quad g(x) = F(\rho_i, m_i)_{i \in \{S,I,R\}}, \quad f(Ax) = \begin{cases} 0 & \text{if } Ax = (0, 0, \gamma \rho_I) \\ \infty & \text{otherwise.} \end{cases}$$

$$Ax = (\partial_t \rho_S + \nabla \cdot m_S - \frac{\eta^2}{2} \Delta \rho_S + \beta \rho_S K * \rho_I,$$

$$\partial_t \rho_I + \nabla \cdot m_I - \frac{\eta^2}{2} \Delta \rho_I - \beta \rho_I K * \rho_S + \gamma \rho_I,$$

$$\partial_t \rho_R + \nabla \cdot m_R - \frac{\eta^2}{2} \Delta \rho_R).$$

Note that the operator A is not linear. In the implementation, we approximate the operator with the following linear operator

$$Ax \approx (\partial_t \rho_S + \nabla \cdot m_S - \frac{\eta^2}{2} \Delta \rho_S + \beta \rho_S,$$

$$\partial_t \rho_I + \nabla \cdot m_I - \frac{\eta^2}{2} \Delta \rho_I + (\gamma - \beta) \rho_I,$$

$$\partial_t \rho_R + \nabla \cdot m_R - \frac{\eta^2}{2} \Delta \rho_R).$$

4.3.2 G-Prox PDHG on SIR variational problem

In this section, we implement G-Prox PDHG to solve the saddle problem (4.2.4). For $i \in \{S, I, R\}$,

$$\rho_i^{(k+1)} = \operatorname*{argmin}_{\rho} \mathcal{L}(\rho, m_i^{(k)}, \phi_i^{(k)}) + \frac{1}{2\tau_i} \|\rho - \rho_i^{(k)}\|_{L^2}^2$$

$$m_i^{(k+1)} = \operatorname*{argmin}_{m} \mathcal{L}(\rho^{(k+1)}, m, \phi_i^{(k)}) + \frac{1}{2\tau_i} \|m - m_i^{(k)}\|_{L^2}^2$$

$$\phi_i^{(k+\frac{1}{2})} = \operatorname*{argmax}_{\phi} \mathcal{L}(\rho^{(k+1)}, m_i^{(k+1)}, \phi) - \frac{1}{2\sigma_i} \|\phi - \phi_i^{(k)}\|_{H^2}^2$$

$$\phi_i^{(k+1)} = 2\phi_i^{(k+\frac{1}{2})} - \phi_i^{(k)}$$

where τ_i, σ_i ($i \in \{S, I, R\}$) are step sizes for the algorithm and by G-Prox PDHG, L^2 norm and H^2 norm are defined as

$$\|u\|_{L^2} = \int_0^T \int_\Omega u(t, x)^2 dx dt$$

$$\|u\|_{H^2} = \int_0^T \int_\Omega (\partial_t u)^2 + \|\nabla u\|^2 + \frac{\eta^4}{4}(\Delta u)^2 dx dt$$

for any $u : [0,T] \times \Omega \to [0,1]$.

By formulating these optimality conditions, we can find explicit formulas for each variable.

$$\rho_S^{(k+1)} = root_+ \left(\frac{\tau_S}{1+c\tau_S} \left(\partial_t \phi_S^{(k)} + \frac{\eta_S^2}{2} \Delta \phi_S^{(k)} - \frac{1}{\tau_S} \rho_S^{(k)} + \beta \left(K * (\phi_I^{(k)} \rho_I^{(k)}) - \phi_S^{(k)} K * \rho_I^{(k)} \right) \right. \right.$$
$$\left. \left. + c(\rho_I + \rho_R) \right), 0, -\frac{\tau_S \alpha_S (m_S^{(k)})^2}{2(1+c\tau_S)} \right)$$

$$\rho_I^{(k+1)} = root_+ \left(\frac{\tau_I}{1+c\tau_I} \left(\partial_t \phi_I^{(k)} + \frac{\eta_I^2}{2} \Delta \phi_I^{(k)} - \frac{1}{\tau_I} \rho_I^{(k)} + \beta \left(\phi_I^{(k)} K * \rho_S^{(k)} - K * (\phi_S^{(k)} \rho_S^{(k)}) \right) \right. \right.$$
$$\left. \left. + \gamma(\phi_R - \phi_I) + c(\rho_S + \rho_R) \right), 0, -\frac{\tau_I \alpha_I (m_I^{(k)})^2}{2(1+c\tau_I)} \right)$$

$$\rho_R^{(k+1)} = root_+ \left(\frac{\tau_R}{1+c\tau_R} \left(\partial_t \phi_R^{(k)} + \frac{\eta_R^2}{2} \Delta \phi_R^{(k)} - \frac{1}{\tau_R} \rho_R^{(k)} + c(\rho_S + \rho_I) \right), 0, -\frac{\tau_R \alpha_R (m_R^{(k)})^2}{2(1+c\tau_R)} \right)$$

$$m_i^{(k+1)} = \frac{\rho_i^{(k+1)}}{\tau \alpha_i + \rho_i^{(k+1)}} \left(m_i^{(k)} - \tau \nabla \phi_i^{(k)} \right), \qquad (i \in \{S, I, R\})$$

$$\phi_S^{(k+1)} = \phi_S^{(k)} + \sigma_S (A_S^T A_S)^{-1} \left(-\partial_t \rho_S^{(k+1)} - \nabla \cdot m_S^{(k+1)} - \beta \rho_S^{(k+1)} K * \rho_I^{(k+1)} + \frac{\eta_S^2}{2} \Delta \rho_S^{(k+1)} \right)$$

$$\phi_I^{(k+\frac{1}{2})} = \phi_I^{(k)} + \sigma_I (A_I^T A_I)^{-1} \left(-\partial_t \rho_I^{(k+1)} - \nabla \cdot m_I^{(k+1)} + \beta \rho_I^{(k+1)} K * \rho_S^{(k+1)} \right.$$
$$\left. - \gamma \rho_I^{(k+1)} + \frac{\eta_I^2}{2} \Delta \rho_I^{(k+1)} \right)$$

$$\phi_R^{(k+\frac{1}{2})} = \phi_R^{(k)} + \sigma_R (A_R^T A_R)^{-1} \left(-\partial_t \rho_R^{(k+1)} - \nabla \cdot m_R^{(k+1)} + \gamma \rho_I^{(k+1)} + \frac{\eta_R^2}{2} \Delta \rho_R^{(k+1)} \right)$$

where $root_+(a,b,c)$ is a positive root of a cubic polynomial $x^3 + ax^2 + bx + c = 0$ and

$$A_S^T A_S = -\partial_{tt} + \frac{\eta_S^4}{4} \Delta^2 - (1 + 2\beta\eta_S)\Delta + \beta^2$$

$$A_I^T A_I = -\partial_{tt} + \frac{\eta_I^4}{4} \Delta^2 - (1 + 2(\gamma - \beta)\eta_S)\Delta + (\gamma - \beta)^2$$

$$A_R^T A_R = -\partial_{tt} + \frac{\eta_R^4}{4} \Delta^2 - \Delta.$$

We use FFTW library to compute $(A_i^T A_i)^{-1}$ $(i \in \{S, I, R\})$ by Fast Fourier Transform (FFT). Computing these inverse operators is $O(n \log n)$ operations per iteration where n is the number of points. Here calculation of convolution is also realized by FFT.

In all, we summarize the algorithm as follows.

Algorithm 1 Algorithm: G-proximal PDHG for mean field game SIR system

---

Input: $\rho_i(0, \cdot)$ $(i \in \{S, I, R\})$

Output: ρ_i, m_i, ϕ_i $(i \in \{S, I, R\})$ for $x \in \Omega$, $t \in [0, T]$

while relative error $>$ tolerance **do**

$$\rho_i^{(k+1)} = \mathrm{argmin}_\rho \, \mathcal{L}(\rho, m_i^{(k)}, \phi_i^{(k)}) + \frac{1}{2\tau_i} \|\rho - \rho_i^{(k)}\|_{L^2}^2$$

$$m_i^{(k+1)} = \mathrm{argmin}_m \, \mathcal{L}(\rho^{(k+1)}, m, \phi_i^{(k)}) + \frac{1}{2\tau_i} \|m - m_i^{(k)}\|_{L^2}^2$$

$$\phi_i^{(k+\frac{1}{2})} = \mathrm{argmax}_\phi \, \mathcal{L}(\rho^{(k+1)}, m_i^{(k+1)}, \phi) - \frac{1}{2\sigma_i} \|\phi - \phi_i^{(k)}\|_{H^2}^2$$

$$\phi_i^{(k+1)} = 2\phi_i^{(k+\frac{1}{2})} - \phi_i^{(k)}$$

end while

Here, the relative error is defined as

$$\text{relative error} = \frac{|P(\rho_i^{(k+1)}, m_i^{(k+1)}) - P(\rho_i^{(k)}, m_i^{(k)})|}{|P(\rho_i^{(k)}, m_i^{(k)})|}.$$

4.4   Numerical Experiments

In this section, we present two sets of numerical experiments using the algorithm with various parameters and all algorithms are coded in C++. Let $\Omega = [0, 1]^2$ be a unit cube in $\mathbb{R}^2$ and

$T = 1$. The domain Ω is discretized with the regular rectangular mesh

$$x_{kl} = \left(\frac{k + 0.5}{N_x}, \frac{l + 0.5}{N_y} \right), \quad k = 0, \cdots, N_x - 1, \quad l = 0, \cdots, N_y - 1$$

$$t_n = \frac{n}{N_t - 1}, \qquad n = 0, \cdots, N_t - 1.$$

where N_x, N_y are the number of data points in space and N_t is the number of data points in time. For all the experiments, we use the same set of parameters,

$$N_x = 128, \quad N_y = 128, \quad N_t = 32$$

$$\sigma = 0.01, \quad c = 0.01 \quad \beta = 0.7, \quad \eta_i = 0.01 \quad (i \in \{S, I, R\})$$

$$\alpha_S = 1, \quad \alpha_I = 10, \quad \alpha_R = 1$$

and a terminal cost functional

$$E(\rho_I(1, \cdot)) = \frac{1}{2} \int_\Omega \rho_I^2(1, x) dx.$$

By setting higher value for α_I, we penalize the movement of infected population more than other populations. Considering the immobility of infected individuals, this is a reasonable choice in terms of real-world applications.

To minimize the terminal cost functional $E(\rho_I)$, a solution needs to minimize the number of infected population. There are mainly two ways of reducing the number of infected. First way is to transition infected to recovered population. However, it may not be feasible if a rate of recovery γ is small. Another way to reduce the number of infected is by separating susceptible population from infected population. The number of infected doesn't increase if there are no susceptible people near infected. However, the total cost increases when densities move due to $\rho_i \|v_i\|^2$ ($i \in \{S, I, R\}$) terms in the running cost. A solution needs to find the optimal balance between the terminal cost and the running cost. The following two sets of experiments show that the algorithm finds the proper solutions based on values of γ given different initial densities.

4.4.1 Experiment 1

In this experiment, initial densities for susceptible, infected, and recovered populations are

$$\rho_S(0, x) = 0.5 \exp\left(-10\big((x_1 - 0.5)^2 + (x_2 - 0.5)^2\big)\right)$$

$$\rho_I(0, x) = 15\big(0.03 - (x_1 - 0.6)^2 - (x_2 - 0.6)^2\big)_+$$

$$\rho_R(0, x) = 0$$

where

$$(x)_+ = \begin{cases} x & \text{if } x > 0 \\ 0 & \text{otherwise.} \end{cases}$$

Susceptible population is a Gaussian distribution centered at $(0.5, 0.5)$ and infected population is concentrated at $(0.6, 0.6)$.

We show two different numerical results with a low rate of recovery $\gamma = 0.1$ (Figure 4.1) and a high rate of recovery $\gamma = 0.5$ (Figure 4.2). In both figures, the evolution of densties ρ_i $(i \in \{S, I, R\})$ are shown at $t = 0, 0.21, 0.47, 0.74, 1$. The total population of each density is indicated as sum in the subtitle of each plot.

When γ is small (Figure 4.1), the solution separates susceptible population from infected population. By separating susceptible from infected, the solution minimizes the terminal cost at $t = 1$. When γ is large (Figure 4.2), susceptible population barely moves over time. The solution minimizes the terminal cost by converting infected to recovered population which is considered to be cheaper than moving susceptible away from infected.

4.4.2 Experiment 2

In this experiment, initial densities for susceptible, infected, and recovered populations are

$$\rho_S(0, x) = 0.5$$

$$\rho_I(0, x) = 70\left(0.005 - \left(\sqrt{(x - 0.5)^2 + (y - 0.5)^2} - 0.25\right)^2\right)_+$$

$$\rho_R(0, x) = 0.$$
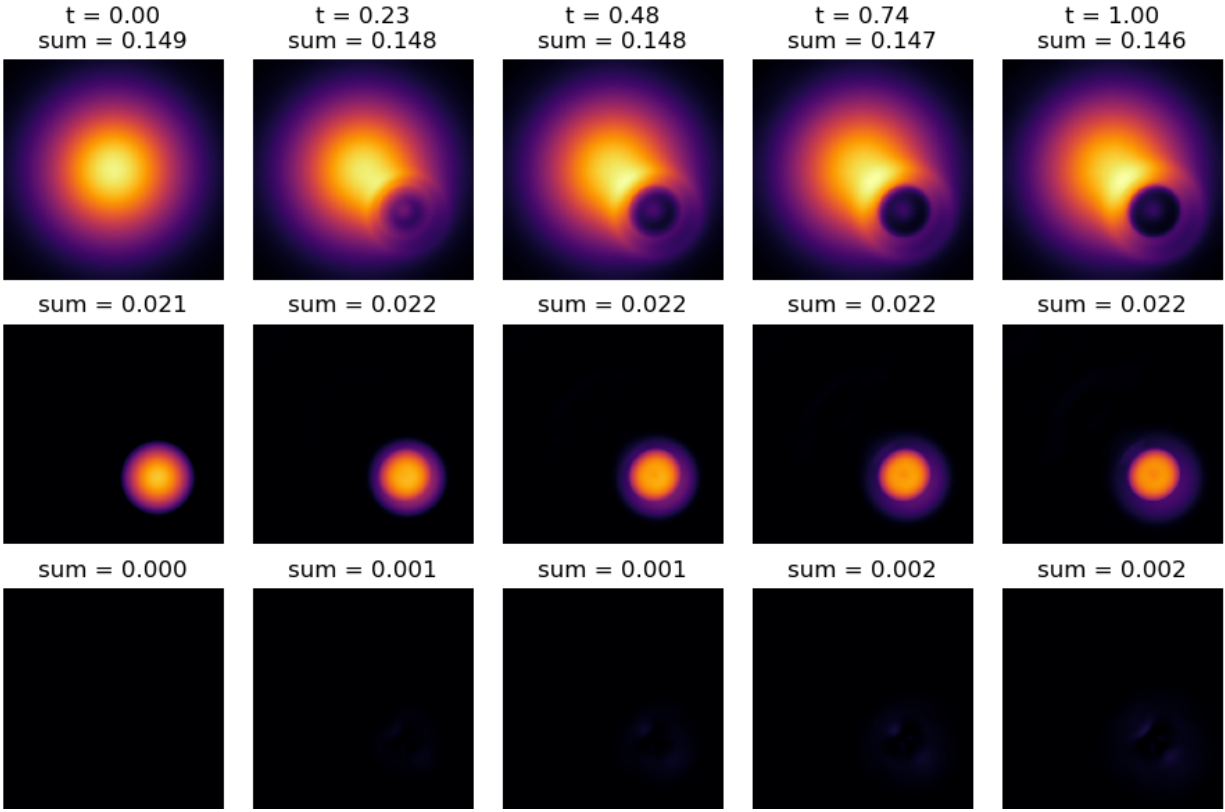
Figure 4.1: Experiment 1. The evolution of populations from $t = 0$ to $t = 1$ with $\beta = 0.7$ and $\gamma = 0.1$. The first row represents susceptible, the second row represents infected, and the last row represents recovered. The solution moves susceptible away from the infected over time.

Susceptible population is a uniform distribution on Ω and infected population is a ring shaped density centered at $(0.5, 0.5)$. We again show that two different numerical results with a low rate of recovery $\gamma = 0.1$ (Figure 4.3) and a high rate of recovery $\gamma = 0.5$ (Figure 4.4). Similar to Experiment 1, we see that the solution minimizes the number of infection by moving susceptible away from infected when γ is small. By separating these two populations, it minimizes the rate of contacts between susceptible and infected. When γ is large, the solution converts infected to recovered population rather than moving susceptible population.
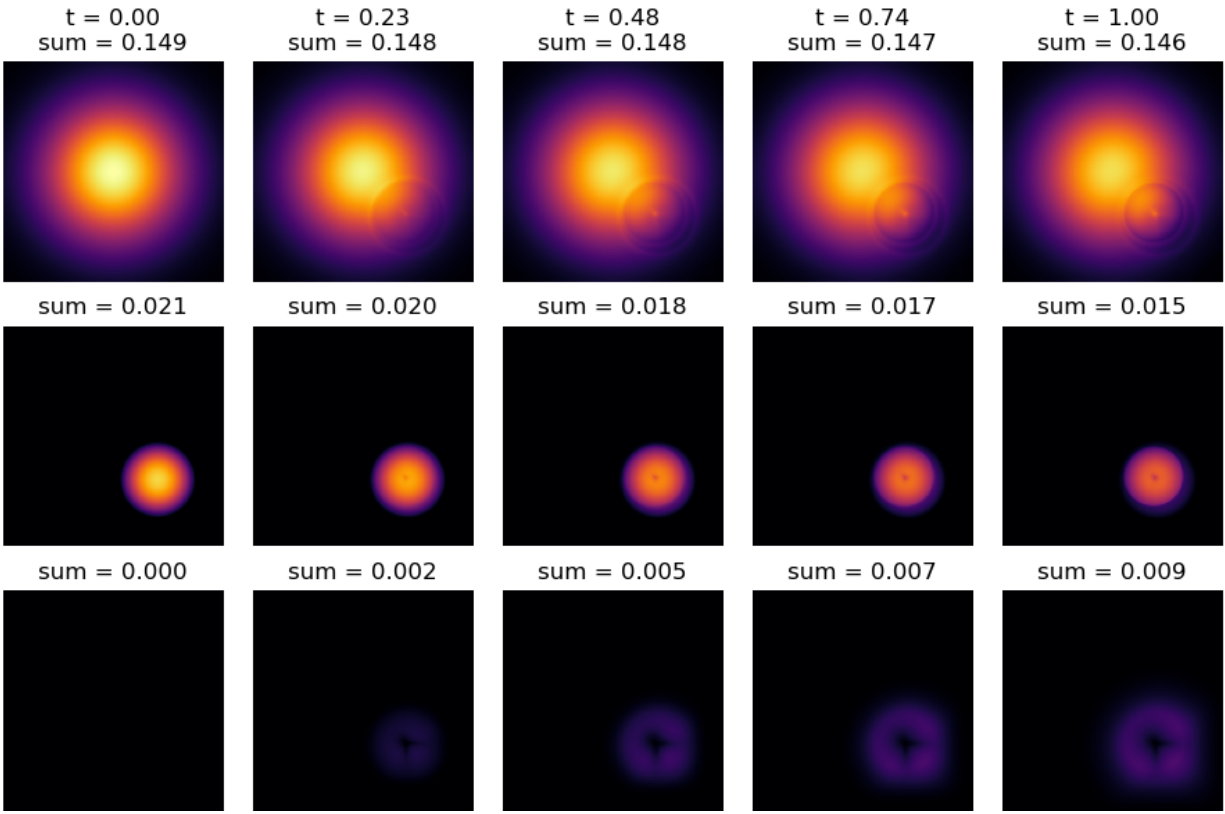
Figure 4.2: Experiment 1. The evolution of populations from $t = 0$ to $t = 1$ with $\beta = 0.7$ and $\gamma = 0.5$. The first row represents susceptible, the second row represents infected, and the last row represents recovered. The solution minimizes the number of infected at time $t = 1$ by recovering infected population.
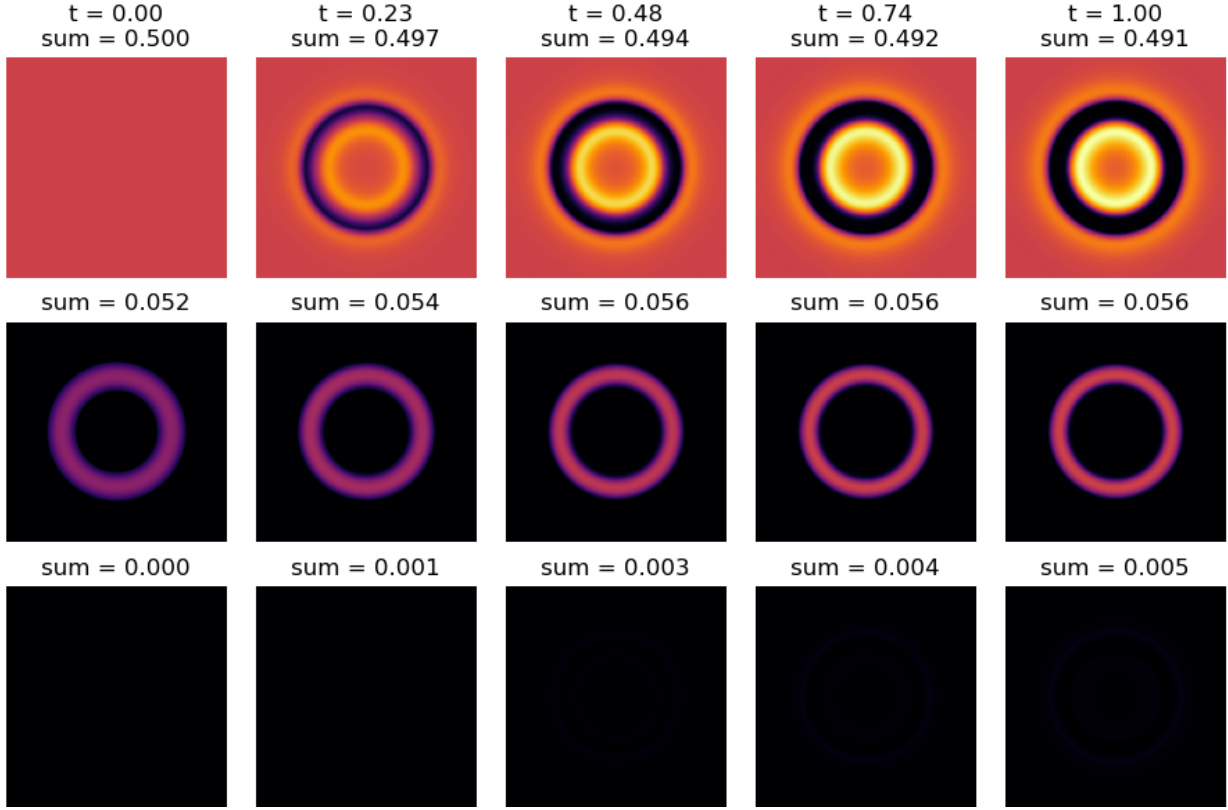
Figure 4.3: Experiment 2. The evolution of populations from $t = 0$ to $t = 1$ with $\beta = 0.7$ and $\gamma = 0.1$. The first row represents susceptible, the second row represents infected, and the last row represents recovered.

4.4.3 Experiment 3

In this experiment, we consider nonsymmetric initial densities.

$$\rho_S(0, x) = 0.45\Big(\exp\big(-15((x - 0.3)^2 + (y - 0.3)^2)\big)$$
$$+ \exp\big(-25((x - 0.5)^2 + (y - 0.75)^2)\big)$$
$$+ \exp\big(-30((x - 0.8)^2 + (y - 0.35)^2)\big)\Big)$$
$$\rho_I(0, x) = 10\big(0.04 - (x - 0.2)^2 - (y - 0.65)^2\big)_+$$
$$+ 12\big(0.03 - (x - 0.5)^2 - (y - 0.2)^2\big)_+$$
$$+ 12\big(0.03 - (x - 0.8)^2 - (y - 0.55)^2\big)_+$$
$$\rho_R(0, x) = 0.$$

91
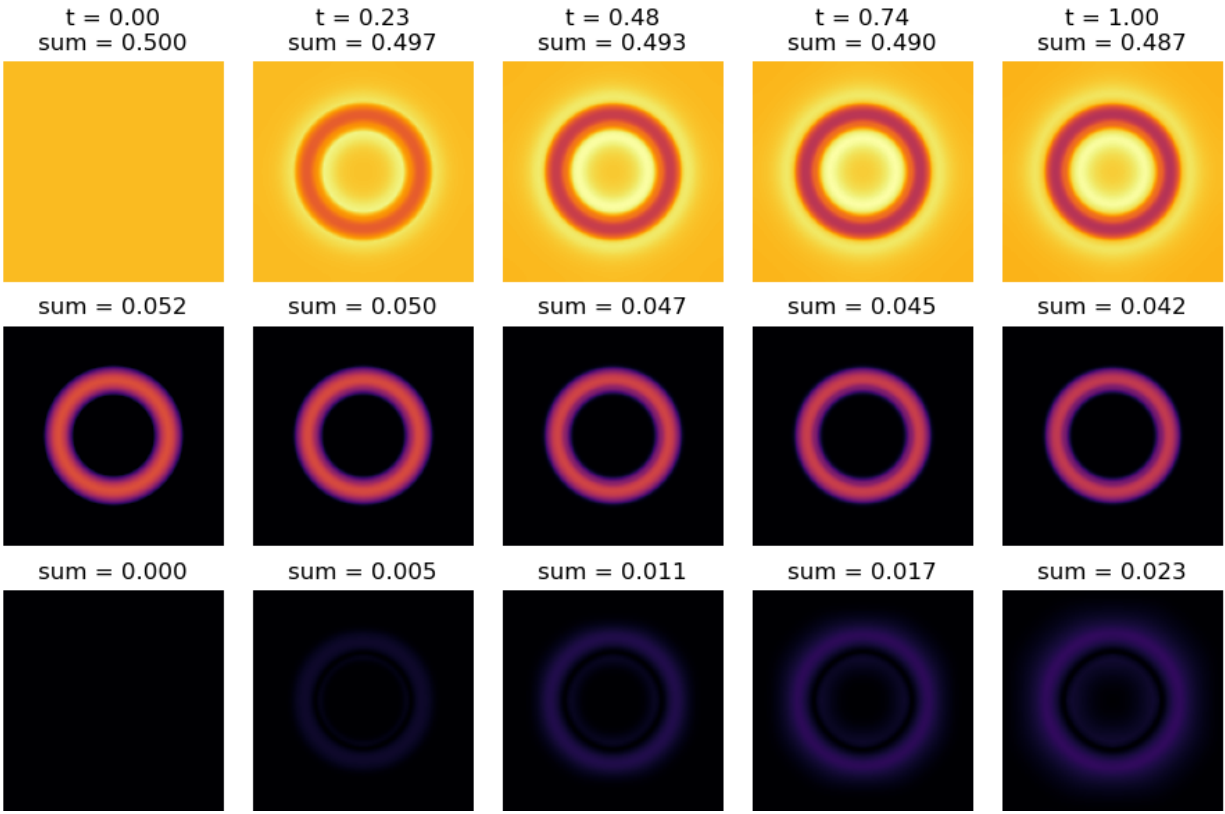
Figure 4.4: Experiment 2. The evolution of populations from $t = 0$ to $t = 1$ with $\beta = 0.7$ and $\gamma = 0.5$. The first row represents susceptible, the second row represents infected, and the last row represents recovered.

Susceptible population is the sum of three Gaussian distributions and infected population is the sum of positive part of quadratic polynomials. We conduct this experiment to show that the algorithm works for nonsymmetric initial densities. Using the same set of parameters, the experiment is repeated twice with $\gamma = 0.1$ and $\gamma = 0.5$. The same behavior of solutions can be observed from Figure 4.5 and Figure 4.6.
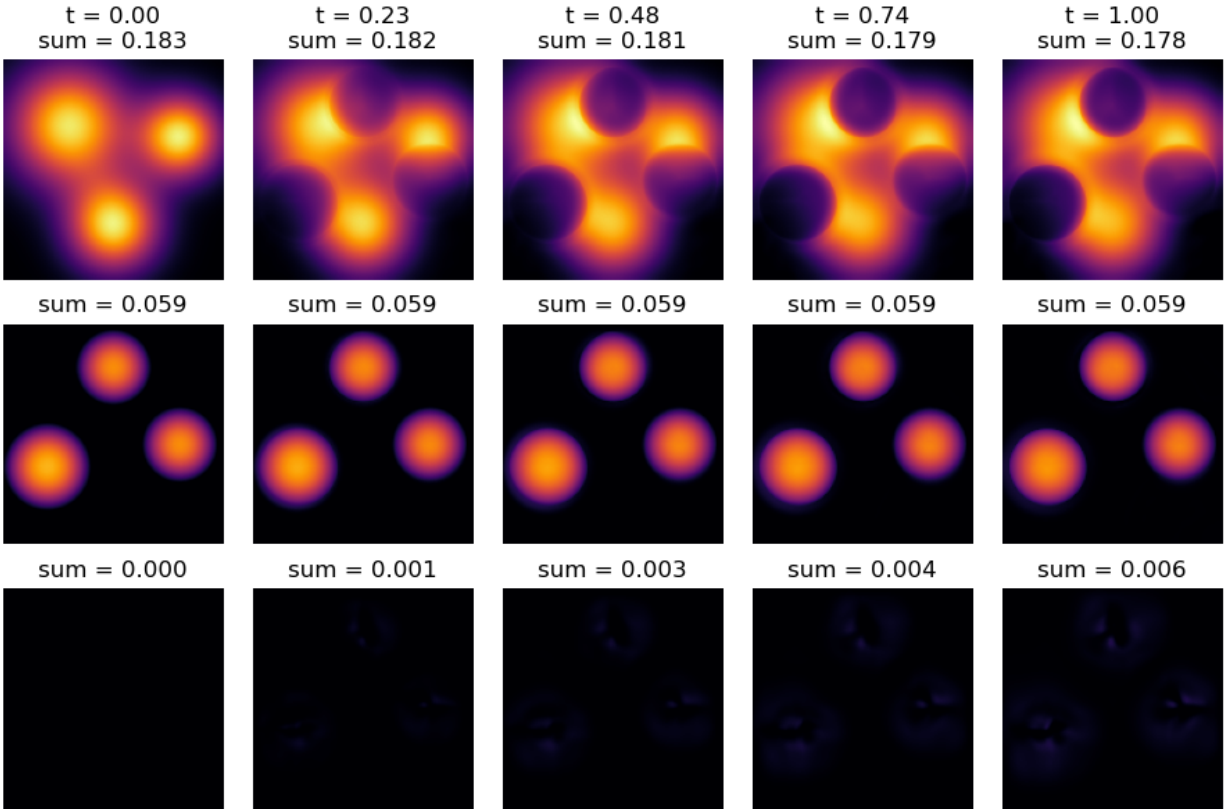
Figure 4.5: Experiment 3. The evolution of populations from $t = 0$ to $t = 1$ with $\beta = 0.7$ and $\gamma = 0.1$. The first row represents susceptible, the second row represents infected, and the last row represents recovered.

4.5 Discussion

In this paper, we chapter a mean-field control model for controlling the virus spreading of a population in a spatial domain, which extends and controls the current SIR model with spatial effect. Here the state variable represents the population status, such as S, I, R, etc with a spatial domain, while the control variable is the velocity of motion of the population. The terminal cost forms the goal of government, which balances the total infection number and maintain suitable physical movement of essential tasks and goods. Numerical algorithms are derived to solve the proposed model. Several experiments demonstrate that our model
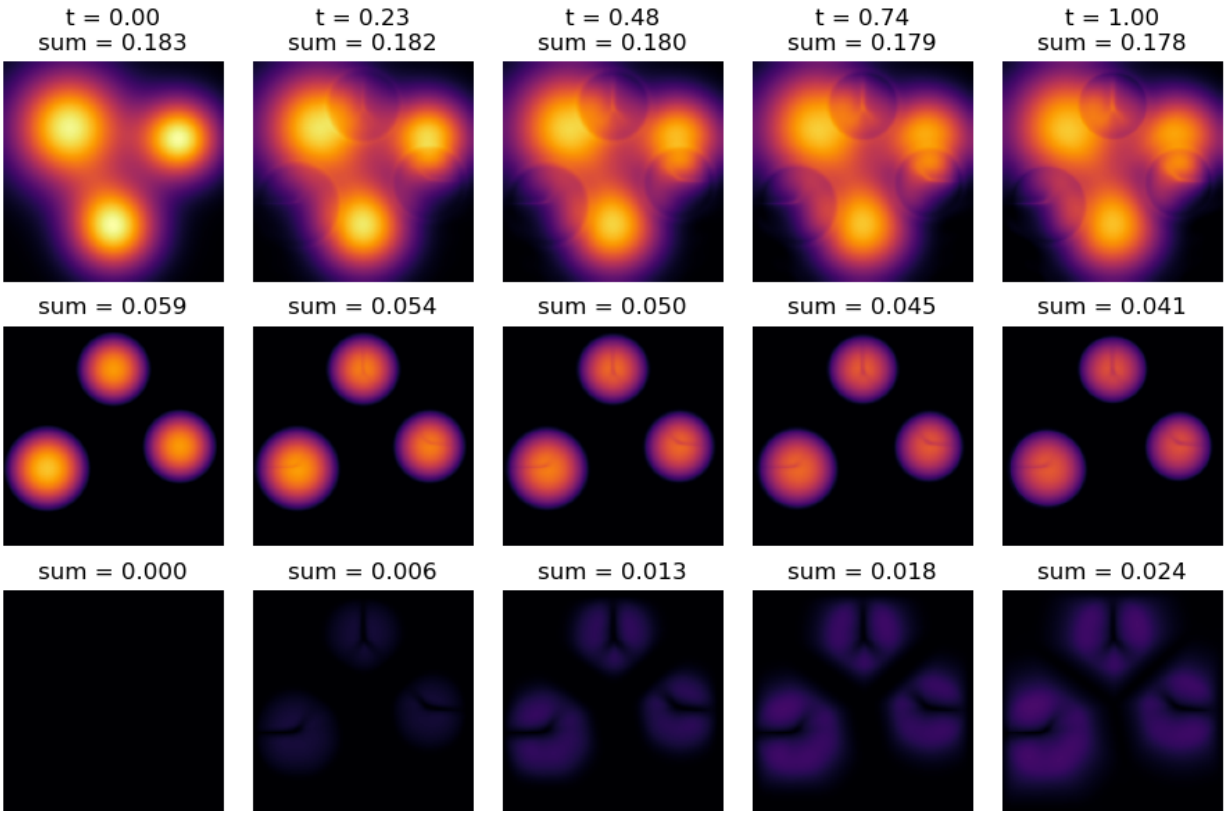
Figure 4.6: Experiment 3. The evolution of populations from $t = 0$ to $t = 1$ with $\beta = 0.7$ and $\gamma = 0.5$. The first row represents susceptible, the second row represents infected, and the last row represents recovered.

can effectively demonstrate how to separate the infected and susceptible population in a spatial domain.

Our model opens the door to many questions in modeling, inverse problems and computations, especially during this COVID-19 pandemic. On the modeling side, first, we are interested in generalize the geometry of the spatial domain. Second, our current model only focuses on the control of population movement. The control of the diffusion operator among populations is also of great interests in future work. Third, the government can also put restrictions on the interaction for different class of populations, depending on their infection status. Fourth, in real life, the spatial domain is often inhomogeneous, containing airports,

schools, subways etc. We also need to formulate our mean-field control model on a discrete spatial graph (network). In addition, our model focus on the forward problem of modeling the dynamics of the virus. In practice, real time data is generated as the virus spreading across different regions. To effectively model this dynamic, a suitable inverse mean-field control problem needs to be constructed. On the computational side, our model involves a non-convex optimization problem, which comes from the multiplicative term of the SIR model itself. In future work, we expect to design a fast and reliable algorithm for these advanced models. We also expect to develop and apply AI numerical algorithms to compute models in high dimensions.

CHAPTER 5

Mean-field Control Problems for Vaccine Distribution

This chapter studies mathematical modeling of mean-field controls. With the invention of the COVID-19 vaccine, shipping and distributing are crucial in controlling the pandemic. We build a mean-field variational problem in a spatial domain, which controls the propagation of pandemics by the optimal transportation strategy of vaccine distribution. Here, we integrate the vaccine distribution into the mean-field SIR model discussed in Chapter4. Numerical examples demonstrate that the proposed model provides practical strategies for vaccine distribution in a spatial domain.

We organize this chapter as follows. In Section 5.1, we review some recent mathematical models proposed to predict and control COVID-19 epidemic, with a focus on optimal control problems. Section 5.2 proposes a novel multi-population mean-field control model and explains how population movement and vaccine distribution are integrated into a constrained optimization problem. Section 5.3 discusses the challenges in numerically solving this mean-field control model, proposes a first-order primal-dual algorithm to solve it, and shows the local convergence of the algorithm. Lastly, in Section 5.4, we present numerical experiments with different model parameter choices and discuss their implications on mean-field controls.

The contributions in this chapter were presented in the joint work with Wonjun Lee, Wuchen Li, and Stanley Osher in[LLL21b].

5.1 Introduction

The COVID-19 pandemic has affected society significantly. Various actions are taken to mitigate the spread of the infections, such as the travel ban, social distancing, and mask-wearing. The recent invention of the vaccine yields breakthroughs in fighting against this infectious disease. According to the recent effectiveness study [FGG21], vaccines including Pfizer, Moderna, and Janssen (J&J) show approximately 66%-95% efficacy at preventing both mild and severe symptoms of COVID-19. Therefore, the deployment of COVID-19 vaccines is an urgent and timely task. Many countries have implemented phased distribution plans that prioritize the elderly and healthcare workers getting vaccinated. Meanwhile, the shipping of vaccines is expensive due to the cold chain transportation [LZL20]. An effective distribution strategy is necessary to eliminate infectious diseases and prevent more death.

In this work, we propose a novel mean-field control model based on [LLT21]. We consider two approaches (controls) to control the pandemic: relocation of populations and distribution of vaccines. The first one has been discussed thoroughly in [LLT21], where we address the spatial effect in pandemic modeling by introducing a mean-field control problem into the spatial SIR model. By applying spatial velocity to the classical disease model, the model finds the most optimal strategy to relocate the different populations (susceptible, infected, and recovered), controlling the epidemic's propagation. We considered several aspects of the vaccine in our model for vaccine distribution, including manufacturing, delivery, and consumption. Our goal is to find an optimal strategy to move the population and distribute vaccines to minimize the total number of infectious, the amount of movement of the people, and the transportation cost of the vaccine with limited vaccine supply. To tackle this question, we ensemble these two controls and propose the following constrained optimization problem:

$$\min_{(\rho_i, v_i)_{i \in \{S,I,R,V\}}, f} G\left((\rho_i, v_i)_{i \in \{S,I,R,V\}}, f\right) \quad (G \text{ defined from } (5.2.7))$$

subject to

$$\begin{cases} \partial_t \rho_S + \nabla \cdot (\rho_S v_S) = -\beta \rho_S K * \rho_I + \dfrac{\eta_S^2}{2} \Delta \rho_S - \theta_1 \rho_V \rho_S & (t,x) \in (0,T) \times \Omega \\[2mm] \partial_t \rho_I + \nabla \cdot (\rho_I v_I) = \beta \rho_S K * \rho_I - \gamma \rho_I + \dfrac{\eta_I^2}{2} \Delta \rho_I & (t,x) \in (0,T) \times \Omega \\[2mm] \partial_t \rho_R + \nabla \cdot (\rho_R v_R) = \gamma \rho_I + \dfrac{\eta_R^2}{2} \Delta \rho_R + \theta_1 \rho_V \rho_S & (t,x) \in (0,T) \times \Omega \\[2mm] \partial_t \rho_V = f(t,x) - \theta_2 \rho_V \rho_S & (t,x) \in (0,T') \times \Omega \\[2mm] \partial_t \rho_V + \nabla \cdot (\rho_V v_V) = -\theta_2 \rho_V \rho_S & (t,x) \in [T',T) \times \Omega \end{cases}$$

and

$$\begin{cases} 0 \leq f(t,x) \leq f_{max} & (t,x) \in [0,T'] \times \Omega_{factory} \\[2mm] f(t,x) = 0 & (t,x) \in [0,T'] \times \Omega \backslash \Omega_{factory} \\[2mm] \rho_V(t,x) \leq C_{factory} & (t,x) \in [0,T'] \times \Omega_{factory} \end{cases}$$

In our model, different populations are described using ρ_i ($i \in \{S,I,R\}$), representing the susceptible, infectious, and recovered. The term $\rho_V(x,t)$ describes the density distribution of the vaccine over the spatial domain at location x and time t. The control variables v_i ($i \in \{S,I,R\}$) create velocity fields over time-space domain that move the corresponding populations. As for vaccines, the control variable v_V represents the vaccine's transportation strategy, and the control variable $f(t,x)$ describes how many vaccines are produced at a specific time and location. The optimization objective function G is the sum of terminal costs $\mathcal{E}_{final}$ and running costs $\mathcal{E}_{running}$. The terminal costs $\mathcal{E}_{final}$ represent the goal of our control to achieve at the terminal time, such as minimizing the total number of infectious individuals and maximizing the total number of recovered (immune) persons. The running costs $\mathcal{E}_{running}$ include the costs of transportation of vaccines and different classes of the populations, etc. We will discuss more details of cost functionals in Section 5.2.2. As for constraints of our optimization problem, the five partial differential equations of ρ_i, v_i ($i \in \{S,I,R,V\}$) describe the dynamics of the different classes of population and vaccines in terms of densities and velocities. The inequalities of $f(t,x)$ model the limitation of vaccine manufacturing. Vaccines are produced at particular factory locations $\Omega_{factory}$ with a daily maximal production rate

f_{max}. The dynamics of the vaccine density ρ_V share some similar aspects to the unnormalized optimal transport [LLL21a]. Specifically, they both study mass transportation with a source term that creates masses.

We solve the main problem using the algorithm based on the first-order Primal-Dual Hybrid Gradient (PDHG) method [CP11, CP16]. Due to the multiplicative interaction terms, $\rho_S K * \rho_I$, $\rho_I K * \rho_S, \rho_V \rho_S$, the optimization problem is based on nonlinear PDE constraints, whereas the PDHG only considers linear constraints. We use the extension of the PDHG [CV17] that solves nonsmooth optimization problems with nonlinear operators between function spaces. We extend the method utilizing the preconditioning operator from [JLL19] which provides a suitable choice of variable norms to achieve a convergence rate independent of the nonlinear operator. As a result, the algorithm converges to the saddle point locally with step length parameters independent of the finite-difference mesh size.

Lots of mathematical models have been invented to predict the future of COVID-19 epidemics. Recently proposed models take more real-world situations into consideration and tend to be more effective in quantitative forecasting. Specifically, there have been studies on the impact of actions such as lockdown, social distancing, wearing a mask [DPT20, DPS20, FMG20]. Data-driven approach and machine learning techniques are also integrated to estimate the parameters for the epidemic better and boost the prediction of the trend of the pandemic model [Ses20, NTS20]. Meanwhile, optimal control serves as an important tool in pandemic control. They seek the optimal strategy to minimize the total number of infected people while keeping certain costs at a minimum. There are work focused on mitigating the epidemic with limited medical supply, such as ICU capacity [CEL20], face masks [LW20], and vaccines [ZKJ08, HD11, KKL16, LLP20, JKL20]. In [JKL20], an optimal vaccine distribution strategy is proposed with a limited total amount of vaccines and maximal daily supply. [LLP20] first uses an inverse problem to determine the parameters of the SIR model. Then it formulates two optimal control problems, with mono- and multi-objective, and solves for the optimal strategy of vaccine administration. Other non-pharmaceutical

interventions are also considered in the scope of optimal control of epidemics, including social distancing, closing schools, and lockdown [GHH21, KK20, SCT21]. [KK20] computes the optimal non-pharmaceutical intervention strategy based on an extended SEIR model with the absence of the vaccine. The mean-field control problem can be viewed as a particular type of optimal control applied to an individual in terms of population density.

Multi-population mean-field game (control) problems have also drawn lots of attention [BHL18, Cir15, Fel13]. This type of problem studies the interactions on two levels: between agents of the same population and between populations. Our model is a multi-population mean-field control problem with population dynamics described using reaction-diffusion equations adopted from the epidemic model and the controls over the vaccine production and distribution. Therefore, we obtain a novel mean-field control problem.

5.2 Models

In this section, we introduce a variational problem to control the SIRV dynamics.

5.2.1 Spatial SIR variational problem with vaccine distribution

Now we consider the optimization problem for the distribution of vaccines. We add an extra function $\rho_V : [0, T] \times \Omega \to [0, \infty)$ which represents the vaccine density in Ω at each time $t \in [0, T]$. The vaccine distribution will be described as the following PDE:

$$
\begin{aligned}
\partial_t \rho_V &= f(t, x) - \theta_2 \rho_V \rho_S \qquad t \in (0, T') \\
\partial_t \rho_V + \nabla \cdot m_V &= -\theta_2 \rho_V \rho_S \quad t \in [T', T), \quad 0 < T' < T,
\end{aligned}
\tag{5.2.1}
$$

where $m_V : [T', T) \times \Omega \to \mathbb{R}^d$ is a momentum, θ_2 represents the utilization rate of vaccines, and $f : (0, T') \times \Omega \to [0, \infty)$ represents the production rate of vaccines in $x \in \Omega$ at $0 < t < T'$. During $0 < t < T'$, the vaccines are produced with a production rate f and used at a rate $\theta_2 \rho_V \rho_S$. During $T' \leq t < T$, the vaccines are delivered to the area where the susceptible

population is located, and they are used at a rate of $\theta_2 \rho_V \rho_S$. In summary, the first part of the PDE describes vaccines' production, and the second part describes the delivery of vaccines. For all time $0 < t < T$, the susceptible population is vaccinated if the vaccines are available in the same area. Now we are ready to introduce the new system of equations for the SIRV model.

$$
\begin{cases}
\partial_t \rho_S + \nabla \cdot m_S = -\beta \rho_S K * \rho_I + \dfrac{\eta_S^2}{2}\Delta \rho_S - \theta_1 \rho_V \rho_S & (t,x) \in (0,T) \times \Omega \\[2mm]
\partial_t \rho_I + \nabla \cdot m_I = \beta \rho_S K * \rho_I - \gamma \rho_I + \dfrac{\eta_I^2}{2}\Delta \rho_I & (t,x) \in (0,T) \times \Omega \\[2mm]
\partial_t \rho_R + \nabla \cdot m_R = \gamma \rho_I + \dfrac{\eta_R^2}{2}\Delta \rho_R + \theta_1 \rho_V \rho_S & (t,x) \in (0,T) \times \Omega \\[2mm]
\partial_t \rho_V = f(t,x) - \theta_2 \rho_V \rho_S & (t,x) \in (0,T') \times \Omega \\[2mm]
\partial_t \rho_V + \nabla \cdot m_V = -\theta_2 \rho_V \rho_S & (t,x) \in [T',T) \times \Omega \\[2mm]
\rho_S(0,\cdot), \rho_I(0,\cdot), \rho_R(0,\cdot), \rho_V(0,\cdot) \text{ are given.}
\end{cases}
\tag{5.2.2}
$$

In the first and third equations, we add the terms $-\theta_1 \rho_V \rho_S$ and $+\theta_1 \rho_V \rho_S$, respectively. The constant θ_1 represents the vaccine efficiency and $\theta_1 \rho_V(t,x)\rho_S(t,x)$ represents the vaccinated population at $(t,x) \in (0,T) \times \Omega$. We denote a set $\mathbb{S} := \{S, I, R, V\}$ and define a nonlinear operator A as follows

$$
\begin{aligned}
A((\rho_i, m_i)_{i \in \mathbb{S}}, f) := \big(&\partial_t \rho_S + \nabla \cdot m_S - \frac{\eta_S^2}{2}\Delta \rho_S + \beta \rho_S K * \rho_I + \theta_1 \rho_S \rho_V, \\
&\partial_t \rho_I + \nabla \cdot m_I - \frac{\eta_I^2}{2}\Delta \rho_I - \beta \rho_S K * \rho_I + \gamma \rho_I, \\
&\partial_t \rho_R + \nabla \cdot m_R - \frac{\eta_R^2}{2}\Delta \rho_R - \gamma \rho_I - \theta_1 \rho_S \rho_V, \\
&\partial_t \rho_V - f \mathcal{X}_{[0,T')}(t) + \nabla \cdot m_V \mathcal{X}_{[T',T]}(t) + \theta_2 \rho_S \rho_V \big),
\end{aligned}
\tag{5.2.3}
$$

where $\mathcal{X}_C : [0,T] \to \mathbb{R}$ is a step function that equals 1 on C and 0 otherwise.

5.2.2 The cost functional

We design the cost functional so that the solution (ρ_i, m_i), $i \in \mathbb{S}$ satisfies the following criteria:

(i) minimize the transportation cost for moving each population;

(ii) minimize the total number of infected people and the total number of susceptible people by maximizing the usage of the vaccines at time T;

(iii) maximize the total number of recovered people at time T;

(iv) avoid high concentration of population and vaccines at each time $t \in (0, T)$;

(v) minimize the amount of vaccines produced during $t \in (0, T')$;

(vi) minimize the transportation cost for delivering vaccines during $t \in (T', T)$.

Item (i) can be described by

$$\int_0^T \int_\Omega F_i(\rho_i(t, x), m_i(t, x)) dx\, dt,$$

for $i \in \{S, I, R\}$ where

$$F_i(\rho_i, m_i) = \begin{cases} \frac{\alpha_i |m_i|^2}{2\rho_i} & \text{if } \rho_i > 0 \\ 0 & \text{if } \rho_i = 0 \text{ and } |m_i| = 0 \\ \infty & \text{if } \rho_i = 0 \text{ and } |m_i| > 0, \end{cases} \tag{5.2.4}$$

which is convex, lower semi-continuous, and 1-homogeneous with respect to (ρ_i, m_i). The parameter α_i characterizes the cost of moving ρ_i with velocity $\frac{m_i}{\rho_i}$. Larger α_i means it is more expensive to move ρ_i. Note that this function comes from the quadratic kinetic energy. To see this, we use the definition $m_i = \rho_i v_i$ and plug into the formula (5.2.4):

$$F_i(\rho_i, m_i) = \frac{\alpha_i |m_i|^2}{2\rho_i} = \frac{\alpha_i}{2} \rho_i |v_i|^2.$$

Item (ii) and (iii) can be described by the terminal costs of the cost functional

$$\mathcal{E}_i(\rho_i(T, \cdot)) = \int_\Omega e_i(\rho_i(T, x))\, dx \quad (i = S, I, V),$$

$$\mathcal{E}_R(\rho_R(T, \cdot)) = \int_\Omega e_R\left(1 - \rho_R(T, x)\right)\, dx,$$

where functions $e : [0, \infty) \to [0, \infty)$ are convex and lower semi-continuous functions. We also minimize the terminal cost for ρ_V because maximizing the usage of vaccines is equivalent to minimizing the number of vaccines left at the terminal time T. The total number of the recovered can be maximized by penalizing the density at the terminal time if the value of $\rho_R(T, x)$ is far away from 1 for $x \in \Omega$. Here, we use a quadratic cost function

$$e_i(t) = \frac{a_i}{2} t^2, \quad (t \in [0, \infty)) \tag{5.2.5}$$

where a_i is some constant.

For Item (iv), the cost functional for the concentration of the total population and vaccines can be represented by

$$\int_0^T \mathcal{G}_P(\rho_S(t, \cdot) + \rho_I(t, \cdot) + \rho_R(t, \cdot)) \, dt, \quad \int_0^T \mathcal{G}_V(\rho_V(t, \cdot)) \, dt,$$

where

$$\mathcal{G}_P(u) = \int_\Omega g_P(u(x)) \, dx, \quad \mathcal{G}_V(u) = \int_\Omega g_V(u(x)) \, dx, \tag{5.2.6}$$

for $u : \Omega \to [0, \infty)$ and convex and lower semi-continuous functions $g_P, g_V : [0, \infty) \to [0, \infty)$. Similar to e_i (5.2.5) from Item (ii), we use quadratic functions for g_P and g_V.

Items (v) and (vi) are criteria specific to the vaccine distribution. From the PDE (5.2.1), the vaccines are produced during $0 < t < T'$ by a function f. We use the similar functional (5.2.6) to minimize the amount of vaccines produced by f. Thus, we set the functional

$$\int_0^{T'} \mathcal{G}_0(f(t, \cdot)) \, dt = \int_0^{T'} \int_\Omega g_0(f(t, x)) \, dx \, dt$$

where $g_0 : [0, \infty) \to [0, \infty)$ is a convex and lower semi-continuous function.

The vaccines are delivered during $T' < t < T$. Similar to the Item (i), we set

$$\int_{T'}^T \int_\Omega F_V(\rho_V, m_V) \, dx \, dt,$$

where F_V has the same definition as (5.2.4).

The total cost functional we consider is then

$$
\begin{aligned}
G((\rho_i, m_i)_{i \in \mathbb{S}}, f) = {}& \sum_{i \in \mathbb{S}} \mathcal{E}_i(\rho_i(T, \cdot)) \\
& + \int_0^T \int_\Omega \sum_{i=S,I,R} F_i(\rho_i, m_i) \, dx \, dt + \int_{T'}^T \int_\Omega F_V(\rho_V, m_V) \, dx \, dt \\
& + \int_0^T \mathcal{G}_P((\rho_S + \rho_I + \rho_R)(t, \cdot)) + \mathcal{G}_V(\rho_V(t, \cdot)) \, dt \\
& + \int_0^{T'} \mathcal{G}_0(f(t, \cdot)) \, dt \\
& + \frac{\lambda}{2} \int_0^T \int_\Omega f^2 + \sum_{i \in \mathbb{S}} \rho_i^2 + |m_i|^2 \, dx \, dt.
\end{aligned} \tag{5.2.7}
$$

In the perspective of a control problem, the first term at the right-hand side in (5.2.7) is the terminal cost, while the rest of the terms accounts for the running costs. The quadratic terms in the last line is a λ-strongly convex functional. The functional F is λ-strongly convex if for any $u = ((\rho_i, m_i)_{i \in \mathbb{S}}, f)$, F satisfies

$$
F(\tilde{u}) \geq F(u) + \partial F(u)(\tilde{u} - u) + \frac{\lambda}{2} \|\tilde{u} - u\|_{L^2}^2, \quad \text{for all } \tilde{u} = ((\tilde{\rho}_i, \tilde{m}_i)_{i \in \mathbb{S}}, \tilde{f})
$$

where $\|\tilde{u} - u\|_{L^2}^2$ is defined as

$$
\int_0^T \int_\Omega (\tilde{f} - f)^2 + \sum_{i \in \mathbb{S}} (\tilde{\rho}_i - \rho_i)^2 + |\tilde{m}_i - m_i|^2 \, dx \, dt
$$

and ∂F denotes the convex subdifferential of F. Since $\mathcal{E}_i$, F_i, $\mathcal{G}_i$ are convex and lower-semicontinuous, G is λ-strongly convex as the sum of convex and λ-strongly convex functionals.

5.2.3 Constraints for vaccine production

In addition to the constraint from (5.2.2), we adapt the following constraints to reflect the limited vaccination coverage:

$$
\begin{aligned}
0 \leq f(t, x) \leq f_{max} \quad & (t, x) \in [0, T'] \times \Omega_{factory} \\
f(t, x) = 0 \quad & (t, x) \in [0, T'] \times \Omega \backslash \Omega_{factory} \\
\rho_V(t, x) \leq C_{factory} \quad & (t, x) \in [0, T'] \times \Omega_{factory}
\end{aligned} \tag{5.2.8}
$$

where $\Omega_{factory} \subset \Omega$ indicates the factory area where vaccines are produced and f_{max} is a nonnegative constant representing the maximum vaccine production rate. In the third inequality, a nonnegative constant $C_{factory}$ limits the total number of vaccines produced during $0 < T < T'$.

$$\int_0^{T'} \int_\Omega \rho_V(t, x) \, dx \, dt \le C_{factory} T' |\Omega_{factory}|.$$

The constraints (5.2.8) can be imposed by having the following functionals for $\mathcal{G}_V$ and $\mathcal{G}_0$.

$$\mathcal{G}_V(\rho_V(t, \cdot)) = \int_\Omega g_V(\rho_V(t, x)) \, dx + i_{[-\infty, C_{factory})}(\rho_V(t, \cdot))$$

$$\mathcal{G}_0(f(t, \cdot)) = \int_\Omega g_0(f(t, x)) + i_{\Omega_{factory}}(x) f(t, x) \, dx + i_{[-\infty, f_{max})}(f(t, \cdot)) \tag{5.2.9}$$

where $\Omega_{factory} \subset \Omega$ indicates the factory area where vaccines are produced. The functionals $i_{[-\infty, C_{factory}]}$ and $i_{[-\infty, f_{max}]}$ are defined as

$$i_{[a,b]}(u) = \begin{cases} 0, & a \le u(x) \le b \quad \text{for all } x \in \Omega \\ \infty, & \text{otherwise} \end{cases}$$

where a, b are constants and $u : \Omega \to \mathbb{R}$ is a function. The function $i_{\Omega_{factory}}(x)$ is defined as

$$i_{\Omega_{factory}}(x) = \begin{cases} 0, & x \in \Omega_{factory} \\ \infty, & x \in \Omega \backslash \Omega_{factory}. \end{cases}$$

This function forces $f(t, x) = 0$ if $(t, x) \in (0, T') \times (\Omega \backslash \Omega_{factory})$, thus vaccines are produced only in $\Omega_{factory}$.

Remark 16. *The formulation is not limited to SIR epidemic model. For example, we can describe the SIRD (Susceptible-Infected-Recovered-Deceased) epidemic model by adding an*

extra population ρ_D for the deceased population with a mortality rate μ.

$$\begin{cases} \partial_t \rho_S + \nabla \cdot m_S = -\beta \rho_S K * \rho_I + \frac{\eta_S^2}{2} \Delta \rho_S - \theta_1 \rho_V \rho_S & (t,x) \in (0,T) \times \Omega \\[2mm] \partial_t \rho_I + \nabla \cdot m_I = \beta \rho_S K * \rho_I - \gamma \rho_I - \mu \rho_I + \frac{\eta_I^2}{2} \Delta \rho_I & (t,x) \in (0,T) \times \Omega \\[2mm] \partial_t \rho_R + \nabla \cdot m_R = \gamma \rho_I + \frac{\eta_R^2}{2} \Delta \rho_R + \theta_1 \rho_V \rho_S & (t,x) \in (0,T) \times \Omega \\[2mm] \partial_t \rho_D = \mu \rho_I + \frac{\eta_D^2}{2} \Delta \rho_D & (t,x) \in (0,T) \times \Omega \\[2mm] \partial_t \rho_V = f(t,x) - \theta_2 \rho_V \rho_S & (t,x) \in (0,T') \times \Omega \\[2mm] \partial_t \rho_V + \nabla \cdot m_V = -\theta_2 \rho_V \rho_S & (t,x) \in [T',T) \times \Omega \\[2mm] \rho_S(0,\cdot), \rho_I(0,\cdot), \rho_R(0,\cdot), \rho_D(0,\cdot), \rho_V(0,\cdot) \text{ are given.} \end{cases}$$

5.2.4 Properties

From the definition of the cost functional and the constraint (5.2.2), we have the following minimization problem:

$$\inf_{(\rho_i, m_i)_{i \in \mathbb{S}}, f} \left\{ G((\rho_i, m_i)_{i \in \mathbb{S}}, f) : \text{subject to } (5.2.2) \right\}.$$

We first define the inner product of vectors of functions in L^2. Given vectors of functions $u = (u_1(t,x), u_2(t,x), \cdots, u_k(t,x))$ and $v = (v_1(t,x), v_2(t,x), \cdots, v_k(t,x))$ with $u_i, v_i : [0,T] \times \Omega \to \mathbb{R}$, the L^2 inner product of vectors u and v and L^2 norm of u are defined by

$$\langle u, v \rangle_{L^2} = \sum_{i=0}^{k} (u_i, v_i)_{L^2}, \quad \|u\|_{L^2}^2 = \langle u, u \rangle_{L^2} \tag{5.2.10}$$

where $(\cdot, \cdot)_{L^2([0,T] \times \Omega)}$ is a L^2 inner product such that

$$(u, v)_{L^2([0,T] \times \Omega)} = \int_0^T \int_\Omega u(t,x) v(t,x) \, dx \, dt.$$

We introduce dual variables $(\phi_i)_{i \in \mathbb{S}}$ for each continuity equation from (5.2.3). Using the dual variables and the definitions of the inner products, we convert the minimization problem into a saddle point problem.

$$\inf_{(\rho_i, m_i)_{i \in \mathbb{S}}, f} \sup_{(\phi_i)_{i \in \mathbb{S}}} \mathcal{L}((\rho_i, m_i, \phi_i)_{i \in \mathbb{S}}, f), \tag{5.2.11}$$

where $\mathcal{L}$ is the Lagrangian functional defined as

$$\mathcal{L}((\rho_i, m_i, \phi_i)_{i \in \mathbb{S}}, f)$$

$$= G((\rho_i, m_i)_{i \in \mathbb{S}}, f) - \langle A((\rho_i, m_i)_{i \in \mathbb{S}}, f), (\phi_i)_{i \in \mathbb{S}} \rangle_{L^2}$$

$$= G((\rho_i, m_i)_{i \in \mathbb{S}}, f)$$

$$- \int_0^T \int_\Omega \phi_S \left(\partial_t \rho_S + \nabla \cdot m_S + \beta \rho_S K * \rho_I + \theta_1 \rho_S \rho_V - \frac{\eta_S^2}{2} \Delta \rho_S \right) dx\, dt$$

$$- \int_0^T \int_\Omega \phi_I \left(\partial_t \rho_I + \nabla \cdot m_I - \beta \rho_S K * \rho_I + \gamma \rho_I - \frac{\eta_I^2}{2} \Delta \rho_I \right) dx\, dt$$

$$- \int_0^T \int_\Omega \phi_R \left(\partial_t \rho_R + \nabla \cdot m_R - \gamma \rho_I - \theta_1 \rho_S \rho_V - \frac{\eta_R^2}{2} \Delta \rho_R \right) dx\, dt$$

$$- \int_0^T \int_\Omega \phi_V \left(\partial_t \rho_V - f \mathcal{X}_{[0,T')}(t) + \nabla \cdot m_V \mathcal{X}_{[T',T]}(t) + \theta_2 \rho_S \rho_V \right) dx\, dt.$$

For brevity, we denote

$$u = ((\rho_i, m_i)_{i \in \mathbb{S}}, f), \quad p = (\phi_i)_{i \in \mathbb{S}}.$$

We can rewrite the Lagrangian as

$$\mathcal{L}(u, p) = G(u) - \langle A(u), p \rangle_{L^2}$$

where the nonlinear operator $A(u)$ is defined as

$$A(u) = (A_S(u), A_I(u), A_R(u), A_V(u)) \tag{5.2.12}$$

$$A_S(u) = \partial_t \rho_S + \nabla \cdot m_S - \frac{\eta_S^2}{2} \Delta \rho_S + \beta \rho_S K * \rho_I + \theta_1 \rho_S \rho_V,$$

$$A_I(u) = \partial_t \rho_I + \nabla \cdot m_I - \frac{\eta_I^2}{2} \Delta \rho_I - \beta \rho_I K * \rho_S + \gamma \rho_I,$$

$$A_R(u) = \partial_t \rho_R + \nabla \cdot m_R - \frac{\eta_R^2}{2} \Delta \rho_R - \gamma \rho_I,$$

$$A_V(u) = \partial_t \rho_V - f \mathcal{X}_{[0,T')}(t) + \nabla \cdot m_V \mathcal{X}_{[T',T]}(t) + \theta_1 \rho_S \rho_V.$$

As noted in [LLT21], the dual gap, the difference between the primal solution and dual solution, may not be zero because the nonconvex functions $(\rho_S, \rho_I) \mapsto \rho_S K * \rho_I$ and $(\rho_S, \rho_V) \mapsto \rho_S \rho_V$ make the feasible set nonconvex. We circumvent the problem by linearizing the nonlinear

operator at a base point $\bar{u}$

$$A(u) \approx \bar{A}_{\bar{u}}(u) = A(\bar{u}) + [\nabla A(\bar{u})](u - \bar{u}).$$

In our formulation, the linearlized operator $\bar{A}_{\bar{u}}(u)$ can be written as follows.

$$\bar{A}_{\bar{u}}(u) = (\bar{A}_{S\bar{u}}(u), \bar{A}_{I\bar{u}}(u), \bar{A}_{R\bar{u}}(u), \bar{A}_{V\bar{u}}(u))$$

$$\bar{A}_{S\bar{u}}(u) = \partial_t \rho_S + \nabla \cdot m_S - \frac{\eta_S^2}{2}\Delta\rho_S + \beta\rho_S K * \bar{\rho}_I + \theta_1\rho_S\bar{\rho}_V,$$

$$\bar{A}_{I\bar{u}}(u) = \partial_t \rho_I + \nabla \cdot m_I - \frac{\eta_I^2}{2}\Delta\rho_I - \beta\rho_I K * \bar{\rho}_S + \gamma\rho_I,$$

$$\bar{A}_{R\bar{u}}(u) = \partial_t \rho_R + \nabla \cdot m_R - \frac{\eta_R^2}{2}\Delta\rho_R - \gamma\bar{\rho}_I,$$

$$\bar{A}_{V\bar{u}}(u) = \partial_t \rho_V - f\mathcal{X}_{[0,T')}(t) + \nabla \cdot m_V \mathcal{X}_{[T',T]}(t) + \theta_1\rho_V\bar{\rho}_S$$

where $\bar{u} = u = ((\bar{\rho}_i, \bar{m}_i)_{i\in\mathbb{S}}, \bar{f})$. We define a linearized Lagrangian as

$$\bar{\mathcal{L}}_{\bar{u}}(u, p) = G(u) - \langle \bar{A}_{\bar{u}}(u), p \rangle_{L^2}.$$

By the first-order optimality conditions (also known as KKT conditions), the saddle point satisfies

$$[\nabla A(u_*)]^T p_* \in \partial G(u_*)$$
$$A(u_*) = 0. \tag{5.2.13}$$

In the next proposition, we present the equations derived from the KKT conditions (5.2.13).

Proposition 4 (Mean-field control SIRV system). *By KKT conditions, the saddle point* $((\rho_i, m_i, \phi_i)_{i\in\mathbb{S}}, f)$ *of* (5.2.11) *satisfies the following equations.*

$$\partial_t\phi_S - \frac{\alpha_S}{2}|\nabla\phi_S|^2 + \frac{\eta_S^2}{2}\Delta\phi_S + \frac{\delta\mathcal{G}_P}{\delta\rho}(\rho_S + \rho_I + \rho_R) + \beta(\phi_I - \phi_S)K * \rho_I$$

$$+ \rho_V\big(\theta_1(\phi_R - \phi_S) - \theta_2\phi_V\big) = 0 \qquad (t, x) \in (0, T) \times \Omega$$

$$\partial_t\phi_I - \frac{\alpha_I}{2}|\nabla\phi_I|^2 + \frac{\eta_I^2}{2}\Delta\phi_I + \frac{\delta\mathcal{G}_P}{\delta\rho}(\rho_S + \rho_I + \rho_R)$$

$$+ \beta K * (\rho_S(\phi_I - \phi_S)) + \gamma(\phi_R - \phi_I) = 0 \qquad (t, x) \in (0, T) \times \Omega$$

$$\partial_t \phi_R - \frac{\alpha_R}{2}|\nabla \phi_R|^2 + \frac{\eta_R^2}{2}\Delta \phi_R + \frac{\delta \mathcal{G}_P}{\delta \rho}(\rho_S + \rho_I + \rho_R) = 0 \qquad (t,x) \in (0,T) \times \Omega$$

$$\partial_t \phi_V + \frac{\delta \mathcal{G}_V}{\delta \rho}(\rho_V) + \rho_S\big(\theta_1(\phi_R - \phi_S) - \theta_2 \phi_V\big) = 0 \qquad (t,x) \in (0,T') \times \Omega$$

$$\partial_t \phi_V - \frac{\alpha_V}{2}|\nabla \phi_V|^2 + \frac{\delta \mathcal{G}_V}{\delta \rho}(\rho_V) + \rho_S\big(\theta_1(\phi_R - \phi_S) - \theta_2 \phi_V\big) = 0 \qquad (t,x) \in (T',T) \times \Omega$$

$$\partial_t \rho_S - \frac{1}{\alpha_S}\nabla \cdot (\rho_S \nabla \phi_S) + \beta \rho_S K * \rho_I + \theta_1 \rho_S \rho_V - \frac{\eta_S^2}{2}\Delta \rho_S = 0 \qquad (t,x) \in (0,T) \times \Omega$$

$$\partial_t \rho_I - \frac{1}{\alpha_I}\nabla \cdot (\rho_I \nabla \phi_I) - \beta \rho_S K * \rho_I + \gamma \rho_I - \frac{\eta_I^2}{2}\Delta \rho_I = 0 \qquad (t,x) \in (0,T) \times \Omega$$

$$\partial_t \rho_R - \frac{1}{\alpha_R}\nabla \cdot (\rho_R \nabla \phi_R) - \gamma \rho_I - \theta_1 \rho_S \rho_V - \frac{\eta_R^2}{2}\Delta \rho_R = 0 \qquad (t,x) \in (0,T) \times \Omega$$

$$\partial_t \rho_V - f + \theta_2 \rho_S \rho_V = 0 \qquad (t,x) \in (0,T') \times \Omega$$

$$\partial_t \rho_V - \frac{1}{\alpha_V}\nabla \cdot (\rho_V \nabla \phi_V) + \theta_2 \rho_S \rho_V = 0 \qquad (t,x) \in (T',T) \times \Omega$$

$$\frac{\delta \mathcal{G}_0}{\delta f}(f) + \phi_V = 0 \qquad (t,x) \in (0,T') \times \Omega$$

$$\phi_i(T,\cdot) = \frac{\delta \mathcal{E}_i}{\delta \rho(T,\cdot)}(\rho_i(T,\cdot)), \quad i \in \mathbb{S}.$$

The terms $\frac{\delta \mathcal{G}_P}{\delta \rho}$, $\frac{\delta \mathcal{G}_V}{\delta \rho}$, $\frac{\delta \mathcal{G}_P}{\delta \rho}$, $\frac{\delta \mathcal{G}_0}{\delta f}$, and $\frac{\delta \mathcal{E}_i}{\delta \rho(T,\cdot)}$ are the functional derivatives. In other words, given $F : \mathcal{H} \to \mathbb{R}$ be a smooth functional where $\mathcal{H}$ is a separable Hilbert space and $\rho \in \mathcal{H}$, we say a map $\frac{\delta F}{\delta \rho}$ is the functional derivative of F with respect to ρ if it satisfies

$$\lim_{\epsilon \to 0} \frac{F(\rho + \epsilon h) - F(\rho)}{\epsilon} = \int_\Omega \frac{\delta F}{\delta \rho}(\rho(x))h(x)\,dx,$$

for any arbitrary function $h : \Omega \to \mathbb{R}$.

The dynamical system models the optimal vector field strategies for S, I, R populations and the vaccine distribution. It combines both strategies from mean field controls and SIRV models. For this reason, we call it *Mean-field control SIRV system*.

Proof of Proposition 4. From the saddle point problem (5.2.11), we can rewrite the problem

as

$$\inf_{(\rho_i,m_i)_{i\in\mathbb{S}},f} \sup_\phi G((\rho_i,m_i)_{i\in\mathbb{S}},f) - \int_0^T \int_\Omega \sum_{i\in\{S,I,R\}} \phi_i\left(\partial_t\rho_i + \nabla\cdot m_i - \frac{\eta_i^2}{2}\Delta\rho_i\right) dx\, dt$$

$$+ \int_0^T \mathcal{Q}((\rho_i,\phi_i)_{i\in\mathbb{S}})\, dt - \int_0^T \int_\Omega \phi_V \partial_t\rho_V\, dx\, dt + \int_0^{T'} \int_\Omega f\phi_V\, dx\, dt - \int_{T'}^T \int_\Omega \phi_V \nabla\cdot m_V\, dx\, dt$$

$$(5.2.14)$$

where a function $\mathcal{Q}:(0,T)\times\Omega\to\mathbb{R}$ is defined as

$$\mathcal{Q}((\rho_i,\phi_i)_{i\in\mathbb{S}}) = \int_\Omega \beta\rho_S(\phi_I-\phi_S)K*\rho_I + \gamma\rho_I(\phi_R-\phi_I) + \rho_S\rho_V\big(\theta_1(\phi_R-\phi_S) - \theta_2\phi_V\big)\, dx.$$

If $((\rho_i,m_i,\phi_i)_{i\in\mathbb{S}},f)$ is the saddle point of the problem, the differential of Lagrangian with respect to ρ_i, m_i, ϕ_i $(i\in\mathbb{S})$, f and $\rho_i(T,\cdot)$ $(i\in\{S,I,V\})$ equal to zero. Thus, from $\frac{\delta\mathcal{L}}{\delta\phi_i}=0$ we have

$$\partial_t\rho_i + \nabla\cdot m_i - \frac{\eta_i^2}{2}\Delta\rho_i + \frac{\delta\mathcal{Q}}{\delta\phi_i}((\rho_i,\phi_i)_{i\in\mathbb{S}}) = 0 \quad (t,x)\in(0,T)\times\Omega, \quad i=S,I,R$$

$$\partial_t\rho_V - f + \frac{\delta\mathcal{Q}}{\delta\phi_V}((\rho_i,\phi_i)_{i\in\mathbb{S}}) = 0 \quad (t,x)\in(0,T')\times\Omega$$

$$\partial_t\rho_V + \nabla\cdot m_V + \frac{\delta\mathcal{Q}}{\delta\phi_V}((\rho_i,\phi_i)_{i\in\mathbb{S}}) = 0 \quad (t,x)\in(T',T)\times\Omega.$$

Using integration by parts, we reformulate the Lagrangian function (5.2.14) as follows.

$$\mathcal{L}((\rho_i,m_i,\phi_i)_{i\in\mathbb{S}},f)$$

$$= \sum_{i\in\mathbb{S}} \mathcal{E}_i(\rho_i(T,\cdot)) + \int_0^T \mathcal{G}_P(\rho_S+\rho_I+\rho_R) + \mathcal{G}_V(\rho_V)\, dt + \int_0^{T'} \mathcal{G}_0(f(t,\cdot))\, dt$$

$$+ \sum_{i=S,I,R} \int_0^T \int_\Omega \frac{\alpha_i|m_i|^2}{2\rho_i} + m_i\cdot\nabla\phi_i + \frac{\eta_i^2}{2}\rho_i\Delta\phi_i\, dx\, dt + \sum_{i\in\mathbb{S}} \int_0^T \int_\Omega \rho_i\partial_t\phi_i\, dx\, dt$$

$$+ \int_{T'}^T \int_\Omega \frac{\alpha_V|m_V|^2}{2\rho_V} + m_V\cdot\nabla\phi_V\, dx\, dt + \int_0^{T'} \int_\Omega f\phi_V\, dx\, dt + \int_0^T \mathcal{Q}((\rho_i,\phi_i)_{i\in\mathbb{S}})\, dt$$

$$+ \sum_{i=S,I,R,V} \int_\Omega \rho_i(0,x)\phi_i(0,x) - \rho_i(T,x)\phi_i(T,x)dx$$

From $\frac{\delta\mathcal{L}}{\delta\rho_i}=0$ $(i\in\{S,I,R\})$,

$$\frac{\delta\mathcal{G}_P}{\delta\rho_i}(\rho_S+\rho_I+\rho_R) + \frac{\delta\mathcal{Q}}{\delta\rho_i}((\rho_i,\phi_i)_{i\in\mathbb{S}}) - \frac{\alpha_i|m_i|^2}{2\rho_i^2} + \frac{\eta_i^2}{2}\Delta\phi_i + \partial_t\phi_i = 0 \quad (t,x)\in(0,T)\times\Omega$$

110

From $\frac{\delta \mathcal{L}}{\delta \rho_V} = 0$,

$$\frac{\delta \mathcal{G}_V}{\delta \rho_V}(\rho_V) + \frac{\delta \mathcal{Q}}{\delta \rho_V}((\rho_i, \phi_i)_{i \in \mathbb{S}}) + \partial_t \phi_V = 0 \quad (t, x) \in (0, T') \times \Omega$$

$$\frac{\delta \mathcal{G}_V}{\delta \rho_V}(\rho_V) + \frac{\delta \mathcal{Q}}{\delta \rho_V}((\rho_i, \phi_i)_{i \in \mathbb{S}}) - \frac{\alpha_V |m_V|^2}{2\rho_V^2} + \partial_t \phi_V = 0 \quad (t, x) \in (T', T) \times \Omega.$$

From $\frac{\delta \mathcal{L}}{\delta \rho_i(T, \cdot)} = 0 \ (i \in \mathbb{S})$,

$$\frac{\delta \mathcal{E}}{\delta \rho_i(T, \cdot)}(\rho_i(T, \cdot)) = \phi_i(T, \cdot).$$

From $\frac{\delta \mathcal{L}}{\delta f} = 0$,

$$\frac{\delta \mathcal{G}_0}{\delta f}(f) + \phi_V = 0, \quad (t, x) \in (0, T') \times \Omega.$$

From $\frac{\delta \mathcal{L}}{\delta m_i} = 0 \ (i \in \mathbb{S})$,

$$\frac{\alpha_i m_i}{\rho_i} = -\nabla \phi_i \quad (t, x) \in (0, T) \times \Omega, \quad i \in \{S, I, R\}$$

$$\frac{\alpha_V m_V}{\rho_V} = -\nabla \phi_V \quad (t, x) \in (0, T') \times \Omega.$$

By replacing $\frac{\alpha_i m_i}{\rho_i} = -\nabla \rho_i$ in $\frac{\delta \mathcal{L}}{\delta \rho_i} = 0$ and $\frac{\delta \mathcal{L}}{\delta \phi_i} = 0$, we derive the result. ∎

5.3   Algorithm

In this section, we propose an algorithm to solve the proposed SIRV variational problem. The algorithm follows the Algorithm 1 proposed in Section 4.3 as a variation of G-Prox PDHG method.

The algorithm takes the following iterative updates:

$$u^{(k+\frac{1}{2})} = \underset{u}{\arg\min} \ g(u) + \langle u, A_{u^{(k)}}^T p^{(k)} \rangle_{L^2} + \frac{1}{2\tau^{(k)}} \|u - u^{(k)}\|_{L^2}^2$$

$$u^{(k+1)} = 2u^{(k+\frac{1}{2})} - u^{(k)}$$

$$p^{(k+1)} = \underset{p}{\arg\max} \ \langle A(u^{(k)}) + A_{u^{(k)}}(u^{(k+1)} - u^{(k)}), p \rangle_{L^2} - f^*(p) - \frac{1}{2\sigma^{(k)}} \|p - p^{(k)}\|_{\mathcal{H}^{(k)}}^2.$$

where the norm $\| \cdot \|_{\mathcal{H}^{(k)}}$ is defined as

$$\|p\|_{\mathcal{H}^{(k)}}^2 = \|A_{u^{(k)}}^T p\|_{L^2}^2.$$

and $A(u)$ defined in Equation 5.2.12.

5.3.1 Implementation of the algorithm

To implement the algorithm to the minimization problem (5.2.7), we set

$$u = ((\rho_i, m_i)_{i \in \mathbb{S}}, f)$$

$$p = (\phi_i)_{i \in \mathbb{S}}$$

$$g(u) = G(u)$$

$$f(A(u)) = \begin{cases} 0 & \text{if } A(u) = 0 \\ \infty & \text{otherwise} \end{cases}$$

$$f^*(p) = 0.$$

We use (5.2.12) for the definition of the operator A. Define the Lagrangian functional as

$$\mathcal{L}(u, p) := G(u) - \langle A(u), p \rangle_{L^2}$$

where $\langle \cdot, \cdot \rangle_{L^2}$ is defined in (5.2.10). We summarize the algorithm as follows.

Here, L^2 and $H_i^{(k)}$ norms are defined as

$$\|u\|_{L^2}^2 = (u, u)_{L^2} = \int_0^T \int_\Omega u^2 dx \, dt, \quad \|p\|_{H_i^{(k)}}^2 = \|[\nabla A_i(u^{(k)})]^T p\|_{L^2}^2, \quad i \in \mathbb{S}$$

for any $u : [0, T] \times \Omega \to [0, \infty)$. Moreover, the relative error is defined as

$$\text{relative error} = \frac{|G(\rho_i^{(k+1)}, m_i^{(k+1)}) - G(\rho_i^{(k)}, m_i^{(k)})|}{|G(\rho_i^{(k)}, m_i^{(k)})|}.$$

In the section 5.4, We use quadratic functions for $\mathcal{E}_i$ ($i \in \{S, I, V\}$), $\mathcal{G}_P$, $\mathcal{G}_V$, $\mathcal{G}_0$. With the definitions (5.2.9), we use

$$\mathcal{E}_i(\rho_i(T, \cdot)) = \int_\Omega \frac{a_i}{2} \rho_i(T, x)^2 \, dx, \quad i = S, I, V$$

$$\mathcal{G}_P(\rho(t, \cdot)) = \int_\Omega \frac{d_P}{2} \rho(t, x)^2 \, dx$$

$$\mathcal{G}_V(\rho(t, \cdot)) = \int_\Omega \frac{d_V}{2} \rho(t, x)^2 \, dx + i_{[-\infty, C_{factory}]}(\rho(t, \cdot))$$

$$\mathcal{G}_0(f(t, \cdot)) = \int_\Omega \frac{d_0}{2} f(t, x)^2 + i_{\Omega_{factory}}(x) f(t, x) \, dx + i_{[-\infty, f_{max}]}(f(t, \cdot))$$

Algorithm 2 Algorithm: G-prox PDHG for mean-field control SIRV system

---

Input: $\rho_i(0, \cdot)$ $(i \in \mathbb{S})$

Output: ρ_i, m_i, ϕ_i $(i \in \mathbb{S})$, f

while relative error $>$ tolerance **for** $i \in \mathbb{S}$ **do**

$$\rho_i^{(k+1)} = \text{argmin}_\rho \, \mathcal{L}((\rho, m^{(k)}, f^{(k)}), \phi^{(k)}) + \frac{1}{2\tau}\|\rho - \rho_i^{(k)}\|_{L^2}^2$$

$$m_i^{(k+1)} = \text{argmin}_m \, \mathcal{L}((\rho^{(k+1)}, m, f^{(k)}), \phi_i^{(k)}) + \frac{1}{2\tau}\|m - m_i^{(k)}\|_{L^2}^2$$

$$f^{(k+1)} = \text{argmin}_f \, \mathcal{L}((\rho^{(k+1)}, m^{(k+1)}, f), \phi^{(k)}) + \frac{1}{2\tau}\|f - f^{(k)}\|_{L^2}^2$$

$$\phi_i^{(k+\frac{1}{2})} = \text{argmax}_\phi \, \mathcal{L}((\rho^{(k+1)}, m^{(k+1)}, f^{(k+1)}), \phi) - \frac{1}{2\sigma}\|\phi - \phi_i^{(k)}\|_{H_i^{(k)}}^2$$

$$\phi_i^{(k+1)} = 2\phi_i^{(k+\frac{1}{2})} - \phi_i^{(k)}$$

end while

Thus, we can write the cost functional as follows

$$G((\rho_i, m_i)_{i \in \mathbb{S}}, f) = \int_\Omega \sum_{i=S,I,V} \frac{a_i}{2} \rho_i(T, \cdot)^2 \, dx$$

$$+ \int_0^T \int_\Omega \sum_{i=S,I,R} F_i(\rho_i, m_i) \, dx \, dt + \int_{T'}^T \int_\Omega F_V(\rho_V, m_V) \, dx \, dt$$

$$+ \int_0^T \int_\Omega \frac{d_P}{2} (\rho_S + \rho_I + \rho_R)^2 + \frac{d_V}{2} \rho_V^2 \, dx \, dt$$

$$+ \int_0^{T'} \int_\Omega \frac{d_0}{2} f^2 + i_{\Omega_{factory}} f \, dx \, dt \qquad (5.3.1)$$

$$+ \int_0^T i_{[-\infty, C_{factory}]}(\rho(t, \cdot)) + i_{[-\infty, f_{max}]}(f(t, \cdot)) \, dt$$

$$+ \frac{\lambda}{2} \int_0^T \int_\Omega f^2 + \sum_{i \in \mathbb{S}} \rho_i^2 + |m_i|^2 \, dx \, dt.$$

where a_i, d_P, d_V, d_0 are nonnegative constants. With this cost functional, we find explicit formula for each variable $\rho_i^{(k+1)}, m_i^{(k+1)}, \phi_i^{(k+1)}$ $(i \in \mathbb{S})$, $f^{(k+1)}$.

Proposition 5. *The variables* $\rho_i^{(k+1)}, m_i^{(k+1)}, \phi_i^{(k+1)}$ *$(i \in \mathbb{S})$, and $f^{(k+1)}$ from the Algorithm 2 satisfy the following explicit formulas:*

$$\rho_S^{(k+1)} = root_+ \left(\frac{\tau}{1 + \tau(d_P + \lambda)} \left(\partial_t \phi_S^{(k)} + \frac{\eta_S^2}{2} \Delta \phi_S^{(k)} - \frac{1}{\tau} \rho_S^{(k)} + \beta \left(\phi_I^{(k)} - \phi_S^{(k)} \right) K * \rho_I^{(k)} \right. \right.$$

$$\left. \left. + \rho_V^{(k)} \left(\theta_1(\phi_R^{(k)} - \phi_S^{(k)}) - \theta_2 \phi_V^{(k)} \right) + d_P(\rho_I^{(k)} + \rho_R^{(k)}) \right), 0, -\frac{\tau \alpha_S |m_S^{(k)}|^2}{2(1 + \tau(d_P + \lambda))} \right)$$

$$\rho_I^{(k+1)} = root_+ \left(\frac{\tau}{1 + \tau(d_P + \lambda)} \left(\partial_t \phi_I^{(k)} + \frac{\eta_I^2}{2} \Delta \phi_I^{(k)} - \frac{1}{\tau} \rho_I^{(k)} + \beta K * \left(\rho_S^{(k)}(\phi_I^{(k)} - \phi_S^{(k)}) \right) \right. \right.$$

$$\left. \left. + \gamma(\phi_R^{(k)} - \phi_I^{(k)}) + d_P(\rho_S^{(k)} + \rho_R^{(k)}) \right), 0, -\frac{\tau \alpha_I |m_I^{(k)}|^2}{2(1 + \tau(d_P + \lambda))} \right) \right)$$

$$\rho_R^{(k+1)} = root_+ \left(\frac{\tau}{1 + \tau(d_P + \lambda)} \left(\partial_t \phi_R^{(k)} + \frac{\eta_R^2}{2} \Delta \phi_R^{(k)} - \frac{1}{\tau} \rho_R^{(k)} + d_P(\rho_S^{(k)} + \rho_I^{(k)}) \right), 0, -\frac{\tau \alpha_R |m_R^{(k)}|^2}{2(1 + \tau(d_P + \lambda))} \right)$$

$$\rho_V^{(k+1)} = \min \left(C_{factory}, \frac{\tau}{1 + \tau(d_V + \lambda)} \left(-\partial_t \phi_V^{(k)} - \rho_S^{(k)}(\theta_1(\phi_R^{(k)} - \phi_S^{(k)}) - \theta_2 \phi_V^{(k)}) + \frac{1}{\tau} \rho_V^{(k)} \right) \right),$$

$$(t, x) \in [0, T'] \times \Omega$$

114

$$\rho_V^{(k+1)} = root_+\left(\frac{\tau}{1+\tau(d_V+\lambda)}\left(\partial_t\phi_V^{(k)} + \rho_S(\theta_1(\phi_R-\phi_S)-\theta_2\phi_V) - \frac{1}{\tau}\rho_V^{(k)}\right), 0, -\frac{\tau\alpha_V|m_V^{(k)}|^2}{2(1+\tau(d_V+\lambda))}\right),$$

$$(t,x) \in (T',T] \times \Omega$$

$$m_i^{(k+1)} = \frac{\rho_i^{(k+1)}}{\tau\alpha_i + (1+\tau\lambda)\rho_i^{(k+1)}}\left(m_i^{(k)} - \tau\nabla\phi_i^{(k)}\right), \qquad (i \in \mathbb{S})$$

$$f^{(k+1)} = \min\left(f_{max}, \frac{\tau}{1+\tau(d_0+\lambda)}\left(\frac{1}{\tau}f^{(k)} - \phi_V^{(k)}\right)\right)\mathcal{X}_{\Omega_{factory}}(x)$$

$$\phi_S^{(k+\frac{1}{2})} = \phi_S^{(k)} + \sigma(A_SA_S^T)^{-1}\left(-\partial_t\rho_S^{(k+1)} - \nabla\cdot m_S^{(k+1)} - \beta\rho_S^{(k+1)}K*\rho_I^{(k+1)} - \theta_1\rho_S^{(k+1)}\rho_V^{(k+1)} + \frac{\eta_S^2}{2}\Delta\rho_S^{(k+1)}\right)$$

$$\phi_I^{(k+\frac{1}{2})} = \phi_I^{(k)} + \sigma(A_IA_I^T)^{-1}\left(-\partial_t\rho_I^{(k+1)} - \nabla\cdot m_I^{(k+1)} + \beta\rho_S^{(k+1)}K*\rho_I^{(k+1)} - \gamma\rho_I^{(k+1)} + \frac{\eta_I^2}{2}\Delta\rho_I^{(k+1)}\right)$$

$$\phi_R^{(k+\frac{1}{2})} = \phi_R^{(k)} + \sigma(A_RA_R^T)^{-1}\left(-\partial_t\rho_R^{(k+1)} - \nabla\cdot m_R^{(k+1)} + \gamma\rho_I^{(k+1)} + \theta_1\rho_S^{(k+1)}\rho_V^{(k+1)} + \frac{\eta_R^2}{2}\Delta\rho_R^{(k+1)}\right)$$

$$\phi_V^{(k+\frac{1}{2})} = \phi_V^{(k)} + \sigma(A_VA_V^T)^{-1}\left(-\partial_t\rho_V^{(k+1)} + f^{(k+1)}\mathcal{X}_{[0,T')}(t) - \nabla\cdot m_V^{(k+1)}\mathcal{X}_{[T',T]}(t) - \theta_1\rho_S^{(k+1)}\rho_V^{(k+1)}\right)$$

where $root_+(a,b,c)$ *is a positive root of a cubic polynomial* $x^3 + ax^2 + bx + c = 0$ *and we approximate the* $A_iA_i^*$ *as follows*

$$A_SA_S^T = -\partial_{tt} + \frac{\eta_S^4}{4}\Delta^2 - (1+(\beta+\theta_1)\eta_S^2)\Delta + (\beta+\theta_1)^2$$

$$A_IA_I^T = -\partial_{tt} + \frac{\eta_I^4}{4}\Delta^2 - (1+(\gamma+\beta)\eta_I^2)\Delta + (\gamma+\beta)^2$$

$$A_RA_R^T = -\partial_{tt} + \frac{\eta_R^4}{4}\Delta^2 - \Delta$$

$$A_VA_V^T = -\partial_{tt} - \Delta + \theta_2^2.$$

Similar to Algorithm 1, we use FFTW library to compute $(A_iA_i^T)^{-1}$ $(i \in \mathbb{S})$ and convolution terms by Fast Fourier Transform (FFT), which is $O(n\log n)$ operations per iteration with n being the number of points. Thus, the algorithm takes just $O(n\log n)$ operations per iteration.

5.4 Numerical Experiments

In this section, we present several sets of numerical experiments using the algorithm 1 with various parameters. We wrote C++ codes to run the numerical experiments. Let $\Omega = [0, 1]^2$ be a unit square in $\mathbb{R}^2$ and the terminal time $T = 1$. The domain $[0, 1] \times \Omega$ is discretized with the regular Cartesian grid below.

$$\Delta x_1 = \frac{1}{N_{x_1}}, \quad \Delta x_2 = \frac{1}{N_{x_2}}, \quad \Delta t = \frac{1}{N_t - 1}$$

$$x_{kl} = ((k + 0.5)\Delta x_1, (l + 0.5)\Delta x_2), \quad k = 0, \cdots, N_{x_1} - 1, \quad l = 0, \cdots, N_{x_2} - 1$$

$$t_n = n\Delta t, \qquad\qquad n = 0, \cdots, N_t - 1$$

where N_{x_1}, N_{x_2} are the number of discretized points in space and N_t is the number of discretized points in time. For all the experiments, we use the same set of parameters,

$$N_{x_1} = 128, \quad N_{x_2} = 128, \quad N_t = 32$$

$$\alpha_S = 10, \quad \alpha_I = 30, \quad \alpha_R = 20, \quad \alpha_V = 0.005$$

$$a_S = 2, \quad a_I = 2, \quad a_R = 0.001, \quad a_V = 0.1$$

$$T' = 0.5, \quad \sigma = 0.01, \quad d_P = 0.4, \quad d_V = 0.4, \quad d_0 = 0.01$$

$$\theta_2 = 0.9 \quad \eta_i = 0.01 \quad (i \in \mathbb{S}).$$

By setting a higher value for α_I, we penalize the infected population's movement more than other populations. Considering the immobility of the infected individuals, this is a reasonable choice in terms of real-world applications. By setting $T' = 1/2$, the solution will produce the vaccines during $0 \le t < 1/2$ and deliver them during $1/2 \le t \le 1$. Furthermore, we fix the parameters for the infection rate and recovery rate

$$\beta = 0.8, \quad \gamma = 0.1.$$

The Chapter 3 describes how the parameters β and γ affect the propagation of the populations. In this chapter, we focus on the vaccine productions and distributions. Recall that from the

116

$$\beta\rho_S\rho_I \qquad \gamma\rho_I$$

$$S \qquad I \qquad R$$

$$\theta_1\rho_S\rho_V$$
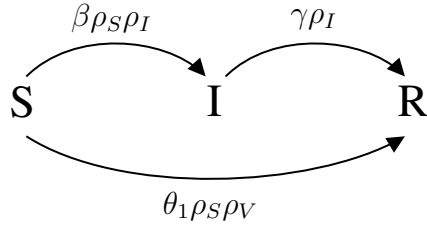
Figure 5.1: Visualization of the flow of three populations. The susceptible transforms to the infected with a rate β and the recovered with a rate θ_1. The infected transforms to the recovered with a rate γ.

formulation (5.3.1), we have terminal functionals

$$\mathcal{E}_i(\rho_i(T, \cdot)) = \int_\Omega \frac{a_i}{2} \rho_i(T, x)^2 \, dx, \quad i \in \{S, I, V\}.$$

Thus, the solution to the problem has to minimize the total number of susceptible, infected, and vaccines at the terminal time T. The solution reduces the total number of infected by recovering them with a rate γ and decreases the total number of susceptible by transforming the susceptible to the infected with a rate β or to the recovered with a rate θ_1 (Figure 5.1). If the β is large and γ is small, the number of infected will grow since there are more inflows from susceptible than the outflows to the recovered. To minimize the total number of the infected, the solution has to vaccinate the susceptible as much as possible to avoid the susceptible becoming infected. Thus, the vaccines need to be produced and delivered to the susceptible efficiently while satisfying the constraint conditions (5.2.8).

We present two experiments that demonstrate how the various factors in the formulation affect the production and the distribution of vaccines.

5.4.1 Experiment 1

In this experiment, we show how the parameters related to ρ_V affect the solution. We set the initial densities for the ρ_i ($i \in \mathbb{S}$) and the factory location $\Omega_{factory}$ as

$$\rho_S(0, x) = \left(2 \exp(-5[(x_1 - 0.7)^2 + (x_2 - 0.7)^2]) - 1.5\right)_+$$
$$\rho_I(0, x) = \left(2 \exp(-5[(x_1 - 0.7)^2 + (x_2 - 0.7)^2]) - 1.8\right)_+$$
$$\rho_R(0, x) = 0 \tag{5.4.1}$$
$$\rho_V(0, x) = 0$$
$$\Omega_{factory} = B_{0.1}(0.3, 0.3)$$

where $(x)_+ = \max(x, 0)$ and $B_r x$ is a ball of a radius r centered at x.
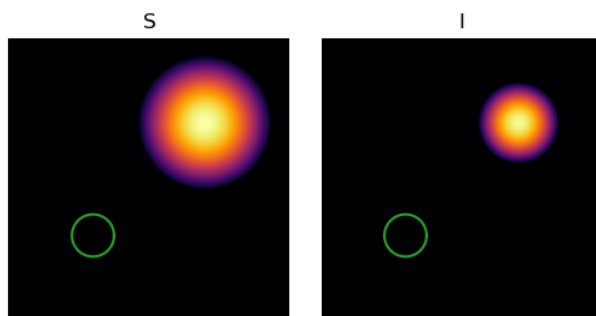
Figure 5.2: Experiment 1: Initial densities of ρ_S (left) and ρ_I (right). The green circle indicates $\Omega_{factory}$.

With the initial densities (5.4.1), we run two simulations with different values for θ_1, θ_2, and f_{max}.

Parameters	Sim 1	Sim 2	Description
θ_1	0.5	0.9	Vaccine efficiency
f_{max}	0.5	10	Maximum production rate of vaccines
$C_{factory}$	0.5	2	Maximum amount of vaccines that can be produced at $x \in \Omega$ during $0 \le t \le \frac{1}{2}$

118

Figure 5.3 shows the comparison between the results from the simulation 1 and the simulation 2. The first three plots (Figure 5.3a) show the total mass of ρ_i $(i = S, I, R)$, i.e.

$$\int_\Omega \rho_i(t, x)\, dx, \quad i = S, I, R, \quad t \in [0, 1].$$

and the last plot (Figure 5.3b) shows the total mass of ρ_V during $0 \le t \le \frac{1}{2}$

$$\int_\Omega \rho_V(t, x)\, dx, \quad t \in \left[0, \frac{1}{2}\right].$$

The total number of vaccines produced from the simulation 1 is smaller than that from the simulation 2 because the solution cannot produce a large amount of vaccines due to the low production rate f_{max}. Furthermore, the solution from the simulation 1 cannot vaccinate a large number of susceptible due to a small θ_1. Thus, there are more susceptible and less recovered at the terminal time in the simulation 1.

5.4.2 Experiment 2

This experiment includes the spatial obstacles and shows how the algorithm effectively finds the solution that utilizes the vaccine production and distribution given spatial barriers. Denote a set $\Omega_{obs} \subset \Omega$ as obstacles. We use the following functionals in the experiment.

$$\mathcal{G}_P(\rho(t, \cdot)) = \int_\Omega \sum_{i \in \{S,I,R\}} \frac{d_i}{2} \rho_i^2(t, x) + i_{\Omega_{obs}}(x) \left(\sum_{i \in \{S,I,R\}} \rho_i(t, x) \right) dx$$

$$\mathcal{G}_V(\rho(t, \cdot)) = \int_\Omega \frac{d_V}{2} \rho_V^2(t, x) + i_{\Omega_{obs}}(x)\rho_V(t, x)\, dx$$

$$\mathcal{E}_i(\rho(1, \cdot)) = \int_\Omega \frac{a_i}{2} \rho_i^2(1, x) + i_{\Omega_{obs}}(x)\rho_i(1, x)\, dx, \quad i \in \{S, I, V\}$$

$$\mathcal{E}_R(\rho(1, \cdot)) = \int_\Omega \frac{a_R}{2} (\rho_R(1, x) - 1)^2 + i_{\Omega_{obs}}(x)\rho_R(1, x)\, dx.$$

The densities ρ_i $(i \in \mathbb{S})$ cannot be positive on Ω_{obs} due to $i_{\Omega_{obs}}$. Thus, the densities transport while avoiding the obstacle Ω_{obs}. We show two sets of experiments based on this setup.

119
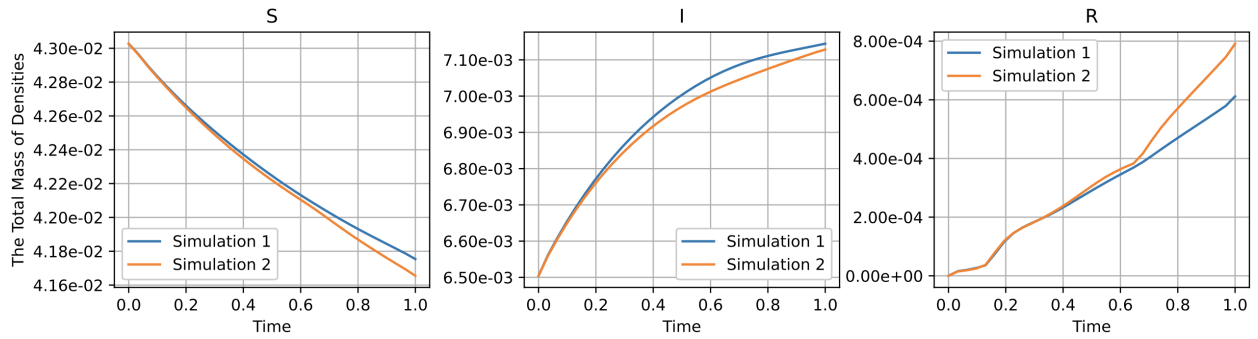
(a) The total populations of ρ_S, ρ_I, ρ_R.
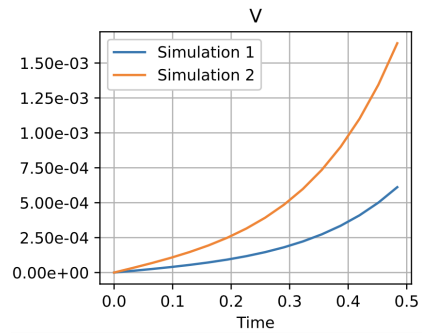
(b) The total mass of vaccines produced during $0 \leq t \leq 0.5$.

Figure 5.3: Experiment 1: The comparison between the results from the simulation 1 and the simulation 2. The first three plots (a) show the total mass of ρ_i ($i = S, I, R$) and the fourth plot (b) shows the total mass of ρ_V produced at the factory area during the production time $0 \leq t < 0.5$.

5.4.2.1 Single factory

We set the initial densities and $\Omega_{factory}$ as follows

$$\rho_S(0, x) = \left(2\exp(-15((x_1 - 0.2)^2 + (x_2 - 0.5)^2)) - 1.6\right)_+$$
$$+ \left(2\exp(-15((x_1 - 0.8)^2 + (x_2 - 0.5)^2)) - 1.6\right)_+$$
$$\rho_I(0, x) = \left(2\exp(-15((x_1 - 0.2)^2 + (x_2 - 0.5)^2)) - 1.8\right)_+$$
$$\rho_R(0, x) = 0$$
$$\rho_V(0, x) = 0$$
$$\Omega_{factory} = B_{0.075}(0.5, 0.5)$$

and fix the parameters

$$\theta_1 = 0.9, \quad f_{max} = 10, \quad C_{factory} = 2.$$

The initial densities are shown in Figure 5.4.

Figure 5.4: Experiment 2: The initial densities ρ_S (left) and ρ_I (right), and the location of the factory (indicated as a green circle).

Figure 5.5 and Figure 5.6 show the evolution of densities with and without obstacles, respectively. In both simulations, the density of vaccines ρ_V (the fourth row) transports to the areas where the susceptible people are present. In Figure 5.6, ρ_V transports while avoiding the obstacle at the right. Figure 5.7 shows the comparison between these two solutions and how the presence of the obstacle affects the production and delivery of vaccines

Figure 5.5: Experiment 2: The evolution of densities ρ_i ($i \in \mathbb{S}$) without the obstacle over time $0 \le t \le 1$. The first row: the susceptible density ρ_S. The second row: the infected density ρ_I. The third row: the recovered density ρ_R. The fourth row: the vaccine density ρ_V.
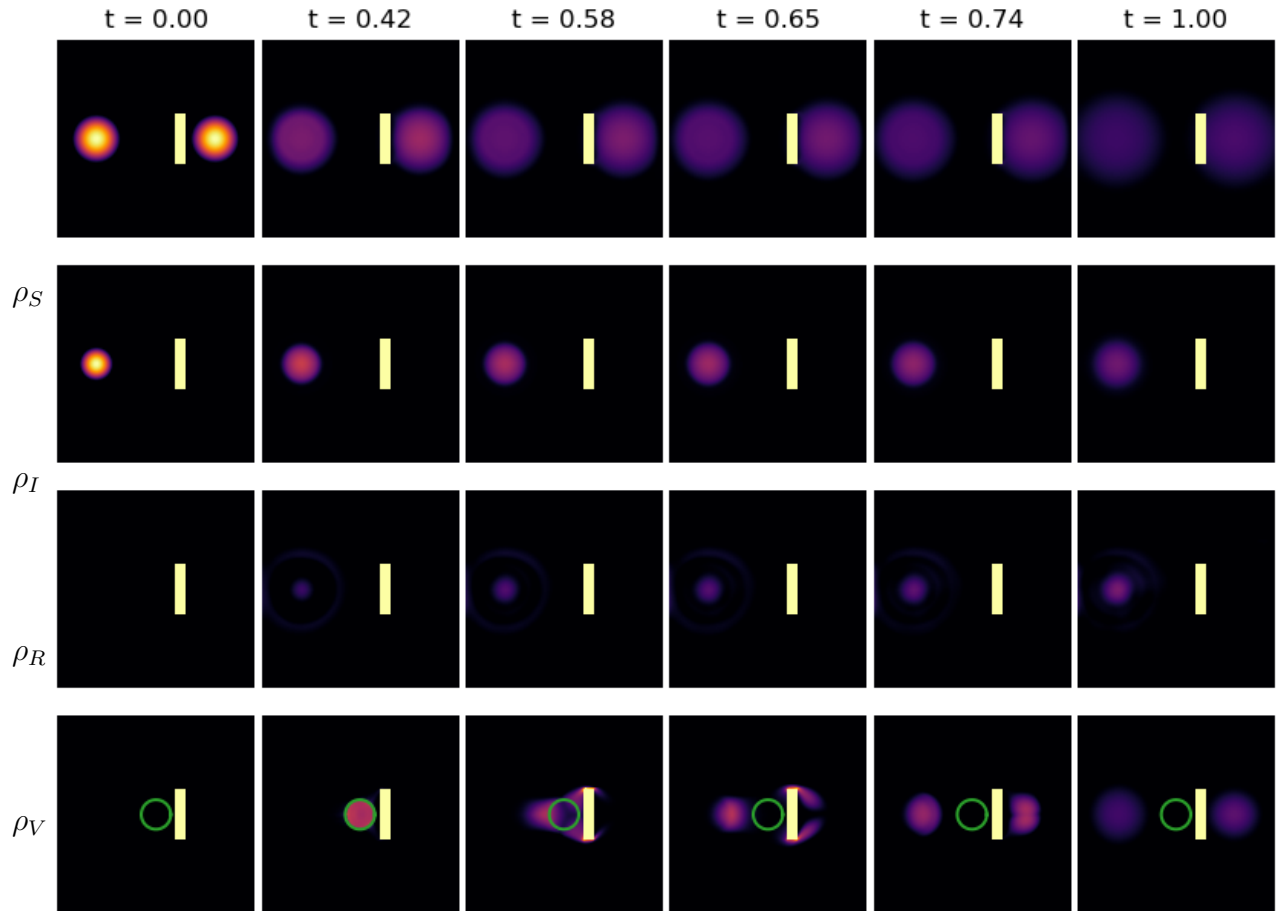
Figure 5.6: Experiment 2: The evolution of densities ρ_i ($i \in \mathbb{S}$) with the obstacle (indicated as a yellow block) over time $0 \le t \le 1$. The first row: the susceptible density ρ_S. The second row: the infected density ρ_I. The third row: the recovered density ρ_R. The fourth row: the vaccine density ρ_V.

quantitatively. Figure 5.7a shows the total mass of the vaccines in the factory area $\Omega_{factory}$ during the production time

$$\int_{\Omega_{factory}} \rho_V(t, x)\, dx, \quad t \in [0, 0.5).$$

Figure 5.7b shows the total mass of the vaccines during the delivery time at the left side and the right side of the domain

$$\int_{\Omega \cap \{x_1 < 0.5\}} \rho_V(t, x)\, dx, \quad \text{Left}$$

$$\int_{\Omega \cap \{x_1 \geq 0.5\}} \rho_V(t, x)\, dx, \quad \text{Right}$$

during $t \in [0.5, 1]$. When there is no obstacle, the vaccines are delivered more to the right than to the left (Figure 5.7b). The number of susceptible people at the left decreases very fast because there are infected people with a high infection rate. When ρ_V starts to transport at time $t = 0.5$, the number of susceptible is lower at the left. Thus, the solution distributes fewer vaccines to the left with less susceptible people. When there is an obstacle, ρ_V has to bypass the obstacle to reach the susceptible areas. Thus, the kinetic energy cost during the delivery time $t \in [0.5, 1]$ increases at the right. The solution cannot deliver the vaccines as much as the case without the obstacle. It results in a fewer number of vaccines produced during $t \in [0, 0.5)$ (Figure 5.7a) and delivered to the right during $t \in [0.5, 1]$ when there is an obstacle (Figure 5.7b).

5.4.2.2 Multiple factories

Similar to the previous experiment, we show how the obstacles in the spatial domain affect the production and distribution of the vaccines. We use more complex initial densities, an obstacle set Ω_{obs}, and three factory locations in this experiment. We set the initial densities and $\Omega_{factory}$ as follows

$$\rho_S(0, x) = \left(2 \exp(-15((x_1 - 0.8)^2 + (x_2 - 0.8)^2)) - 1.6\right)_+$$

124
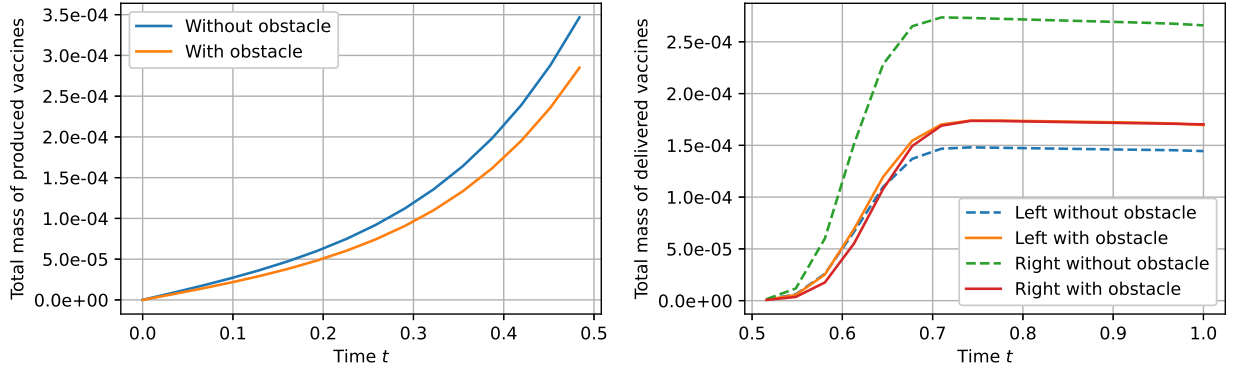
(a) The total mass of ρ_V during $t \in [0, 0.5)$ (b) The total mass of ρ_V during $t \in [0.5, 1]$

Figure 5.7: Experiment 2: The left plot shows the total mass of vaccine density ρ_V during the production time $t \in [0, 0.5)$. The right plot shows the total mass of ρ_V at the left side of the domain $\Omega \cap \{x_1 < 0.5\}$ and at the right side of the domain $\Omega \cap \{x_1 \geq 0.5\}$.

$$
\begin{aligned}
&+ \left(2\exp(-15((x_1 - 0.2)^2 + (x_2 - 0.7)^2)) - 1.6\right)_+ \\
&+ \left(2\exp(-15((x_1 - 0.8)^2 + (x_2 - 0.3)^2)) - 1.6\right)_+ \\
&+ \left(2\exp(-15((x_1 - 0.2)^2 + (x_2 - 0.2)^2)) - 1.6\right)_+ \\
\rho_I(0, x) = &\left(2\exp(-15((x_1 - 0.2)^2 + (x_2 - 0.7)^2)) - 1.8\right)_+ \\
&+ \left(2\exp(-15((x_1 - 0.2)^2 + (x_2 - 0.2)^2)) - 1.8\right)_+ \\
\rho_R(0, x) = &\; 0 \\
\rho_V(0, x) = &\; 0 \\
\Omega_{factory} = &\; B_{0.075}(0.5, 0.2) \,\cup\, B_{0.075}(0.5, 0.5) \,\cup\, B_{0.075}(0.5, 0.8)
\end{aligned}
$$

and fix the parameters

$$
\theta_1 = 0.9, \quad f_{max} = 10, \quad C_{factory} = 2.
$$

The initial densities are shown in Figure 5.8.

Figure 5.9 and Figure 5.10 show the evolution of densities with and without obstacles, respectively. The experiment demonstrates that even with the complex initial densities, the algorithm successfully converges to the reasonable solution that coincides with the previous
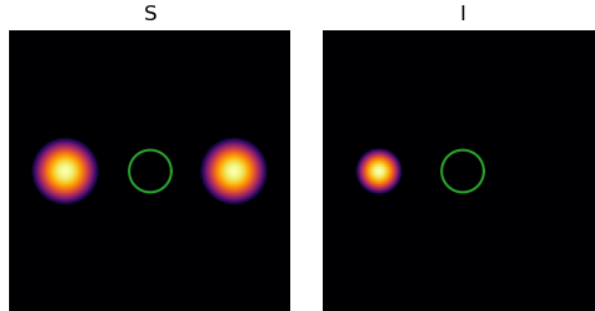
Figure 5.8: Experiment 2: The initial densities ρ_S (left) and ρ_I (right), and the location of the factory (indicated as green circles).
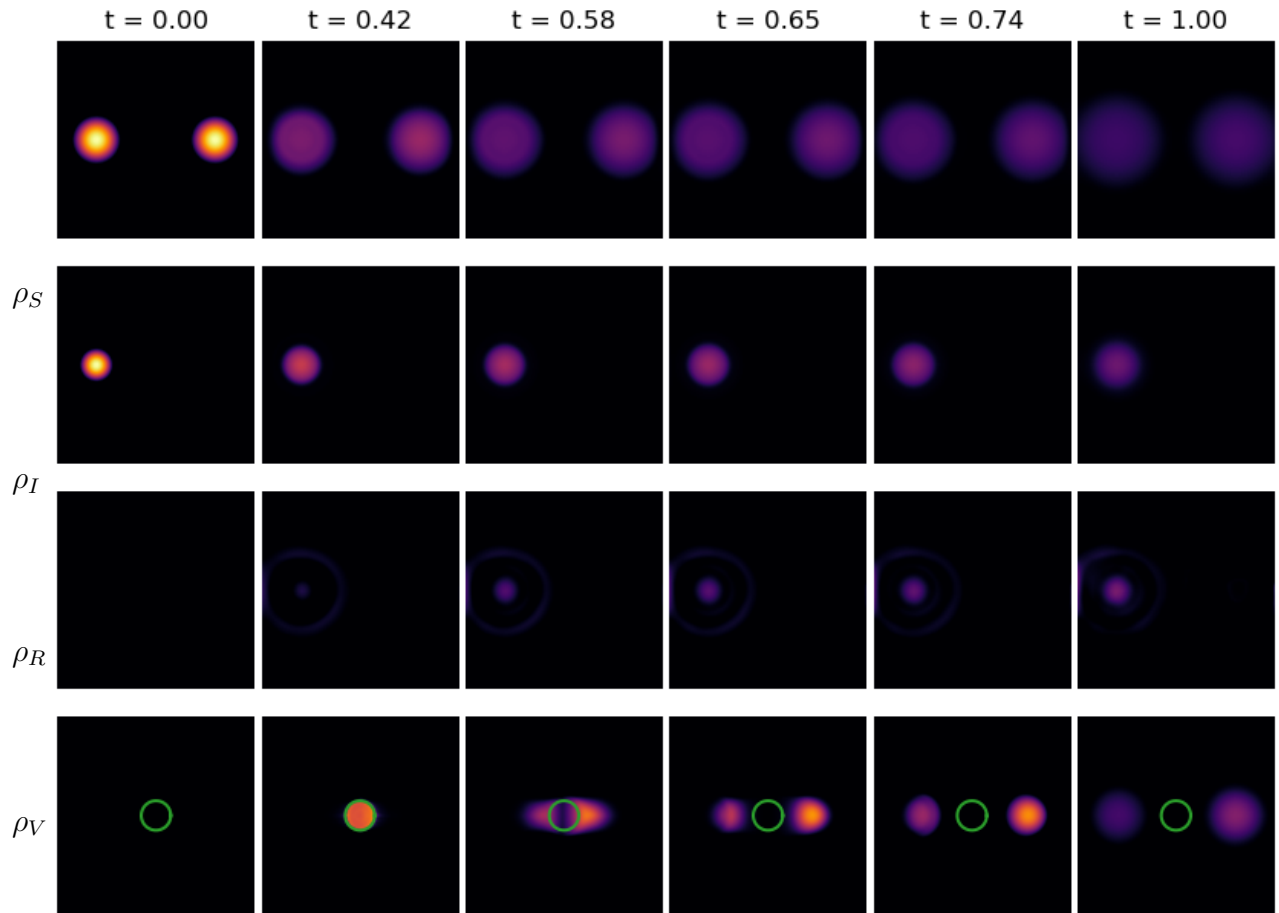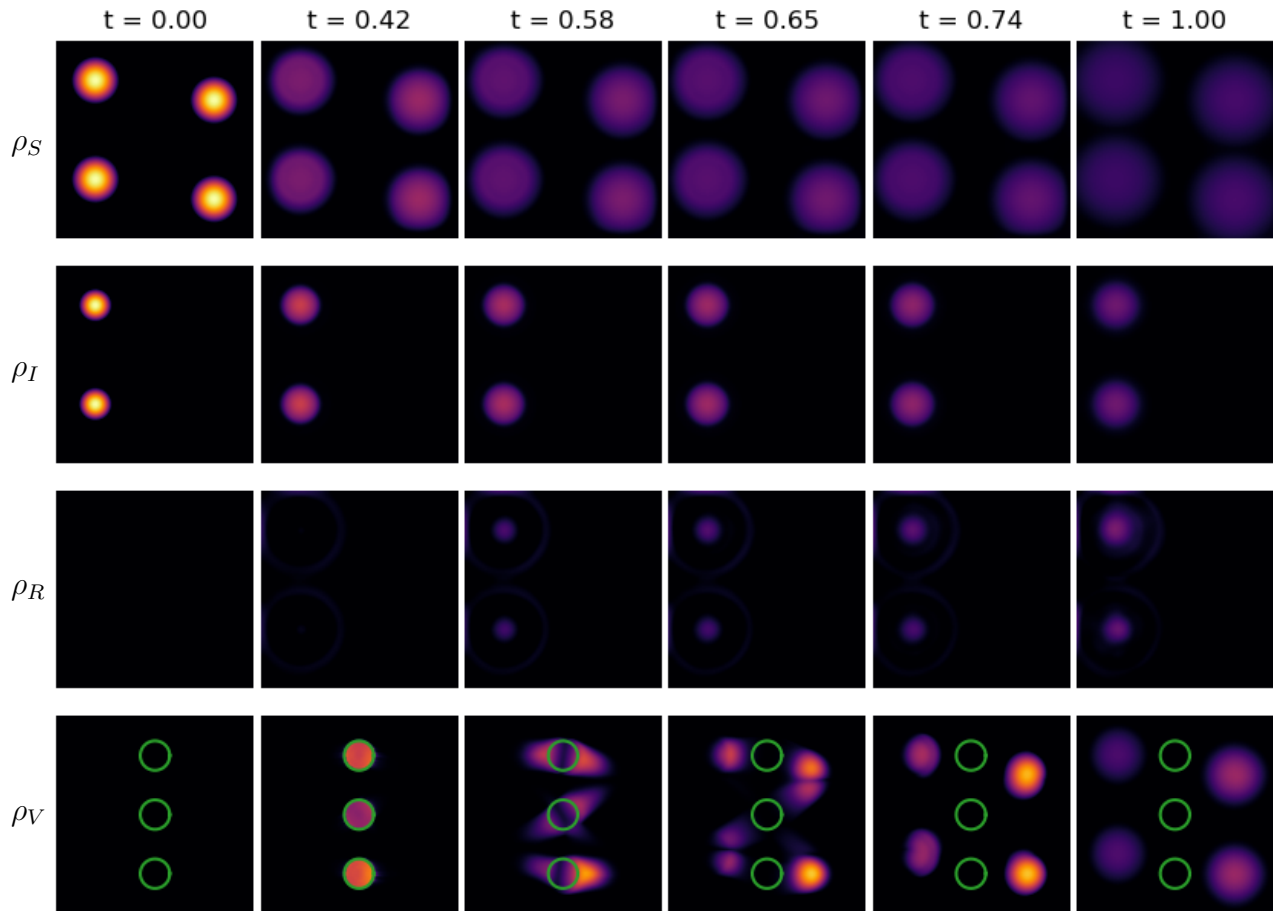

Figure 5.9: Experiment 2: The evolution of densities ρ_i ($i \in \mathbb{S}$) without the obstacle over time $0 \leq t \leq 1$. The first row: the susceptible density ρ_S. The second row: the infected density ρ_I. The third row: the recovered density ρ_R. The fourth row: the vaccine density ρ_V.

126
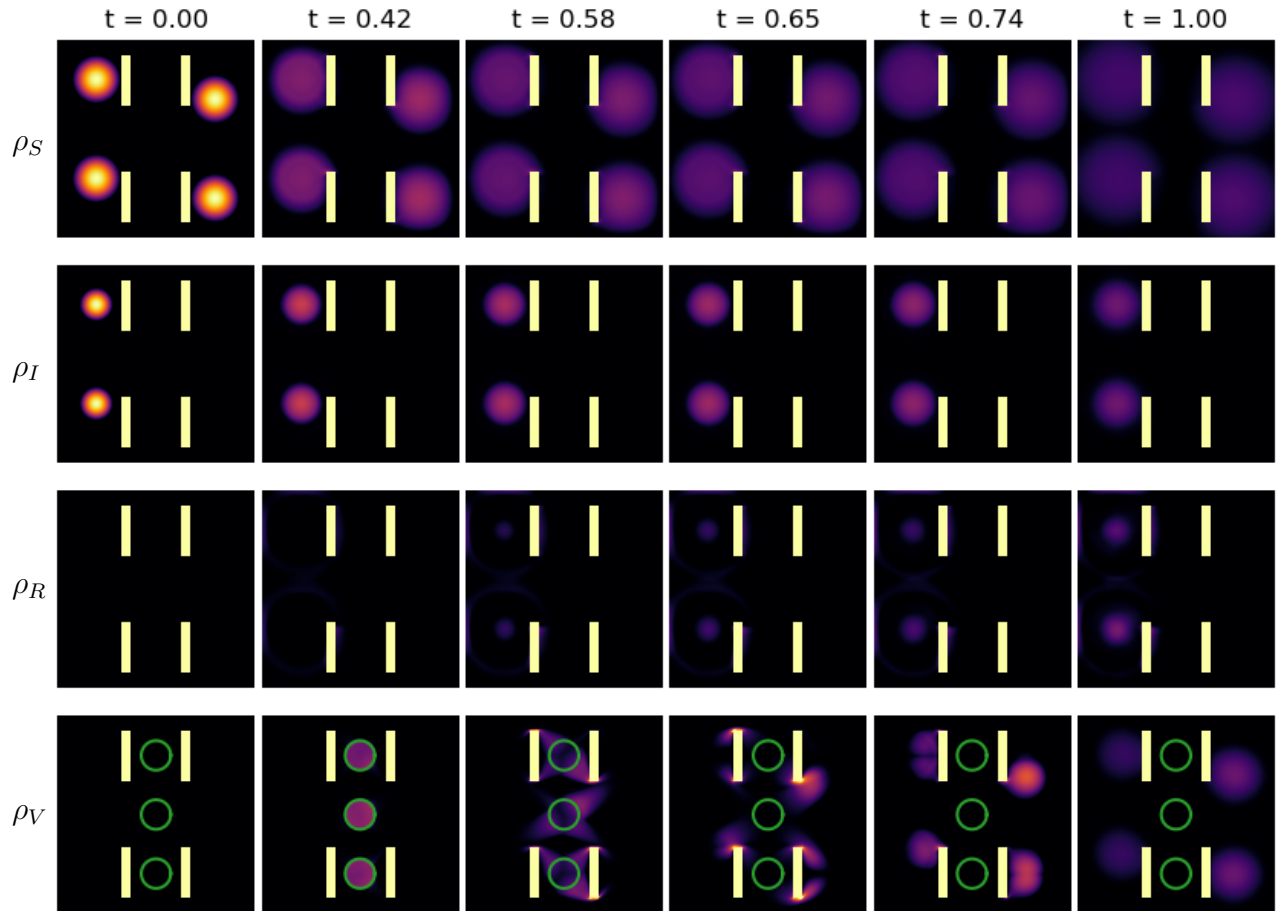
Figure 5.10: Experiment 2: The evolution of densities ρ_i ($i \in \mathbb{S}$) with the obstacle (colored yellow) over time $0 \le t \le 1$. The first row: the susceptible density ρ_S. The second row: the infected density ρ_I. The third row: the recovered density ρ_R. The fourth row: the vaccine density ρ_V.

experiments. The density of vaccines ρ_V (the fourth row) transports to the areas where the susceptible people are present while avoiding the obstacles.

Figure 5.11a shows the total mass of the vaccines produced during the production time at each factory location. Without the obstacles, the total mass of ρ_V at the middle is the lowest at time 0.5 because the factory at the middle is the farthest away from the susceptible people. It is more efficient to produce the vaccines at the factories closer to the susceptible (the top and the bottom) to reduce the kinetic energy cost during the delivery time $t \in [0.5, 1]$. However, the vaccines are produced the most at the middle factory with the obstacles. Since the obstacles block the paths between the top and the bottom factories and the susceptible people, ρ_V has to bypass them to reach the target area. The pathways from the middle factory to the susceptible people are not blocked as much as from the top and the bottom factories. Thus, producing more vaccines at the middle factory is more efficient.

Figure 5.11b shows the total mass of the vaccines during the delivery time at different locations. The lines in the plot represent the following quantities:

$$\int_{\Omega \cap \{x_1 < 0.5\} \cap \{x_2 \geq 0.5\}} \rho_V(t, x) \, dx, \quad \text{Top Left} \qquad \int_{\Omega \cap \{x_1 \geq 0.5\} \cap \{x_2 \geq 0.5\}} \rho_V(t, x) \, dx, \quad \text{Top Right}$$

$$\int_{\Omega \cap \{x_1 < 0.5\} \cap \{x_2 < 0.5\}} \rho_V(t, x) \, dx, \quad \text{Bottom Left} \qquad \int_{\Omega \cap \{x_1 \geq 0.5\} \cap \{x_2 < 0.5\}} \rho_V(t, x) \, dx, \quad \text{Bottom Right}$$

over $t \in [0.5, 1]$. With the obstacles, the kinetic energy cost increases since ρ_V has to bypass to reach to the targets when it transports from the top and the bottom factories. As a result, the vaccines are not produced as much as the simulation without the obstacles, and there are less vaccines reached to the targets.

5.4.3   Experiment 3

This experiment compares the vaccine production strategy generated by the algorithm and the strategy with the fixed rates of production without using the algorithm. The initial
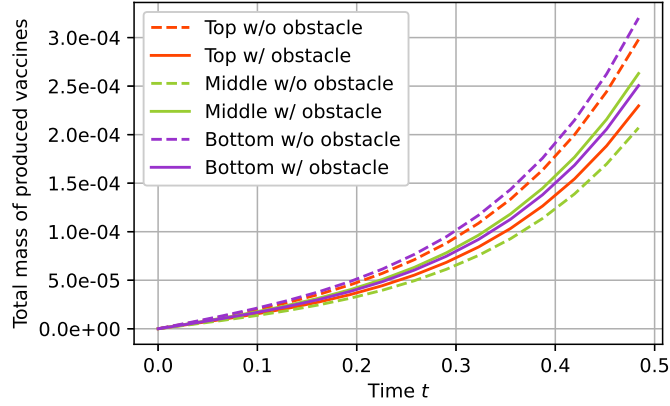
(a) The total mass of ρ_V during $t \in [0, 0.5)$
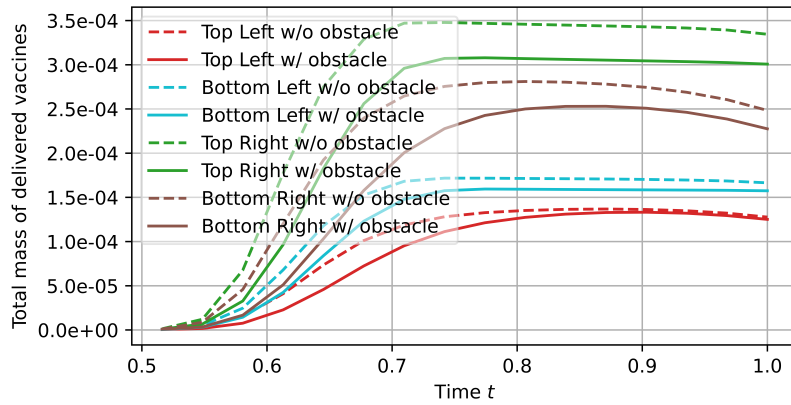
(b) The total mass of ρ_V during $t \in [0.5, 1]$

Figure 5.11: Experiment 2: The top plot shows the total mass of vaccine density ρ_V at three factory locations during the production time $t \in [0, 0.5)$. The bottom plot shows the total mass of ρ_V at the top left area of the domain $\Omega \cap \{x_1 < 0.5\} \cap \{x_2 \geq 0.5\}$, at the bottom left area $\Omega \cap \{x_1 < 0.5\} \cap \{x_2 < 0.5\}$, at the top right area $\Omega \cap \{x_1 \geq 0.5\} \cap \{x_2 \geq 0.5\}$, and at the bottom right area $\Omega \cap \{x_1 \geq 0.5\} \cap \{x_2 < 0.5\}$ during the distribution time $t \in [0.5, 1]$.

densities and $\Omega_{factory}$ are set as follows

$$\rho_S(0, x) = \left(4\exp(-15((x_1 - 0.5)^2 + (x_2 - 0.55)^2)) - 1.6\right)_+$$

$$\rho_I(0, x) = \left(4\exp(-15((x_1 - 0.5)^2 + (x_2 - 0.55)^2)) - 1.8\right)_+$$

$$\rho_R(0, x) = 0$$

$$\rho_V(0, x) = 0$$

$$\Omega_{factory} = B_{0.04}(0.1, 0.3) \cup B_{0.04}(0.5, 0.3) \cup B_{0.04}(0.9, 0.4).$$

We fix the parameters

$$\theta_1 = 0.9, \quad f_{max} = 5, \quad C_{factory} = 1.$$

The initial densities and locations of factories are shown in Figure 5.12.
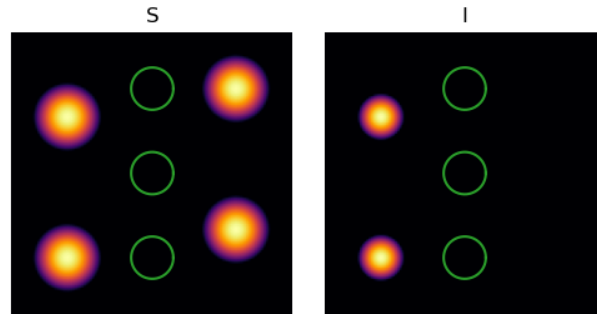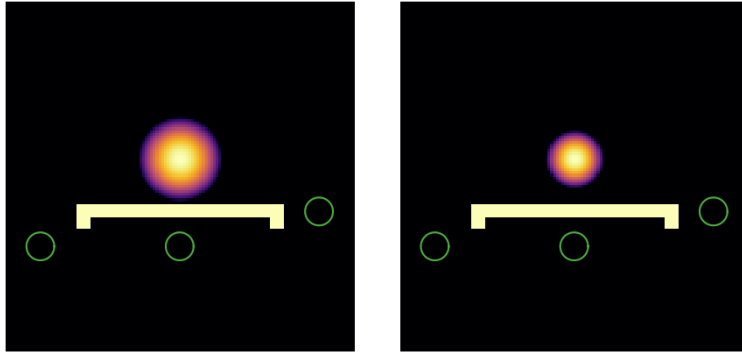

Figure 5.12: Experiment 3: The initial densities ρ_S (left) and ρ_I (right), the location of the factory (indicated as green circles), and the obstacle (colored yellow).

To fairly compare the effect of the optimal vaccine production strategy, we remove the momentum of S, I, R groups; thus, removing the spatial movements defined by m_S, m_I, m_R.

We consider the following PDEs:

$$\partial_t \rho_S = -\beta \rho_S K * \rho_I + \frac{\eta_S^2}{2}\Delta\rho_S - \theta_1\rho_V\rho_S \quad (t,x) \in (0,T) \times \Omega$$

$$\partial_t \rho_I = \beta \rho_S K * \rho_I - \gamma\rho_I + \frac{\eta_I^2}{2}\Delta\rho_I \qquad (t,x) \in (0,T) \times \Omega$$

$$\partial_t \rho_R = \gamma\rho_I + \frac{\eta_R^2}{2}\Delta\rho_R + \theta_1\rho_V\rho_S \qquad (t,x) \in (0,T) \times \Omega$$

$$\partial_t \rho_V = f(t,x) - \theta_2\rho_V\rho_S \qquad\qquad (t,x) \in (0,T') \times \Omega$$

$$\partial_t \rho_V + \nabla \cdot m_V = -\theta_2\rho_V\rho_S \qquad\qquad (t,x) \in [T',T) \times \Omega.$$

Furthermore, by taking out the momentum terms from S, I, R groups, the cost functional for this experiment is

$$G((\rho_i, m_i)_{i\in\mathbb{S}}, f) = \int_\Omega \frac{a_V}{2}\rho_V(T,\cdot)^2\,dx + \int_{T'}^T \int_\Omega F_V(\rho_V, m_V)\,dx\,dt + \int_0^T \int_\Omega \frac{d_V}{2}\rho_V^2\,dx\,dt$$

$$+ \int_0^{T'} \int_\Omega \frac{d_0}{2}f^2 + i_{\Omega_{factory}}f\,dx\,dt$$

$$+ \int_0^T i_{\{\rho(t,\cdot)\le C_{factory}\}}(\rho(t,\cdot)) + i_{\{f(t,\cdot)\le f_{max}\}}(f(t,\cdot))\,dt$$

$$+ \frac{\lambda}{2}\int_0^T \int_\Omega f^2 + \rho_V^2 + |m_V|^2\,dx\,dt.$$

With the PDEs and the cost functionals above, we compare two results. The first result is using the optimal vaccine production and distribution strategy generated by the algorithm 1. The second result is using the fixed vaccine production rate and the algorithm's distribution strategy. In the second result, the factory variable f is fixed as

$$f(t,x) = \begin{cases} 1.2, & (t,x) \in [0,T'] \times \Omega_{factory} \\ 0, & (t,x) \in [0,T'] \times \Omega\backslash\Omega_{factory}. \end{cases}$$

Figure 5.13 shows the comparison between these two results. The result from the fixed production rate is "without control", and the result from the optimal vaccine production strategy is "with control". The labels "left", "middle", and "right" are the locations of the factories in Figure 5.12. The solid lines, the result with the same fixed rates of production, show that all three factories produce identical amounts of vaccines. The dotted lines show the

least amount of vaccines in the middle factory and much more in the left and right factories. When vaccines produce at the middle factory, one needs to pay more transportation costs because they bypass the obstacles. The obstacle does not block the paths from the left and right factories to the susceptible. Thus, it's an optimal choice to utilize the left and right more than the middle to minimize the transportation costs.
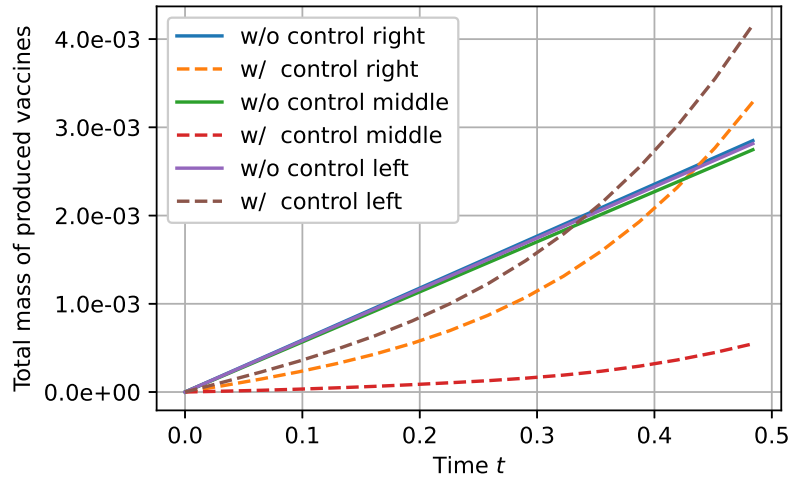
Figure 5.13: Experiment 3: The plot shows the total mass of vaccine densities $\int_0^t \int_\Omega \rho_V \, dx \, dt$ during production $t \in [0, T']$ at each factory location: left, middle, and right. The dotted lines are from the optimal strategy from the Algorithm 1, and the solid lines are from the fixed production rates.

Table 5.1 is the quantitative comparison between the two results.

The first row of the table shows that more vaccines are produced with a fixed rate of production. However, the result of the fixed-rate vaccinizes fewer susceptible people; as a result, more infected people at the terminal time. Furthermore, the result from the fixed rate shows higher transportation costs. The algorithm finds the more efficient strategy with fewer vaccines produced.

Quantity	Description	Algorithm 1	Fixed rates
$\int_\Omega \rho_V(\frac{1}{2}, x)\, dx$	The total amount of vaccines produced.	7.997×10^{-3}	8.411×10^{-3}
$\int_\Omega \rho_S(1, x)\, dx$	The number of susceptible people at the terminal time.	1.520×10^{-2}	1.525×10^{-2}
$\int_\Omega \rho_I(1, x)\, dx$	The number of infected people at the terminal time.	5.133×10^{-3}	5.134×10^{-3}
$\int_{\frac{1}{2}}^{1} \int_\Omega \frac{|m_V|^2}{2\rho_V}\, dx\, dt$	The transportation cost of vaccines.	7.339×10^{-3}	7.544×10^{-3}

Table 5.1: Comparison of vaccine production of fixed and non-fixed rate.

CHAPTER 6

A Numerical Algorithm for Inverse Problem from Partial Boundary Measurement Arising from Mean-Field Game Problem

This chapter considers a new inverse problem arising from mean-field games. We aim to recover the MFG model parameters that govern the underlying interactions among the population based on a limited set of noisy partial observations of the population dynamics under the fixed aperture. Due to its severe ill-posedness, maintaining high quality in the reconstruction is very difficult. Nonetheless, it is vital to recover the model parameters stably and efficiently to uncover the underlying causes of population dynamics for practical needs. Our work focuses on the simultaneous recovery of running cost and interaction energy in the MFG equations from a finite number of boundary measurements of population profile and movement. We formalize the inverse problem as a constrained optimization problem of a least squared residual functional under suitable norms to achieve this goal. Then we develop a fast and robust operator splitting algorithm to solve the optimization using techniques including harmonic extensions, the three-operator splitting scheme, and the primal-dual hybrid gradient method. The numerical experiments illustrate the effectiveness and robustness of the algorithm.

This chapter is organized as follows. Firstly in Section 6.1, we discuss the motivation for studying inverse mean-field games and related studies. In Section 6.2, we introduce an abstract inverse problem with a saddle point constraint and a generic algorithm to solve it.

In Section 6.3, we present the inverse MFG formulation. Next, in Section 6.4 we discuss the implementation of the algorithm in Section 6.2 for the inverse MFG in Section 6.3. Section 6.5 contains three numerical examples to demonstrate the robustness and effectiveness of our algorithm. Finally, Section 6.6 contains a discussion and concluding remarks.

The contributions in this chapter were first presented in the joint work with Yat Tin Chow, Samy Wu Fung, Levon Nurbekyan, and Stanley Osher in[CFL22].

6.1 Introduction

The basis for the MFG framework is the concept of Nash equilibrium, where agents cannot unilaterally improve their objectives. Under suitable regularity assumptions, a common MFG model reduces to the following system of partial differential equations (PDE):

$$
\begin{cases}
-\partial_t \phi(x,t) - \nu \Delta \phi(x,t) + H(x, \nabla_x \phi(x,t)) = F(x, \rho(\cdot,t)), \text{ in } \Omega' \times (0,1), \\
\partial_t \rho(x,t) - \nu \Delta \rho(x,t) - \nabla_x \cdot (\rho(x,t) \nabla_p H(x, \nabla_x \phi(x,t))) = 0, \text{ in } \Omega' \times (0,1), \\
\rho(x,0) = \rho_0(x), \ \phi(x,1) = g(x), \text{ in } \Omega'.
\end{cases}
$$

Here, $\rho(\cdot,t)$, $t \in [0,1]$ represents the population distribution over the state space Ω' at time t satisfying a Fokker-Planck equation, and $\phi(x,t)$ is the value function of each player that satisfies a Hamilton-Jacobi equation and governs optimal actions of players. The Hamiltonian, H, is the Legendre transform of the Lagrangian, L, representing the running cost for each agent. Furthermore, F represents an interaction between the agents and the population. Typical choices for H, L, F in crowd motion applications are

$$
H(x,p) = \frac{1}{2}\kappa(x)|p|^2, \ L(x,v) = \frac{1}{2\kappa(x)}|v|^2, \ F(x,\rho) = \int_{\Omega'} K(x,y)\rho(y)dy. \quad (6.1.2)
$$

MFG is an actively growing field that provides a flexible tremendously powerful descriptions ranging from socioeconomics to biodiversity ecology, and have recently gained enormous attention. They significantly advancing the understanding of social cooperation and economics

[ABL14, CL18, GNP15], biological systems [SB18], election dynamics [YYT18], population games [LT20], robotic control [LWL18], machine learning [ROL20, LFL21], dynamics of multiple populations [Cir15]. Recently, they are utilized to understand pandemic modeling and control such as COVID-19 [LLT21].

With the significant descriptive power of MFGs, it is vital to consider inverse problems arising in MFGs. We aim to reconstruct MFG parameters for a class of nonlocal problems, including the geometry of the underlying space and the interactions between large crowds, based on partial population observations. More specifically, we are interested in the following problem.

Problem 1. *Given a part of the solution to an MFG system* (6.1.1), (6.1.2), *for instance,*

$$\Big(\rho\left(x, s\right), -\rho\left(x, s\right) \nabla_p H(x, \nabla_x \phi(x, t))\Big)\big|_{\partial\Omega \times (0, T)},$$

for finitely many examples of ρ_0 and terminal cost g, can we numerically recover the speed field $\kappa(x)$ and the interaction kernel $K(x, y)$ from observations?

Such a model-recovery algorithm can help understand the underlying population dynamics in numerous problems, such as migration flow or contagious rate of COVID-19. We further envision applications to include rescue and exploration team management, policymaking, diplomacy, election modeling, catastrophe management, and evacuation planning.

Note that $m(x, s) = -\rho\left(x, s\right) \nabla_p H(x, \nabla_x \phi(x, s))$ represents the flux of the agents through the state x at time s as a result of optimal actions. The interpretation of the flux is straightforward for crowd-dynamics models and can be measured by counting people crossing checkpoints or parts of the border. For such models, the value function $\phi(x, s)$ could represent the travel cost for a traveller who is at location x at time s. Hence, one could also consider an inverse problem where one observes the value function, instead of the flux, by looking at travel companies' expenses or consumer ticket prices (discounted for the companies' profit margins).

For economic and finance models [GPV16, ABL14, CL18] the state variables typically represent asset (wealth, income, inventory) levels instead of a physical location. Hence, the value function represents maximal utility for agents with a given asset level, and the flux represents the total amount of transactions performed by them. Interestingly, in economic models one often has *implicit* mean-field interactions reflected in *market-clearing* type conditions instead of an explicit interaction functional $F(x, \rho)$. Hence, a related inverse problem is to find an appropriate market-clearing condition or tune its parameters for a given economy. This chapter addresses explicit models with flux data leaving the implicit ones with other data types for future work.

6.1.1 Related work

Despite of the large body of work on theory, numerical methods, and applications [ACD20], inverse problems arisen from MFG is still quite an unexplored terrain. To the best of our knowledge, only [DLO20, KAS15, BPW20] study such problems. The work in [DLO20] is the closest to our objective but considers the case with a full space-time measurement of data in the sampling domain. However, most inverse problems in practice only have partial boundary measurements available, either obtained via non-invasive measurement methods or because of the limited access to the sampling domain. Compared with the case with full space-time measurement in the domain, inverse problems with only partial boundary measurements are generally known to be more severely ill-posed. In this work, we focus on the recovery problem with only boundary measurements coming from several measurement events.

6.2 An inverse problem with a saddle point forward model

In this section, we formulate an abstract inverse problem with a saddle point forward model. We discuss suitable Karush-Kuhn-Tucker (KKT) conditions and a generic algorithm to solve such inverse problems.

6.2.1   A forward saddle point problem

Consider a saddle point problem

$$\min_{x \in \mathcal{X}} \max_{y \in \mathcal{Y}} F(u, x, y, c), \tag{6.2.1}$$

where $F : \mathcal{U} \times X \times Y \times \mathcal{D} \to \mathbb{R} \bigcup \{\pm\infty\}$ a smooth functional such that $(x, y) \mapsto F(u, x, y, c)$ is strongly convex-concave. Here, x is the primal variable, and y is the dual variable in the forward problem. Commonly, y is either used to handle constraints in the forward problem or linearize nonlinear components via some splitting scheme. The variable c represents model parameters associated with the functional F, while u represents boundary and initial-terminal conditions. Given model parameters c, we define a boundary measurement map Λ_c as follows:

$$\Lambda_c : \mathcal{U} \quad \to \quad \Pi_B X \times \Pi_B Y$$

$$u \quad \mapsto \quad (\Pi_{B,x}(x), \Pi_{B,y}(y)) \text{ where } (x, y) \in \underset{x}{\operatorname{argmin}} \underset{y}{\operatorname{argmax}} F(u, x, y, c),$$

where $\Pi_{B,x}, \Pi_{B,y}$ denote a projection operator that represent the partial boundary measurements of x, y available. We note that u corresponds to boundary conditions of the forward problem, whereas B is the subset of the domain where the partial measurements are collected.

6.2.2   The inverse problem and a generic algorithm

Assume that

$$(\tilde{r}_{B,i}, \tilde{s}_{B,i}) \approx \Lambda_c(u_i) = ([\Pi_{B,x}(x)](u_i), [\Pi_{B,y}(y)](u_i))$$

are noisy measurements for a given $\{u_i\}_{i=1}^N \in \mathcal{U}$. Our goal is to recover $c \in \mathcal{D}$. We formulate this problem as a constrained optimization problem

$$\inf_{\{x_i, y_i\}_{i=1}^N, c} \left\{ \sum_{i=1}^N \frac{1}{2} \|\Pi_{B,x}(x_i) - \tilde{r}_{B,i}\|^2 + \sum_{i=1}^N \frac{1}{2} \|\Pi_{B,y}(y_i) - \tilde{s}_{B,i}\|^2 + R(c) : \right.$$

$$\left. (x_i, y_i) \in \underset{x}{\operatorname{argmin}} \underset{y}{\operatorname{argmax}} F(u_i, x, y, c) \right\}, \tag{6.2.2}$$

where R is a suitable regularizer and $\| \cdot \|$ are suitable choices of (semi)-norms. Introducing Lagrange multipliers (dual variables) $(\lambda_{x_i}, \lambda_{y_i})$, (6.2.2) reduces to

$$\inf_{\{x_i, y_i\}_{i=1}^N, c} \sup_{\{\lambda_{x_i}, \lambda_{y_i}\}_{i=1}^N} \left\{ \sum_{i=1}^N \frac{1}{2} \|\Pi_{B,x}(x_i) - \tilde{r}_{B,i}\|^2 + \sum_{i=1}^N \frac{1}{2} \|\Pi_{B,y}(y_i) - \tilde{s}_{B,i}\|^2 + R(c) \right.$$
$$\left. + \sum_{i=1}^N \langle \partial_{x_i} F(u_i, x_i, y_i, c), \lambda_{x_i} \rangle - \sum_{i=1}^N \langle \partial_{y_i} F(u_i, x_i, y_i, c), \lambda_{y_i} \rangle \right\}.$$
$$(6.2.3)$$

Thus, the KKT condition for (6.2.2), (6.2.3) are as follows:

$$\begin{cases} \Pi_{B,x}^*[\Pi_{B,x}(x_i) - \tilde{r}_{B,i}] + \partial_{x_i,x_i}^2 F(u_i, x_i, y_i, c)\lambda_{x_i} & = 0, \\[2mm] \Pi_{B,y}^*[\Pi_{B,x}(y_i) - \tilde{s}_{B,i}] - \partial_{y_i,y_i}^2 F(u_i, x_i, y_i, c)\lambda_{y_i} & = 0, \\[2mm] \partial_c R(c) + \sum_{i=1}^N \langle \partial_c \partial_{x_i} F(u_i, x_i, y_i, c), \lambda_{x_i} \rangle - \sum_{i=1}^N \langle \partial_c \partial_{y_i} F(u_i, x_i, y_i, c), \lambda_{y_i} \rangle & = 0, \\[2mm] \partial_{x_i} F(u_i, x_i, y_i, c) & = 0, \\[2mm] -\partial_{y_i} F(u_i, x_i, y_i, c) & = 0, \end{cases}$$

for $i = 1, \ldots, N$. Here, $\Pi_{B,x}^*, \Pi_{B,y}^*$ are the adjoints of $\Pi_{B,x}, \Pi_{B,y}$, respectively.

Finally, we formulate these KKT conditions as an inclusion problem

$$0 \in A\left(c, (x,y), (\lambda_x, \lambda_y)\right) + C\left(c, (x,y), (\lambda_x, \lambda_y)\right),$$

where

$$A\left(c, (x,y), (\lambda_x, \lambda_y)\right) = \begin{pmatrix} \partial_c R(c) \\ (0,0) \\ (0,0) \end{pmatrix},$$

and

$$C\left(c, (x,y), (\lambda_x, \lambda_y)\right)$$

$$= \begin{pmatrix} \sum_{i=1}^{N} \langle \partial_c \partial_{x_i} F(u_i, x_i, y_i, c), \lambda_{x_i} \rangle - \sum_{i=1}^{N} \langle \partial_c \partial_{y_i} F(u_i, x_i, y_i, c), \lambda_{y_i} \rangle \\ \\ \left(\partial_{x_i} F(u_i, x_i, y_i, c), -\partial_{y_i} F(u_i, x_i, y_i, c) \right) \\ \\ \left(\partial^2_{x_i, x_i} F(u_i, x_i, y_i, c) \lambda_{x_i} + \Pi^*_{B,x} [\Pi_{B,x}(x_i) - \tilde{r}_{B,i}], \right. \\ \\ \left. -\partial^2_{y_i, y_i} F(u_i, x_i, y_i, c) \lambda_{y_i} + \Pi^*_{B,y} [\Pi_{B,x}(y_i) - \tilde{s}_{B,i}] \right) \end{pmatrix}.$$

Note that A is monotone but C is not known to be monotone in general.

6.2.3   A generic algorithm

Here, we outline an iterative algorithm for solving (6.2.3). At $(n + 1)$-th iteration, we first update the adjoint variables $\{(\lambda_{x_i}, \lambda_{y_i})\}_{i=1}^{N}$ using the Chambolle-Pock method [CP11]; then we update c for the inverse problem by taking a proximal gradient step; next we use the Chambolle-Pock method again to compute forward problems $\{(x_i, y_i)\}_{i=1}^{N}$. Summarizing, a high level description of the $(n + 1)$-th iteration is as follows:

$$\begin{cases} \begin{cases} \lambda_{y_i}^{n+1} &= [1 - \alpha_{\lambda_{y_i}} \partial^2_{y_i, y_i} F(u_i, x_i^n, y_i^n, c^n)]^{-1} \left(\lambda_{y_i}^n - \alpha_{\lambda_{y_i}} \Pi^*_{B,y} [\Pi_{B,y}(y_i^n) - \tilde{s}_{B,i}] \right) \\ \lambda_{x_i}^{n+1,\text{temp}} &= [1 + \alpha_{\lambda_{x_i}} \partial^2_{x_i, x_i} F(u_i, x_i^n, y_i^n, c^n)]^{-1} \left(\lambda_{x_i}^n - \alpha_{\lambda_{x_i}} \Pi^*_{B,x} [\Pi_{B,x}(x_i^n) - \tilde{r}_{B,i}] \right) \\ \lambda_{x_i}^{n+1} &= 2\lambda_{x_i}^{n+1,\text{temp}} - \lambda_{x_i}^{n,\text{temp}} \end{cases} \\ \begin{cases} c^{n+1} &= (I + \alpha_c \partial_c R)^{-1} \Big[c^n - \alpha_c \sum_{i=1}^{N} \langle \partial_c \partial_{x_i} F(u_i, x_i^n, y_i^n, c^n), \lambda_{x_i}^{n+1} \rangle \\ &\quad + \alpha_c \sum_{i=1}^{N} \langle \partial_c \partial_{y_i} F(u_i, x_i^n, y_i^n, c^n), \lambda_{y_i}^{n+1} \rangle \Big] \end{cases} \\ \begin{cases} x_i^{n+1} &= [1 + \alpha_{x_i} \partial_{x_i} F(u_i, \cdot, y_i^n, c^{n+1})]^{-1}(x_i^n) \\ y_i^{n+1,\text{temp}} &= [1 - \alpha_{y_i} \partial_{y_i} F(u_i, x_i^{n+1}, \cdot, c^{n+1})]^{-1}(y_i^n) \\ y^{n+1} &= 2y_i^{n+1,\text{temp}} - y_i^{n,\text{temp}}, \end{cases} \end{cases}$$

where $(\alpha_{\lambda_{x_i}}, \alpha_{\lambda_{y_i}}, \alpha_c, \alpha_{x_i}, \alpha_{y_i})$ are the corresponding time steps.

In what follows, we specify the MFG inverse problem and the implementation of the algorithm above for it.

6.3 An inverse MFG problem

Here, we explain the saddle point problem formulation of nonlocal MFG [NS18, LJL21, LN21] and formulate the inverse MFG problem of our interest.

6.3.1 Saddle point formulation of MFG via feature-space expansions

Consider the following MFG system with nonlocal couplings:

$$
\begin{cases}
-\phi_t(x,t) - \nu\Delta\phi(x,t) + \frac{\kappa(x)}{2}\|\nabla\phi(x,t)\|^2 = \int_{\Omega'} K(x,y)\rho(y,t)dy & \text{in } \Omega' \times (0,1), \\
\rho_t(x,t) - \nu\Delta\rho(x,t) - \nabla\cdot(\kappa(x)\rho(x,t)\nabla\phi(x,t)) = 0 & \text{in } \Omega' \times (0,1), \\
(\kappa(x)\rho(x,t)\nabla\phi(x,t))\cdot n = 0 & \text{on } \partial\Omega' \times (0,1), \\
\rho(x,0) = \rho_0(x), \ \phi(x,1) = g(x) & \text{in } \Omega'.
\end{cases}
\tag{6.3.1}
$$

We assume that K is positive definite and translation invariant, which yields that the mean-field interaction satisfies the Lasry-Lions monotonicity condition [LL07] and agents are crowd averse. Moreover, (6.3.1) admits a saddle point formulation

$$
\begin{aligned}
\inf_{\phi}\sup_{\rho,m} \Big\{ &-\int_{\Omega'}\phi(x,0)\rho_0(x)dx - \int_{\Omega'}\int_0^1 (\rho\phi_t + \nu\rho\Delta\phi + m\cdot\nabla\phi)\,dtdx \\
&- \int_{\Omega'}\int_0^1 \frac{1}{2\kappa(x)}\frac{\|m\|^2}{2\rho}dtdx - \frac{1}{2}\int_{\Omega'\times\Omega'} K(x,y)\rho(x,t)\rho(y,t)dxdy - \chi_{\rho\geq 0} + \chi_{\phi(x,1)=g(x)} \Big\}
\end{aligned}
\tag{6.3.2}
$$

Here, $\chi_Z(z)$ is the indicator function over the set Z defined by

$$
\chi_Z(z) = \begin{cases} 0, & \text{if } z \in Z \\ \infty, & \text{otherwise.} \end{cases}
$$

Modeling the interaction term

$$
\frac{1}{2}\int_{\Omega'\times\Omega'} K(x,y)\rho(x,t)\rho(y,t)dxdy
$$

directly is costly for both forward model and the inverse problem. Moreover, based on the works from [NS18, LJL21, LN21, ALF22], we model and approximate this term using feature-space expansions. More specifically, based on Bochner's theorem [Ron98], we postulate that

$$K(x, y) = \sum_{k=1}^{r} \mu_k^2 \cos(\omega_k \cdot (x - y))$$

$$= \sum_{k=1}^{r} \left(\mu_k^2 \cos(\omega_k \cdot x) \cos(\omega_k \cdot y) + \mu_k^2 \sin(\omega_k \cdot x) \sin(\omega_k \cdot y) \right)$$

for some $\{\omega_k\} \subset \mathbb{R}^d$, and $\{\mu_k^2\} \subset \mathbb{R}_+$. Denoting by

$$\mu = \left(\mu_{1,1}, \mu_{1,2}, \mu_{2,1}, \cdots, \mu_{r,1}, \mu_{r,2} \right) \quad \omega = \left(\omega_{1,1}, \omega_{1,2}, \omega_{2,1}, \cdots, \omega_{r,1}, \omega_{r,2} \right)$$

$$C_{\text{odd=even}} = \left\{ (x_{1,1}, x_{1,2}, x_{2,1}, \cdots, x_{r,1}, x_{r,2}) : x_{i,1} = x_{i,2} \right\}$$

$$\zeta(x; \mu, \omega) = \left(\mu_{1,1} \cos(\omega_{1,1} \cdot x), \mu_{1,2} \sin(\omega_{1,2} \cdot x), \cdots, \mu_{r,1} \cos(\omega_{r,1} \cdot x), \mu_{r,2} \sin(\omega_{r,2} \cdot x) \right)$$

we obtain

$$K(x, y) = \zeta(x; \mu, \omega) \cdot \zeta(y; \mu, \omega), \quad \mu, \omega \in C_{\text{odd=even}}.$$

Using this representation, we obtain

$$\frac{1}{2} \int_{\Omega' \times \Omega'} K(x, y) \rho(x, t) \rho(y, t) dt = \frac{1}{2} \left\| \int_{\Omega'} \zeta(x; \mu, \omega) \rho(x, t) dx \right\|^2$$

$$= \sup_a \left\{ a(t) \cdot \int_{\Omega'} \zeta(x; \mu, \omega) \rho(x, t) dx - \frac{1}{2} \int_0^1 \|a(t)\|^2 dt \right\},$$

where $a(t) = (a_{1,1}(t), a_{1,2}(t), .., a_{r,1}(t), a_{r,2}(t))$ are auxiliary dual variables. The last equality is a result from [NS18]. Hence, (6.3.2) transforms to

$$\inf_{\phi, a} \sup_{\rho, m} \left\{ \frac{1}{2} \int_0^1 \|a(t)\|^2 dt - \int_{\Omega'} \phi(x, 0) \rho_0(x) dx - \int_{\Omega'} \int_0^1 (\rho \phi_t + \nu \rho \Delta \phi + m \cdot \nabla \phi) \, dt dx \right.$$

$$\left. - \int_{\Omega'} \int_0^1 \left(\frac{1}{2\kappa(x)} \frac{\|m\|^2}{2\rho} + \rho \, a(t) \cdot \zeta(x; \mu, \omega) \right) dt dx - \chi_{\rho \geq 0} + \chi_{\phi(x,1) = g(x)} \right\}$$

$$:= \inf_{\phi, a} \sup_{\rho, m} \left\{ -\mathcal{L}\Big((\rho_0, g), (\rho, m), (\phi, a), (\kappa, \mu) \Big) \right\},$$

$$(6.3.3)$$

142

For more details on representation of nonlocal MFG interactions via a basis and computational methods, see [NS18, LN21, LJL21, ALF22]. We also attach an example Algorithm 3 here for calculating the nonlocal mean-field game problem.

Algorithm 3 Iterative algorithm for the nonlocal mean-field game system

---

Input: (ρ_0, g), (κ, μ), a set of initial guess $(\rho^0, m^0, \phi^0, a^0)$, e_{tol}, a set of stepsizes $(\alpha_\rho^j, \alpha_m^j, \alpha_\phi^j, \alpha_a^j)$

Output: $(\rho^*, m^*, \phi^*, a^*)$

while iteration $j < \mathcal{J}_{\max}$ and primal-dual gap $\mathrm{PD}(\rho^j, m^j, \phi^j, a^j) \geq e_{tol}$ **do**

$$
\begin{cases}
\begin{aligned}
(\rho^{j+1}, m^{j+1}) \quad &= \mathrm{argmin}_{(\rho,m)} \Bigg\{ \mathcal{L}\bigg((\rho_0, g), (\rho, m), (a^j, \phi^j), (\kappa, \mu) \bigg) \\
&\quad + \frac{1}{2\alpha_\rho^j} \|\rho^j - \rho\|_{L^2_{x,t}}^2 + \frac{1}{2\alpha_m^j} \|m^j - m\|_{L^2_{x,t}}^2 \Bigg\} \\
(\phi^{j+1,\mathrm{temp}}, a^{j+1,\mathrm{temp}}) \quad &= \mathrm{argmin}_{(a,\phi)} \Bigg\{ -\mathcal{L}\bigg((\rho_0, g), (\rho^{n+1}, m^{n+1}), (a, \phi), (\kappa, \mu) \bigg) \\
&\quad + \frac{1}{2\alpha_\phi^j} \|\phi^j - \phi\|_{H^1_{x,t}}^2 + \frac{1}{2\alpha_a^j} \|a^j - a\|_{L^2_t}^2 \Bigg\} \\
(\phi^{j+1}, a^{j+1}) \quad &= 2(\phi^{j+1,\mathrm{temp}}, a^{j+1,\mathrm{temp}}) - (\phi^j, a^j)
\end{aligned}
\end{cases}
$$

$\quad j \leftarrow j + 1$

end while

return $(\rho^j, m^j, \phi^j, a^j)$

6.3.2   An inverse mean-field game problem

Denoting by

$$
u = (\rho_0, g), \quad x = (\rho, m), \quad y = (\phi, a), \quad c = (\kappa, \mu),
$$
$$
F\big((\rho_0, g), (\rho, m), (\phi, a), (\kappa, \mu) \big) = \mathcal{L}\big((\rho_0, g), (\rho, m), (\phi, a), (\kappa, \mu) \big),
$$

we place the MFG forward model in the abstract framework (6.2.1). Next, we assume that $\Omega \subset \Omega'$ and $\kappa(x)$ is known in the domain $\Omega' \backslash \Omega$. We refer to Ω and Ω' as sampling and

computational domains, respectively. An example is shown in Figure 6.1, where the Ω' is the large square domain, while Ω is the inner square with its boundary highlighted in red.
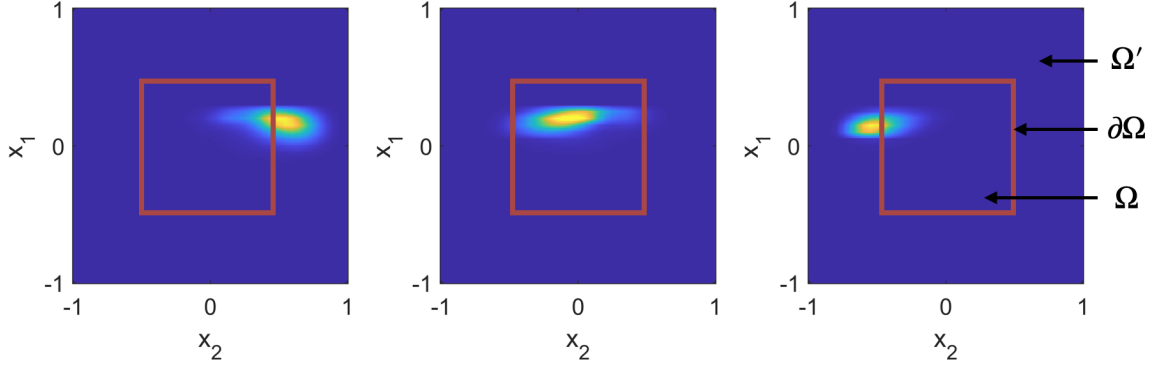
Figure 6.1: Denote ρ as the solution to the mean-field game system. From left to right, the pictures display the density distribution ρ at time $t = 0.1, 0.5, 0.9$. The solid red line represents the boundary of domain Ω. In this mean-filed game, the density travels from the right towards the left, crossing the boundary $\partial\Omega$ twice.

Next, we take

$$\Pi_{B,(\rho,m)}\left(\rho, m\right) := \left.(\rho, m \cdot n)\right|_{[0,T] \times \partial\Omega^+}, \quad \Pi_{B,(a,\phi)}(a, \phi) := (0, 0),$$

for the partial boundary measurement along the boundary $\partial\Omega$. Here, $\partial\Omega^+$ means that the normal vector n is pointing outward. Measuring the density and flux through $\partial\Omega$ is reasonable based on physical meaning of the variables. We cannot measure a directly because it is a non-physical auxiliary variable introduced specifically for an efficient representation of nonlocal interactions.

We assume that the ground truth parameters (κ, μ) represent a disturbance of background parameters (κ_0, μ_0). Therefore, given an additional parameter $\varepsilon \geq 0$, we would also like to have a regularization term in the form of $R_\beta = \chi_{\beta \geq \varepsilon}(\beta)$. We also write $R(\kappa, \mu) = R_1(\kappa, \mu) + R_2(\kappa, \mu)$, where

$$R_1(\kappa, \mu) = \tilde{R}_1(\kappa) + \tilde{R}_2(\mu) := \gamma_\kappa \|\kappa - \kappa_0\|_{L^1} + \gamma_\mu \|\mu - \mu_0\|_{L^1},$$

144

$$R_2(\kappa, \mu) := \chi_{\kappa \geq \varepsilon_1}(\kappa) + \chi_{\mu^2 \leq \varepsilon_2}(\mu).$$

It is also possible to have other choices of regularization for (κ, μ), such as TV, H^1, Wavelet norms.

Now, we can formulate the inverse MFG as follows:

$$
\inf_{\substack{\{(\rho_i, m_i), (\phi_i, a_i)\}_{i=1}^N, \\ \kappa, \mu}} \left\{ \sum_{i=1}^N \frac{1}{2} \|\Pi_B(\rho_i, m_i) - \tilde{r}_{B,i}\|^2 + R(\kappa, \mu) : \right.
$$

$$
\left. (\rho_i, m_i), (\phi_i, a_i) \in \operatorname*{argmin}_{\rho, m} \operatorname*{argmax}_{\phi, a} F((\rho_{0,i}, g_i), (\rho, m), (\phi, a), (\kappa, \mu)) \right\}.
$$

$(6.3.4)$

6.3.3 The KKT conditions of the inverse mean-field game problem

We denote by

$$\mathcal{L}(\cdot) := \mathcal{L}\left((\rho_{0,i}, g_i), (\rho_i, m_i), (a_i, \phi_i), (\kappa, \mu)\right),$$

the function $\mathcal{L}$ defined in Equation 6.3.3 for simplicity. The KKT conditions for the inverse mean-field game problem are then

$$
\begin{cases}
\Pi^*_{B,(\rho,m)}[\Pi_{B,(\rho,m)}(\rho_i, m_i) - \tilde{r}_{B,i}] + \partial^2_{(\rho_i,m_i),(\rho_i,m_i)}\mathcal{L}(\cdot)\lambda_{(\rho_i,m_i)} = 0, \quad i = 1, ..., N, \\[2mm]
\Pi^*_{B,(a,\phi)}[\Pi_{B,(a,\phi)}(a_i, \phi_i) - \tilde{s}_{B,i}] - \partial^2_{(a_i,\phi_i),(a_i,\phi_i)}\mathcal{L}(\cdot)\lambda_{(a_i,\phi_i)} = 0, \quad i = 1, ..., N, \\[2mm]
\partial_{(\kappa,\mu)}R_1(\kappa, \mu) + \partial_{(\kappa,\mu)}R_2(\kappa, \mu) + \sum_{i=1}^N \left\langle \partial_{(\kappa,\mu)}\partial_{(\rho_i,m_i)}\mathcal{L}(\cdot), \lambda_{(\rho_i,m_i)} \right\rangle, \\[2mm]
- \sum_{i=1}^N \left\langle \partial_{(\kappa,\mu)}\partial_{(a_i,\phi_i)}\mathcal{L}(\cdot), \lambda_{(a_i,\phi_i)} \right\rangle = 0, \\[2mm]
\partial_{(\rho_i,m_i)}\mathcal{L}(\cdot) = 0, \quad i = 1, ..., N, \\[2mm]
-\partial_{(a_i,\phi_i)}\mathcal{L}(\cdot) = 0, \quad i = 1, ..., N.
\end{cases}
$$

Furthermore, the derivatives of $\mathcal{L}$ are given by

$$
\partial_{(\rho_i,m_i)}\mathcal{L} = \left(\partial_t \phi + \nu \Delta \phi - \frac{1}{2\kappa}\frac{|m|^2}{\rho^2} + a \cdot \zeta(\cdot; \mu, \omega), \nabla \phi + \frac{1}{\kappa}\frac{m}{\rho} \right)
$$

$$
\partial_{(a_i,\phi_i)}\mathcal{L} = \left(-a + \int_{\Omega'} \rho(y)\,\zeta(y; \mu, \omega)dx, -\partial_t \rho + \nu \Delta \rho - \nabla \cdot m \right)
$$

145

$$\partial^2_{(\rho_i, m_i),(\rho_i, m_i)}\mathcal{L} \;=\; \begin{pmatrix} \frac{1}{\kappa}\frac{|m|^2}{\rho^3} & -\frac{1}{\kappa}\frac{m}{\rho^2} \\[2ex] -\frac{1}{\kappa}\frac{m}{\rho^2} & \frac{1}{\kappa\rho}I \end{pmatrix}$$

$$\partial^2_{(a_i, \phi_i),(a_i, \phi_i)}\mathcal{L} \;=\; \begin{pmatrix} I & 0 \\[2ex] 0 & 0 \end{pmatrix}$$

$$\partial_{(\kappa,\mu)}\partial_{(\rho_i, m_i)}\mathcal{L} \;=\; \begin{pmatrix} \frac{1}{2\kappa^2(x)}\frac{|m|^2}{\rho^2} & -\frac{1}{\kappa^2(x)}\frac{m}{\rho} \\[2ex] \Lambda_1(\omega,\cdot)\,a & 0 \end{pmatrix}$$

$$\partial_{(\kappa,\mu)}\partial_{(a_i, \phi_i)}\mathcal{L} \;=\; \begin{pmatrix} 0 & 0 \\[2ex] \int_{\Omega'}\rho(y)\,\Lambda_1(\omega,y)dy & 0 \end{pmatrix}$$

where the variable $\Lambda_1(\omega, x)$ is defined as follows

$$\Lambda_1(\omega, x) = \begin{pmatrix} \begin{pmatrix} \cos(\omega_1 \cdot x) & 0 \\ 0 & \sin(\omega_1 \cdot x) \end{pmatrix} & \cdots & & 0 \\[3ex] & \vdots & \ddots & 0 \\[3ex] & 0 & \cdots & \begin{pmatrix} \cos(\omega_r \cdot x) & 0 \\ 0 & \sin(\omega_r \cdot x) \end{pmatrix} \end{pmatrix}.$$

6.4   The algorithm

We propose an inverse algorithm adapted from the three-operator splitting method [DY17], which has also been shown to predict Nash equilibria in traffic flows [HML21]. We also discuss stabilizing techniques that are essential in practice.

6.4.1 The three-operator splitting scheme

Denoting by $\lambda_{(\rho,m)} := (\lambda_\rho, \lambda_m)$ and $\lambda_{(a,\phi)} := (\lambda_a, \lambda_\phi)$ and applying the framework in Section 6.2 to (6.3.4) we obtain the following inclusion formulation of the inverse MFG problem:

$$0 \in A(\kappa, \mu) + B(\kappa, \mu) + C\left((\kappa, \mu), ((\rho, m), (a, \phi)), (\lambda_{(\rho,m)}, \lambda_{(a,\phi)})\right),$$

where

$$A(\kappa, \mu) = \begin{pmatrix} \partial R_1(\kappa, \mu) \\ (0,0) \\ (0,0) \end{pmatrix}, \quad B(\kappa, \mu) = \begin{pmatrix} \partial R_2(\kappa, \mu) \\ (0,0) \\ (0,0) \end{pmatrix},$$

and

$$C\left((\kappa, \mu), ((\rho, m), (a, \phi)), (\lambda_{(\rho,m)}, \lambda_{(a,\phi)})\right)$$

$$= \begin{pmatrix} \sum_{i=1}^{N} \left\langle \partial_{(\kappa,\mu)} \partial_{(\rho_i, m_i)} \mathcal{L}, \lambda_{(\rho_i, m_i)} \right\rangle \\ - \sum_{i=1}^{N} \left\langle \partial_{(\kappa,\mu)} \partial_{(a_i, \phi_i)} \mathcal{L}, \lambda_{(a_i, \phi_i)} \right\rangle \\ \left(\partial_{(\rho_i, m_i)} \mathcal{L}, -\partial_{(a_i, \phi_i)} \mathcal{L} \right) \\ \left(\partial^2_{(\rho_i, m_i),(\rho_i, m_i)} \mathcal{L} \lambda_{(\rho_i, m_i)} + \Pi^*_{B,(\rho,m)}[\Pi_{B,(\rho,m)}(\rho_i, m_i) - \tilde{r}_{B,i}], \right. \\ \left. -\partial^2_{(a_i, \phi_i),(a_i, \phi_i)} \mathcal{L} \lambda_{(a_i, \phi_i)} \right) \end{pmatrix}.$$

The three-operator splitting scheme in [DY17] applies to optimization problems of the form

$$\text{find} \quad z \in \mathcal{H} \quad \text{such that} \quad 0 \in Az + Bz + Cz, \tag{6.4.2}$$

147

where A, B, C are maximal monotone operators defined on a Hilbert space $\mathcal{H}$, and C is cocoercive. Denote by $I_{\mathcal{H}}$ the identity map in $\mathcal{H}$, and $J_S := (I + S)^{-1}$ the resolvent of a monotone operator S. The splitting scheme for solving (6.4.2) can be summarized as follows

$$z^{k+1} := (1 - \lambda_k)z^k + \lambda_k T z^k,$$

$$T := I_{\mathcal{H}} - J_{\gamma B} + J_{\gamma A} \circ (2J_{\gamma B} - I_{\mathcal{H}} - \gamma C \circ J_{\gamma B}),$$

where γ is a scalar. If an operator S is of the sub-differential forms; that is, $S = \partial f_S$ for some functional f_S, the resolvent J_S reduces to the proximal map $x \mapsto \underset{y}{\operatorname{argmin}} f_S(y) + \frac{1}{2}\|x - y\|^2$.

Overall, the algorithm for (6.4.1) follows three components of the generic framework in Section 6.2.3, upon some modification. In what follows, we discuss each component separately.

6.4.1.1 Update of the adjoint problem

Firstly, we choose $\|\cdot\|_{(\rho,m)}$ and $\|\cdot\|_{(a,\phi)}$ with $L^2([0,T], H^{-1/2}(\partial\Omega)) \times L^2([0,T], H^{1/2}(\partial\Omega))$ semi-norm, and $L_t^2 \times L_{x,t}^2$ norms, respectively. Here the $H^{\frac{1}{2}}(\partial\Omega)$ and $H^{-\frac{1}{2}}(\partial\Omega)$ semi-norm are taken as follows:

$$|v|^2_{H^{\frac{1}{2}}(\partial\Omega)} := \min_{v_0 \in H^1(\Omega),\, v_0 = v \text{ on } \partial\Omega} |v_0|^2_{H^1(\Omega)},$$

$$|v|^2_{H^{-\frac{1}{2}}(\partial\Omega)} := \min_{v_0 \in H_0^1(\Omega),\, \partial_n v_0 = \partial_n v \text{ on } \partial\Omega} |v_0|^2_{H^1(\Omega)},$$

where the right hand side denotes the standard $H^1(\Omega)$ semi-norm.

Assuming appropriate regularity of (ρ, m), we recall that the operator $\Pi_{B,(\rho,m)}$ is the restriction/trace operator onto the appropriate Sobolev space on the boundary $L^2\big([0,T], H^{-1/2}(\partial\Omega)\big) \times L^2\big([0,T], H^{1/2}(\partial\Omega)\big)$

$$\Pi_{B,(\rho,m)}(\rho, m) := (\rho, m \cdot n)\big|_{[0,T]\times\partial\Omega^+}.$$

With the aforementioned choice of the semi-norms, we naturally have the (formal) adjoint of $\Pi_{B,(\rho,m)}$, $\Pi^*_{B,(\rho,m)}$, as the Dirichlet and Neumann harmonic extension operators by definition; that is,

$$(\eta_i, \nabla\xi_i) := \Pi^*_{B,(\rho,m)}[\Pi_{B,(\rho,m)}(\rho_i^n, m_i^n) - \tilde{r}_{B,i}],$$

148

where (η_i, ξ_i) satisfy

$$\begin{cases} \begin{cases} \Delta\eta_i^{n+1} = 0 \text{ in } \Omega \\ \eta_i^{n+1} = \rho_i^n - \mathrm{pr}_1\tilde{r}_{B,i} \text{ on } \partial\Omega^+ \\ \Delta\eta_i^{n+1} = 0 \text{ in } \Omega'\backslash\Omega \\ \eta_i^{n+1} = \rho_i^n - \mathrm{pr}_1\tilde{r}_{B,i} \text{ on } \partial\Omega^- \\ \eta_i^{n+1} = 0 \text{ on } \partial\Omega' \end{cases} \quad \begin{cases} \Delta\xi_i^{n+1} = 0 \text{ in } \Omega \\ \partial_n\xi_i^{n+1} = m_i^n \cdot n - \mathrm{pr}_2\tilde{r}_{B,i} \text{ on } \partial\Omega^+ \\ \Delta\xi_i^{n+1} = 0 \text{ in } \Omega'\backslash\Omega \\ \partial_n\xi_i^{n+1} = m_i^n \cdot n + \mathrm{pr}_2\tilde{r}_{B,i} \text{ on } \partial\Omega^- \\ \partial_n\xi_i^{n+1} = 0 \text{ on } \partial\Omega' \end{cases} \end{cases} \quad (6.4.3)$$

Here we use $\mathrm{pr}_1, \mathrm{pr}_2$ to denote the projection from the noisy data. The harmonic extension is taken at each time $t \in [0,1]$ independently. In the implementation, we use a standard finite difference scheme to compute the harmonic extension on spatial grids for each time grid point. Note that if we assume $\kappa = \kappa_0$ to be known outside of domain Ω, the measurements of m and $\nabla\phi$ are equivalent, as $-\kappa_0(x)\rho(x)\partial_n\phi(x) = m(x) \cdot n$ on $\partial\Omega^+$.

We remark that the techniques of harmonic extension have been applied to various other problems, e.g. over point clouds and in machine learning [SST18].

It is clear to see that λ_ϕ is redundant and $\lambda_a = 0$ whenever $0 \in A + B + C$. Hence, we can consider only $C\big((\kappa, \mu), ((\rho, m), (a, \phi)), (\lambda_{(\rho,m)}, (0,0))\big)$. In this case, we preform a primal-dual hybrid gradient method for updating $\lambda_{(\rho,m)}$:

$$\begin{cases} \begin{pmatrix} \lambda_{\rho_i}^{n+1,\text{temp}} \\ \lambda_{m_i}^{n+1,\text{temp}} \end{pmatrix} = \\ \left[I + \alpha_{\lambda_{(\rho_i,m_i)}}^n \rho_i^n \begin{pmatrix} \frac{1}{\kappa^n} \frac{|m_i^n|^2}{(\rho_i^n)^3} & -\frac{1}{\kappa^n} \frac{m_i^n}{(\rho_i^n)^2} \\ -\frac{1}{\kappa^n} \frac{m_i^n}{(\rho_i^n)^2} & \frac{1}{\kappa^n \rho_i^n} I \end{pmatrix} \right]^{-1} \left(\begin{pmatrix} \lambda_{\rho_i}^n \\ \lambda_{m_i}^n \end{pmatrix} - \alpha_{\lambda_{(\rho_i,m_i)}}^n \rho_i^n \begin{pmatrix} \eta_i^{n+1} \\ \nabla\xi_i^{n+1} \end{pmatrix} \right) \\ \begin{pmatrix} \lambda_{\rho_i}^{n+1} \\ \lambda_{m_i}^{n+1} \end{pmatrix} = 2 \begin{pmatrix} \lambda_{\rho_i}^{n+1,\text{temp}} \\ \lambda_{m_i}^{n+1,\text{temp}} \end{pmatrix} - \begin{pmatrix} \lambda_{\rho_i}^{n,\text{temp}} \\ \lambda_{m_i}^{n,\text{temp}} \end{pmatrix} \end{cases} \quad (6.4.4)$$

6.4.1.2 Update of the inverse problem

In this part, we focus on the update for the inverse problem variables (κ, μ).

$$
\begin{cases}
\begin{cases}
\kappa^{n+1,\text{temp}} &= S_{\alpha_\kappa^n \gamma}\left(2\kappa^n - \tilde{\kappa}^n - \alpha_\kappa^n \sum_{i=1}^N \Lambda_\kappa(\kappa^n, m_i^n, \rho_i^n, \lambda_{\rho_i}^{n+1}, \lambda_{m_i}^{n+1}) - \kappa_0\right) + \kappa_0 \\
\tilde{\kappa}^{n+1} &= \tilde{\kappa}^n + \kappa^{n+1,\text{temp}} - \kappa^n \\
\kappa^{n+1} &= \max\left\{\varepsilon_1, \tilde{\kappa}^{n+1}\right\}
\end{cases} \\
\begin{cases}
\mu^{n+1,\text{temp}} &= S_{\alpha_\mu^n \gamma}\left(2\Pi_\mu^*(\mu^n) - \tilde{\mu}^n - \alpha_\mu^n \sum_{i=1}^N \Lambda_\mu(\lambda_{\rho_i}^{n+1}, a_i^n) - \Pi_\mu^*(\mu_0)\right) + \Pi_\mu^*(\mu_0) \\
\tilde{\mu}^{n+1} &= \tilde{\mu}^n + \mu^{n+1,\text{temp}} - \mu^n \\
\mu^{n+1} &= \Pi_\mu\left(\min\left\{\varepsilon_2, \tilde{\mu}^{n+1}\right\}\right)
\end{cases}
\end{cases}
$$

(6.4.5)

where $S_\alpha(r)$ is the shrinkage operator given as $S_\alpha(r) = \text{sign}(r)\max\{|r| - \alpha, 0\}$, and

$$
\Lambda_\kappa(\kappa, m, \rho, \lambda_\rho, \lambda_m) = \int_0^T \frac{1}{2(\kappa)^2} \frac{\|m(\cdot, s)\|^2}{(\rho(\cdot, s))^2} \lambda_\rho(\cdot, s) - \frac{1}{(\kappa)^2} \frac{m(\cdot, s)}{\rho(\cdot, s)} \lambda_m(\cdot, s) ds,
$$

$$
\Lambda_\mu(\lambda_\rho, a) = \int_0^T \int_{\Omega'} \Lambda_1(\omega, y) \lambda_\rho(y, s) a(s) dy ds.
$$

Since we have the $\mu, \omega \in C_{\text{odd=even}} := \{(x_{1,1}, x_{1,2}, x_{2,1}, x_{2,2}, ..., x_{r,1}, x_{r,2}) : x_{i,1} = x_{i,2} \forall i = 1, ..., r\}$, we write the projector $\partial \chi_{C_{\text{odd=even}}}$ (where we identify $C_{\text{odd=even}}$ with $\mathbb{R}^r$) as

$$
\Pi_\mu : \mathbb{R}^{2r} \to C_{\text{odd=even}} \cong \mathbb{R}^r
$$

$$
(x_{1,1}, x_{1,2}, x_{2,1}, x_{2,2}, ..., x_{r,1}, x_{r,2}) \mapsto \left(\frac{x_{1,1} + x_{1,2}}{2}, \frac{x_{2,1} + x_{2,2}}{2}, ..., \frac{x_{r,1} + x_{r,2}}{2}\right)
$$

and its adjoint as

$$
\Pi_\mu^* : \mathbb{R}^r \to \mathbb{R}^{2r}
$$

$$
(x_1, x_2, ..., x_r) \mapsto (x_1, x_1, x_2, x_2, ..., x_r, x_r).
$$

6.4.1.3 Update of the forward problem

As for the forward problem, we use primal–dual hybrid gradient method (PDHG) [CP11] to update $((\rho_i, m_i), (\phi_i, a_i))$ for each event i, for $1 \le i \le N$. The iterative updates contains

three parts: firstly a proximal gradient descent step for (ρ_i, m_i) with stepsizes $(\alpha^n_{\rho_i}, \alpha^n_{m_i})$; then a proximal gradient ascent step for (ϕ_i, a_i) of stepsizes $(\alpha^n_{\phi_i}, \alpha^n_{a_i})$; lastly an extrapolating step for (ϕ_i, a_i). Note that we make the choice of norm $\|\phi\|^2_{H^1_{x,t}} = \|\phi_t\|^2_{L^2_{x,t}} + \|\nabla_x \phi\|^2_{L^2_{x,t}}$ for ϕ, based on the General-proximal Primal-Dual Hybrid Gradient (G-prox PDHG) method [JLL19] that can be interpreted as a preconditioning step for obtaining a mesh-size-free convergence rate for the algorithm. Overall, the computation for the forward model follows the computational method proposed in [LJL21, LN21].

$$
\begin{cases}
(\rho_i^{n+1}, m_i^{n+1}) & = \mathrm{argmin}_{(\rho,m)} \Bigg\{ \mathcal{L}\Big((\rho_{0,i}, g_i), (\rho, m), (a_i^n, \phi_i^n), (\kappa^{n+1}, \mu^{n+1}) \Big) \\
& \quad + \frac{1}{2\alpha^n_{\rho_i}} \|\rho_i^n - \rho\|^2_{L^2_{x,t}} + \frac{1}{2\alpha^n_{m_i}} \|m_i^n - m\|^2_{L^2_{x,t}} \Bigg\} \\
(\phi_i^{n+1,\mathrm{temp}}, a_i^{n+1,\mathrm{temp}}) & = \mathrm{argmin}_{(a,\phi)} \Bigg\{ -\mathcal{L}\Big((\rho_{0,i}, g_i), (\rho^{n+1}, m^{n+1}), (a, \phi), (\kappa^{n+1}, \mu^{n+1}) \Big) \\
& \quad + \frac{1}{2\alpha^n_{\phi_i}} \|\phi_i^n - \phi\|^2_{H^1_{x,t}} + \frac{1}{2\alpha^n_{a_i}} \|a_i^n - a\|^2_{L^2_t} \Bigg\} \\
(\phi_i^{n+1}, a_i^{n+1}) & = 2(\phi_i^{n+1,\mathrm{temp}}, a_i^{n+1,\mathrm{temp}}) - (\phi_i^n, a_i^n)
\end{cases}
$$

(6.4.6)

Assembling all three components described above, we arrive at the following Algorithm 4 for solving the inverse problem (6.4.1).

6.4.2 Stabilizing techniques

Here, we discuss key numerical strategies for stabilizing Algorithm 4. We refer to Algorithm 5 for more implementation details.

While the change of κ^{n+1} is made from the accumulation of all measurement events (through $(\lambda^{n+1}_{\rho_i}, \lambda^{n+1}_{m_i})$), there is sometimes unexpected change of $\kappa^{n+1}(x)$ that makes the algorithm highly unstable. For instance, there may be a large $\kappa^{n+1}(x)$ at a single grid point. Moreover, we are using harmonic expansion method to update $(\lambda^{n+1}_{\rho_i}, \lambda^{n+1}_{m_i})$, which causes large variances of $\kappa(x)$ along the boundary $\partial\Omega$. Therefore, we add a cut-off function and

Algorithm 4 Inverse method for the nonlocal mean-field game system

---

Input: $(\rho_{0,i}, g_i, \tilde{r}_{B,i})$ for $i = 1, ..., N$, (κ_0, μ_0)

Output: (κ^n, μ^n) for $n = 1, ..., \mathcal{N}_{\max}$

while iteration $n < \mathcal{N}_{\text{maximal}}$ **do**

    1.Update for the adjoint problem:

        compute $(\lambda_{\rho_i}^{n+1}, \lambda_{m_i}^{n+1,})$ use (6.4.3)(6.4.4) for $i = 1, ..., N$.

    2. Update for the inverse problem:

        compute $(\kappa^{n+1}, \mu^{n+1})$ use (6.4.5)

    3. Update forward problem:

        compute $(\rho_i^{n+1}, m_i^{n+1}, \phi_i^{n+1}, a_i^{n+1})$ use (6.4.6) for $i = 1, ..., N$.

    $n \leftarrow n + 1$

end while

---

a convolution kernel to the step (6.4.5) to have a smoother change in $\kappa^{n+1}(x)$ in space. Specifically, we have

$$\begin{cases} \tilde{\kappa}^{n+1} & = \tilde{\kappa}^n + \mathcal{T}_{mask}(\kappa^{n+1,\text{temp}}, \kappa_0) - \kappa^n \\ \kappa^{n+1} & = \max\left\{\varepsilon_1, \tilde{\kappa}^{n+1} * \psi\right\} \end{cases},$$

where $\mathcal{T}_{mask}$ is a cut–off function that truncates the change of κ near $\partial\Omega$ given by

$$\mathcal{T}_{mask}(\kappa, \kappa_0)(x) = \xi(x)(\kappa - \kappa_0)(x) + \kappa_0(x),$$

for a function $\xi(x)$ vanishing near $\partial\Omega$. As for the convolution

$$\kappa^{n+1}(x) = \max\left\{\varepsilon_1, \int_{\Omega'} \tilde{\kappa}^{n+1}(y)\psi(x - y)dy\right\},$$

where the convolution kernel $\psi(x)$ satisfies $\int_\Omega \psi(x)dx = 1$.

On the other hand, after the inverse problem parameters $(\kappa^{n+1}, \mu^{n+1})$ are updated, we get new pair of parameters for a set of mean-field game problems. It is unclear whether starting

from $(\rho_i^n, m_i^n, \phi_i^n, a_i^n)$ and taking the update rule (6.4.6) once produces physical solutions for the new mean-field game system due to highly nonlinear dependence of the solution on the system parameters. Therefore, instead of preforming one iteration for the forward problem, we apply the PDHG algorithm for the forward problem until its error reaches a preset tolerance. More specifically, at every iteration n, with new system parameters $(\kappa^{n+1}, \mu^{n+1})$, we use $(\rho_i^n, m_i^n, \phi_i^n, a_i^n)$ as an initial guess and calculate the mean-field game solution accurately so that the primal–dual gap is smaller than residual the preset tolerance.

We summarize the inversion algorithm for the nonlocal mean-field game system in details in Algorithm 5.

6.5 Numerical examples

This section demonstrates the efficiency and robustness of the inverse mean-field game algorithm with three examples. We also discuss details on the rule we used to choose the best reconstruction parameters.

6.5.1 Numerical implementation details

In this section, we present several numerical examples to illustrate the effectiveness of the new algorithm for the reconstruction of parameters in the mean-field game problem.

We consider the spatial-time domain $\Omega' \times [0, T] = [-1, 1]^2 \times [0, 1]$. In the following examples, the partial boundary measurements are taken along the domain $\Omega = [-0.5, 0.5]^2$, we refer as $\partial \Omega$. The Figure 6.1 gives an example of the forward measurement event.

In order to collect our observed data of the forward problem, we solve a set of mean-field game problem (6.3.3) with given $(\rho_{0,i}, g_i)$ and (κ, μ) by finite difference method with a mesh of size $(0.05, 0.04)$ in space-time. Each problem is solved via primal-dual optimization approach with primal-dual gap $e_{tol} < 2e - 3$. The initial density function $\rho_{0,i}$ is the average of two

Algorithm 5 A detailed inversion algorithm for the nonlocal mean-field game system

Input: $(\rho_{0,i}, g_i, \tilde{r}_{B,i})$ for $i = 1, ..., N$, (κ_0, μ_0)

Output: (κ^n, μ^n) for $n = 1, ..., \mathcal{N}_{\max}$

while iteration $n < \mathcal{N}_{\text{maximal}}$ **do**

    1.Update for the adjoint problem by computing $(\lambda_{\rho_i}^{n+1}, \lambda_{m_i}^{n+1,})$

$$
\left\{
\begin{aligned}
&\left\{
\begin{aligned}
&\Delta \eta_i^{n+1} = 0 \text{ in } \Omega \\
&\eta_i^{n+1} = \rho_i^n - \mathrm{pr}_1 \tilde{r}_{B,i} \text{ on } \partial\Omega^+ \\
&\Delta \eta_i^{n+1} = 0 \text{ in } \Omega'\backslash\Omega \\
&\eta_i^{n+1} = \rho_i^n - \mathrm{pr}_1 \tilde{r}_{B,i} \text{ on } \partial\Omega^- \\
&\eta_i^{n+1} = 0 \text{ on } \partial\Omega'
\end{aligned}
\right. \\
&\left\{
\begin{aligned}
&\Delta \xi_i^{n+1} = 0 \text{ in } \Omega \\
&\partial_n \xi_i^{n+1} = m_i^n \cdot n - \mathrm{pr}_2 \tilde{r}_{B,i} \text{ on } \partial\Omega^+ \\
&\Delta \xi_i^{n+1} = 0 \text{ in } \Omega'\backslash\Omega \\
&\partial_n \xi_i^{n+1} = m_i^n \cdot n + \mathrm{pr}_2 \tilde{r}_{B,i} \text{ on } \partial\Omega^- \\
&\partial_n \xi_i^{n+1} = 0 \text{ on } \partial\Omega'
\end{aligned}
\right.
\end{aligned}
\right.
$$

$$
\left\{
\begin{aligned}
&\begin{pmatrix} \lambda_{\rho_i}^{n+1,\text{temp}} \\ \lambda_{m_i}^{n+1,\text{temp}} \end{pmatrix} = \\
&\left[I + \alpha_{\lambda_{(\rho_i, m_i)}}^n \rho_i^n \begin{pmatrix} \frac{1}{\kappa^n} \frac{|m_i^n|^2}{(\rho_i^n)^3} - \frac{1}{\kappa^n} \frac{m_i^n}{(\rho_i^n)^2} \\ -\frac{1}{\kappa^n} \frac{m_i^n}{(\rho_i^n)^2} \frac{1}{\kappa^n \rho_i^n} I \end{pmatrix} \right]^{-1} \left(\begin{pmatrix} \lambda_{\rho_i}^n \\ \lambda_{m_i}^n \end{pmatrix} - \alpha_{\lambda_{(\rho_i, m_i)}}^n \rho_i^n \begin{pmatrix} \eta_i^{n+1} \\ \nabla \xi_i^{n+1} \end{pmatrix} \right) \\
&\begin{pmatrix} \lambda_{\rho_i}^{n+1} \\ \lambda_{m_i}^{n+1} \end{pmatrix} = 2 \begin{pmatrix} \lambda_{\rho_i}^{n+1,\text{temp}} \\ \lambda_{m_i}^{n+1,\text{temp}} \end{pmatrix} - \begin{pmatrix} \lambda_{\rho_i}^{n,\text{temp}} \\ \lambda_{m_i}^{n,\text{temp}} \end{pmatrix}
\end{aligned}
\right.
$$

2. Update for the inverse problem by computing $(\kappa^{n+1}, \mu^{n+1})$

$$
\begin{cases}
\begin{cases}
\kappa^{n+1,\text{temp}} &= S_{\alpha_\kappa^n \gamma}\left(2\kappa^n - \tilde{\kappa}^n - \alpha_\kappa^n \sum_{i=1}^N \Lambda_\kappa(\kappa^n, m_i^n, \rho_i^n, \lambda_{\rho_i}^{n+1}, \lambda_{m_i}^{n+1}) - \kappa_0\right) + \kappa_0 \\[2ex]
\tilde{\kappa}^{n+1} &= \tilde{\kappa}^n + \mathcal{T}_{mask}(\kappa^{n+1,\text{temp}}, \kappa_0) - \kappa^n \\[2ex]
\kappa^{n+1} &= \max\left\{\varepsilon_1, \tilde{\kappa}^{n+1} * \psi\right\}
\end{cases} \\[6ex]
\begin{cases}
\mu^{n+1,\text{temp}} &= S_{\alpha_\mu^n \gamma}\left(2\Pi_\mu^*(\mu^n) - \tilde{\mu}^n - \alpha_\mu^n \sum_{i=1}^N \Lambda_\mu(\lambda_{\rho_i}^{n+1}, a_i^n) - \Pi_\mu^*(\mu_0)\right) + \Pi_\mu^*(\mu_0) \\[2ex]
\tilde{\mu}^{n+1} &= \tilde{\mu}^n + \mu^{n+1,\text{temp}} - \mu^n \\[2ex]
\mu^{n+1} &= \Pi_\mu(\min\{\varepsilon_2, \tilde{\mu}^{n+1}\})
\end{cases}
\end{cases}
$$

3. Update forward problem by computing $(\rho_i^{n+1}, m_i^{n+1}, \phi_i^{n+1}, a_i^{n+1})$ with the forward mean-field game algorithm for $i = 1, ..., N$.

Apply the iterative Algorithm 3 given input $(\rho_{0,i}, g_i)$, $(\kappa^{n+1}, \mu^{n+1})$, e_{tol} with initial guess $(\rho_i^n, m_i^n, \phi_i^n, a_i^n)$, and assign

$$(\rho_i^{n+1}, m_i^{n+1}, \phi_i^{n+1}, a_i^{n+1}) := (\rho_i^*, m_i^*, \phi_i^*, a_i^*)$$

$n \leftarrow n + 1$

end while

Gaussian functions with centers $x_G \in \Omega' \backslash \Omega$. The final cost function $g(x)$ is smooth and has a smaller value around a single point $x_g \in \Omega' \backslash \Omega$ such that densities are concentrated in the neighborhood of x_g at the final time. We want to point out that there is room to improve the initial density function and final cost function choices. We choose this set of $(\rho_{0,i}, g_i)$ to ensure that the density's movement covers the domain Ω as completely as possible. We also expect the nonlocal interaction among agents to be better reflected at the partial boundary measurements by setting the initial density as two Gaussians rather than one.

We only take 16 forward measurement events for each of the following numerical examples. The partial boundary measurement means that we only collect the ρ, m along the boundary $\partial \Omega$ in each event. Therefore, the resulting inverse problem is severely ill-posed.

To test the robustness of our reconstruction algorithm, we add some random noise to the measurements as follows:

$$(\rho, m \cdot n)^{\delta}(t_i, x_j) = ((1 + \epsilon_n \delta_{ij,1})\rho, (1 + \epsilon_n \delta_{ij,2})m \cdot n)(t_i, x_j),$$

where $\{(t_i, x_j)\}_{i=1,..,I,j=1,...,J} \in [0, T] \times \partial \Omega^+$ represents sampling points on the measurement boundary $[0, T] \times \partial \Omega^+$, $\{\delta_{ij,1}, \delta_{ij,2}\}_{i=1,..,I,j=1,...,J}$ are i.i.d. random variables uniformly distributed on the interval $[-0.5, 0.5]$ and ϵ_n corresponds to the noise level in the data, which is always set to be $\epsilon_n = 10\%$ in all our examples.

From the noisy observed data $\{(\rho, m \cdot n)^{\delta}(t_i, x_j)\}_{i=1,..,I,j=1,...,J}$ on the sampling points of the measurement surface, we then use the algorithm to reconstruct the forward problem parameters (κ, μ). Recall that we paramatrized the running cost $L(x, v) := \frac{1}{2\kappa(x)}|v|^2$ by κ and nonlocal kernel $K(x, y) := \zeta(x; \mu, \omega) \cdot \zeta(y; \mu, \omega)$ by μ. Since we aim at recovering the model on a given domain with fixed grid points, we fix the choice of ω, and only seek sparse recovery of μ.

In the following examples, we use a set of parameters uniformly, without tuning. $\gamma_c = 0.2, \gamma_\mu = 0.1, \alpha_c = 0.1, \alpha_\mu = 0.1, \alpha_\lambda = 10$. We set the lower-bound projection parameter $\varepsilon_1 = \kappa_c$, this is based on the additional assumption of the model parameters that $\kappa(x) \geq$

κ_c for $x \in \Omega'$. The projection parameter for kernel coefficient is $\varepsilon_2 = 1$.

To account for unknown ground truth of the model parameters, we introduce Res to quantify the quality of the reconstructed parameters.

$$\mathrm{Res}^n = \sum_i \int_{\partial\Omega^+} \left(\|\rho_i^n - \mathrm{pr}_1 \tilde{r}_{B,i}\|^2 + \|m_i^n \cdot n - \mathrm{pr}_2 \tilde{r}_{B,i}\|^2 \right),$$

where ρ_i^n, m_i^n are the solution of the forward mean-field game problem with i-th choice of initial density and final cost function with the reconstructed parameter (κ^n, μ^n) at the n-th iteration of the algorithm. The boundary residual Res measures how much the new boundary measurements of the mean-field game model with the recovered parameters deviate from the given partial measurements. If $(\kappa, \mu) = (\kappa_{true}, \mu_{true})$, we would expect that Res is close to 0. Therefore, we pick the reconstructed parameters at n_{opt}-th iteration by taking

$$n_{opt} = \operatorname*{argmin}_n \mathrm{Res}^n,$$

$$(\kappa_{opt}, \mu_{opt}) = (\kappa^{n_{opt}}, \mu^{n_{opt}}).$$

When we implemented the algorithm, we observed that the quantity Res^n first decreased then increased with respect to the iteration. We also observed that with large enough number of iterations, (for example, 1500), the inverse problem is contaminated and the reconstruction of mean-field game coefficients are very bad. In the following examples, we take fixed number of iterations $N = 1500$ for the inverse algorithm, and pick the reconstructed model parameters accordingly.

6.5.2 Example 1

This example tests a running cost $\kappa(x)$ with a bump at point $(0.25, 0.25)$, which means the density that travel crossing near this point has a lower cost than other routes. The density are also expected to accelerate when they travel across this point. The nonlocal kernel $K(x, y)$ is constructed via a Gaussian function plus some sparse terms in forms of $\mu_k^2 \cos(\omega_k \cdot x)$. The nonlocal kernel, in general, penalizes being too concentrated. The amplify of certain Fourier

frequencies determines the agents' particular interaction preferences. Specifically, we have the following:

$$\kappa(x) = 2 + 4 \exp\left(-\frac{(x_1 - 0.25)^2 + (x_2 - 0.25)^2}{0.1^2}\right),$$

$$\kappa_0(x) = 2,$$

$$K(x, y) = K_0(x, y) + K_s(x, y) + k_0,$$

$$K_0(x, y) = \frac{1}{5} \exp\left(-\frac{1}{2}\frac{x^2 + y^2}{0.4^2}\right),$$

$$K_s(x, y) = 0.2094^2 \left(\cos\left(\pi(x_1 - y_1)\right) + \cos\left(\pi(x_2 - y_2)\right)\right)$$

$$+ 0.2613^2 \left(\cos\left(\pi(x_1 - y_1) + \pi(x_2 - y_2)\right) + \cos\left(-\pi(x_1 - y_1) + \pi(x_2 - y_2)\right)\right),$$

where $x = [x_1, x_2], y = [y_1, y_2]$. We have μ_0, which represents $K_0(x, y)$ via the expansions form $\mu_k^2 \cos(\omega_k \cdot x)$, known. The variable k_0 is a given constant value that makes the kernel integration $\int\int K(x, y)dxdy = 1$. Varying this constant corresponding to changing the coefficient of the zero Fourier mode $(0, 0)$. This constant k_0 does not change the intensity of repulsion effect among the agents, since $\int k_0\rho(y)dy = k_0 \int \rho_0(y)dy$ is uniform over the domain Ω'. With $K(x, y) = \zeta(x; \mu, \omega) \cdot \zeta(y; \mu, \omega)$ for $\mu, \omega \in C_{odd=even}$, we omit the even entries (eg. $\mu_{k,2}, \omega_{k,2}$) and express the kernel K_s as follows:

$$\mu_s = (0.2094, 0.2094, 0.2613, 0.2613),$$

$$\omega_s = ((\pi, 0), (0, \pi), (\pi, \pi), (-\pi, \pi)).$$

Here, we also assume that $\kappa_c = 2$ and $\kappa(x) = 2$ for $x \in \Omega'\backslash\Omega$ is known.

Given (κ_0, μ_0) and the noisy partial boundary measurements with corresponding event parameters $(\rho_{0,i}, g_i, \tilde{r}_{B,i})$, we apply our inverse algorithm. The results are shown in Figure 6.2, 6.3. In Figure 6.2, we plot the residual Res^n and the $\max_x \kappa^n(x)$ along the iteration. We see that the residual oscillates and decreases first, then bounces back and increases. In Figure 6.3, we show the reconstruction of model parameters by taking $n_{opt} = \text{argmin}_n \text{Res}^n$, $(\kappa_{opt}, \mu_{opt}) = (\kappa^{n_{opt}}, \mu^{n_{opt}})$. We see that the reconstructed $\kappa_{opt}(x)$ has a single bump sits near $(0.25, 0.25)$.
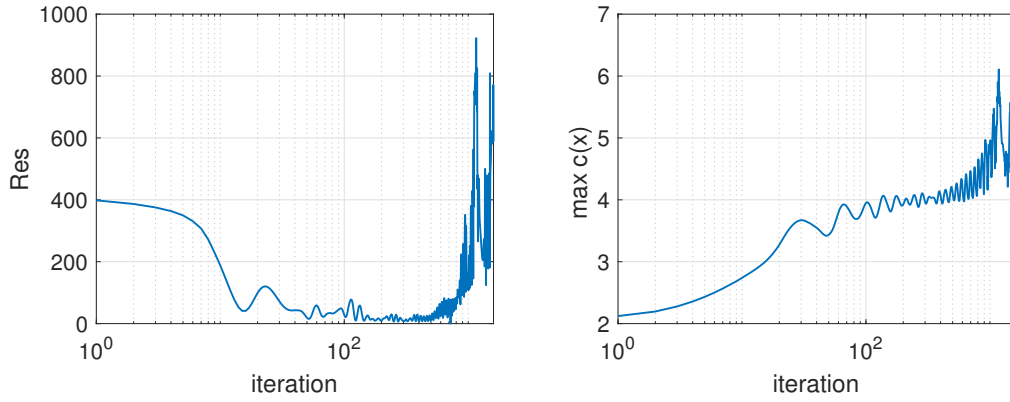
Figure 6.2: The residual Res^n and the $\max_x \kappa^n(x)$ at n-th iteration.

Figure 6.3: From left to right: the true running cost $\kappa(x)$; the reconstructed running cost $\kappa_{opt}(x)$ at iteration n_{opt}; the coefficient representation of nonlocal kernel $K(x, y)$ in vector form, where x-axis represents different Fourier mode ω and the y-axis corresponds to the coefficients μ.

The shape of the bump is not as sharp as the ground truth κ. The maximal value of running cost $\max_x \kappa_{true}(x) = 6$; while $\max_x \kappa_{opt}(x) = 4$. As for the non-local kernel, we have μ_{opt} nicely reconstructed, where $\mu_{true} = \mu_0 + \mu_s \approx \mu_{opt}$. This example shows that our inverse algorithm is robust to noise and can recover the model parameters (κ, μ) simultaneously.

6.5.3 Example 2

In this example, we make the $\kappa(x)$ more complicated by having two bumps sitting diagonally. We except that if the density travels across these two bumps, it will accelerate twice. The model set-up is as follows:

$$\kappa(x) = 2 + 4\exp\left(-\frac{(x_1 + 0.25)^2 + (x_2 - 0.25)^2}{0.1^2}\right) + 4\exp\left(-\frac{(x_1 - 0.25)^2 + (x_2 + 0.25)^2}{0.1^2}\right),$$

$$\kappa_0(x) = 2, \kappa_c = 2,$$

$$K(x, y) = K_0(x, y) + K_s(x, y) + k_0,$$

$$K_0(x, y) = \frac{1}{5}\exp\left(-\frac{1}{2}\frac{x^2 + y^2}{0.4^2}\right),$$

$$\mu_s = (0.3374, 0.3374, 0.2942, 0.2942),$$

$$\omega_s = ((\pi, 0), (0, \pi), (2\pi, 0), (0, 2\pi)).$$

We can see from the Figure 6.4 that recovered bumps are well separated, and their locations are accurately captured. Reconstructed bumps are more spread compared to the ground truth, and there is some noise on upper left and bottom right corners of the domain Ω'. The nonlocal kernel is reconstructed nicely as shown in Figure 6.4(right). A precise sparse representation of $K_s(x, y)$ is recovered. Considering the severe ill-posedness of the inverse problem with 10% multiplicative noise added to the boundary measurements, the reconstruction quality is quite satisfactory.
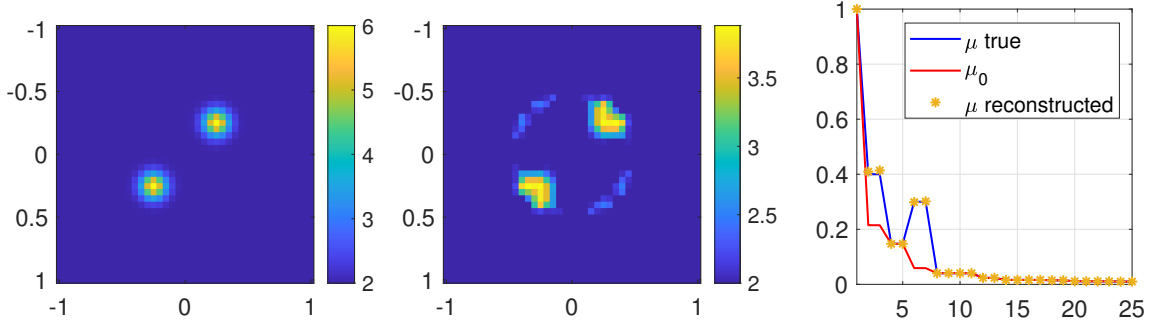
Figure 6.4: From left to right: the true running cost $\kappa(x)$; the reconstructed running cost $\kappa_{opt}(x)$ at iteration n_{opt}; the coefficient representation of nonlocal kernel $K(x, y)$ in vector form.

6.5.4 Example 3

In this example, we modify the $\kappa(x)$ by having two bumps sitting in parallel. Similar to the Example 2, the density would prefer to move crossing these bumps. We set the nonlocal kernel with K_s containing Fourier modes with higher frequency.

$$\kappa(x) = 2 + 4 \exp\left(-\frac{(x_1 - 0.25)^2 + (x_2 - 0.25)^2}{0.1^2}\right) + 4 \exp\left(-\frac{(x_1 - 0.25)^2 + (x_2 + 0.25)^2}{0.1^2}\right).$$

$$\kappa_0(x) = 2, \kappa_c = 2,$$

$$K(x, y) = K_0(x, y) + K_s(x, y) + k_0,$$

$$K_0(x, y) = \frac{1}{5} \exp\left(-\frac{1}{2}\frac{x^2 + y^2}{0.4^2}\right),$$

$$\mu_s = (0.2973, 0.2973, 0.2973, 0.2973),$$

$$\omega_s = ((2\pi, -\pi), (2\pi, \pi), (\pi, 2\pi), (\pi, -2\pi)).$$

We have the reconstruction result shown in Figure 6.5. The two parallel sitting bumps are well separated and located with reasonable accuracy. Again, the bumps are diffused with some noise near the upper boundary of Ω. The nonlocal kernel is recovered very nicely.
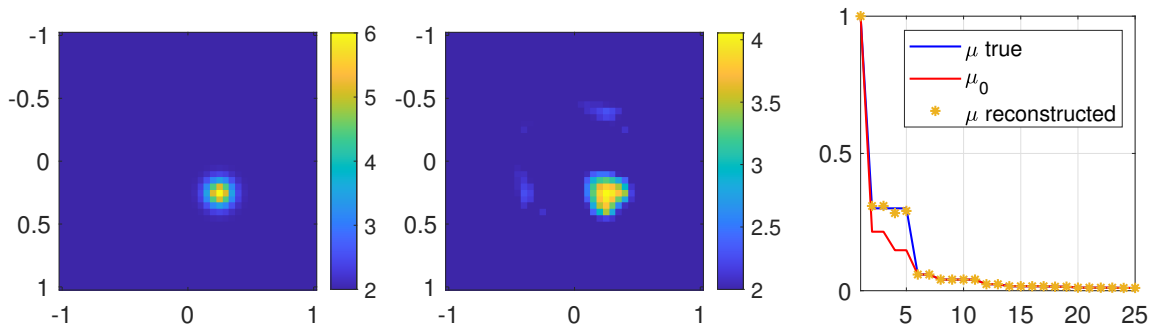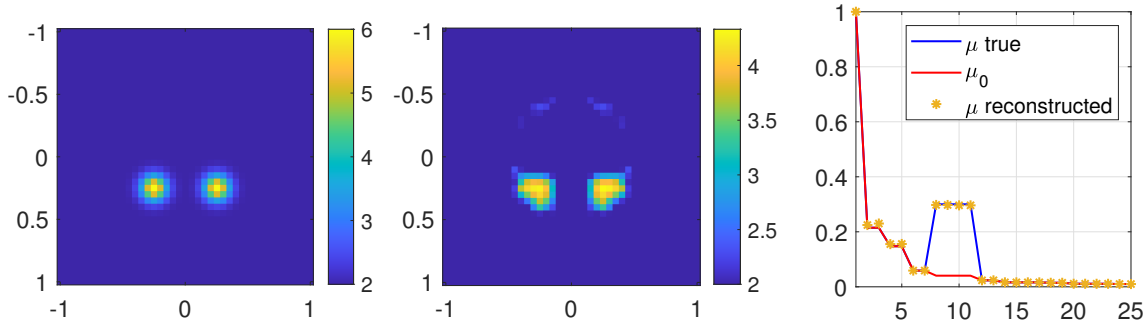
Figure 6.5: From left to right: the ground true running cost $\kappa(x)$; the reconstructed running cost $\kappa_{opt}(x)$ at iteration n_{opt}; the coefficient representation of nonlocal kernel $K(x, y)$ in vector form.

6.6 Conclusion

In this chapter, we formulate a new class of inverse mean-field game problems given only partial boundary measurements. A novel model recovery algorithm is proposed based on the saddle point formulation of MFGs. We demonstrate the robustness and effectiveness of the numerical inverse algorithm with several examples, where the MFG model parameters are reconstructed accurately. Our algorithm can be further generalized to other inverse problems with saddle point structure in the forward problem.

REFERENCES

[ABL14]   Yves Achdou, Francisco J. Buera, Jean-Michel Lasry, Pierre-Louis Lions, and Benjamin Moll. "Partial differential equation models in macroeconomics." *Philos. Trans. R. Soc. Lond. Ser. A Math. Phys. Eng. Sci.*, **372**(2028):20130397, 19, 2014.

[AC10]   Yves Achdou and Italo Capuzzo-Dolcetta. "Mean field games: numerical methods." *SIAM Journal on Numerical Analysis*, **48**(3):1136–1162, 2010.

[ACC12]   Yves Achdou, Fabio Camilli, and Italo Capuzzo-Dolcetta. "Mean field games: numerical methods for the planning problem." *SIAM Journal on Control and Optimization*, **50**(1):77–109, 2012.

[ACC13]   Yves Achdou, Fabio Camilli, and Italo Capuzzo-Dolcetta. "Mean field games: convergence of a finite difference method." *SIAM Journal on Numerical Analysis*, **51**(5):2585–2612, 2013.

[ACD20]   Yves Achdou, Pierre Cardaliaguet, François Delarue, Alessio Porretta, and Filippo Santambrogio. *Mean field games*, volume 2281 of *Lecture Notes in Mathematics*. Springer, Cham; Centro Internazionale Matematico Estivo (C.I.M.E.), Florence, [2020] ©2020. Edited by Pierre Cardaliaguet and Alessio Porretta, Fondazione CIME/CIME Foundation Subseries.

[ACD22]   Alexander Aurell, Rene Carmona, Gokce Dayanikli, and Mathieu Lauriere. "Optimal incentives to mitigate epidemics: a Stackelberg mean field game approach." *SIAM Journal on Control and Optimization*, (0):S294–S322, 2022.

[Ach13]   Yves Achdou. "Finite difference methods for mean field games." In *Hamilton-Jacobi equations: approximations, numerical analysis and applications*, volume 2074 of *Lecture Notes in Math.*, pp. 1–47. Springer, Heidelberg, 2013.

[AD11]   Daniel Andersson and Boualem Djehiche. "A maximum principle for SDEs of mean-field type." *Applied Mathematics & Optimization*, **63**(3):341–356, 2011.

[AD18]   Alexander Aurell and Boualem Djehiche. "Mean-field type modeling of nonlocal crowd aversion in pedestrian crowd dynamics." *SIAM J. Control Optim.*, **56**(1):434–455, 2018.

[AFG17]   Noha Almulla, Rita Ferreira, and Diogo Gomes. "Two numerical approaches to stationary mean-field games." *Dynamic Games and Applications*, **7**(4):657–682, 2017.

[AFL21]   Andrea Angiuli, Jean-Pierre Fouque, and Mathieu Lauriere. "Reinforcement learning for mean field games, with applications to economics." *arXiv preprint arXiv:2106.13755*, 2021.

[AFL22]   Andrea Angiuli, Jean-Pierre Fouque, and Mathieu Laurière. "Unified reinforcement Q-learning for mean field game and control problems." *Mathematics of Control, Signals, and Systems*, pp. 1–55, 2022.

[AHL17]   Yves Achdou, Jiequn Han, Jean-Michel Lasry, Pierre-Louis Lions, and Benjamin Moll. "Income and Wealth Distribution in Macroeconomics: A Continuous-Time Approach." Working Paper 23732, National Bureau of Economic Research, August 2017.

[AKK19]   L. Briceño Arias, D. Kalise, Z. Kobeissi, M. Laurière, Á. Mateos González, and F. J. Silva. "On the implementation of a primal-dual algorithm for second order time-dependent mean field games with local couplings." In *CEMRACS 2017—numerical methods for stochastic models: control, uncertainty quantification, mean-field*, volume 65 of *ESAIM Proc. Surveys*, pp. 330–348. EDP Sci., Les Ulis, 2019.

[AKS18]   L. M. Briceño Arias, D. Kalise, and F. J. Silva. "Proximal methods for stationary mean field games with local couplings." *SIAM J. Control Optim.*, **56**(2):801–836, 2018.

[AL16]   Yves Achdou and Mathieu Laurière. "Mean field type control with congestion (II): An augmented Lagrangian method." *Applied Mathematics & Optimization*, **74**(3):535–578, 2016.

[AL19]   Yves Achdou and Jean-Michel Lasry. "Mean field games for modeling crowd motion." In *Contributions to partial differential equations and applications*, volume 47 of *Comput. Methods Appl. Sci.*, pp. 17–42. Springer, Cham, 2019.

[AL20]   Yves Achdou and Mathieu Laurière. "Mean field games and applications: Numerical aspects." *Mean Field Games*, pp. 249–307, 2020.

[ALF22]   Sudhanshu Agrawal, Wonjun Lee, Samy Wu Fung, and Levon Nurbekyan. "Random features for high-dimensional nonlocal mean-field games." *Journal of Computational Physics*, p. 111136, 2022.

[And17]   Roman Andreev. "Preconditioning the augmented Lagrangian method for instationary mean field games with diffusion." *SIAM Journal on Scientific Computing*, **39**(6):A2763–A2783, 2017.

[Aro77]   DG Aronson. "The asymptotic speed of propagation of a simple epidemic." In *Nonlinear diffusion*, volume 14, pp. 1–23. Pitman London, 1977.

[Bar12]   Martino Bardi. "Explicit solutions of some linear-quadratic mean field games." *Networks & Heterogeneous Media*, **7**(2):243, 2012.

[BB00]   Jean-David Benamou and Yann Brenier. "A computational fluid mechanics solution to the Monge-Kantorovich mass transfer problem." *Numerische Mathematik*, **84**(3):375–393, 2000.

[BB14]   Fabio Bagagiolo and Dario Bauso. "Mean-field games and dynamic demand management in power grids." *Dynamic Games and Applications*, **4**(2):155–176, 2014.

[BC13]   Luis M Briceno-Arias and Patrick L Combettes. "Monotone operator methods for Nash equilibria in non-potential games." In *Computational and analytical mathematics*, pp. 143–159. Springer, 2013.

[BC15a]   J.-D. Benamou and G. Carlier. "Augmented Lagrangian methods for transport optimization, mean field games and degenerate elliptic equations." *J. Optim. Theory Appl.*, **167**(1):1–26, 2015.

[BC15b]   Jean-David Benamou and Guillaume Carlier. "Augmented Lagrangian methods for transport optimization, mean field games and degenerate elliptic equations." *Journal of Optimization Theory and Applications*, **167**(1):1–26, 2015.

[BCS17]   Jean-David Benamou, Guillaume Carlier, and Filippo Santambrogio. "Variational mean field games." In *Active Particles, Volume 1*, pp. 141–171. Springer, 2017.

[BDL09]   Rainer Buckdahn, Boualem Djehiche, Juan Li, and Shige Peng. "Mean-field backward stochastic differential equations: a limit approach." *The Annals of Probability*, **37**(4):1524–1565, 2009.

[BDM14]   Martin Burger, Marco Di Francesco, Peter A. Markowich, and Marie-Therese Wolfram. "Mean field games with nonlinear mobilities in pedestrian dynamics." *Discrete Contin. Dyn. Syst. Ser. B*, **19**(5):1311–1333, 2014.

[BF16]   Martino Bardi and Ermal Feleqi. "Nonlinear elliptic systems and mean-field games." *Nonlinear Differential Equations and Applications NoDEA*, **23**(4):1–32, 2016.

[BFY13]   Alain Bensoussan, Jens Frehse, Phillip Yam, et al. *Mean field games and mean field type control theory*, volume 101. Springer, 2013.

[BFY15]   Alain Bensoussan, Jens Frehse, and Sheung Chi Phillip Yam. "The master equation in mean field theory." *Journal de Mathématiques Pures et Appliquées*, **103**(6):1441–1474, 2015.

[BHL18]   Alain Bensoussan, Tao Huang, and Mathieu Laurière. "Mean field control and mean field game models with several populations." *arXiv preprint arXiv:1810.00783*, 2018.

[BKK19]   Luis Briceño-Arias, Dante Kalise, Ziad Kobeissi, Mathieu Laurière, A Mateos González, and Francisco J Silva. "On the implementation of a primal-dual algorithm for second order time-dependent mean field games with local couplings." *ESAIM: Proceedings and Surveys*, **65**:330–348, 2019.

[BKS18]   Luis M Briceno-Arias, Dante Kalise, and Francisco J Silva. "Proximal methods for stationary mean field games with local couplings." *SIAM Journal on Control and Optimization*, **56**(2):801–836, 2018.

[BLP21]   J Frédéric Bonnans, Pierre Lavigne, and Laurent Pfeiffer. "Generalized conditional gradient and learning in potential mean field games." *arXiv:2109.05785*, 2021.

[BLY21]   Reginald A Banez, Lixin Li, Chungang Yang, and Zhu Han. "A Survey of Mean Field Game Applications in Wireless Networks." In *Mean Field Game and its Applications in Wireless Networks*, pp. 61–82. Springer, 2021.

[BPW20]   Martin Burger, Jan-Frederik Pietschmann, and Marie-Therese Wolfram. "Data assimilation in price formation." *Inverse Problems*, **36**(6):064003, may 2020.

[BRR20]   Henri Berestycki, Jean-Michel Roquejoffre, and Luca Rossi. "Propagation of epidemics along lines with fast diffusion." *arXiv preprint arXiv:2005.01859*, 2020.

[BSY16]   Alain Bensoussan, KCJ Sung, Sheung Chi Phillip Yam, and Siu-Pang Yung. "Linear-quadratic mean field games." *Journal of Optimization Theory and Applications*, **169**(2):496–529, 2016.

[BTB16]   Dario Bauso, Hamidou Tembine, and Tamer Basar. "Opinion Dynamics in Social Networks through Mean-Field Games." *SIAM Journal on Control and Optimization*, **54**(6):3225–3257, 2016.

[Car13a] P. Cardaliaguet. "Notes on Mean Field Games.", 2013. https://www.ceremade.dauphine.fr/ cardaliaguet/.

[Car13b] Pierre Cardaliaguet. "Long time average of first order mean field games and weak KAM theory." *Dynamic Games and Applications*, **3**(4):473–488, 2013.

[Car15]   Pierre Cardaliaguet. "Weak solutions for first order mean field games with local coupling." In *Analysis and geometry in control theory and its applications*, pp. 111–158. Springer, 2015.

[CC10]   Settapat Chinviriyasit and Wirawan Chinviriyasit. "Numerical modelling of an SIR epidemic model with diffusion." *Applied Mathematics and Computation*, **216**(2):395–409, 2010.

[CC18]   Piermarco Cannarsa and Rossana Capuani. "Existence and uniqueness for mean field games with state constraints." In *PDE models for multi-agent phenomena*, volume 28 of *Springer INdAM Ser.*, pp. 49–71. Springer, Cham, 2018.

[CCC19]   Piermarco Cannarsa, Rossana Capuani, and Pierre Cardaliaguet. "$C^{1,1}$-smoothness of constrained solutions in the calculus of variations with application to mean field games." *Math. Eng.*, **1**(1):174–203, 2019.

[CCC21]   Piermarco Cannarsa, Rossana Capuani, and Pierre Cardaliaguet. "Mean field games with state constraints: from mild to pointwise solutions of the PDE system." *Calculus of Variations and Partial Differential Equations*, **60**(3):108, 2021.

[CCS21]   Steven Campbell, Yichao Chen, Arvind Shrivats, and Sebastian Jaimungal. "Deep learning for principal-agent mean field games." *arXiv preprint arXiv:2110.01127*, 2021.

[CD13a]   René Carmona and François Delarue. "Mean field forward-backward stochastic differential equations." *Electronic Communications in Probability*, **18**:1–15, 2013.

[CD13b]   René Carmona and François Delarue. "Probabilistic analysis of mean-field games." *SIAM Journal on Control and Optimization*, **51**(4):2705–2734, 2013.

[CD14]   René Carmona and Francois Delarue. "The master equation for large population equilibriums." In *Stochastic analysis and applications 2014*, pp. 77–128. Springer, 2014.

[CDL19]   Pierre Cardaliaguet, François Delarue, Jean-Michel Lasry, and Pierre-Louis Lions. *The master equation and the convergence problem in mean field games*. Princeton University Press, 2019.

[CEL20]   Arthur Charpentier, Romuald Elie, Mathieu Laurière, and Viet Chi Tran. "COVID-19 pandemic control: balancing detection policy and lockdown intervention under ICU sustainability." *Mathematical Modelling of Natural Phenomena*, **15**:57, 2020.

[CFL22]   Yat Tin Chow, Samy Wu Fung, Siting Liu, Levon Nurbekyan, and Stanley Osher. "A numerical algorithm for inverse problem from partial boundary measurement arising from mean field game problem." *arXiv:2204.04851*, 2022.

[CGC02]   Thomas Caraco, Stephan Glavanakov, Gang Chen, Joseph E Flaherty, Toshiro K Ohsumi, and Boleslaw K Szymanski. "Stage-structured infection transmission and a spatial epidemic: a model for Lyme disease." *The American Naturalist*, **160**(3):348–359, 2002.

[CGP15]   Pierre Cardaliaguet, P Jameson Graber, Alessio Porretta, and Daniela Tonon. "Second order mean field games with degenerate diffusion and local coupling." *Nonlinear Differential Equations and Applications NoDEA*, **22**(5):1287–1317, 2015.

[CH17]   Pierre Cardaliaguet and Saeed Hadikhanloo. "Learning in mean field games: the fictitious play." *ESAIM: Control, Optimisation and Calculus of Variations*, **23**(2):569–591, 2017.

167

[Cir15]   Marco Cirant. "Multi-population mean field games systems with Neumann boundary conditions." *Journal de Mathématiques Pures et Appliquées*, **103**(5):1294–1315, 2015.

[CJ19]   Philippe Casgrain and Sebastian Jaimungal. "Algorithmic Trading in Competitive Markets with Mean Field Games." *SIAM News*, **52**(2), 2019.

[CJ20]   Philippe Casgrain and Sebastian Jaimungal. "Mean-field games with differing beliefs for algorithmic trading." *Mathematical Finance*, **30**(3):995–1034, 2020.

[CL15]   René Carmona and Daniel Lacker. "A probabilistic weak formulation of mean field games and applications." *The Annals of Applied Probability*, **25**(3):1189–1231, 2015.

[CL18]   Pierre Cardaliaguet and Charles-Albert Lehalle. "Mean field game of controls and an application to trade crowding." *Mathematics and Financial Economics*, **12**(3):335–363, 2018.

[CLL12]   Pierre Cardaliaguet, Jean-Michel Lasry, Pierre-Louis Lions, and Alessio Porretta. "Long time average of mean field games." *Networks & Heterogeneous Media*, **7**(2):279, 2012.

[CLM15]   Geoffroy Chevalier, Jerome Le Ny, and Roland Malhamé. "A micro-macro traffic model based on mean-field games." In *2015 American Control Conference (ACC)*, pp. 1983–1988. IEEE, 2015.

[CLO19]   Yat Tin Chow, Wuchen Li, Stanley Osher, and Wotao Yin. "Algorithm for Hamilton–Jacobi equations in density space via a generalized Hopf formula." *Journal of Scientific Computing*, **80**(2):1195–1239, 2019.

[CLT19]   René Carmona, Mathieu Laurière, and Zongjun Tan. "Model-free mean-field reinforcement learning: mean-field MDP and mean-field Q-learning." *arXiv:1910.12802*, 2019.

[CP11]   Antonin Chambolle and Thomas Pock. "A First-Order Primal-Dual Algorithm for Convex Problems with Applications to Imaging." *Journal of Mathematical Imaging and Vision*, **40**(1):120–145, 2011.

[CP16]   Antonin Chambolle and Thomas Pock. "On the ergodic convergence rates of a first-order primal-dual algorithm." *Math. Program.*, **159**(1-2, Ser. A):253–287, 2016.

[CP19]   Pierre Cardaliaguet and Alessio Porretta. "Long time behavior of the master equation in mean field game theory." *Analysis & PDE*, **12**(6):1397–1453, 2019.

[CPP20]   Sheryl L Chang, Mahendra Piraveenan, Philippa Pattison, and Mikhail Prokopenko. "Game theoretic modelling of infectious disease dynamics and intervention methods: a review." *Journal of Biological Dynamics*, **14**(1):57–89, 2020.

[CS12]   Fabio Camilli and Francisco Silva. "A semi-discrete in time approximation for a model 1st order-finite horizon mean field game problem." *Networks and heterogeneous media*, **7**(2):263–277, 2012.

[CS14]   Elisabetta Carlini and Francisco J Silva. "A fully discrete semi-Lagrangian scheme for a first order mean field game problem." *SIAM Journal on Numerical Analysis*, **52**(1):45–67, 2014.

[CS15]   Elisabetta Carlini and Francisco J Silva. "A semi-Lagrangian scheme for a degenerate second order mean field game system." *Discrete & Continuous Dynamical Systems*, **35**(9):4269, 2015.

[CS18]   Elisabetta Carlini and Francisco J Silva. "On the Discretization of Some Nonlinear Fokker–Planck–Kolmogorov Equations and Applications." *SIAM Journal on Numerical Analysis*, **56**(4):2148–2177, 2018.

[CV17]   Christian Clason and Tuomo Valkonen. "Primal-dual extragradient methods for nonlinear nonsmooth PDE-constrained optimization." *SIAM Journal on Optimization*, **27**(3):1314–1339, 2017.

[Die79]   Odo Diekmann. "Run for your life. A note on the asymptotic speed of propagation of an epidemic." *Journal of Differential Equations*, **33**(1):58–73, 1979.

[DLO20]   Lisang Ding, Wuchen Li, Stanley Osher, and Wotao Yin. "A mean field game inverse problem." *arXiv preprint arXiv:2007.11551*, 2020.

[DLR20]   François Delarue, Daniel Lacker, and Kavita Ramanan. "From the master equation to mean field game limit theory: Large deviations and concentration of measure." *The Annals of Probability*, **48**(1):211–263, 2020.

[DPS20]   Laura Di Domenico, Giulia Pullano, Chiara E Sabbatini, Pierre-Yves Boëlle, and Vittoria Colizza. "Impact of lockdown on COVID-19 epidemic in Île-de-France and possible exit strategies." *BMC medicine*, **18**(1):1–13, 2020.

[DPT20]   Giacomo Dimarco, Benoît Perthame, Giuseppe Toscani, and Mattia Zanella. "Social contacts and the spread of infectious diseases." *arXiv preprint arXiv:2009.01140*, 2020.

[DTT17]   Boualem Djehiche, Alain Tcheukam, and Hamidou Tembine. "A mean-field game of evacuation in multilevel building." *IEEE Transactions on Automatic Control*, **62**(10):5154–5169, 2017.

[DY17]   Damek Davis and Wotao Yin. "A three-operator splitting scheme and its optimization applications." *Set-valued and variational analysis*, **25**(4):829–858, 2017.

[EB92]   Jonathan Eckstein and Dimitri P Bertsekas. "On the Douglas–Rachford splitting method and the proximal point algorithm for maximal monotone operators." *Mathematical Programming*, **55**(1):293–318, 1992.

[EB19]   Karthik Elamvazhuthi and Spring Berman. "Mean-field models in swarm robotics: a survey." *Bioinspiration & Biomimetics*, **15**(1):015001, 2019.

[EHT20]   Romuald Elie, Emma Hubert, and Gabriel Turinici. "Contact rate epidemic control of COVID-19: an equilibrium view." *Mathematical Modelling of Natural Phenomena*, **15**:35, 2020.

[FC17]   Dena Firoozi and Peter E Caines. "An optimal execution problem in finance targeting the market trading speed: An MFG formulation." In *2017 IEEE 56th Annual Conference on Decision and Control (CDC)*, pp. 7–14. IEEE, 2017.

[Fel13]   Ermal Feleqi. "The derivation of ergodic mean field game equations for several populations of players." *Dynamic Games and Applications*, **3**(4):523–536, 2013.

[FG00]   Michel Fortin and Roland Glowinski. *Augmented Lagrangian methods: applications to the numerical solution of boundary-value problems*. Elsevier, 2000.

[FG18]   Rita Ferreira and Diogo Gomes. "Existence of weak solutions to stationary mean-field games through variational inequalities." *SIAM J. Math. Anal.*, **50**(6):5969–6006, 2018.

[FGG21]   Andre Ian Francis, Saudah Ghany, Tia Gilkes, and Srikanth Umakanthan. "Review of COVID-19 vaccine subtypes, efficacy and geographical distributions." *Postgraduate Medical Journal*, 2021.

[FGT21]   Rita Ferreira, Diogo Gomes, and Teruo Tada. "Existence of weak solutions to time-dependent mean-field games." *Nonlinear Analysis*, **212**:112470, 2021.

[FH16]   István Faragó and Róbert Horváth. "Qualitatively adequate numerical modelling of spatial SIRS-type disease propagation." *Electronic Journal of Qualitative Theory of Differential Equations*, **2016**(12):1–14, 2016.

[FJN20]   Chris Finlay, Jörn-Henrik Jacobsen, Levon Nurbekyan, and Adam Oberman. "How to train your neural ODE: the world of Jacobian and kinetic regularization." In *International Conference on Machine Learning*, pp. 3154–3164. PMLR, 2020.

[FMG20]   Seth Flaxman, Swapnil Mishra, Axel Gandy, H Juliette T Unwin, Thomas A Mellan, Helen Coupland, Charles Whittaker, Harrison Zhu, Tresnia Berah, Jeffrey W Eaton, et al. "Estimating the effects of non-pharmaceutical interventions on COVID-19 in Europe." *Nature*, **584**(7820):257–261, 2020.

[GBK01]   Bryan T Grenfell, Ottar N Björnstad, and Jens Kappey. "Travelling waves and spatial hierarchies in measles epidemics." *Nature*, **414**(6865):716–723, 2001.

[GHH21]   Prakhar Godara, Stephan Herminghaus, and Knut M Heidemann. "A control theory approach to optimal pandemic mitigation." *PloS one*, **16**(2):e0247445, 2021.

[GHX19]   Xin Guo, Anran Hu, Renyuan Xu, and Junzi Zhang. "Learning mean-field games." In *Advances in Neural Information Processing Systems*, pp. 4967–4977, 2019.

[GHX20]   Xin Guo, Anran Hu, Renyuan Xu, and Junzi Zhang. "A General Framework for Learning Mean-Field Games." *arXiv preprint arXiv:2003.06069*, 2020.

[GLB22]   Hao Gao, Alex Lin, Reginald Banez, Wuchen Li, Zhu Han, Stanley Osher, and Vincent Poor. "Opinion Evolution in Social Networks: Connecting Mean Field Games to Generative Adversarial Nets." *IEEE Transactions on Network Science and Engineering*, 2022.

[GLK22]   Hao Gao, Wonjun Lee, Yuhan Kang, Wuchen Li, Zhu Han, Stanley Osher, and Vincent Poor. "Energy-Efficient Velocity Control for Massive Numbers of UAVs: A Mean Field Game Approach." *IEEE Transactions on Vehicular Technology*, 2022.

[GLL11]   Olivier Guéant, Jean-Michel Lasry, and Pierre-Louis Lions. "Mean field games and applications." In *Paris-Princeton Lectures on Mathematical Finance 2010*, volume 2003 of *Lecture Notes in Math.*, pp. 205–266. Springer, Berlin, 2011.

[GLY13]   Tom Goldstein, Min Li, Xiaoming Yuan, Ernie Esser, and Richard Baraniuk. "Adaptive primal-dual hybrid gradient methods for saddle-point problems." *arXiv:1305.0546*, 2013.

[GM18]   P. Jameson Graber and Alpár R. Mészáros. "Sobolev regularity for first order mean field games." *Ann. Inst. H. Poincaré Anal. Non Linéaire*, **35**(6):1557–1576, 2018.

[GM20]   Wilfrid Gangbo and Alpár R Mészáros. "Global well-posedness of Master equations for deterministic displacement convex potential mean field games." *arXiv preprint arXiv:2004.01660*, 2020.

[GMS19]   P Jameson Graber, Alpár R Mészáros, Francisco J Silva, and Daniela Tonon. "The planning problem in mean field games as regularized mass transport." *Calculus of Variations and Partial Differential Equations*, **58**(3):1–28, 2019.

[GNP15]   Diogo A Gomes, Levon Nurbekyan, and Edgard A Pimentel. *Economic models and mean-field games theory*. IMPA Mathematical Publications. Instituto Nacional de Matemática Pura e Aplicada (IMPA), Rio de Janeiro, 2015.

[GNT08]   Wilfrid Gangbo, Truyen Nguyen, Adrian Tudorascu, et al. "Hamilton-Jacobi equations in the Wasserstein space." *Methods and Applications of Analysis*, **15**(2):155–184, 2008.

[GPS12]   Diogo A Gomes, Gabriel E Pires, and Héctor Sánchez-Morgado. "A-priori estimates for stationary mean-field games." *Networks & Heterogeneous Media*, **7**(2):303, 2012.

[GPV16]   Diogo A. Gomes, Edgard A. Pimentel, and Vardan Voskanyan. *Regularity theory for mean-field game systems*. SpringerBriefs in Mathematics. Springer, [Cham], 2016.

[GS14]   Diogo A. Gomes and J. Saúde. "Mean field games models—a brief survey." *Dyn. Games Appl.*, **4**(2):110–154, 2014.

[GS15]   Wilfrid Gangbo and Andrzej Święch. "Existence of a solution to an equation arising from the theory of mean field games." *Journal of Differential Equations*, **259**(11):6573–6643, 2015.

[GS21]   Diogo A. Gomes and João Saúde. "Numerical Methods for Finite-State Mean-Field Games Satisfying a Monotonicity Condition." *Applied Mathematics & Optimization*, **83**(1):51–82, 2021.

[Gue09]   Olivier Guéant. "A reference case for mean field games models." *Journal de mathématiques pures et appliquées*, **92**(3):276–294, 2009.

[Had17]   Saeed Hadikhanloo. "Learning in anonymous nonatomic games with applications to first-order mean field games." *arXiv:1704.00378*, 2017.

[HCM07]   M. Huang, P. E. Caines, and R. P. Malhamé. "Large-population cost-coupled LQG problems with nonuniform agents: individual-mass behavior and decentralized ϵ-Nash equilibria." *IEEE Trans. Automat. Control*, **52**(9):1560–1571, 2007.

[HD11]   Elsa Hansen and Troy Day. "Optimal control of epidemics with limited resources." *Journal of mathematical biology*, **62**(3):423–451, 2011.

[HI95]   Yuzo Hosono and Bilal Ilyas. "Traveling waves for a simple diffusive epidemic model." *Mathematical Models and Methods in Applied Sciences*, **5**(07):935–966, 1995.

[HL22]   Ruimeng Hu and Mathieu Laurière. "Recent Developments in Machine Learning Methods for Stochastic Control and Games." 2022.

[HMC06]   M. Huang, R. P. Malhamé, and P. E. Caines. "Large population stochastic dynamic games: closed-loop McKean-Vlasov systems and the Nash certainty equivalence principle." *Commun. Inf. Syst.*, **6**(3):221–251, 2006.

[HML21]   Howard Heaton, Daniel McKenzie, Qiuwei Li, Samy Wu Fung, Stanley Osher, and Wotao Yin. "Learn to Predict Equilibria via Fixed Point Networks." *arXiv preprint arXiv:2106.00906*, 2021.

[HS19]   Saeed Hadikhanloo and Francisco J Silva. "Finite mean field games: fictitious play and convergence to a first order continuous mean field game." *Journal de Mathématiques Pures et Appliquées*, **132**:369–397, 2019.

[JC14]   Atit Jaichuang and Wirawan Chinviriyasit. "Numerical modelling of influenza model with diffusion." *International Journal of Applied Physics and Mathematics*, **4**(1):15, 2014.

[JKL20]   Junyoung Jang, Hee-Dae Kwon, and Jeehyun Lee. "Optimal control problem of an SIR reaction–diffusion model with inequality constraints." *Mathematics and Computers in Simulation*, **171**:136–151, 2020.

[JL20]   Matt Jacobs and Flavien Léger. "A fast approach to optimal transport: The back-and-forth method." *Numerische Mathematik*, **146**(3):513–544, 2020.

[JLL19]   Matt Jacobs, Flavien Léger, Wuchen Li, and Stanley Osher. "Solving large-scale optimization problems with a convergence rate independent of grid size." *SIAM Journal on Numerical Analysis*, **57**(3):1100–1123, 2019.

[Kal84]   Anders Källén. "Thresholds and travelling waves in an epidemic model for rabies." *Nonlinear Analysis: Theory, Methods & Applications*, **8**(8):851–856, 1984.

[KAS15]   Pushkin Kachroo, Shaurya Agarwal, and Shankar Sastry. "Inverse problem for non-viscous mean field control: Example from traffic." *IEEE Transactions on Automatic Control*, **61**(11):3412–3421, 2015.

[KC12]   Arman C Kizilkale and Peter E Caines. "Mean field stochastic adaptive control." *IEEE Transactions on Automatic Control*, **58**(4):905–920, 2012.

[Ken65]   David G Kendall. "Mathematical models of the spread of infection." *Mathematics and computer science in biology and medicine*, pp. 213–225, 1965.

[KK20]   Markus Kantner and Thomas Koprucki. "Beyond just "flattening the curve": Optimal control of epidemics with purely non-pharmaceutical interventions." *Journal of Mathematics in Industry*, **10**(1):1–23, 2020.

[KKL16]   Jungeun Kim, Hee-Dae Kwon, and Jeehyun Lee. "Constrained optimal control applied to vaccination for influenza." *Computers & Mathematics with Applications*, **71**(11):2313–2329, 2016.

[KLZ21] Yuhan Kang, Siting Liu, Hongliang Zhang, Wuchen Li, Zhu Han, Stanley Osher, and H. Vincent Poor. "Joint Sensing Task Assignment and Collision-Free Trajectory Optimization for Mobile Vehicle Networks Using Mean-Field Games." *IEEE Internet of Things Journal*, **8**(10):8488–8503, 2021.

[KM27] William Ogilvy Kermack and Anderson G McKendrick. "A contribution to the mathematical theory of epidemics." *Proceedings of the royal society of london. Series A, Containing papers of a mathematical and physical character*, **115**(772):700–721, 1927.

[KSM19] Arman C Kizilkale, Rabih Salhab, and Roland P Malhamé. "An integral control formulation of mean field game based large scale coordination of loads in smart grids." *Automatica*, **100**:312–322, 2019.

[Lau21] Mathieu Lauriere. "Numerical methods for mean field games and mean field type control." *Mean Field Games*, **78**:221, 2021.

[LES18] A Lahrouz, H El Mahjour, A Settati, and A Bernoussi. "Dynamics and optimal control of a non-linear epidemic model with relapse and cure." *Physica A: Statistical Mechanics and its Applications*, **496**:299–317, 2018.

[LFL21] Alex Tong Lin, Samy Wu Fung, Wuchen Li, Levon Nurbekyan, and Stanley J Osher. "Alternating the population and control neural networks to solve high-dimensional stochastic mean-field games." *Proceedings of the National Academy of Sciences*, **118**(31), 2021.

[LJL21] Siting Liu, Matthew Jacobs, Wuchen Li, Levon Nurbekyan, and Stanley J. Osher. "Computational Methods for First-Order Nonlocal Mean Field Games with Applications." *SIAM Journal on Numerical Analysis*, **59**(5):2639–2668, 2021.

[LL06a] Jean-Michel Lasry and Pierre-Louis Lions. "Jeux à champ moyen. I. Le cas stationnaire." *C. R. Math. Acad. Sci. Paris*, **343**(9):619–625, 2006.

[LL06b] Jean-Michel Lasry and Pierre-Louis Lions. "Jeux à champ moyen. II. Horizon fini et contrôle optimal." *C. R. Math. Acad. Sci. Paris*, **343**(10):679–684, 2006.

[LL07] Jean-Michel Lasry and Pierre-Louis Lions. "Mean field games." *Jpn. J. Math.*, **2**(1):229–260, 2007.

[LLL16] Aimé Lachapelle, Jean-Michel Lasry, Charles-Albert Lehalle, and Pierre-Louis Lions. "Efficiency of the price formation process in presence of high frequency participants: a mean field game analysis." *Math. Financ. Econ.*, **10**(3):223–262, 2016.

[LLL21a] Wonjun Lee, Rongjie Lai, Wuchen Li, and Stanley Osher. "Generalized unnormalized optimal transport and its fast algorithms." *Journal of Computational Physics*, p. 110041, 2021.

[LLL21b] Wonjun Lee, Siting Liu, Wuchen Li, and Stanley Osher. "Mean field control problems for vaccine distribution." *arXiv preprint arXiv:2104.11887*, 2021.

[LLP20] Gustavo Barbosa Libotte, Fran Sérgio Lobato, Gustavo Mendes Platt, and Antônio J Silva Neto. "Determination of an optimal control strategy for vaccine administration in COVID-19 pandemic treatment." *Computer methods and programs in biomedicine*, **196**:105664, 2020.

[LLT21] Wonjun Lee, Siting Liu, Hamidou Tembine, Wuchen Li, and Stanley Osher. "Controlling propagation of epidemics via mean-field control." *SIAM Journal on Applied Mathematics*, **81**(1):190–207, 2021.

[LN21] Siting Liu and Levon Nurbekyan. "Splitting methods for a class of non-potential mean field games." *Journal of Dynamics & Games*, **8**(4):467–486, 2021.

[LRO18] Wuchen Li, Ernest K. Ryu, Stanley Osher, Wotao Yin, and Wilfrid Gangbo. "A parallel method for earth mover's distance." *J. Sci. Comput.*, **75**(1):182–197, 2018.

[LRS19] Zongxi Li, A Max Reppen, and Ronnie Sircar. "A mean field games model for cryptocurrency mining." *arXiv preprint arXiv:1912.01952*, 2019.

[LT20] Mathieu Laurière and Ludovic Tangpi. "Convergence of large population games to mean field games with interaction through the controls." *arXiv preprint arXiv:2004.08351*, 2020.

[LW11] Aimé Lachapelle and Marie-Therese Wolfram. "On a mean field game approach modeling congestion and aversion in pedestrian crowds." *Transp. Res. Part B: Methodol.*, **45**(10):1572 – 1589, 2011.

[LW20] Jun Liu and Xiang-Sheng Wang. "Optimal allocation of face masks during the COVID-19 pandemic: a case study of the first epidemic wave in the United States." *arXiv preprint arXiv:2101.03023*, 2020.

[LWL18] Zhiyu Liu, Bo Wu, and Hai Lin. "A mean field game approach to swarming robots control." In *2018 Annual American Control Conference (ACC)*, pp. 4293–4298. IEEE, 2018.

[LZL20] Qi Lin, Qiuhong Zhao, and Benjamin Lev. "Cold chain transportation decision in the vaccine supply chain." *European Journal of Operational Research*, **283**(1):182–195, 2020.

[LZM19]   Kezan Li, Guanghu Zhu, Zhongjun Ma, and Lijuan Chen. "Dynamic stability of an SIQS epidemic network and its optimal control." *Communications in Nonlinear Science and Numerical Simulation*, **66**:84–95, 2019.

[MLT13]   François Mériaux, Samson Lasaulce, and Hamidou Tembine. "Stochastic differential games and energy-efficient power control." *Dynamic Games and Applications*, **3**(1):3–23, 2013.

[MRT18]   Mehryar Mohri, Afshin Rostamizadeh, and Ameet Talwalkar. *Foundations of machine learning*. Adaptive Computation and Machine Learning. MIT Press, Cambridge, MA, 2018. Second edition of [MR3057769].

[Mur01]   JD Murray. *Mathematical biology II: spatial models and biomedical applications*. Springer New York, 2001.

[MYZ22]   Chenchen Mou, Xianjin Yang, and Chao Zhou. "Numerical methods for mean field games based on Gaussian processes and Fourier features." *Journal of Computational Physics*, p. 111188, 2022.

[MZ19]   Chenchen Mou and Jianfeng Zhang. "Wellposedness of second order master equations for mean field games with nonsmooth data." *arXiv preprint arXiv:1903.09907*, 2019.

[NCM11]   Mojtaba Nourian, Peter E Caines, and Roland P Malhamé. "Mean field analysis of controlled Cucker-Smale type flocking: Linear analysis and perturbation equations." *IFAC Proceedings Volumes*, **44**(1):4471–4476, 2011.

[NH12]   Son Luu Nguyen and Minyi Huang. "Linear-quadratic-Gaussian mixed games with continuum-parametrized minor players." *SIAM Journal on Control and Optimization*, **50**(5):2907–2937, 2012.

[NS18]   Levon Nurbekyan and J. Saúde. "Fourier approximation methods for first-order nonlocal mean-field games." *Port. Math.*, **75**(3-4):367–396, 2018.

[NTS20]   Babacar Mbaye Ndiaye, Lena Tendeng, and Diaraf Seck. "Analysis of the COVID-19 pandemic by SIR model and machine learning technics for forecasting." *arXiv preprint arXiv:2004.01574*, 2020.

[Nur18]   Levon Nurbekyan. "One-dimensional, non-local, first-order stationary mean-field games with congestion: a Fourier approach." *Discrete Contin. Dyn. Syst. Ser. S*, **11**(5):963–990, 2018.

[ONL21a]   Derek Onken, Levon Nurbekyan, Xingjian Li, Samy Wu Fung, Stanley Osher, and Lars Ruthotto. "A neural network approach applied to multi-agent optimal control." In *2021 European Control Conference (ECC)*, pp. 1036–1041. IEEE, 2021.

[ONL21b] Derek Onken, Levon Nurbekyan, Xingjian Li, Samy Wu Fung, Stanley Osher, and Lars Ruthotto. "A Neural Network Approach for High-Dimensional Optimal Control." *arXiv preprint arXiv:2104.03270*, 2021.

[OWL21] D Onken, S Wu Fung, Xingjian Li, and L Ruthotto. "OT-Flow: Fast and Accurate Continuous Normalizing Flows via Optimal Transport." In *Proceedings of the AAAI Conference on Artificial Intelligence*, volume 35, 2021.

[ROL20] Lars Ruthotto, Stanley J Osher, Wuchen Li, Levon Nurbekyan, and Samy Wu Fung. "A machine learning framework for solving high-dimensional mean field game and mean field control problems." *Proceedings of the National Academy of Sciences*, **117**(17):9183–9193, 2020.

[Ron98] Xiaochun Rong. "A Bochner theorem and applications." *Duke mathematical journal*, **91**(2):381–392, 1998.

[Rua07] Shigui Ruan. "Spatial-temporal dynamics in nonlocal epidemiological models." In *Mathematics for life science and medicine*, pp. 97–122. Springer, 2007.

[SB18] Leonardo Stella and Dario Bauso. "Mean-field games for bio-inspired collective decision-making in dynamical networks." *arXiv preprint arXiv:1802.03435*, 2018.

[SCT21] Cristiana J Silva, Carla Cruz, Delfim FM Torres, Alberto P Muñuzuri, Alejandro Carballosa, Iván Area, Juan J Nieto, Rui Fonseca-Pinto, Rui Passadouro, Estevão Soares Dos Santos, et al. "Optimal control of the COVID-19 pandemic: controlled sanitary deconfinement in Portugal." *Scientific reports*, **11**(1):1–15, 2021.

[Ses20] Jörn Lothar Sesterhenn. "Adjoint-based data assimilation of an epidemiology model for the Covid-19 pandemic in 2020." *arXiv preprint arXiv:2003.13071*, 2020.

[SPB19] Hamid Shiri, Jihong Park, and Mehdi Bennis. "Massive autonomous UAV path planning: A neural network based mean-field game theoretic approach." In *2019 IEEE Global Communications Conference (GLOBECOM)*, pp. 1–6. IEEE, 2019.

[SS78] Suresh P Sethi and Preston W Staats. "Optimal control of some simple deterministic epidemic models." *Journal of the Operational Research Society*, **29**(2):129–136, 1978.

[SS21] Filippo Santambrogio and Woojoo Shim. "A Cucker–Smale Inspired Deterministic Mean Field Game with Velocity Interactions." *SIAM Journal on Control and Optimization*, **59**(6):4155–4187, 2021.

[SST18] Zuoqiang Shi, Jian Sun, and Minghao Tian. "Harmonic extension on the point cloud." *Multiscale Modeling & Simulation*, **16**(1):215–247, 2018.

[Thi77]   HR Thieme. "A model for the spatial spread of an epidemic." *Journal of Mathematical Biology*, **4**(4):337–351, 1977.

[V 13]   Bang Công Vũ. "A variable metric extension of the forward-backward-forward algorithm for monotone operators." *Numer. Funct. Anal. Optim.*, **34**(9):1050–1065, 2013.

[WHL19]   E Weinan, Jiequn Han, and Qianxiao Li. "A mean-field optimal control formulation of deep learning." *Research in the Mathematical Sciences*, **6**(1):10, 2019.

[WW10]   Zhi-Cheng Wang and Jianhong Wu. "Travelling waves of a diffusive Kermack–McKendrick epidemic model with non-local delayed transmission." *Proceedings of the Royal Society A: Mathematical, Physical and Engineering Sciences*, **466**(2113):237–261, 2010.

[YYT18]   Jiachen Yang, Xiaojing Ye, Rakshit Trivedi, Huan Xu, and Hongyuan Zha. "Learning Deep Mean Field Games for Modeling Large Population Behavior." In *International Conference on Learning Representations (ICLR)*, 2018.

[ZKJ08]   Gul Zaman, Yong Han Kang, and Il Hyo Jung. "Stability analysis and optimal vaccination of an SIR epidemic model." *BioSystems*, **93**(3):240–249, 2008.

[ZYL19]   Yue Zhang, Chungang Yang, Jiandong Li, and Zhu Han. "Distributed interference-aware traffic offloading and power control in ultra-dense networks: Mean field game with dominating player." *IEEE Transactions on Vehicular Technology*, **68**(9):8814–8826, 2019.